CHEMIA

S T U D I A
UNIVERSITATIS BABEŞ-BOLYAI CHEMIA

2,
Tom I

CUPRINS – CONTENT – SOMMAIRE – INHALT

Studia Universitatis Babes-Bolyai Chemia has been selected for coverage in Thomson Reuters products and custom information services. Beginning with V. 53 (1) 2008, this publication is indexed and abstracted in the following:
- Science Citation Index Expanded (also known as SciSearch®)
- Chemistry Citation Index®
- Journal Citation Reports/Science Edition

CONCISE SYNTHESIS OF SOME (4-AMINOPHENOXY)ALKANOIC ACIDS BASED ON PARACETAMOL

CRISTINA MORAR[a], LAVINIA COST[a], MIRCEA DARABANTU[a,*]

ABSTRACT. Starting from *N*-(4-hydroxyphenyl)acetamide (*Paracetamol*), a three steps synthesis of (4-aminophenoxy)acetic acid and 4-(4-aminophenoxy) butyric acid is comparatively discussed.

Keywords: *(4-aminophenoxy)acetic acid, 4-(4-aminophenoxy)butyric acid, Williamson etherification, acidolysis*

INTRODUCTION

(4-Aminophenoxy)acetic acid **1a** and 4-(4-aminophenoxy)butyric acid **1b** (Scheme 1) are known compounds as early as for the end of XIX-century and the starting of XX-century [1-4].

1a (n=1), **1b** (n=3)
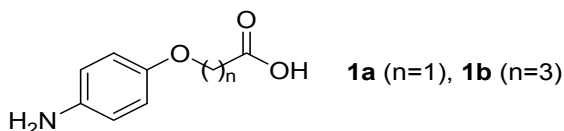
Scheme 1

The first reported synthesis of (4-aminophenoxy)acetic acid consisted of reduction of its corresponding nitro precursor, the last one being available from Williamson etherification of 4-nitrophenol with monochloroacetic acid in alkaline conditions [1-3]. Closer to our days, the same etherification strategy still was actual by using, in the key step, *N*-(4-hydroxyphenyl)acetamide (*Paracetamol*) in reaction with monochloroacetic acid [5, 6] with yields around 60%. However, the expected soft nucleophilicity of the conjugated *p*-substituted phenoxides[1] prompted other authors to explore the use of

---

[a] *Babeş-Bolyai University, Faculty of Chemistry and Chemical Engineering, Department of Chemistry, 11 Arany Janos St., RO-400028, Cluj-Napoca, Romania.*
[*] *Corresponding author: darab@chem.ubbcluj.ro*
[1] pKa (*Paracetamol*): 9.38; pKa (4-nitrophenol): 7.16

bromoacetic acid [7] or of its low alkyl esters against deprotonated forms of *Paracetamol* [8a] or even *p*-nitrophenol [8b]. Overall, the nowadays increased interest in (*N,O*-masked) forms of (4-aminophenoxy)acetic acid arises from their bioimpact, i.e. when targeting new analgesic, antipyretic and anti-inflammatory agents [6], new potential antisickling agents [7], bioabsorbable as biocompatible polyurethanes and polyamides for medical [8] devices.

In contrast, there are very few reports concerning the synthesis of 4-(4-aminophenoxy)butyric acid **1b** (Scheme 1) in spite of its first mentioning in the literature in 1917 [4]. Similar to its lower homologue **1a**, **1b** can be obtained by reduction of 4-(4-nitrophenoxy)butyric acid resulted, from the regioselective ring cleavage of γ-butyrolactone upon treatment with sodium 4-nitrophenoxide (Scheme 2) [9a, 9b] or by Williamson etherification of the latter, as reported very recently [9c, 9d].

Scheme 2
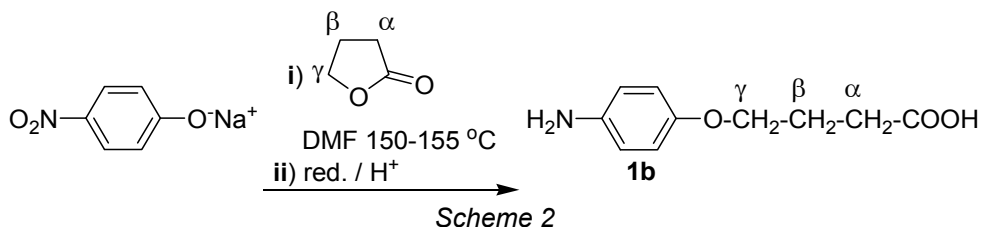
Lately, the use of **1b** as polyconjugate for delivery of RNA triggers to tumor cells *in vivo* [9c], as intermediate in the synthesis of new anti-*Helicobacter pylori* agents [10] and side-chain component of some cancer inhibitors of the cellular checkpoint kinase Wee1 [11] was reported.

Therefore, the aim of the present preliminary communication is to present a common and concise synthetic pathway towards (4-aminophenoxy)alkanoic acids **1a** and **1b** (Scheme 1) based on a Williamson approach.

RESULTS AND DISCUSSION

The chemistry we performed is resumed in Scheme 3.

(4-Aminophenoxy)acetic acid hydrochloride **3a** was prepared in two steps, **I** and **II**, both inspired from Bezwada's recent Patent [8a]. They consisted of Williamson etherification of *Paracetamol* (**I**, 90% yield against lit. 80% [8a]) followed by acidolysis of the amidoester **2a** (**II**, 92% yield against lit. 77.6% [8a]), hence, an overall yield of 83% (lit. 62%, [8a]). In step **III**, we isolated the free amine **1a** by manipulating its solubility in water in such a way that we avoided contamination with potassium chloride.

In order to access 4-(4-aminophenoxy)butyric acid **1b**, we first planned the ring opening of γ-butyrolactone with the use of sodium phenoxide of *Paracetamol* in similar conditions with those already reported in the case of sodium 4-nitrophenoxide (Scheme 2) [9a]. In our hands no reaction occurred, the starting *N*-(4-hydroxyphenyl)acetamide being recovered. That is, once more we moved our interest towards Williamson

I
Br-(CH$_2$)$_n$-CO-OEt
K$_2$CO$_3$

Ac-HN—⬡—OH → Ac-HN—⬡—O-(CH$_2$)$_n$-CO-OEt

Paracetamol

2a (n=1) 90%; **2b** (n=3) 75%

II
concd. HCl →

n=1 → ⁻Cl⁺H$_3$N—⬡—O-CH$_2$-COOH
3a (92%)

III
0.5 equiv.
K$_2$CO$_3$ aq.

H$_2$N—⬡—O-(CH$_2$)$_n$-COOH

1a (n=1) 81%; **1b** (n=3) 73%

⁻Cl⁺H$_3$N—⬡—O-(CH$_2$)$_3$-COOH
3b (71%)

n=3 → Ac-HN—⬡—O-(CH$_2$)$_3$-COOH
3c

⁻Cl⁺H$_3$N—⬡—OH
3d

Acidolysis of compound **2b**

Time (h)	Molar composition (%)			
	2b	**3b**	**3c**	**3d**
13	0	80	0	20
2	0	100	0	0
1	0	90	10	0

Key
 I (n=1) **2a**: 3.93 equiv. anh. K$_2$CO$_3$, 1.36 equiv. ethyl bromoacetate / acetone, 52 °C,15 h
 I (n=3) **2b**: 3.93 equiv. anh. K$_2$CO$_3$, 1.10 equiv. ethyl 4-bromobutyrate / DMF / 70 °C, 16 h / r.t., 72 h
 II (n=1, 3): 69.0 equiv HCl as aq. soln. 37% / reflux, 13 h (**3a**), 2 h (**3b**)
 III (n=1, 3) **1a**, **1b**: 0.50 equiv. K$_2$CO$_3$ / H$_2$O / r.t., 1 h

Scheme 3

methodology. Thus, inspired from the similar reactivity of *N*-(4-hydroxyben-zyl)acetamide [10], we obtained (**I**) the amidoester **2b** with good yield[2]. However, acidolysis (**II**) of **2b** carried out in identical conditions as for **2a**, resulted in a crude reaction mixture whose ^{1}H NMR spectrum revealed, besides formation of the desired **3b**, the existence of the hydrochloride of 4-aminophenol **3d** issued from the acidolysis of the etheric connection (Figure 1). ^{1}H NMR monitoring of the process showed the reaction reaching completion within 2 h, i.e. in a much shorter time in comparison with **3a** (Scheme 3). As for **1a**, the free amine **1b** was isolate simply (**III**) by modulating its solubility in water against that of potassium chloride. To conclude, the overall yield in the synthesis of **1b** was 39%.

---

[2] Compound **2b** was previously mentioned by Katsura and co-workers in 2000 (Ref. [10]) with no experimental assignment (synthesis and / or analytical data)

CONCLUSIONS

Starting from *N*-(4-hydroxyphenyl)acetamide, we described a three steps expeditious synthetic pathway in the direction of two (4-aminophenoxy)alkanoic acids. The common key step, a Williamson etherification yielding amidoesters of the target aminoacids, appears to be a good option if ethyl bromoalkanoates are used. In contrast, the key step,
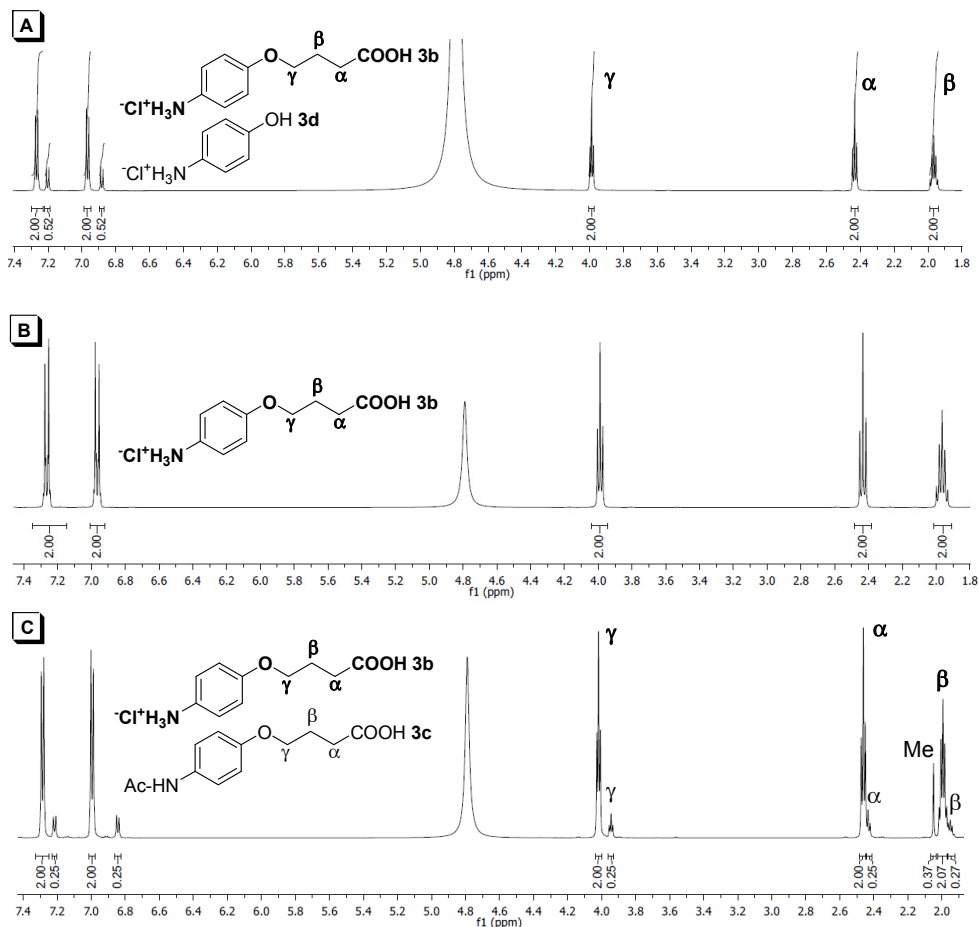
Figure 1. ^{1}H NMR monitoring of acidolysis of amidoester **2b** (600 MHz, D$_2$O, 298 K): crude reaction mixture after 13 h (**A**), 2 h (**B**), 1 h (**C**).

N,O-deprotection of the resulting amidoesters by acidolysis, strongly depends on the size of the (poly)methylenic chain (n=1 vs. n=3).

EXPERIMENTAL SECTION

General. Melting points were measured on an Electrothermal® instrument and are not corrected. NMR spectra were recorded on Bruker® AV 400, or AV 600 instruments operating at 400 or 600 MHz for ^{1}H and at 100 or 150 MHz for ^{13}C nuclei respectively. All chemical shifts (δ values) are given in parts per million (ppm); all homocoupling patterns ($^n J_{H,H}$ values) are given in Hertz. TLC was performed by using aluminium sheets with silica gel 60 F_{254} (Merck®). IR spectra were recorded on a Bruker® FT-IR Vector 22 Spectrometer. Microanalyses were performed on a Carlo Erba® CHNOS 1160 apparatus. Mass spectra were carried out on a Schimadzu® GC-MS QP-2010 PLUS instrument equipped with a Column HP-5MS under EI (70 eV) ionisation. All solvents and reagents were of analytical grade and required no purification prior to use.

Typical procedure for Williamson etherification. Preparation of compound **2b**. Into a DMF (30 mL) solution containing *N*-(4-hydroxyphenyl) acetamide (3.00 g, 19.85 mmol) and ethyl 4-bromobutyrate (3.14 mL, 4.26 g, 21.83 mmol), anhyd. K_2CO_3 (10.81 g, 78.2 mmol) was added with vigorous stirring. The resulted suspension was heated at 70 °C for 16 h then let to stir at room temperature for additional 72 h. Water (50 mL) and ethyl acetate (100 mL) were added to the reaction mixture with stirring, then the resulted two layers were separated. The organic layer was washed with water to complete removal of DMF (5 × 50 mL), dried over anhyd. Na_2SO_4 and evaporated under reduced pressure. The crude solid product was crystallised from min. amount of ethyl acetate to afford 3.95 g pure compound **2b** [75% yield with respect to *N*-(4-hydroxyphenyl)acetamide] as a white solid.

Ethyl (4-N-acetylamino)phenoxyacetate (**2a**); yield 90% [1.41 g **2a** starting from 1.00 g *N*-(4-hydroxyphenyl)acetamide], white powder, mp 102.3-103.5 °C (toluene/hexane 1:5 v/v) (Lit. [8a]: 104.2-106.2 °C); [Found: C, 61.05; H, 6.57; N, 6.24%. $C_{12}H_{15}NO_4$ (237.10) requires: C, 60.75; H, 6.37; N, 5.90 %]; R_f (ligroin/acetone 2:1 v/v) 0.51. $v_{max.}$ (KBr) 3382 (m), 2994 (w), 1741(s), 1678 (m), 1532 (m), 1510 (s), 1428 (w), 1408 (w), 1322 (w), 1251 (m), 1215 (s), 1175 (w), 1089 (m), 1015 (w), 833 (m), 810 (m), 678 (w), 595 (w) cm^{-1}. ^{1}H NMR (400 MHz, DMSO-d_6, 298 K) δ_H 1.20 (3 H, t, $^3 J_{H,H}$=7.0 Hz, CH$_2$C*H$_3$*), 2.00 (3 H, s, CH$_3$), 4.15 (2 H, q, $^3 J_{H,H}$=7.0 Hz, C*H$_2$*CH$_3$), 4.71 (2 H, s, CH$_2$), 6.86 (2 H, d, $^3 J_{H,H}$=9.2 Hz, H-3, -5, Ar), 7.47 (2 H, d, $^3 J_{H,H}$=9.2 Hz, H-2, -6, Ar), 9.83 (1 H, s, NH) ppm. ^{13}C NMR in J_{mod} (100 MHz, DMSO-d_6, 298 K) δ_C 14.1 (CH$_2$*CH$_3$*), 23.8 (CH$_3$), 60.6 (*CH$_2$*CH$_3$), 64.9 (CH$_2$), 114.6 (C-3, -5, Ar), 120.5 (C-2, -6, Ar), 133.2 (C-4, Ar), 153.4 (C-1, Ar), 167.9 (NH-CO), 168.9 (COO) ppm. GC-MS (MeOH) *m/z* (rel. int. %) 223 [M, - CH$_3$] (23); [APCI(+), MeCN] *m/z* (rel. int. %) 238.11 [M+1].

Ethyl 4-(4-N-acetylamino)phenoxybutyrate (**2b**); yield 75% [3.95 g **2b** starting from 3.00 g *N*-(4-hydroxyphenyl)acetamide], white crystals, mp 88-90 °C (ethyl acetate); [Found: C, 63.56; H, 7.10; N, 5.34%. $C_{14}H_{19}NO_4$ (265.13) requires: C, 63.38; H, 7.22; N, 5.28%]; R_f (CHCl$_3$/MeOH 5:0.5 v/v) 0.51. $\nu_{max.}$ (KBr) 3325 (m), 2992 (w), 2944 (w), 2914 (w), 2874 (w), 1730 (s), 1659 (s), 1533 (s), 1513 (m), 1409 (m), 1377 (m), 1319 (m), 1266 (m), 1249 (m), 1179 (s), 1101 (w), 1055 (m), 1032 (w), 965 (m), 943 (w), 828 (m), 603 (w) cm^{-1}. ^{1}H NMR (400 MHz, DMSO-d_6, 298 K) δ_H 1.16 (3 H, t, $^3J_{H,H}$=7.2 Hz, CH$_2$CH_3), 1.93 (2 H, tt app. qv., $^3J_{H,H}$=6.8 Hz, β-CH$_2$), 1.99 (3 H, s, CH$_3$), 2.43 (2 H, t, $^3J_{H,H}$=6.0 Hz, α-CH$_2$), 3.92 (2 H, t, $^3J_{H,H}$=6.2 Hz, γ-CH$_2$), 4.05 (2 H, q, $^3J_{H,H}$=7.2 Hz, CH_2CH$_3$), 6.83 (2 H, d, $^3J_{H,H}$=9.2 Hz, H-3, -5, Ar), 7.45 (2 H, d, $^3J_{H,H}$=8.8 Hz, H-2, -6, Ar), 9.79 (1 H, s, NH) ppm. ^{13}C NMR in J_{mod} (100 MHz, DMSO-d_6, 298 K) δ_C 14.2 (CH$_2$CH$_3$), 23.9 (CH$_3$), 24.4 (β-CH$_2$), 30.3 (α-CH$_2$), 60.0 (γ-CH$_2$), 66.7 (CH$_2$CH$_3$), 114.5 (C-3, -5, Ar), 120.6 (C-2, -6, Ar), 132.6 (C-4, Ar), 154.3 (C-1, Ar), 167.9 (NH-CO), 172.7 (COO) ppm. GC-MS (MeOH) *m*/*z* (rel. int. %) 265.1 [M$^+$] (5).

Typical procedure for acidolysis. Preparation of compound **3b**. Ethyl 4-(4-*N*-acetylamino)phenoxybutyrate **2b** (3.95 g, 14.90 mmol) was added to aq. concd. 37% HCl soln. (86 mL solution, 1028.10 mmol HCl) and the reaction mixture was refluxed for 2 h. The resulted white suspension was cooled at 0 °C for 24 h, filtered off and washed with anh. THF to afford 2.45 g pure compound **3b** (71% yield with respect to **2b**) as white crystals.

(4-Aminophenoxy)acetic acid hydrochloride (**3a**); yield 92% (5.31 g **3a** starting from 6.70 g **2a**), beige powder, mp 219.6-220.9 °C (aq. HCl) (Lit. [8a]: 224-226 °C); [Found: C, 47.51; H, 4.64; N, 6.94%. $C_8H_{10}ClNO_3$ (203.03) requires: C, 47.19; H, 4.95; N, 6.88%]; R_f (EtOH 100%) 0.43. $\nu_{max.}$ (KBr) 3101 (s), 3016 (s), 2968 (s), 2850 (s), 2585 (m), 1761 (m), 1736 (s), 1614 (w), 1574 (w), 1500 (s), 1435 (w), 1407 (w), 1309 (w), 1277 (w), 1242 (w), 1178 (s), 1073 (m), 1053 (m), 812 (m), 771 (m), 732 (m), 672 (w), 629 (w) cm^{-1}. ^{1}H NMR (400 MHz, D$_2$O, 298 K) δ_H 4.68 (2 H, s, CH$_2$), 7.00 (2 H, ddd app. dt, $^3J_{H,H}$=9.6 Hz, $^4J_{H,H}$=$^5J_{H,H}$= 2.8 Hz, H-3, -5, Ar), 7.29 (2 H, ddd app. dt, $^3J_{H,H}$=9.7 Hz, $^4J_{H,H}$=$^5J_{H,H}$= 2.8 Hz, H-2, -6, Ar) ppm. ^{13}C-RMN in J_{mod} (100 MHz, D$_2$O, 298 K) δ_C 65.0 (CH$_2$), 115.8 (C-3, -5, Ar), 123.4 (C-4, Ar) 124.4 (C-2, -6, Ar), 157.3 (C-1, Ar), 173.1 (C=O) ppm. GC-MS (MeOH) *m*/*z* (rel. int. %) 169 [M, - HCl, + CH$_3$] (24).

4-(4-Aminophenoxy)butyric acid hydrochloride (**3b**); yield 71% (2.45 g **3b** starting from 3.95 g **2b**), white crystals, mp 191-193 °C (aq. HCl); [Found: C, 52.06; H, 6.15; N, 5.96%. $C_{10}H_{14}ClNO_3$ (231.07) requires: C, 51.84;

H, 6.09; N, 6.05%]; R_f (ligroin/acetone 1:1 v/v) 0.5. $\nu_{max.}$ (KBr) 3119 (m), 3026 (s), 2918 (s), 2868 (s), 2604 (w), 2559 (w), 1734 (s), 1616 (m), 1565 (m), 1503 (s), 1465 (m), 1440 (w), 1406 (m), 1378 (w), 1345 (w), 1261 (s), 1172 (s), 1118 (w), 1050 (m), 943 (m), 840 (m), 814 (m), 768 (w), 645 (w) cm^{-1}. ^{1}H NMR (400 MHz, D_2O, 298 K) δ_H 1.96 (2 H, tt app. qv., $^3J_{H,H}$=6.7 Hz, β-CH_2), 2.43 (2 H, t, $^3J_{H,H}$=7.0 Hz, α-CH_2), 3.99 (2 H, t, $^3J_{H,H}$=6.0 Hz, γ-CH_2), 6.97 (2 H, ddd app. dt, $^3J_{H,H}$=9.6 Hz, $^4J_{H,H}$=$^5J_{H,H}$= 3.1 Hz, H-3, -5, Ar), 7.26 (2 H, ddd app. dt, $^3J_{H,H}$=9.6 Hz, $^4J_{H,H}$=$^5J_{H,H}$=3.1 Hz, H-2, -6, Ar) ppm. ^{13}C NMR in J_{mod} (100 MHz, D_2O, 298 K) δ_C 23.8 (β-CH_2), 30.5 (α-CH_2), 67.6 (γ-CH_2), 115.8 (C-3, -5, Ar), 122.6 (C-4, Ar), 124.2 (C-2, -6, Ar), 158.3 (C-1, Ar), 178.1 (C=O) ppm. GC-MS (MeOH) m/z (rel. int. %) 209 [M -HCl, + CH_3] (20).

Typical procedure for isolation of (4-aminophenoxy)alkanoic acids as free amine. Isolation of compound 1b. 4-(4-aminophenoxy)butyric acid hydrochloride **3b** (2.45 g, 10.60 mmol) was dissolved in distilled water (20 mL). To this solution, anhyd. K_2CO_3 (0.73 g, 5.30 mmol) was added portionwise. The resulted suspension was stirred for 1 h at r.t. then filtered off to give 1.51 g pure compound **1b** (73% yield with respect to **3b**) as a white powder.

(4-Aminophenoxy)acetic acid (**1a**); yield 81% (0.20 g **1a** starting from 0.30 g **3a**), white powder, mp 214 °C (dec.) (Lit. 312 ºC [2], 220 ºC [3], 215-220 ºC [7]); [Found: C, 57.58; H, 5.88; N, 8.25%. $C_8H_9NO_3$ (167.06) requires: C, 57.48; H, 5.43; N, 8.38%]; R_f (EtOH 100%) 0.54. $\nu_{max.}$ (KBr) 2931 (m), 2870 (m), 2630 (m), 2100 (w), 1619 (m), 1592 (m), 1544 (m), 1511 (s), 1411 (m), 1338 (w), 1301 (w), 1258 (m), 1227 (m), 1182 (w), 1057 (m), 916 (w), 822 (m), 729 (m), 596 (w), 578 (w) cm^{-1}. ^{1}H NMR (600 MHz, DMSO-d_6, 298 K) δ_H 4.47 (2 H, s, CH_2), 5.51 (3 H, br s, NH_2 ⇆ COOH exchangeable), 6.52 (2 H, d, $^3J_{H,H}$=9.0 Hz, H-3, -5, Ar), 6.64 (2 H, d, $^3J_{H,H}$=9.0 Hz, H-2, -6, Ar) ppm. ^{13}C-RMN in J_{mod} (150 MHz, DMSO-d_6, 298 K) δ_C 65.5 (CH_2), 115.2 (C-3, -5, Ar), 115.5 (C-2, -6, Ar), 142.5 (C-4, Ar), 149.5 (C-1, Ar), 170.9 (C=O) ppm. GC-MS (MeOH) m/z (rel. int. %) 109 [M+1, - CO_2, - CH_3] (100).

4-(4-Aminophenoxy)butyric acid (**1b**); yield 73% (1.51 g **1b** starting from 2.45 g **3b**), white powder, mp 143-145 °C (H_2O) (Lit. 145.5-146 ºC [4]).; [Found: C, 61.75; H, 6.48; N, 6.95%. $C_{10}H_{13}NO_3$ (195.09) requires: C, 61.53; H, 6.71; N, 7.18;%]; R_f (ligroin/acetone 1:1 v/v) 0.5. $\nu_{max.}$ (KBr) 2959 (m), 2872 (m), 2590 (m), 2148 (w), 1623 (m), 1601 (m), 1519 (s), 1507 (s), 1405 (m), 1387 (w), 1302 (m), 1216 (w), 1174 (w), 1077 (w), 1050 (w), 1024 (w), 832 (m), 810 (w), 766 (w), 663 (w) cm^{-1}. ^{1}H NMR (600 MHz, DMSO-d_6, 298 K) δ_H 1.86 (2 H, tt app. qv., $^3J_{H,H}$=6.9 Hz, β-CH_2), 2.35 (2 H, t, $^3J_{H,H}$=7.2 Hz, α-CH_2), 3.81 (2 H, t, $^3J_{H,H}$=6.3 Hz, γ-CH_2), 6.51 (2 H, d, $^3J_{H,H}$=9.0 Hz, H-3, -5, Ar),

6.64 (2 H, d, $^3J_{H,H}$=8.4 Hz, H-2, -6, Ar) ppm. ^{13}C NMR in J_{mod} (100 MHz, DMSO-d_6, 298 K) δ_C 24.6 (β-CH$_2$), 30.3 (α-CH$_2$), 67.1 (γ-CH$_2$), 115.1 (C-3, -5, Ar), 115.5 (C-2, -6, Ar), 142.3 (C-4, Ar), 150.0 (C-1, Ar), 174.4 (C=O) ppm. GC-MS (MeOH) m/z (rel. int. %) 195 [M$^+$] (10).

ACKNOWLEDGMENT

REFERENCES

1. J. Fritzsche, *J. Prakt. Chem.* (Leipzig), **1879**, *2*, 283
2. J. Kym, *J. Prakt. Chem.* (Leipzig), **1897**, *2*, 122
3. W.A. Jacobs, M. Heidelberger, *J. Am. Chem. Soc.*, **1917**, *39*, 1435
4. W.A. Jacobs, M. Heidelberger, *J. Am. Chem. Soc.*, **1917**, *39*, 2188
5. P.M. Mistry, R. Bradbury, US Pat. 6 559 292/06.05.**2003**
6. R. Kumar, S. Jain, N. Jain, *Der Pharma Chem.*, **2013**, *5*, 73
7. D.J. Abraham, P.E. Kennedy, A.S. Mehanna, D.C. Patwa, F.L. Williams, *J. Med. Chem.*, **1984**, *27*, 967
8. a) R.S. Bezwada, US Pat. 8 143 325 B2/03.27.**2012**; b) K. Hidaka, T. Kimura, A.J. Ruben, T. Uemura, M. Kamiya, A. Kiso, T. Okamoto, Y. Tsuchiya, Y. Hayashi, E. Freire, Y. Kiso, *Bioorg. Med. Chem.*, **2008**, *16*, 10049–10060
9. a) V.A. Barashkin, *J. Org. Chem. USSR* (English Translation), **1970**, *6*, 2274; *Zh. Org. Khim.*, **1970**, *6*, 2266; b) M. Nutiu, R. Bacaloglu, M. Darabantu, Z. Pap *Scientific and Technical Bulletin of Polytechnic Institute "Traian Vuia" Timisoara, Chemistry Series,* **1981**, *26*, 79; c) W. Cheng, S. Wong, A.M. Almeida, D.B. Rozema, A.V. Blokhin, J.C. Carlson, US Pat. 2015/45573 A1/02.12. **2015**; d) X. Zhang, B. Bao, X. Yu, L. Tong, Y. Luo, Q, Huang, M. Su, L. Sheng, J. Li, H. Zhu, B. Yang, X. Zhang, Y. Chen, W. Lu, *Bioorg. Med. Chem.*, **2013**, *21*, 6981
10. Y. Katsura, T. Tomishi, Y. Inoue, K. Sakane, Y. Matsumoto, C. Morinaga, H. Ishikawa, H. Takasugi, *J. Med. Chem.*, **2000**, *43,* 3315
11. B.D. Palmer, J.B. Smaill, G.W. Rewcastle, E.M. Dobrusin, A. Kraker, C.W. Moore, R.W. Steinkampf, W. Denny, *Bioorg. Med. Chem. Lett.*, **2005**, *15*, 1931

SILICA GEL MODIFIED WITH FUNCTIONALIZED CALIXARENES. PREPARATION AND CHARACTERIZATION

RAUL RANETE[a], PETRONELA M. PETRAR[a], RALUCA ŞEPTELEAN[a], IOANA PERHAIŢĂ[b], GABRIELA NEMEŞ[a*]

ABSTRACT. This work presents the synthesis and characterization of novel products obtained by the chemical bonding of lower rim substituted calix[4]- and calix[8]arene macrocycles to silica gel surfaces modified with aminopropyl chains. The products were investigated by thermogravimetric analysis (DTG, EGA), surface area analysis (BET), as well as by electron microscopy (TEM, SEM).

Keywords: functionalized silica gel, calixarenes, thermal analyses, electronic microscopy.

INTRODUCTION

Calix[n]arenes (n = 4 – 20) are phenolic metacyclophanes obtained by the condensation of para- substituted phenol with formaldehyde or paraformaldehyde [1] and they can be functionalized with organic groups by esterification, etherification, sulphonation, nitration or alkylation reactions [2, 3, 4, 5] at the lower rim (the OH phenol groups) or the upper rim (the para position of the phenyl rings). The cavity formed by the phenolic rings and the possibility of functionalizing the calixarenic framework with various organic groups, make these organic macrocycles very interesting for a wide range of applications including biomedical research [6], chromatography [7, 8], selective metal extraction [9, 10], electrochemical and luminescent sensors [11], catalysis [12], and selective gas adsorption [13]. In recent years, more emphasis was put on the immobilization of calixarenes on silica gel substrates, thus improving their possible application in separation sciences [14,15]. One of the most accessible ways to bond calixarene macrocycles to the SiO_2 layer is through alcoxysilanes of the type $X-(CH_2)_n-Si(OR')_3$ [16,17], where X is a functional group that allows coupling reactions with the calixarenic system, usually at the lower rim.

---

[a] *Facultatea de Chimie şi Inginerie Chimică, Universitatea Babeş-Bolyai Cluj-Napoca, Str. Arany Janos, nr 11, RO-400028.*
[b] *Institutul de Cercetări în Chimie Raluca Ripan, Str. Fântânele, nr. 30, Cluj-Napoca RO-400294*
[*] *Corresponding author: sgabi@chem.ubbcluj.ro*

Following this trend, we have studied the preparation of modified silica gel, using 3-aminopropyl-tri-methoxy-silane (APTMS) as a spacer, in order to obtain new products with possible applications in ion metal separation. The reactions were performed in anhydrous conditions by the nucleophilic attack of hydroxyl groups from the silica gel surface at the APTMS spacer, with the elimination of methanol [18].

RESULTS AND DISCUSSION

New modified silica gel with 3-aminopropyl-tri-methoxy-silane (APTMS) and the compound obtained by attaching of this system to the acetylated p-tertbutyl calix[n]arene (n = 4, 8) were synthesized and investigated by specific physico-chemical methods.

A first stage in the synthesis of functionalized calixarenes linked to the silica gel substrate through an aminopropyl spacer requires the preparation of lower rim substituted calixarenes. The starting p-tertbutyl calix[n]arenes (n = 4, 8) and their acetyl derivatives were synthesized according to the methods described in the literature [1,19,20] (Scheme 1, compounds **1**, **2**).
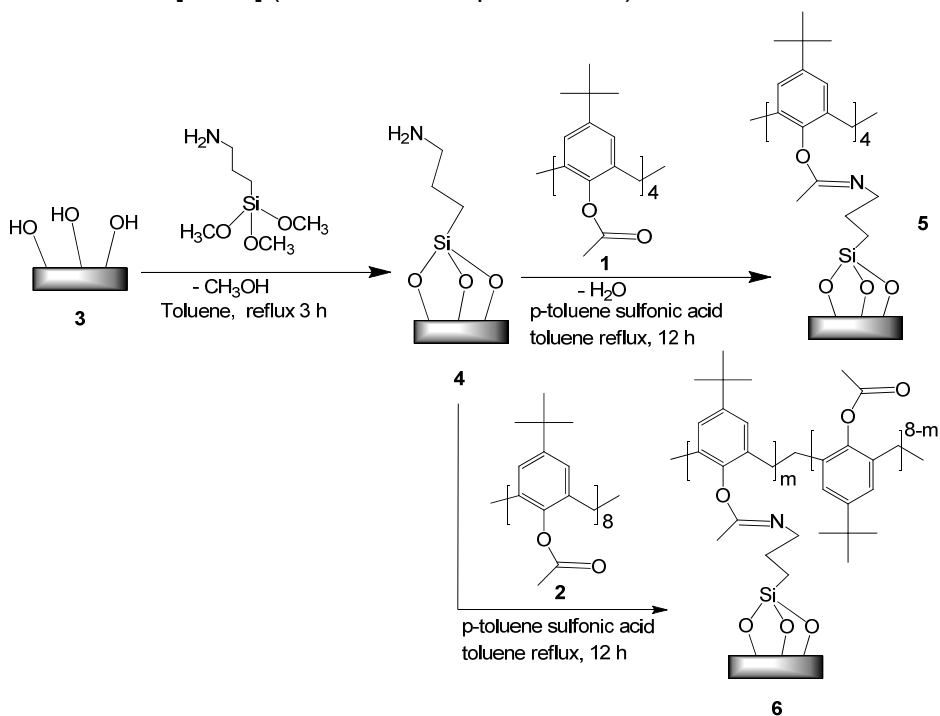
Scheme 1

The APTMS-chemosorbed silica gel **4** was prepared starting from pre-activated silica gel by heating it at 600 °C under reduced pressure (10^{-6} bar) for an hour and products 5 and 6 was performed by a modified literature method [21].

The acetyl functionalized calixarene precursors **1** and **2** were characterized by ^{1}H-NMR and IR spectroscopy, all the obtained data being in agreement with published results [1,19,20]. The new products **5** and **6** were characterized by thermogravimetric methods, surface electron microscopy (SEM), transmission electron microscopy (TEM) and Brunauer-Emmett-Teller surface analysis (BET).

The binding of the functionalized calixarenes to the silica surface, with the formation of products **5** and **6** (Scheme 1), was investigated using thermal analysis and electron microscopy (SEM and TEM). The results suggest that the functionalized calixarenic systems **1** and **2** are chemically bonded to the ATPMS modified silica, most likely by means of a C=N bond.

Thermal analysis

Thermal analysis for the new products has been carried out. The thermograms were also recorded for the heat-activated silica gel **3** and the APTMS-modified silica **4**, for comparison. After the treatment of the modified silica **4** with p-tertbutyl calix[4]arene tetra-acetate and the calix[8]arene analogue, the derivative thermogravimetric plots (DTG) differ sharply from those of the calixarene-free materials, as shown in Figure 1 and Table 1.

Table 1. Thermogravimetric analysis data for products 1, 2, 4, 5, and 6.

Product	Quantity (mg)	Thermogravimetric (TG) and (DTG) analysis			
		Total mass loss (Δm_T)	Temperature range	Partial mass loss (Δm_p)	T_{max} (°C)
1	36.5506	86.00 %	25 -260 °C	6.23 %	177
			260 -480 °C	63.48 %	413
			480 -1100 °C	16.30 %	506
2	7.9157	87.26 %	25 -230 °C	4.37%	90
			230 -480 °C	60.12 %	402
			480 -1100 °C	22.81 %	482
4	40.0067	17.15 %	25 -140 °C	3.94 %	70
			140 -800 °C	11.01 %	464
			800 -1100 °C	2.21 %	1008

Product	Quantity (mg)	Thermogravimetric (TG) and (DTG) analysis			
		Total mass loss (Δm_T)	Temperature range	Partial mass loss (Δm_P)	T_{max} (°C)
5	50.8478	36.97 %	25 -160 °C	3.24 %	64
			160 -430 °C	24.51 %	368
			430 -790 °C	7.05 %	458
			790-1100 °C	2.32 %	796
6	26.9450	37.02 %	25 -140 °C	3.39 %	68
			140 -350 °C	17.83 %	279
			350-450 °C	8.83 %	377
			450 – 794 °C	5.18 %	449
			794-1100 °C	1.96 %	815

The thermal analysis data for product **5** indicates that the acetylated p-tertbutyl calix[4]arene is bonded to the silica surface through the APTMS spacer (Figure 1c). The mass loss interval at 160 – 430 °C (24.5 %) is correlated with the elimination of the macrocycle from the system. Another significant mass loss (7 %), between 430 and 600 °C, can be attributed to the decomposition of the aminopropylic chain tethered to the surface.

For derivative **6**, the significantly higher total mass loss (Table 1) indicates the bonding of the organic macrocycles within the new material.

The recorded DTG curve for APTMS-modified silica gel shows a mass loss in the 360-450 °C range, attributed to the decomposition of the APTMS (Figure 1b). The full thermogravimetric data recorded for products **1** – **6** are presented in Table 1.

The comparison of the two DTG recorded for **5** and **6** suggests a stronger bonding of the acetylated calix[4]arene (Figure 1c) on the inorganic surface than in the case of the calix[8]arene analogue (Figure 1d), as the first significant mass loss occurs at higher temperature values for product **5** (Table 1). This can be explained by the preference of calix[4]arenes for a basket geometry, which means that all the acetyl groups in derivative **1** are on the same side of the macrocycle cone [22]. However, larger calixarenes (n = 5, 6, 8), are conformationally mobile, and the cone conformation is almost never preferred. Therefore, it can be assumed that the acetylated calix[8]arene would adopt a conformation allowing fewer connectivity points to the APTMS-modified silica gel via chemical bonding, while physical interactions between the calixarenic unit and the modified substrates are still possible. The coupling of the calix[4]arene to the APTMS-modified silica gel surface through all its connective points can be correlated to the higher decomposition temperature.
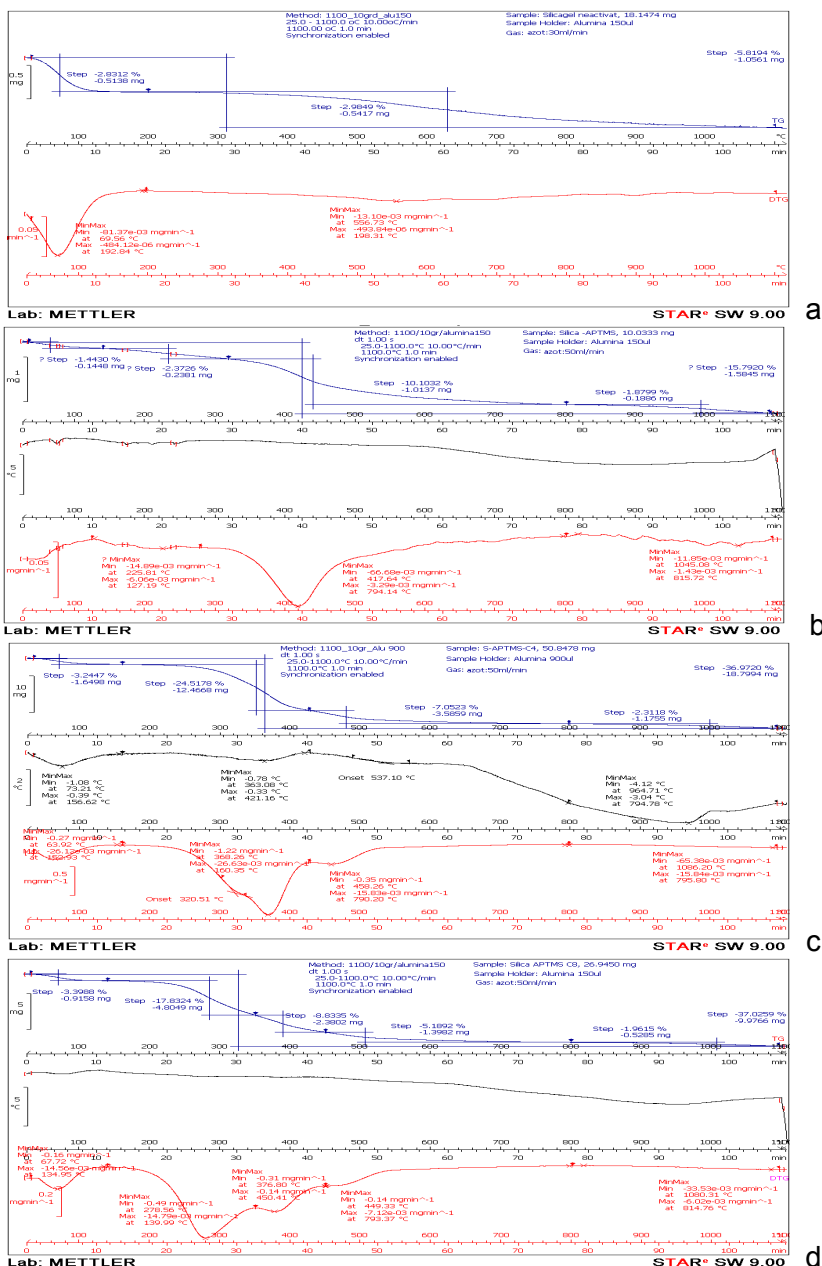
Figure 1. TG and DTG plots for (a) silica gel, (b) APTMS-modified silica gel **4**, (c) silica gel-APTMS-acetyl-p-tertbutyl calix[4]arene **5**, (d) silica gel-APTMS-acetyl-p-tertbutyl calix[8]arene **6**.

Complementary analysis of the new products **5** and **6** by EGA correlates the decomposition of the organic layer to the TG-DTG data. Figure 2 details the recorded EGA data for product **5** (silica gel-APTMS-acetylated calix[4]arene) compared to the starting acetylated calix[4]arene and the APTMS-modified silica gel.

a

b

c
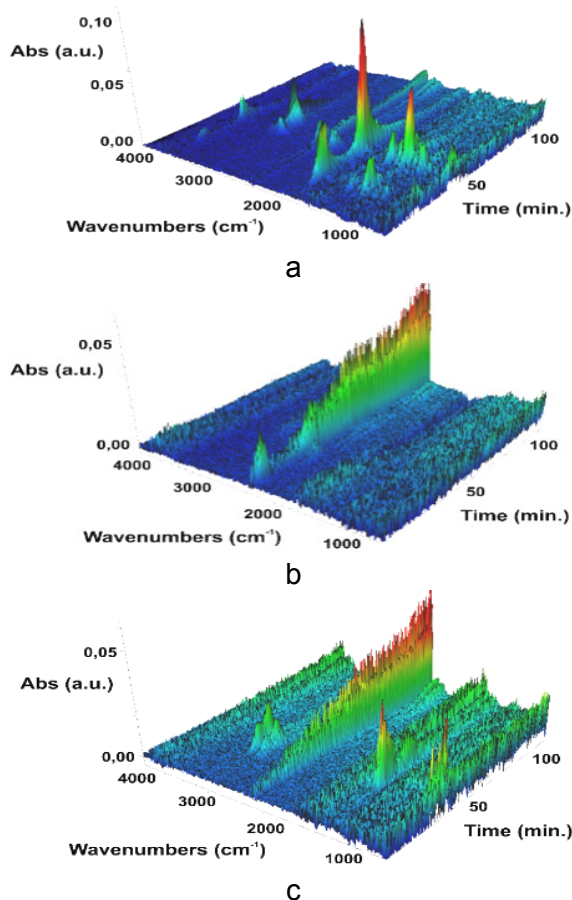
Figure 2. EGA 3D plots for (a) tetra-acetyl derivative of p-tertbutyl calix[4]arene **1**, (b) functionalized silica gel with APTMS **4**, (c) product **5**.

The pattern in the EGA - 3D plot recorded for the decomposition of compound **5** (Figure 2c) indicates the presence of both a calixarene moiety and APTMS fragments, which suggests that the calixarene system is bonded to the inorganic substrate. Similar results were obtained for the calix[8]arene-containing material.

Brunauer–Emmett–Teller surface area analysis

The new products and the starting materials were also investigated through BET surface analysis. As expected, the pore volume of the APTMS functionalized silica gel is much lower than that of the unfunctionalized silica gel due to the covering of the pores with the organic phase (the pore volume decreases from 0.83 cm^3/g to 0.48 cm^3/g). Furthermore, the pore volume in the case of material **5** differs significantly from that obtained for **6**. The larger pore volume of silica gel-APTMS-acetyl-calix[8]arene (0.15 cm^3/g) by comparison with the silica gel-APTMS-acetyl-calix[4]arene system (0.03 cm^3/g) can be explained by a larger cavity of the calix[8] derivative together with a better covering of the silica surfacein the case of **5** (Figure 3).

The pore sizes are relatively small and with a narrow distribution in the meso-porous range (20 - 500 Å). A reduction in pore size was noticed, from an interval of about 50-100 Å determined for the unmodified silica gel to about 35-70 Å for the final product silica gel-APTMS- acetyl calix[8]arene (**6**), (Figure 3). The same pore size interval was determined for the product obtained with the calix[4]arene tetra-acetate (**5**).
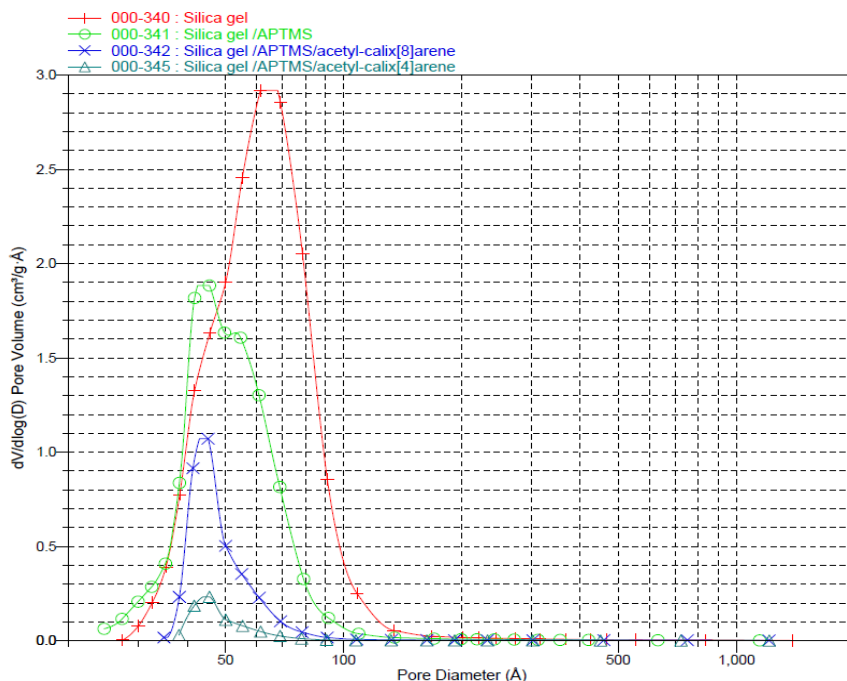
Figure 3. BJH desorbtion pore volume distribution curve according to pore diameter for silica gel (red), silica gel-APTMS **4** (green), silica gel-APTMS-acetyl-calix[4]arene **5** (dark green) and silica gel-APTMS-acetyl-calix[8]arene **6** (blue).

The BET analysis clearly shows that a decrease in pore volume is noticeable after the treatment of the inorganic substrate with APTMS and the calixarene macrocycles, proving that the organic layer covers the silica surface. The BET surface area decreases from 462.20 m²/g for the silica gel to 301.47 m²/g for the APTMS modified silica gel and 63.99 m²/g for product **6** and 11.75 m²/g for product **5** respectively.

Scanning electron and transmission electron microscopy investigations

SEM images suggest that in both cases the lower rim functionalized calix[n]arenes have been deposited on the APTMS-modified silica gel surface (Figure 4). The images show a relative smooth surface for the unmodified silica gel (Figure 4a), when compared with the products containing either APTMS or the calix[4]arene macrocycle. The APTMS covering of the silica surface does not seem to be uniform (Figure 4b). The same can be told about product **5**, for which the covering of the inorganic substrate is discontinuous. It can be hypothesized that the covering occurred only at the regions on the surfaces already modified with the amino-propyl spacer. By contrast, a smoother surface is observed in the case of product **6**. This, together with the thermal analysis data indicate that the surface is covered uniformly with an organic layer of calix[8]arene.
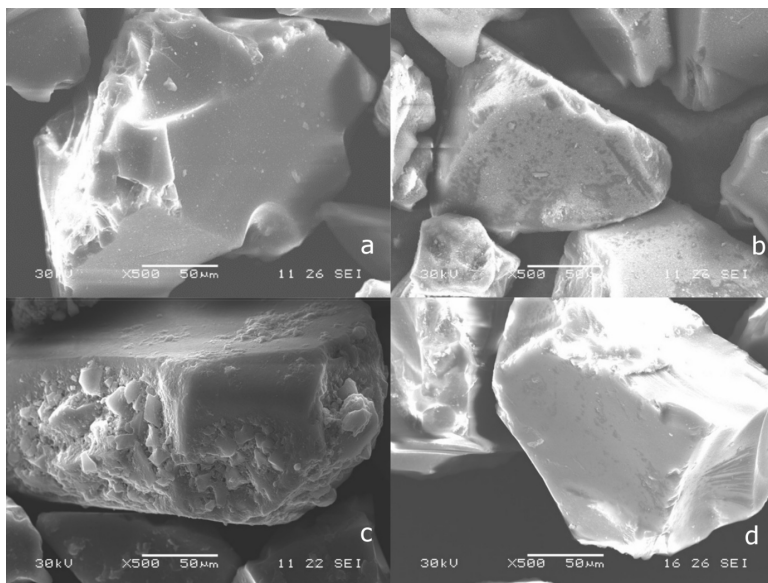
Figure 4. SEM images of (a) silicagel, (b) silica gel-APTMS **4**, (c) silica gel-APTMS-acetyl-calix[4]arene **5** and (d) silica gel-APTMS-acetyl-calix[8]arene **6**.

The new obtained products were also investigated by TEM. Images of the starting activated, unmodified silica gel as well as of the APTMS-modified silica gel are presented for comparison (Figure 5a and b).
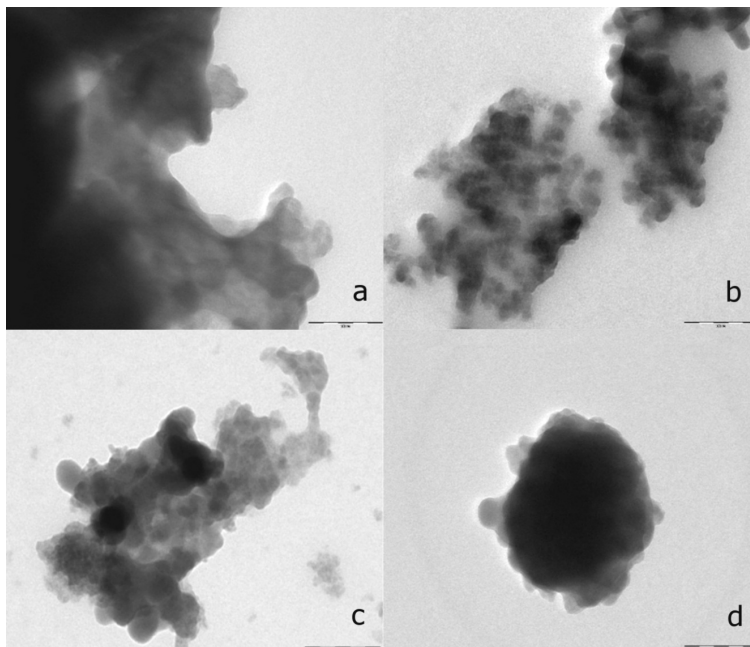
Figure 5. TEM images (Scale: 100 nm) of (a) silica gel, (b) silica gel-APTMS **4**, silica gel-APTMS-acetyl-calix[4]arene **5** and (d) silica gel-APTMS-acetyl-calix[8]arene **6**.

The TEM images of silica gel-APTMS-acetyl-calix[4] arene **5** (Figure 5c) and silica gel-APTMS- acetyl- calix[8]arene **6** (Figure 5d) show that in the case of product **6**, the silica particles aggregate in a higher degree by comparison to the analogue product **5**. This is consistent with the thermogravimetry data suggesting the possibility of calix[8]arene - based material to contain multi-directional bonds of the organic layer to the silica particles while a macrocycle of acetylated calix[4]arene would bond to only one particle.

CONCLUSIONS

This work presents the successful binding of functionalized calix[n]arene (n = 4, 8) derivatives to silica gel by means of 3-aminopropyl trimethoxysilane. The silica substrate was thermally and chemically activated with 3-aminopropyl

trimethoxysilane according to literature procedures. The new silica gel-APTMS-acetyl-calix[n]arene systems were characterized by specific methods including DTG, EGA, SEM and TEM, which prove the chemical bonding of the calixarenic macrocycles to the inorganic substrate.

EXPERIMENTAL

All the chemicals were used as purchased from chemical suppliers (Merck, Sigma Aldrich), without any further purification. All reactions have been carried out under argon.

The ^{1}H NMR spectra were recorded on a Bruker Avance 400 MHz spectrometer in CDCl$_3$, with TMS as reference at a frequency of 400.13 MHz.

Thermogravimetric analysis (TGA) was performed using a Mettler Toledo TGA/SDTA851e Thermal Analysis System. All the experiments were done in an alumina crucible (900 μl), with a heating speed of 10°C/min in an interval ranging from 25 to 1100 °C. The measurements were carried out in a nitrogen atmosphere with a flow of 50 ml/min.

The evolved gas analysis (EGA) was performed on a Thermo Scientific Nicolet 6700 FT-IR spectrometer equipped with a TG module, operating at 280 °C. Surface area measurements were done on a Tristar II 3020 – Micromeritics (nitrogen adsorption at 77 K, sample decontamination at 150 °C for 24 h, under nitrogen flow).The scanning electron microscopy experiments were performed on a Jeol JSM5510LV (Jeol, Japan) –3.5 nm rezolution, accelerating voltage 0.5-30 kV system. The transmission electron microscopy images were obtained with a Hitachi Automatic TEM H7650 system (accelerating voltage 40-120 kV, zoom 200x-600000x).

Preparation of APTMS-modified silica gel 4. The silica gel was pre-activated by heating it at 600 °C under reduced pressure (10^{-6} bar) for an hour [23]. After the system returned to room temperature, 3-aminopropyl-trimethoxysilane (1.8 mmoles, 0.33 ml) in 20 ml of toluene was added under inert gas and the system was heated to reflux for 3 h. The obtained solid **4** was washed with toluene for 12 h in a Soxhlet extractor.

Synthesis of products 5 and 6. Product **5** was obtained from 2 g of **4**, 0.33 g of **1** and 0.017 g anhydrous p-toluene sulphonic acid in 100 ml of toluene. The mixture was refluxed for 12 h and the resulting solid was then washed with toluene for 12 h in a Soxhlet extractor. Product **6** was obtained in similar conditions from 0.33 g of p-tertbutyl-calix[8]arene octa-acetate **2**.

ACKNOWLEDGMENTS

REFERENCES

[1]. C.D. Gutsche, J.F. Stoddart, Calixarenes Revisited, The Royal Society of Chemistry, Cambridge, **1998**.

[2]. B. Dhawan, S.-I. Chen, C.D. Gutsche, *Macromolecular Chemistry and Physics*, **1997**, *188* (5), 921.

[3]. A. Saponar, E.-J.Popovici, N. Popovici, E. Bica, G. Nemes, P. Petrar, I. Silaghi-Dumitrescu, *Revista de Chimie*, **2009**, *60* (3), 278.

[4]. A. Saponar, E-J. Popovici, R. Grecu, I. Silaghi-Dumitrescu, N. Popovici, *Studia UBB Chemia*, **2009**, *44* (4), 203.

[5]. S. Saying, M. Yilmaz, M. Tavasli, *Tetrahedron*, **2011**, *67*, 3743.

[6]. R.V. Rodik, V.I. Boyko, V.I. Kalcheno, *Current Medicinal Chemistry*, **2009**, *16* (13), 1630.

[7]. B. Mokhtari, K. Pourabdollah, N. Dalali, *Chromatographia*, **2011**, *73* (9-10), 829.

[8]. M. Sliwka-Kaszynka, *Critical Reviews in Analytical Chemistry*, **2007**, *37* (3), 211.

[9]. A. Saponar, E.-J. Popovici, R. Septelean, E. Bica, I. Perhaita, G. Nemes, *Revista de Chimie*, **2013**, *64* (1), 55.

[10]. A. Saponar, E.-J. Popovici, G. Nemes, N. Popovici, I. Perhaita, E. Bica, I. Silaghi-Dumitrescu, *Revista de Chimie,* **2012**, *63* (3), 249.

[11]. J.S. Kim, D.T. Quang, *Chemical Reviews*, **2007**, *107* (9), 3780.

[12]. Y. Kurusu, D.C. Neckers, *Journal of Organic Chemistry*, **1991**, *56* (6), 1981.

[13]. E. Soto-Cantu, R. Cueto, J. Koch, P.S. Russo, *Langmuir*, **2012**, *28* (13), 5562.

[14]. S. Sayin, F. Ozcan, M. Yilmaz, *Journal of Hazardous Materials*, **2010**, *178* (1 - 3), 312.

[15]. C. Ding, K. Qu, Y. Li, K. Hu, H. Liu, B. Ye, Y. Wu, S. Zhang, J*ournal of Chromatography A*, **2007**, *1170* (1 - 2), 73.

[16]. K. Miyatake, O. Ohama, Y. Kawahara, A. Urano, A. Kimura, *SEI Technical Review,* **2007**, 65.

[17]. K.C. Vrancken, L. De Coster, P.V. Der Voort, P.J. Grobet, E.F. Vansant, *Journal of Colloid and Interface Science*, **1995**, *170* (1), 71.

[18]. B. Arkles, *CHEMTECH 7,* **1977**, 766.

[19]. G.D. Andreetti, V. Böhmer, J.G. Jordon, M. Tabatabai, F. Ugozzoli, W. Vogt, A. Wolff, *Journal of Organic Chemistry,* **1993**, *58*, 4023.

[20]. C.D. Gutsche, L.G. Lin, *Tetrahedron*, **1986**, *42* (6), 1633.

[21]. V. Ivanovskia, M. Bukleskia, M. Madalska, E. Hey-Hawkins, Vibrational Spectroscopy, **2013**, *69*, 57.
[22]. C.D. Gutsche, B. Dhawan, J.A. Levine, K.H. No, L.J. Bauer, **1983**, *39* (3), 409.
[23]. V. Ivanovskia, M. Bukleskia, M. Madalska, E. Hey-Hawkins, *Vibrational Spectroscopy*, **2013**, *69*, 57.

INFLUENCE OF GRAIN AND CRYSTALLITE SIZE ON THE GIBBSITE TO BOEHMITE THERMAL TRANSFORMATION

VIKTOR ZSOLT BARANYAI[a,b], FERENC KRISTÁLY[c,*], ISTVÁN SZŰCS[a]

ABSTRACT. Thermal decomposition processes of three different samples of hydrated alumina: Bayer precipitated size fractioned, Bayer precipitated ground and fine precipitated, were studied. These were investigated with special regard to evolution of boehmite. The original samples contained 75-85 wt% of gibbsite, while remaining material with gibbsite-like Al_2O_3-H_2O ratio did not show long range order crystallinity. Decomposition reactions were observed by thermal analysis and reaction products were investigated by powder X-ray diffraction. Grain sizes were determined by laser diffraction and morphological changes of grains were observed by scanning electron microscopy. Boehmite formation is influenced mainly by grain and crystallite sizes of starting materials, while degree of crystallinity is of less importance. Transformation of gibbsite to boehmite was most pronounced in the case of coarse grains, nevertheless in fine particles boehmite evolution seemed retarded.

Keywords: gibbsite decomposition, boehmite evolution, nanocrystalline boehmite, Rietveld-refinement

INTRODUCTION

Gibbsite (γ–Al(OH)$_3$), end-product of the Bayer cycle is essential raw material of calcined alumina (Al_2O_3). Utilization of aluminum oxide in ceramic technologies has long history [1], however beyond the prevalent technologies, application of gibbsite or boehmite in ceramic green bodies, green fibers has appeared for increasing the final porosity of sintered material [2-4] or stabilizing of alumina foams [5, 6]. In this case the chemically bound water content of raw material is removed during sintering.

[a] *University of Miskolc, Department of Combustion Technology and Thermal Energy, H-3515 Miskolc-Egyetemváros, Hungary*

[b] *Bay Zoltán Nonprofit Ltd. for Applied Research, Department of Advanced Materials, H-3519 Miskolc, Iglói út 2.*

[c] *University of Miskolc, Institute of Mineralogy and Geology, H-3515 Miskolc-Egyetemváros, Hungary*

[*] *Corresponding author: kristalyf@gmail.com*

The Bayer precipitated particles are agglomerates of single pseudohexagonal plate-like crystallites. The structure and properties of the particles are influenced by the processes during formation: nucleation, agglomeration, crystal growth and attrition [7, 8]. During calcination the wet gibbsite loses its adhesive moisture first, further the bound water (~34 % referring to the dry hydrated material) exits. All of decomposition pathways are closed by the formation of the only thermodynamically stable oxide phase, corundum (α-Al_2O_3) [1]. The decomposition pathway is influenced by the factors of calcination. The major factors are the physicochemical properties of the initial raw (untreated) material (e.g. particle size, shape, substituting elements) and the circumstances of the heat treatment (temperature, heating rate, composition of the atmosphere, pressure) [9, 10].

The thermal decomposition reactions of aluminum-hydroxides has been reported since the middle of 20th century in a row of papers. Figure 1. summarizes the reaction pathways depending on the conditions of thermal treatment and the physical properties of particles. The following decomposition reactions are given for normal atmospheric air pressure. Dehydroxylation of gibbsite begins above the temperature of 200-300 °C. At higher temperatures different amorphous and crystalline alumina phases appear. The last step of all decomposition pathways is the formation of corundum (α-Al_2O_3). Over 200 °C a part of gibbsite loses two moles of H_2O and changes into oxi-hydroxide, as boehmite. Above 300 °C gibbsite decomposes directly into aluminum-oxide. Boehmite loses the remaining one mole of H_2O at 450-550 °C [1]. Decomposition temperatures are influenced by heating rate: the faster the temperature increase, the higher the starting temperature of decomposition is [11, 12].
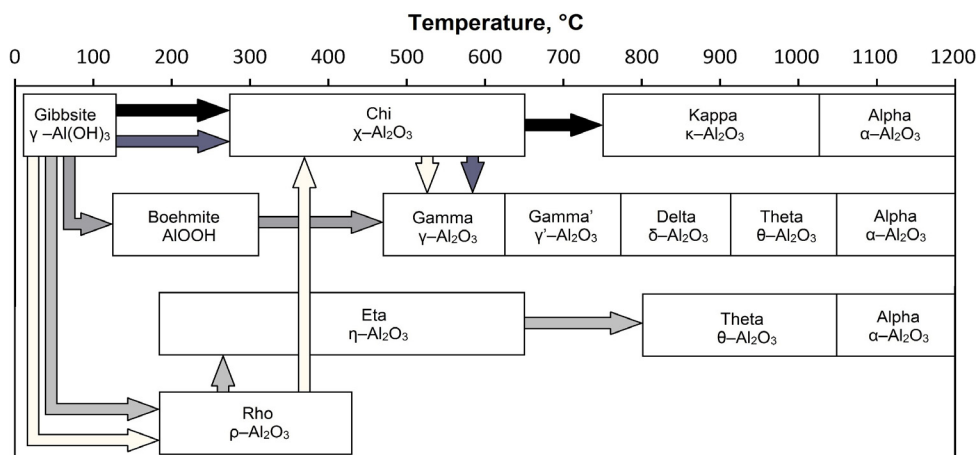
Figure 1. Thermal decomposition pathways of gibbsite, adapted from Perander [10].

Phenomenon of boehmite formation is explained by several authors, in different ways. Conditions causing higher internal steam pressure within the particle (coarse particles, high heating rate, and high concentration of water steam) favor the decomposition via boehmite. With slow heating, fine particles retard the formation of boehmite, favoring the direct decomposition into oxides [13, 14]. These predicates are prevalent in case of heat treatment at normal atmospheric pressure. If the pressure is lower (vacuum) or higher (overpressure) as normal atmospheric pressure, the decomposition processes are different [15-17]. Opposed to the above arguing, Mercury et al. [9] states that gibbsite decomposes to boehmite irrespective of particle size distribution. In case of amorphous material, the decomposition yields oxides, without boehmite formation [9, 18].

Effect of long term grinding of gibbsite is the amorphisation and appearing of gel-like hydroxide phases. The original water content of gibbsite remains invariable or slightly decreases. The product of thermal decomposition of gel-like hydroxides is amorphous oxide which transforms to crystalline form at elevated temperature [19, 20].

Several authors investigated the thermal decomposition processes of long term ground materials, like gibbsite, bayerite and boehmite [21-24].

Physical properties of alumina products applied as adsorbents, catalysts or catalyst carriers are highly influenced by decomposition processes of gibbsite [23, 25, 26]. The accompanying phenomena of dehydroxilation are in number of cases undesired. Ceramics industry utilizes boehmite when large shrinkage and porosity formation must be avoided [27, 28]. Plastics and electronics industries use increasingly boehmite as fire retardant filler, because boehmite is more stable at higher temperatures compared to gibbsite [29]. The above examples prove the necessity of knowledge expansion over gibbsite thermal decomposition processes.

Present study compares thermal decomposition of three aluminum hydroxide materials: Bayer precipitated, fine precipitated, and short term ground. All of the three samples consisted prevailingly of gibbsite. We attempted to find out, how grain and crystallite size influences the thermal decomposition processes, considering the formation of boehmite as intermediate product.

RESULTS AND DISCUSSION

1. Chemical composition and particle size of starting materials

Chemical composition of C and FP samples is shown in Table 1. As expected, only trace amounts of contaminant elements were detected. Loss on ignition values confirm the $Al(OH)_3$ composition of samples. The measured

Na_2O content is normal for these materials, as residual component from the Bayer-process. Altogether, no chemical compounds were observed that would influence the results of thermal behavior.

Particle size distribution of "original Bayer precipitated" material, CU, GU and FPU can be seen in Figure 2. The "original Bayer precipitated" sample has wide distribution of particle diameter, the size of the finest 10 % of particles is below 30 μm, while the coarsest 10 % of particles exceed 120 μm of size. Size fractionation made the mean particle size overrepresented: limits of finest and coarsest 10 % were 52 and 99 μm, respectively. Grinding reduced the median size of original material to 13 μm. Above figures of ground particle diameter are in accordance with the results of Tsuchida et al. [19]. Further milling causes only moderate decrease in particle size, but degrades the crystal structure. FPU sample has shown the finest particle distribution with median diameter at 1.9 μm.

Table 1. Chemical composition of samples

wt%	SiO_2	Al_2O_3	CaO	Na_2O	K_2O	Fe_2O_3	MnO	TiO_2	P_2O_5	L.O.I
C	0.01	65.4	0.01	0.10	0.05	0.03	0.001	n.d.	0.001	34.398
FP	0.02	65.4	0.01	0.13	0.05	0.02	0.001	n.d.	0.001	34.368
ppm	S	Cu	Zn	Pb	As	Ga	Zr	In	Ge	Sr
C	653	30	275	22	n.d	93	n.d.	n.d	n.d.	n.d
FP	468	12	178	24	n.d	91	n.d.	n.d.	n.d.	n.d
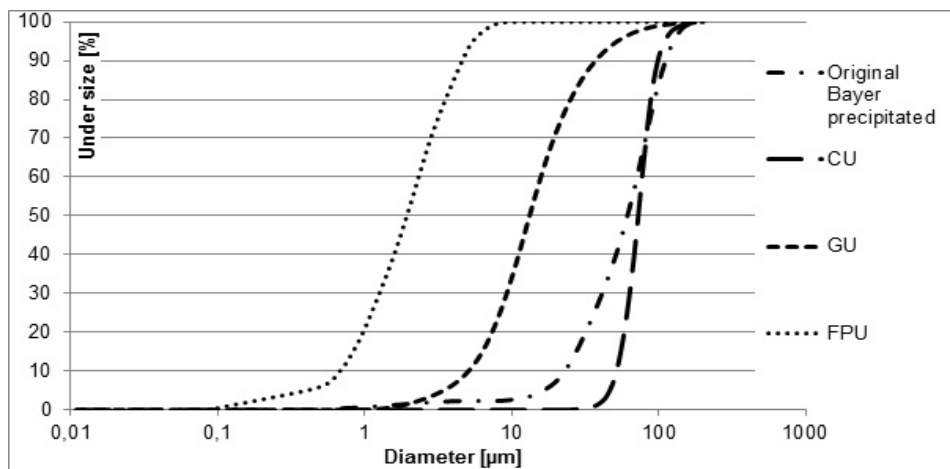
Figure 2. Cumulative particle size distribution of original Bayer precipitated, classified, ground and fine precipitated samples

2. Evaluation of experimental results

2.1. Weight loss during thermal treatment at 260 °C

Boehmite during thermal decomposition of gibbsite evolves between 200-300 °C and remains stable until 400-450 °C [9, 19, 30]. The course of boehmite evolution is followed by direct transformation of gibbsite to oxide. The intersection of the two partially overlapped processes appears between 250-270 °C depending on the conditions of heating. The temperature of heat treatment was chosen as 260 °C, according to our previous survey [31]. We have heated 10 grams of each sample in programmable furnace (Nabertherm, with ±5 °C thermal inertia) at 260 °C for 30 minutes.

Table 2 summarizes the codes of heat treated and unheated samples.

Table 2. Sample codes

Sample	Classified	Ground	Fine precipitated
unheated	CU	GU	FPU
heated	C260	G260	FP260

The weight losses of samples are 18.24 % for C, 22.57 % for G and 9.00 % for FP. The remarkable differences may be caused by different properties of sample materials. At the chosen temperature of heat treatment the coexistence of gibbsite-boehmite and gibbsite-oxide transition reactions is observable. Taken into consideration that at the above temperature the reactions are not finished, it is ascertainable that the extent of mass loss is highly influenced by residence time, properties of material (packing density, heat conductivity) and experimental conditions like water vapor pressure. Diminished mass loss during thermal treatment of FP sample can be referred to the fine sized particles and small packing density [32, 33]. Beyond the experimental and material conditions, the effect of mechanical treatment is assumable too. Largest mass loss was detectable on ground sample, suggesting that the evolved grain structure (higher porosity, flat shape) benefits the escape of water [22, 23, 34].

2.2. X-ray powder diffraction

Boehmite was not detected in the starting materials, and variable material contents without long range order were determined (Table 3). Due to a large deviation of crystallite size values, a complex peak broadening occurred. This was not readily modelled by available options in software, neither did strain refinement and modelling give a solution. As an empirical approach, two similar crystal structures were applied to fit the gibbsite peaks: one for nanocrystalline (<300 nm) and one for microcrystalline (>300 nm) fractions. Crystallite shape effects produced strong preferred

orientation for (*00l*) peaks, modelled by March-Dollase model. Minor preferred orientation was also observed and corrected for (*hk0*) peaks. The C samples gave a similar content for the <100 nm and >500 nm mean crystallite size fractions. The grinded material had mainly microcrystalline fraction, which is realistic for original Bayer process Al-hydroxide [35]. Thus, comparing C and G samples, sieving helped in uniformization of macro- to nanocrystalline fraction ratio. In a contrasting way, FP sample is dominantly nanocrystalline, according to mean crystallite sizes (Table 3A), also indicated by BET results.

Table 3. Mineralogical composition of aluminum hydroxide samples
(CS_m=mean crystallite sizes in nanometer)

A						
	CU		GU		FPU	
Phase Name	wt%	CS_m [nm]	wt%	CS_m [nm]	wt%	CS_m [nm]
Gibbsite-n	44.3	78	8.6	220	7.4	270
Gibbsite	40.7	4800	75.4	2000	67.6	350
Crystallinity undetectable	14.0		16.0		25.0	
B						
Phase Name	C260		G260		FP260	
Gibbsite-n	7.2	95	10.0	55		
Gibbsite	42.9	600			62.3	350
Boehmite	27.9	55	14.0	53	8.7	60
Crystallinity undetectable	22.0		76.0		29.0	

Phases with undetectable crystallinity were observed as two separate humps (Figure 3.), attributed to the differences in chemical composition. However, the hump centered between 10 Å and 8 Å marks an angular ranger, where the main peaks of scarbroite group minerals have their main XRD peaks. Scarbroite [$Al_5(CO_3)(OH)_{13} \cdot 5(H_2O)$, $d_{(003)}$=8.660 Å – $I_{\%}$=100, $d_{(-102)}$=8.340 Å – $I_{\%}$=40] and hydroscarbroite [$Al_{14}(CO_3)_3(OH)_{36} \cdot (H_2O)$, $d_{(100)}$=9.000 Å – $I_{\%}$=100] are hydrated Al-hydroxide-carbonates. Our presumption is that similar compounds may appear during precipitation, in low amounts and rather low crystallite sizes, thus their presence may not be detected. In our unheated samples these broad peaks gave crystallite sizes of a few nanometers only, therefore we chose to fit them as amorphous humps. The second hump at ~4.3 Å is considered to be an amorphous phase of gibbsite composition, as not crystallized residuum of precipitation. The

amorphous content slightly increased with grinding, due to minor amorphisation. The elevated amorphous content of FP sample is derived from its technological process and is supposed to be of Al-hydroxide composition.
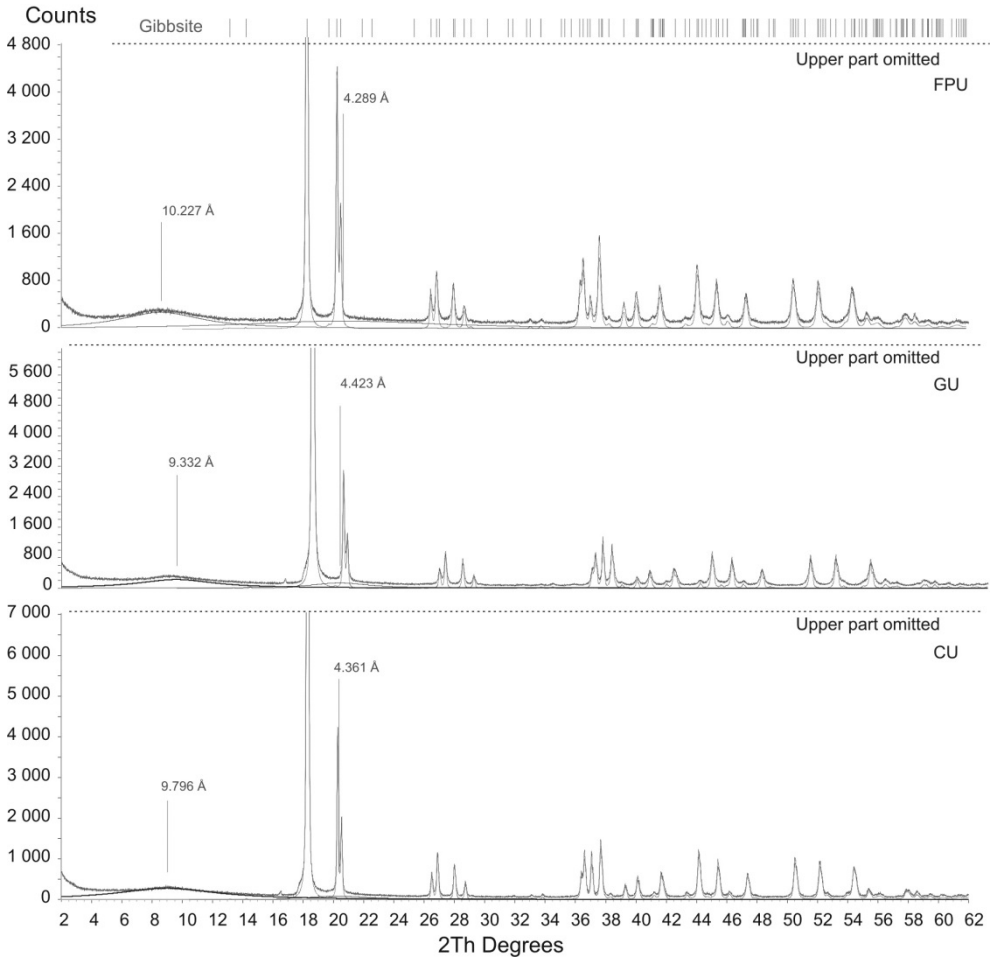
Figure 3. Rietveld-refinement results on XRD patterns for unheated samples

After heat treatment, the microcrystalline fractions were reduced or eliminated, transformed into nanocrystalline fraction (Table 3B). The amorphous content was highly raised in G sample, while only a moderate and minor increase was observed for C and FP samples, respectively. The amorphous hump at ~10Å was shifted to higher d(Å) values in G and FP, and was reduced in C sample (Figure 4). The persistence of ~10Å hump is assumed

to the presence of larger grains in unground material. The new broad peaks are due to the formation of partly dehydroxylated $Al(OH)_{3-x}$ or oxide phases. However, we did not found any similar results among available published data. Boehmite also was formed in different amounts for each material type. In C sample its amount is the highest, which is partly due to the higher nanocrystalline gibbsite content, which is readily transformed into boehmite in this stage. The boehmite to gibbsite ratio is higher in G material, but the boehmite amount is low, most of the microcrystalline and nanocrystalline gibbsite was decomposed. The lowest boehmite formation was observed in FP material, with almost all of the gibbsite being retained. To explain this behavior we have to take into account several influencing factors.
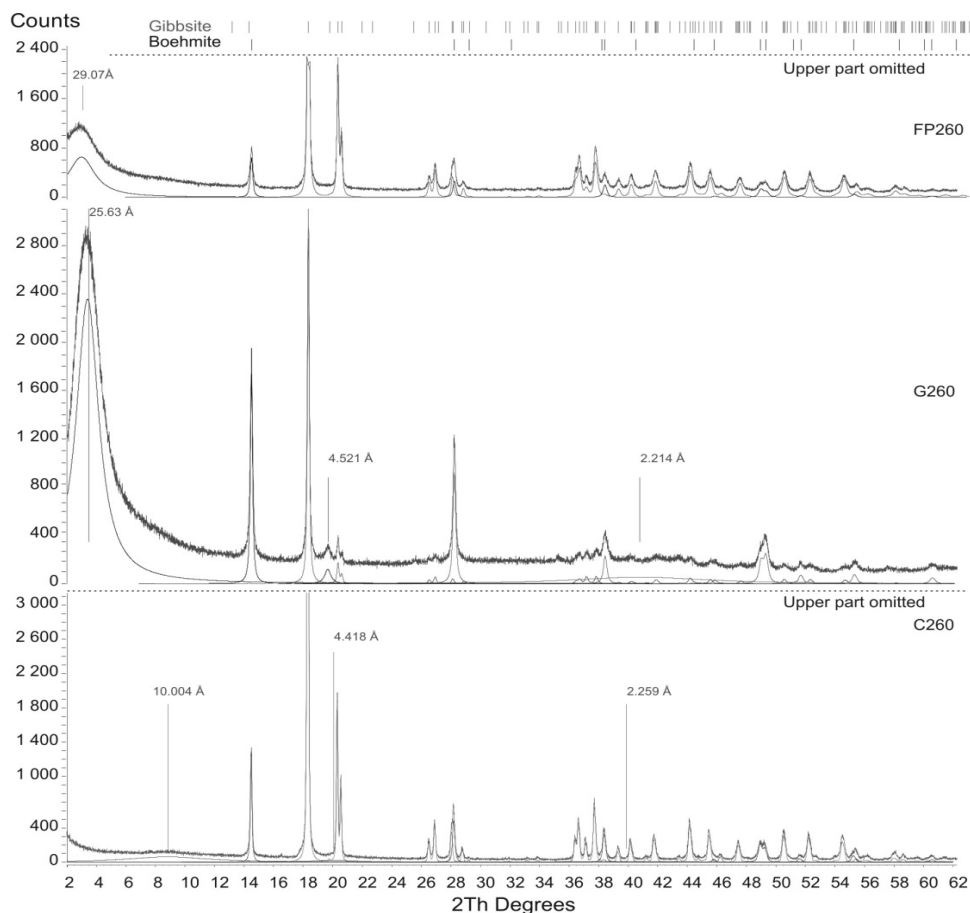
Figure 4. Rietveld-refinement results on XRD patterns for heat treated samples

The small particle diameters do not promote the hydrothermal conditions necessary for boehmite formation within the core of crystals [14, 15, 23, 36, 37]. Considerable affecting factors can be the retarded heat transfer mechanism in the volume of material and consequently the decelerated warming rate and the shorter soaking time. The finer grained the material, the more closed pores can be formed in the intergranular space, by agglomeration, reducing thermal conductivity. In the meantime, due to the increases in grain boundary ratio with decreasing grain size, and small packing densities, diffusion of heat is also slowed down [32, 33]. We must also take into account the higher amorphous content of FP sample. If the amorphous material is present as a layer on Al-hydroxide grains, by dehydration may form a coating layer, which is also inhibiting the rising of boehmite. These factors together may result in the low boehmite formation and gibbsite retaining in FP260 sample.

According to our XRD evaluations, the crystallite size also suffered variations during thermal treatment. In both C and G samples the mean crystallite size of retained gibbsite is <100 nm and the resulted boehmite gave results of ~50 nm. In FP sample, most of the microcrystalline gibbsite was retained, with high crystallite size (unaffected by heating) but the resulted boehmite also gave values of ~60 nm (Table 3B).

2.3. Thermal analysis

Individual sub-processes of thermal decomposition of gibbsite are more or less distinguishable on TG-DTA curves, depending on the conditions of analysis. Experimental curves were divided into the following four steps: I. loosing of adsorbed water (up to 200 °C); II. transformation of gibbsite to boehmite (beginning: 200-220 °C, end: 260-285 °C); III. transformation of gibbsite to oxide (beginning: 260-280 °C, end: 385-440 °C); IV. dissociation of boehmite to oxide (beginning: 435-480 °C, end: 560-595 °C). Some of the above processes are partly overlapped (step II. and step III.), making impossible the exact evaluation of data. Step I. was negligible in case of unheated samples. During step IV. not only the boehmite contained by the sample, but boehmite evolved during step II. is decomposed. Evaluated data are shown in Table 4 and Figure 5.

Step I. is only detectable on heat treated samples. Water which escapes during step I. is derived not from original sample, but adsorbed during the time passed between heat treatment and analysis. Summing the mass decrements of thermal analysis (on basis of unheated material) and mass decrement of heat treatment results in higher total loss, in case of

C260 and G260 samples, than the stoichiometric calculated (34.6 %) loss. Subtracting mass decrement during step I. from total loss yields a result approximating eligibly the theoretic mass loss.

Table 4. TG changes and DTA peak areas during thermal analysis

		Unheated			Heat treated		
		C	G	FP	C	G	FP
Step I.	TG decrement [%]	n.d.	n.d.	n.d.	2.5	3.3	1.8
	TG decrement calculated for U sample [%]				2.0	2.5	1.6
	DTA peak area [uV s/mg]				17.4	17.8	8.6
Step II.	TG decrement [%]	5.5	2.2	n.d.	n.d.	n.d.	n.d.
	TG decrement calculated for U sample [%]	-	-				
	DTA peak area [uV s/mg]	43.2	13.3				
Step III.	TG decrement [%]	21.6	25.6	30.5	14.5	9.0	21.9
	TG decrement calculated for U sample [%]	-	-	-	11.8	6.9	19.9
	DTA peak area [uV s/mg]	237.4	244.3	274.2	130.8	37.3	180.1
Step IV.	TG decrement [%]	3.9	2.9	1.5	5.3	3.7	2.7
	TG decrement calculated for U sample [%]	-	-	-	4.4	2.9	2.4
	DTA peak area [uV s/mg]	36.2	15.5	5.4	41.6	12.2	5.0
Total mass loss [%]		34.1	33.6	34.5	23.3	17.4	27.7
Total mass loss calculated for U sample [%]		-	-	-	19.1	13.5	25.2

The unheated samples contain phases considered as amorphous. Those phases exhibit crystalline hydroxide-like behavior during thermal analysis. Presence of above phases has not caused observable deviance between stoichiometric and measured weight loss, nor resulted in surplus peaks. Thermal decomposition under 200 °C can be attributed to mechanically amorphised hydroxides, and is characteristic in case of prolonged/intensive grinding [19, 22, 23]. Neither GU nor G260 samples have shown signs of grinding caused amorphisation.

Step II. is detectable only in case of untreated samples, what suggests that remaining gibbsite content of heat treated samples will not transform to boehmite. Difference between TG decrements and DTA peaks (C>G>FP) of unheated samples during Step II. indicates different amounts of boehmite evolved due to the dissimilar particle and crystalline sizes of powders.

All of samples had shown TG decrease during step III. The total mass losses of untreated samples are comparatively correspondent. Consequently the extent of step III. is influenced by boehmite evolution and decomposition (boehmite evolves at expense of gibbsite). Remaining hydroxide content, therefore mass loss during step III., of heat treated samples is affected by losses during previous decomposition processes.

Step IV. indicates the decomposition of boehmite formed during Step II. or previous heat treatment. Similarly to Step II., extent of TG decrement and DTA area during Step IV. correlates to the inclination of boehmite formation of original samples, what is influenced by particle and crystalline sizes. Largest TG decrease and DTA area belongs to C samples (heat treated and untreated too) while G samples show considerably smaller, and FP samples indicate the smallest values. This suggests that during calcination of Bayer precipitated coarse aluminum-hydroxide particles the decomposition pathway via boehmite is more significant compared to ground or fine precipitated materials. Considerable differences were not experienced between heat treated and unheated samples in extent of Step IV.
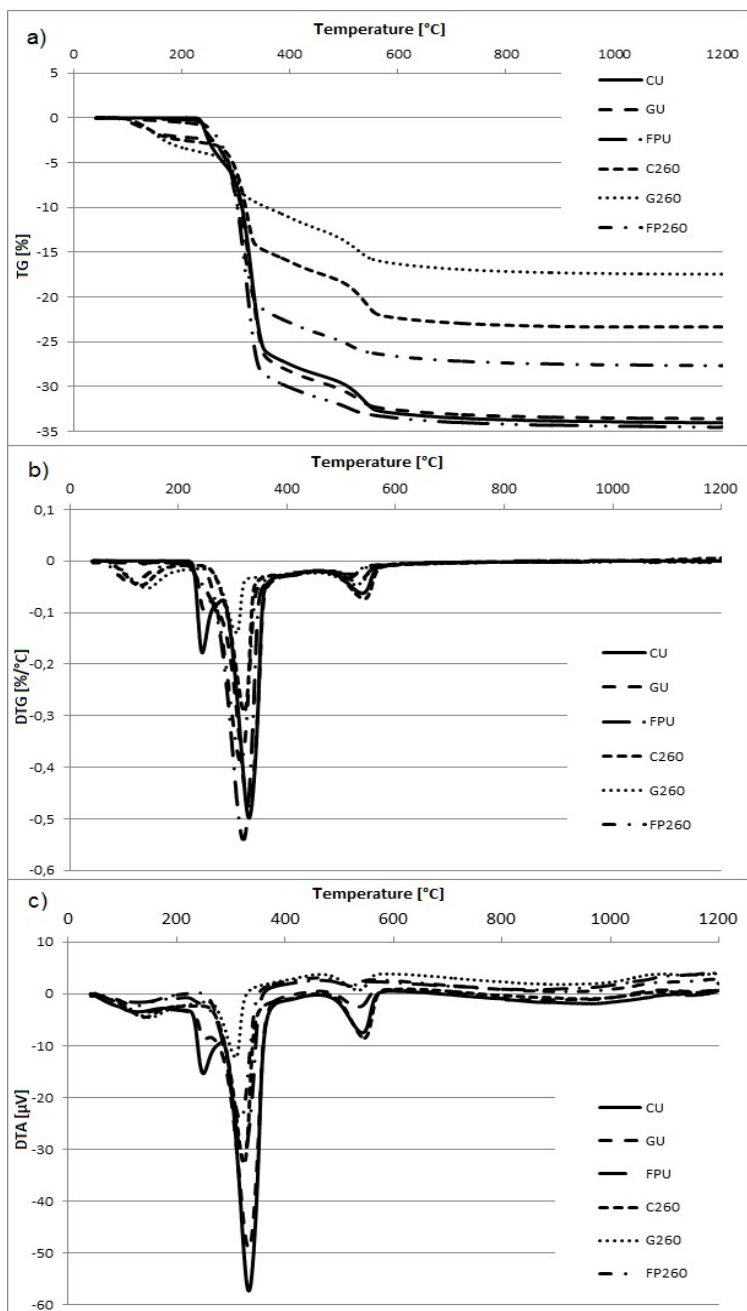
Figure 5. Thermoanalytical curves of samples: a) TG, b) DTG, c) DTA

2.4. Specific surface area

BET specific surface areas of the samples are visible on Figure 6. CU sample has the smallest value (0.12 m^2/g), while grinding increased that to 4.33 m^2/g. FPU is the finest sample (difference in particle size between FP and G is approximately one order of magnitude), the BET specific surface are of FPU is 2.96 m^2/g. It suggests that bigger surface area caused by grinding evolves not only because of attrition and emerging new surfaces, but contribution of porosity can be considerable too. Initial stage of calcination causes rapid growing of porosity and specific surface area. This is attributable to evolved water molecules escaping to the particle surface, forming slit shaped pores parallel to the 001 plane [10, 36]. As it is noticed, BET specific surface areas of C260 and FP260 samples are approximately equivalent (97.29 m^2/g and 101.24 m^2/g, respectively), while in case of G260 sample it is larger (234.34 m^2/g). It must be taken into account that heat treatment of different samples resulted in different degree of decomposition.
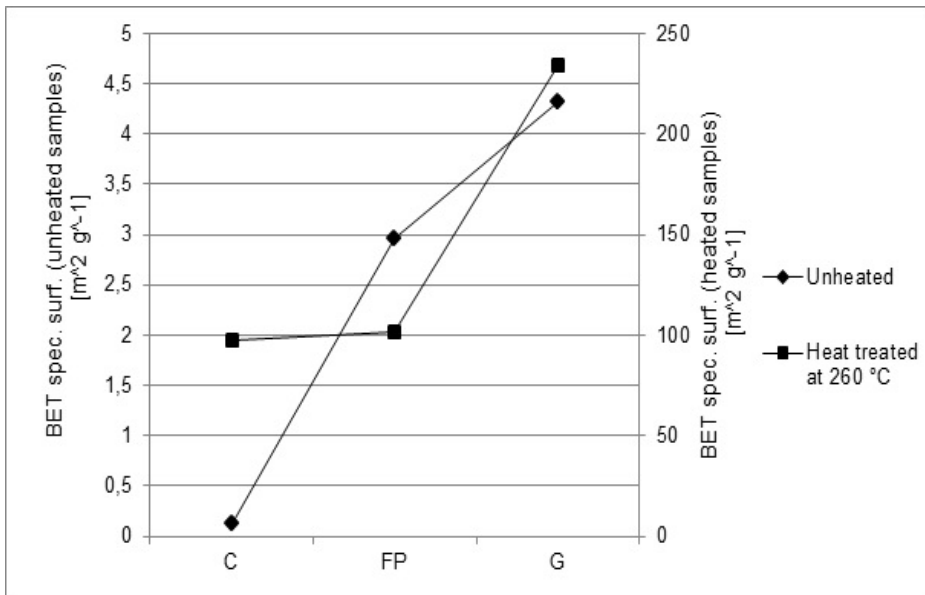
Figure 6. BET specific surface area of unheated (left axis) and heated (right axis) samples

2.5. Scanning electron microscopy

CU sample particles are agglomerates of single pseudohexagonal platy crystallites (Figure 7a). Heat treatment at 260 °C has not caused change on morphological appearance, while the long-shaped pores parallel to 001 plane are distinguishable (Figure 7b). Grinding caused considerable decrease of particle size, however particle fragments above size of 30 µm are observable too. Those relatively big particle fragments are plate like shaped, cracked along the 001 plane (Figure 7c). Craks are perceptible on the sides parallel to 001 plane of the lumps within heat treated sample (Figure 7d). Difference between particle size of GU and FPU samples is approximately one order of magnitude. Occurrence of particles with diameter above 1 µm is extremely rare in FPU. Morphological differences between FPU and FP260 samples with available method was not detectable (Figure 7e-f).

CONCLUSIONS

Both the L.O.I. values at XRF measurements and TG weight loss proved that all the samples have a $Al(OH)_3$ ($\pm H_2O$) chemical composition, regardless of their crystalline or amorphous state. The possible presence of hydrated (and carbonated?) Al-hydroxide was indicated by XRD, considered as amorphous.

The phases with undetectable crystallinity calculated from XRD are not influencing the weight losses by heating, but in the case of FP sample it might have a role in inhibiting boehmite formation. According to TG results, the higher weight loss was recorded in FPU sample, with the lowest crystallite sizes for gibbsite. Accordingly, the lowest weight loss was observed for GU samples, with the highest microcrystalline gibbsite content.

Specific surface area is increased by grinding, due to the opening of closed nanopores by disaggregation. The highest degree of amorphous formation happened in the material with highest specific surface area, proving the importance of free grain surfaces in gibbsite decomposition.

Boehmite formation is mainly promoted by aggregate grain size and internal morphology (relevant for steam pressure generation) but also the microcrystalline nature of gibbsite, as a secondary factor.

As we could observe, thermal treatment affected the grain integrity of samples, cracking appeared on crystallographic directions, mainly in the (001) plane. From XRD results also a decrease in crystallite size for gibbsite is observed. This indicates, that the cracking observed by SEM is affecting the integrity of crystallites.
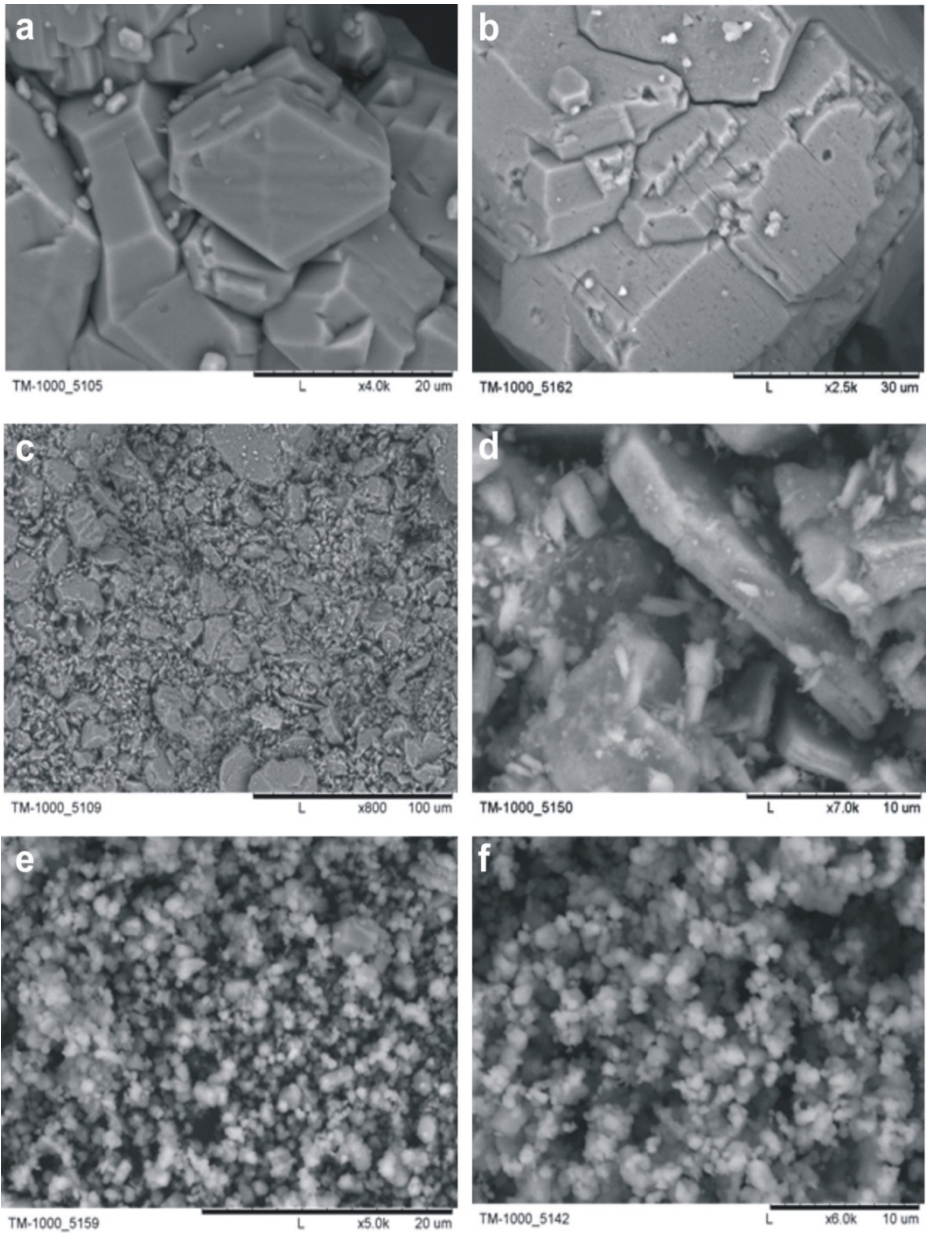
Figure 7. SEM images of samples; a) CU, b) C260, c) GU, d) G260, e) FPU, f) FP260

EXPERIMENTAL SECTION

1. Instrumentation

Particle size determinations were done on a Horiba LA-950 laser scattering particle size distribution analyzer in presence of sodium pyrophosphate solution. Samples were dispersed in ultrasonic bath for one minute before the measurement.

The chemical composition of C and FP samples was measured by X-ray Fluorescence Spectrometry (XRF, Rigaku Supermini200, WD-system, Pd source, 50kV-4nA).

X-ray powder diffraction (XRD) was performed for each material (Bruker D8 Advance, Cu-Kα source, 33 kV and 50 mA, Bragg-Brentano with Våntec-1 position sensitive detector). Measurement time of 5 minutes was allowed, to avoid rehydration of heated samples. Quantitative results were obtained by Rietveld-refinement, in Bruker TOPAS4 software, using ICSD database, unit cell parameters were refined and mean crystallite sizes determined.

Thermal analysis by simultaneous differential thermal analysis (DTA), thermogravimetry (TG) and derivative thermogravimetry (DTG) was made on a Setaram Setsys 24 instrument (heating rate 10 K min^{-1} up to 1200 °C, 55-60 mg sample, dispensed into ceramic crucible, in synthetic high flow air atmosphere). The base-line correction of DTA curves was done with measured correction data (α-Al$_2$O$_3$), smoothing of TG and DTA data was unnecessary.

Scanning electron microscopy (SEM) for morphological examinations were performed on a Hitachi TM 1000 instrument at 15 kV acceleration voltage and 10nA probe current. The powder samples were deposited on self-adhering carbon plates, without surface coating, in low vacuum chamber, to avoid morphology and aggregate structure deterioration. Back-scattered electron (BSE) images were recorded.

Specific surface area was measured on TriStar 3000 analyzer by multipoint BET method (77.35 K temperature, N$_2$ adsorptive, 0.3-0.5 g sample).

2. Materials

Examined materials were obtained from original Bayer precipitated, by sieving – size fractioned Bayer precipitated (C), and grinding – ground Bayer precipitated (G) aluminum hydroxide. Sieving was done in dry state between sieves with mesh size of 63 and 100 μm, shaken for 5 minutes. Size fractionation allows to avoid the disturbing effects in analytical results, caused by extremely fine and coarse particles. Ground sample was prepared in planetary mill by dry grinding (Fritsch Pulverisette 6). Six grams of C Al-hydroxide was

charged into an agate jar of 250 ml together with six agate balls (18 mm diameter). Duration of grinding was 15 minutes at a rotational speed of 500 rpm, stopped in every five minutes, to remove the adhered material from the inner wall of jar. Conditions of milling corresponded to our former experiment [31].

Also a fine precipitated (FP) aluminum hydroxide, with a finer grains size, was used in experiments, to compare its behavior with C and G. Original Bayer precipitated and fine precipitated materials were purchased from MAL Co. Ltd. Ajka Plant (Hungary). Purity of fine precipitated aluminum hydroxide (type of ALOLT 60DLS) is above 99.5 %, analyzed contaminations are SiO_2: 0.004 mass % and Fe_2O_3: 0.006 mass % (results given by MAL Co. Ltd.).

ACKNOWLEDGMENTS

REFERENCES

1. W.H. Gitzen, „Alumina as a Ceramic Material", American Ceramic Society, Westerville, **1970**.
2. R. Salomão, J. Brandi, *Ceram. Int.,* **2013**, *39*, 8227.
3. R. Salomão, M.O.C. Villas Bôas, V.C. Pandolfelli, *Ceram. Int.*, **2011**, *37*, 1393.
4. L. Peng, X. Xu, Z. Lv, J. Song, M. He, Q. Wang, L. Yan, Y. Li, Z. Li, *J. Therm. Anal. Calorim.*, **2012**, *110*, 749.
5. W.J. Tseng, P. Wu, *Ceram. Int.*, **2012**, *38*, 4461.
6. W.J. Tseng, P. Wu, *Ceram. Int.*, **2012**, *38*, 2711.
7. F. Habashi, "Extractive Metallurgy of Aluminum", in G.E. Totten, D.S. MacKenzie, "Handbook of Aluminum: Volume 2: Alloy Production and Materials Manufacturing", Taylor & Francis, New York, Basel, **2003**.
8. A.R. Hind, K.S. Bhargava, C.S. Grocott, *Colloid. Surface*, **1999**, *146*, 359.
9. J.M.R. Mercury, P. Pena, A.H.D. Aza, D. Sheptyakov, X. Turrillas, *J. Am. Ceram. Soc.*, **2006**, *89*, 3728.
10. L.M. Perander, "Evolution of Nano- and Microstructure During the Calcination of Bayer Gibbsite to Produce Alumina", PhD thesis, The University of Auckland, Auckland, **2010.**
11. B. Zhu, B. Fang, X. Li, *Ceram. Int.*, **2010**, *36*, 2493.

12. B. Xu, P. Smith, *Thermochim. Acta*, **2012**, *531*, 46.
13. B.K. Gan, I.C. Madsenb, J.G. Hockridge, *J. Appl. Crystallogr.*, **2009**, *42*, 697.
14. J. Rouquerol, F. Rouquerol, M. Ganteaume, *J. Catal.*, **1975**, *36*, 99.
15. J. Rouquerol, M. Ganteaume, *J. Therm. Anal.*, **1977**, *11*, 201.
16. N. Koga, S. Yamada, *Solid State Ionics*, **2004**, *172*, 253.
17. C. Novák, G. Pokol, V. Izvekov, T. Gál, *J. Therm. Anal.*, **1990**, *36*, 1895.
18. I.N. Bhattacharya, S.C. Das, P.S. Mukherjee, S. Paul, P.K. Mitra, *Scand. J. Metall.*, **2004**, *33*, 211.
19. T. Tsuchida, N. Ichikawa, *React. Solid.*, **1989**, *7*, 207.
20. J. Temuujin, K.J.D. MacKenzie, M. Schmücker, H. Schneider, J. McManus, S. Wimperis, *J. Eur. Ceram. Soc.*, **2000**, *20*, 413.
21. T.C. Alex, *J. Therm. Anal. Calorim.*, **2014**, *117*, 163.
22. K.J.D. MacKenzie, J. Temuujin, K. Okada, *Thermocim. Acta*, **1999**, *327*, 103.
23. N. Koga, *J. Therm. Anal. Calorim.*, **2005**, *81*, 595.
24. N. Koga, T. Fukagawa, H. Tanaka, *J. Therm. Anal. Calorim.*, **2001**, *64*, 965.
25. E.E. Kiss, G.C. Boskovic, *Rev. Roum. Chim.*, **2013**, *58*, 3
26. C. Dan, E.-J. Popovici, F. Imre, E. Indrea, P. Mărginean, I. Silaghi-Dumitrescu, *Studia UBB Chemia*, **2007**, *LII*, 91.
27. S. Cassiano-Gaspar, D. Bazer-Bachi, J. Chevalier, E. Lécolier, Y. Jorand, L. Rouleau, *Powder Technol.*, **2014**, *255*, 74.
28. K. Okada, T. Nagashima, Y. Kameshima, A. Yasumori, *Ceram. Int.*, **2003**, *29*, 533.
29. C.J. Oh, Y.K. Yi, S.J. Kim, T. Tran, M.J. Kim, *Powder Technol.*, **2013**, *235*, 556.
30. M. Földvári, "Handbook of thermogravimetric system of minerals and its use in geological practice", Magyar Állami Földtani Intézet, Budapest, **2011**.
31. V.Z. Baranyai, F. Kristály, I. Szűcs, *Materials Science and Engineering: A Publication of the University of Miskolc*, **2013**, *38*, 15.
32. H.W. Zhang, Q. Zhou, H.L. Xing, H. Muhlhaus, *Powder Technol.*, **2011**, *205*, 172.
33. K.C. Smith, T.S. Fisher, *Int. J. Hydrogen Energy*, **2012**, *37*, 13417.
34. K.J.D. MacKenzie, J. Temuujin, M.E. Smith, P. Angerer, Y. Kameshima, *Thermochim. Acta*, **2000**, *359*, 87.
35. D.A. Ksenofontov, Y.K. Kabalov, *Inorg. Mater.*, **2012**, *48*, 142.
36. B. Whittington, D. Ilievski, *Chem. Eng. J.*, **2004**, *98*, 89.
37. V. Balek, J. Šubrt, J. Rouquerol, P. Llewellyn, V. Zeleòák, I. M. Bountsewa, I.N. Beckman, K. Györyová, *J. Therm. Anal. Calorim.*, **2003**, *71*, 773.

POROUS TITANIUM - AN ENHANCED SUPPORT FOR HUMAN OSTEOBLASTS AFTER ANODIZATION AND c-RGD IMMOBILIZATION

ANA-MARIA SALANTIU[a,*], OLGA SORITAU[b], NOEMI DIRZU[b], FLORIN POPA[a], LIANA MURESAN[c], VIOLETA POPESCU[a], PETRU PASCUTA[a], CATALIN POPA[a]

ABSTRACT. Porous titanium is the material of choice for hard tissue implants but an enhanced osseointegration can be achieved only through subsequent surface conditioning. In this work, we aimed to study the effect of both surface conditioning and immobilization of cyclic Arg-Gly-Asp (RGD) peptide onto two types of porous titanium samples designed for endosseous applications and obtained by Powder Metallurgy (PM) in view of osteoblast cells attachment and proliferation. Cyclic RGD peptide was chosen as bioactive target and was covalently immobilized on anodized PM porous titanium. The samples, formerly pressed with 200 or 400 MPa and sintered at 1100°C in vacuum, were first anodized using a constant voltage of 2V for 1 hour with 0.25 M sulphuric acid to enhance the thickness of titanium oxide layer. An intermediary aminoalkylsilane molecule (APTES) was then covalently linked to the oxide layer, followed by the covalent binding of cyclic RGD peptide to the free terminal NH_2 groups using polyethylenglycol diglycidyl ether (PEGDE) as coupling agent. The samples were characterized by micro CT, X-ray diffraction (XRD), scanning electron microscopy (SEM) and Fourier transform infrared spectroscopy (FT-IR). Anodized titanium samples display anatase and rutile on the surface and, after functionalization, two important amide characteristic regions, confirming the presence of cyclic RGD peptide. Cells seeded on samples pressed with 400 MPa, anodized and c-RGD immobilized, displayed a more flattened shape and a more obvious tendency of spreading into pores.

Keywords: *porous titanium, cyclic RGD, anodic oxidation, human osteoblasts*

---

[a] *Technical University of Cluj-Napoca, Faculty of Materials and Environmental Engineering, 103-105 Muncii Avenue, RO-400641, Cluj-Napoca, Romania,*

[b] *"Prof. I.Chiricuta" Oncological Institute, 34-36 Republic str., RO- 400015, Cluj-Napoca, Romania,*

[c] *Babeş-Bolyai University, Faculty of Chemistry and Chemical Engineering, 11 Arany Janos str., RO-400028, Cluj-Napoca, Romania.*

[*] *Corresponding author: bolfa_anamaria@yahoo.com*

A.-M. SALANTIU, O. SORITAU, N. DIRZU, F. POPA, L. MURESAN, V. POPESCU, P. PASCUTA, C. POPA

INTRODUCTION

Ti and Ti alloys are intensively studied for most dental and orthopedic applications [1,2]. Porous structures gained an increased interest for medical applications due to their low elastic modulus, matching that of bones [3,4]. A porous surface enhances the implant/ bone bonding by growth of tissue into the pores [5]. To this aim, it was reported that the optimal pore size for bone ingrowth should be between 100 μm and 600 μm [6]. Besides the use of porous surfaces, osseointegration of titanium implants is influenced also by surface properties which are often the basis of successful endosseous implantology [7,8]. Various techniques have been studied and applied to improve the osseointegration of titanium implants [9], such as acid etching, plasma spraying, anodizing [10,11] and also by the use of bioactive coatings [12]. Titanium surface conditioning *via* anodizing has been reported to increase the surface area and the activity of the contacting cells [13]. On the other hand, bioactive coatings have the role to create a strong interface between bone tissues and implant [14]. It is fundamental that the method used to attach a biomolecule to the implant surface is stable enough to keep the biomolecule in place until the desired response is triggered [15].

A method commonly employed to covalently attach biomolecules onto hydroxylated surfaces is functionalization using an aminosilane reaction and subsequent chemical attachment using crosslinkers [15,16]. 3-Aminopropyltriethoxysilane (APTES) is a silane molecule commonly used in the biomedical literature to bond an assortment of materials [16]. The presence of NH_2 end groups on the silanized surface has a major importance in biological applications as it allows proteins or other biomolecules to be attached in a simple way [17]. Bioactive peptides have been used to promote cell adhesion, in particular extensive scientific investigations have been described using RGD peptide, a short amino acid sequence present in several adhesive extracellular matrix proteins, for improving cell adhesion *via* cell membrane integrins reactions [18-20]. It was reported that RGD-related peptides influence also osteoblast mineralization, cytoskeleton reorganization and migration *in vitro* [21].

The purpose of this study was to evaluate the influence of both surface conditioning and c-RGD peptide immobilization on porous titanium with respect to osteoblast adhesion and proliferation.

RESULTS AND DISCUSSION

Microstructural analysis of porous titanium samples

The linear analysis performed on optical images of surfaces revealed an average porosity of 33% for samples pressed with 200 MPa

and 28% for 400 MPa pressed ones, while the average pore size was of 31 µm and 26 µm respectively. Nevertheless, large pores with the conventional diameter of more than 100 µm can be observed for both types of samples (Figure 1a and b). The shape of pores is irregular, with sharp edges; interconnected pores are representing the majority, as it can be observed also by micro CT images of the cross section of samples (Figure 1b'). This aspect of structure is well suited for osseointegration, while providing a low Young's modulus.
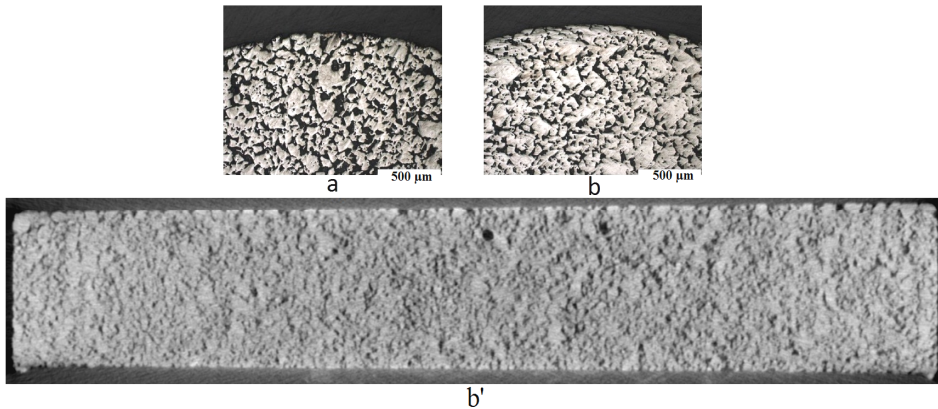
Figure 1. Optical images for titanium pressed samples with 200 MPa (a) and 400 MPa (b) and microCT image for the titanium sample pressed with 400 MPa (b').

Electrochemical behaviour of anodized PM porous titanium

To inspect the influence of manufacturing conditions for the titanium samples pressed with 200 or 400 MPa, chronoamperometric tests were devoted to analyse the influences upon the titanium oxide formation. The curves are shown in Figure 2. The current density / time measurements showed that overall process can be described in two stages. The first stage represents the nucleation of a titanium oxide layer on the porous surface, which lowers the current density in the circuit. In the last stage, the current density remained stable, increasing the thickness of the titanium oxide layer.

When comparing the chronoamperograms results for the different types of titanium samples, Figure 2, it was found that samples pressed with 200 MPa presented the highest intensity of oxidation / dissolution reactions. Such behaviour is explained by the increased active surface of the electrode. In contrast, the curve for the sample pressed with 400 MPa, after the first stage, present an increasing tendency of current density, a certain

instability, which could be related with the sharp edges pores that are more pronounced on this sample (see Figure 1).

Lattice structure of anodized Ti oxide

Figure 3 shows the XRD patterns for untreated porous titanium and anodically oxidized porous titanium in 0.25 M H_2SO_4 for 1hour at 2V and then heat treated at 700°C. For any temperature of the heat treatment below 700°C, no peak corresponding to any of the oxides occurred. Only the peaks of titanium could be observed for the untreated porous Ti sample (Figure 3a). The peaks of rutile and anatase occurred for titanium samples pressed with 200 MPa and then oxidized at 2V (Figure 3b). From Figure 3c it can be seen that a higher compaction pressure of 400 MPa resulted in a decrease of the peak intensity of the rutile phase while no peaks for anatase phase appeared. The trends in anatase and rutile formation should be attributed to the higher thermodynamic stability of the rutile phase with respect to the anatase phase, which makes rutile more likely to form. The differences in the oxide nucleation and growth for the two types of samples, as seen in Figures 2 and 3, are supposed to be generated by the effects at the bottom of pores, as both porosity and pores size display small differences.

Chemical functionalization of anodized porous titanium surfaces and cyclic RGD immobilization

FTIR spectra in the range from 4000 cm^{-1} to 500 cm^{-1} for APTES and PEGDE/c-RGD films grafted on the porous titanium surfaces are shown in Figures 4 and 5. APTES films prepared from toluene solution show similar features in the range presented before, on the anodized titanium samples pressed with 200 and 400 MPa (Figures 4b and 5b). Around 3400 cm^{-1}, the symmetric and asymmetric –NH stretch modes from amino group in APTES were very weak in the spectra. In Figure 4b and also in Figure 5b, between 2800 and 3000 cm^{-1} are found several CH stretch modes corresponding to APTES backbone and ethoxy groups [14]. The most important structural information regarding APTES films is found between 1800-900 cm^{-1}. A vibrational mode around 1655 cm^{-1} is due to the presence of an imine group formed by the oxidation of an amine bicarbonate salt. Two dominating vibrational modes are found around 1575 and 1485 cm^{-1}. Such vibrational modes arise when surface amino groups form bicarbonate salts in a reaction with atmospheric CO_2, as was reported previously [22]. The mode near 1195 cm^{-1} arise from unhydrolyzed ethoxy moieties in APTES ($-OCH_2CH_3$). The peak located around 1110 cm^{-1} is attributed to Si-O-Si from polymerized APTES indicating that the silane agent had been grafted onto the surface of anodized titanium surfaces [23].

Curing of silanes at elevated temperature, 110°C, seemed to enhance the siloxane layer formation on the TiO_2 surface of titanium substrate.

FTIR spectra corresponding to PEGDE/c-RGD peptide films grafted on silanized titanium samples pressed with 200 and 400 MPa are presented in Figures 4c and 5c. The intense band at approximately 2870 cm^{-1} was attributed to the symmetric stretch of the methylene group. Bands in the region 1500-1100 cm^{-1} were generally due to the bending, wagging and twisting modes of the CH_3 and CH_2 groups and the methylenes of the O-CH_2-CH_2-O group. The most intense band at 1093 cm^{-1} was assigned to the asymmetric C-O-C stretch [24].

The ATR-FTIR spectrum of c-RGD-PEGDE for both of the two types of samples show all the characteristic peaks presented before, which demonstrates that c-RGD/PEGDE films have the similar base structure as PEGDE films. However, cRGD/PEGDE films show two more important characteristic regions at 1650 cm^{-1} and at 1559 cm^{-1}, which correspond to the vibrations of amide (-CO-NH) I and II, respectively [25].

These amide groups are from the c-RGD peptide, indicating that c-RGD peptide is present on the films surface anchored on porous titanium samples.
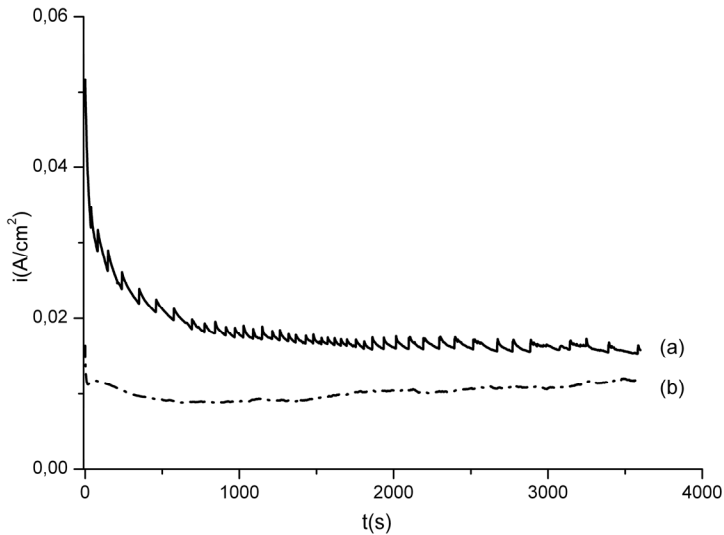
Figure 2. Chronoamperograms for anodic oxidation of titanium samples pressed with 200 MPa (a) and 400 MPa (b).
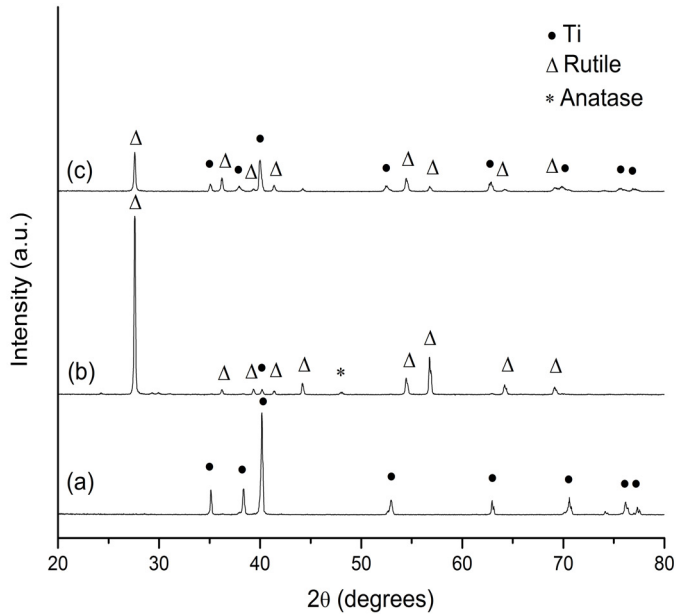
Figure 3. XRD patterns of untreated porous titanium (a) and anodized titanium samples pressed with 200 MPa (b) and 400 MPa (c) at 2V for 1h and then heat treated at 700°C.

Adhesion and proliferation of human osteoblasts

Adhesion and proliferation were evaluated on untreated and on modified (TiO_2, c-RGD) porous titanium samples. To assess cell attachment and morphology, PKH26 marked osteoblast cells were analysed by fluorescence microscopy after 1 hour, 4 days and 14 days of cultivation on the samples mentioned before. The presence of c-RGD peptide increased cell attachment one hour after seeding on both 200 and 400 MPa titanium pressed samples (Figure 6a). After 4 days of osteoblasts cultivation, 200 and 400 MPa titanium pressed samples coated with c-RGD peptide (Figure 6b), sustained a higher number of cells. Cell spreading was observed especially on anodized titanium samples. The best cell proliferation rate after 14 days was observed for c-RGD coated samples pressed with both 200 and 400 MPa, Figure 6c, as well as for untreated and anodized titanium samples pressed with 400MPa.

Cells counting of PKH26 stained cells was performed after the capture of images in three different microscopic fields randomly selected and the obtained results are shown in Figure 7 as cells number/mm^2. After one hour, 400 MPa-RGD samples displayed by far the highest number of attached cells, while the 400 MPa-anodizing samples displayed the lowest. The latter one might be due to the oxidation instability proven in Figure 2b. The same trend could be observed after 4 hours, but all differences were smaller. After 14 days, the highest number of cells corresponds to 400 MPa-anodizing samples and RGD samples come after. The increased fluorescence intensity observed in the optical images for c-RGD coated samples (Figure 6), could be explained by the presence of cells on the RGD samples surface due to cell capture by the peptide sequences, capture which does not allowed their migration into the pores of the samples, as in the case of only anodized samples. For these ones, it seems that along the 14 days, the oxide layer became stable enough.
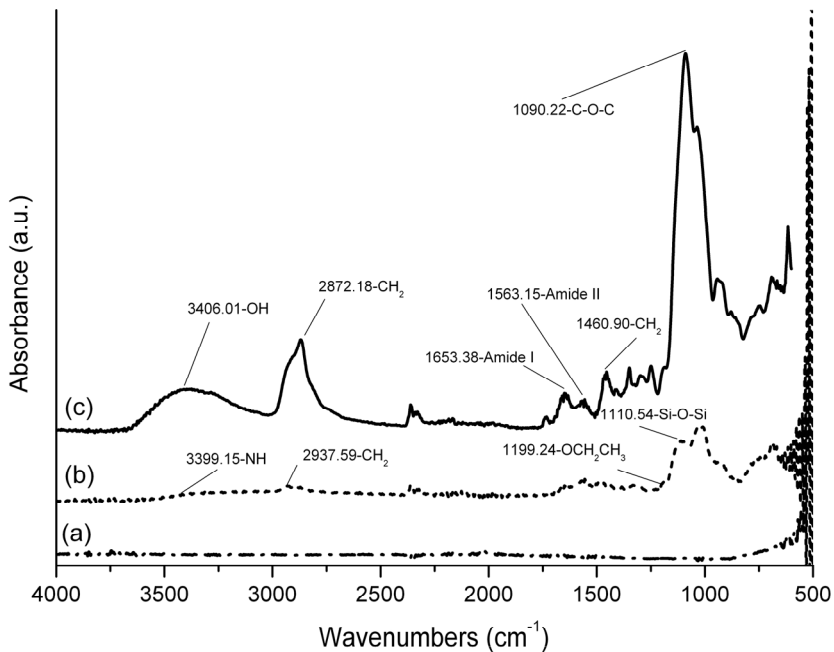
Figure 4. FTIR spectra of (a) anodized, (b) silanized and (c) c-RGD peptide grafting on titanium sample pressed with 200 MPa.
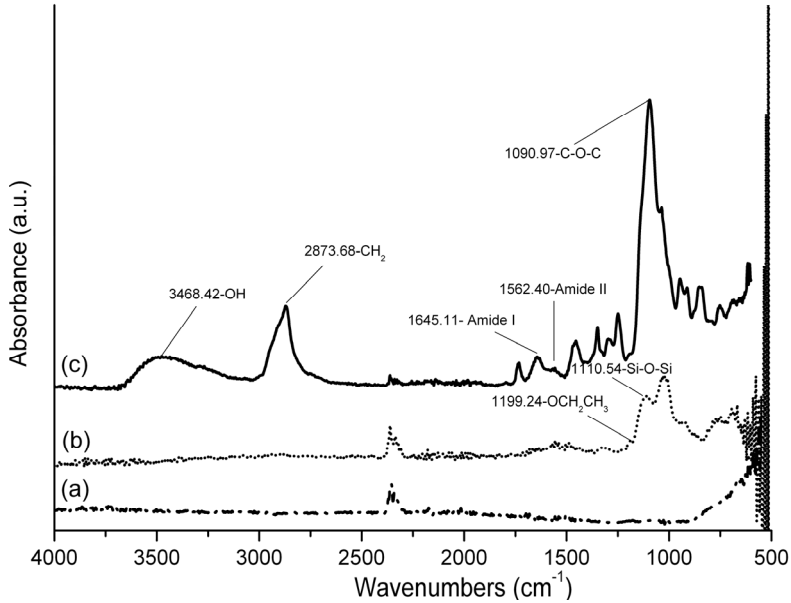
Figure 5. FTIR spectra of (a) anodized, (b) silanized and (c) c-RGD peptide grafting on titanium sample pressed with 400 MPa.

SEM morphological analysis

Figure 8 illustrates the surface SEM micrographs of untreated and modified titanium samples pressed with 200 and 400 MPa without and with osteoblast cells. After 29 days of culture, cells on untreated titanium samples pressed with 400 MPa, Figure 8a, appeared in higher number, more spread and with traces of mineralization in comparison with the sample pressed with 200 MPa. On the anodized titanium sample pressed with 200 MPa without osteoblast cells seeded, Figure 8b, an advanced coverage of the pores with a titanium dioxide layer occurred. For the other type of samples, the difference between untreated and anodized state is not so visible because the coverage with a titanium dioxide layer was reduced. In Figure 8b it can be seen that the osteoblast cells migrated and adhered into the pores of anodized titanium samples, which is consistent to the conclusions for Figure 7.

The presence of c-RGD peptide attachment on the surface of TiO_2 after coating with an intermediate layer of APTES without osteoblast cells seeded was observed as irregular deposits. For the titanium sample pressed with 400 MPa and coated with c-RGD, (Figure 8c), we can observe

the presence of c-RGD attachment at the surface but also in the pores. The presence of the c-RGD peptide on titanium samples pressed with 400 MPa induced a more flattened cell shape with tendency of cell spreading into pores in contrast with the round shape of cells cultivated on c-RGD surface coated titanium samples pressed with 200 MPa, also consistent with the conclusions referring to Figures 6 and 7.
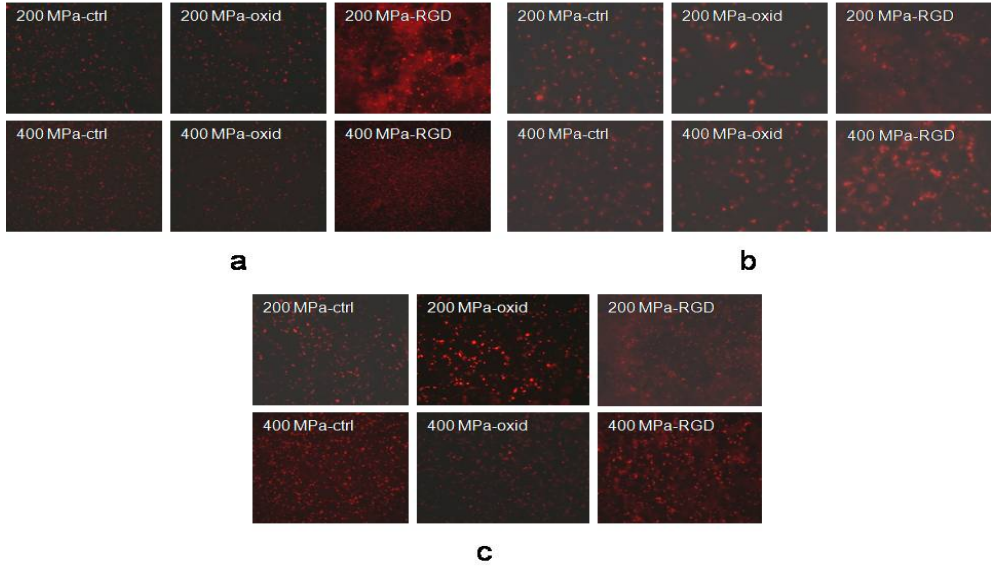
Figure 6. Fluorescence microscopy images (10x) of osteoblast cells stained with PKH26 dye and cultivated on different surface treatment of porous Ti substrate after 1 hour (magnification X100) (a), 4 days (magnification X200) (b) and 14 days (magnification X100) (c).
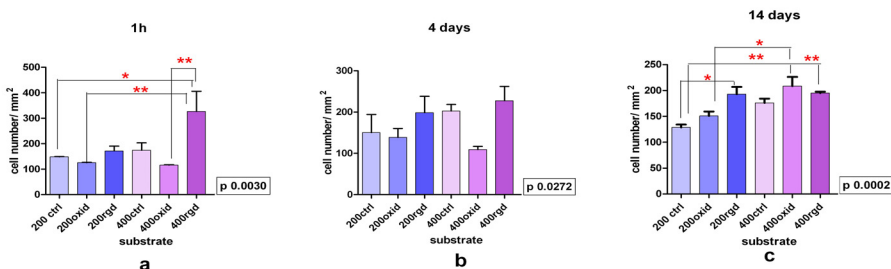
Figure 7. Cell counting graphs for evaluating the cell adhesion one hour after osteoblasts seeding (a) and proliferation rates of osteoblasts on different uncoated and coated titanium surfaces after 4 days (b) and 14 days (c) of cultivation. * indicates a significant statistical difference ($p < 0.05$).
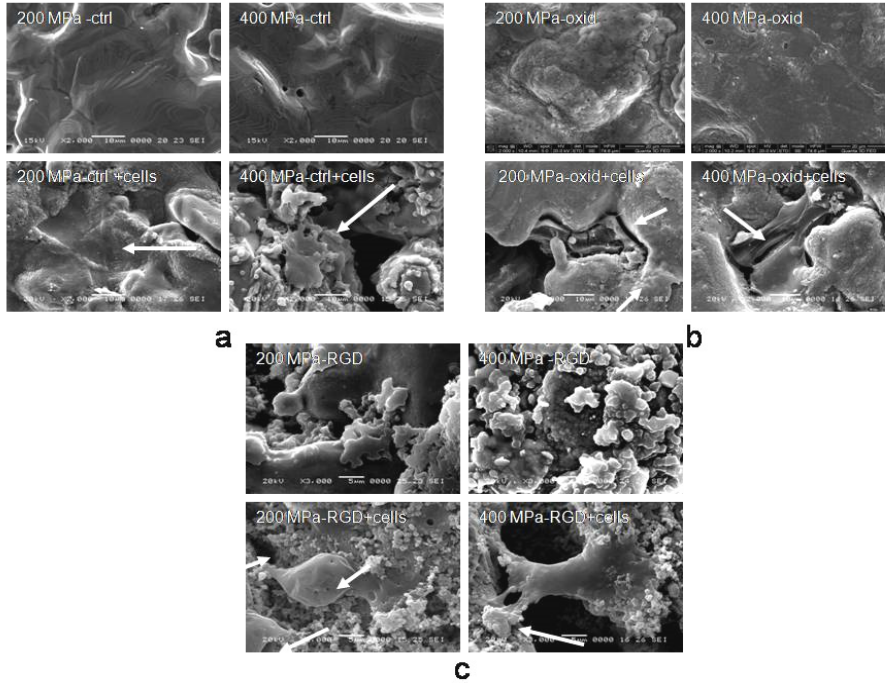
Figure 8. SEM micrographs of untreated titanium samples pressed with 200 MPa and 400 MPa (a), following anodizing (b) and c-RGD immobilization (c) without and with osteoblast cells after 29 days of culture. Arrows indicate adhered cells on samples surface.

CONCLUSIONS

In this study, c-RGD peptide was successfully covalently grafted onto the surface of anodized TiO_2 after coating with an intermediary layer of APTES. Furthermore, the c-RGD peptide promoted the adhesion and proliferation of osteoblast cells. The results of *in* vitro tests showed that c-RGD peptide accelerated the initial attachment of osteoblast cells, phenomenon which is not consistent for a longer time. Therefore, we believe that applying an RGD coating onto TiO_2 anodically grown on porous Ti implants may contribute to the improvement of osseointegration for a design of the implant that provides also other surfaces (i.e. surfaces that were only anodized) to take over the process after the first stages after implantation (weeks time). The porosity resulted after PM processing with various compacting pressures plays also a role in the enhancement of the

biocompatibility for porous titanium. In the conditions of this work, we found that the best behaviour is unexpectedly obtained for pressing with 400 MPa before sintering, leading to a smaller porosity compared to 200 MPa pressing.

EXPERIMENTAL SECTION

Samples preparation

The CP Ti powder (with a purity higher than 99.5%) obtained by hydration-milling-dehydration process with powder particles size lower than 150 μm was used to manufacture porous samples with 11.5 mm diameter. Closed die pressing was performed with 200 and 400 MPa and sintering of the specimens was carried out at 1100°C for 1h in a high vacuum furnace using a heating and cooling rate of 10°C/min and a minimum vacuum level of 10^{-5} Torr was guaranted.

Microstructural characterization of the porous titanium samples was performed on the surface by optical/ electron microscopy (Olympus GX51) and in volume by microCT (Bruker microCT analyzer).

Anodizing

Anodic oxidation was performed using a conventional three electrode cell with a porous titanium disk (samples pressed with 200 and 400 MPa) as the working electrode, a platinum electrode as the counter electrode and a saturated calomel electrode (SCE) as the reference electrode. Electrochemical measurements (chronoamperometric investigations) were conducted using a commercial potentiostat PAR 2273 at room temperature. The anodic oxidation was performed at 2V during 1hour in 0.25 M H_2SO_4 solution. All solutions were prepared from reagent grade chemicals and deionized water. After the anodizing, the samples were rinsed with deionized water, dried at 60°C, and then heat treated at 700°C for 1h to crystallize the as-formed amorphous titanium oxide. The film lattice structure was examined by X-ray diffraction (Shimadzu XRD 6000).

Silanization and c-RGD immobilization on porous titanium surfaces

Silanization of porous titanium oxidised samples was performed in 3% Aminopropyl-triethoxysilane (APTES; Sigma Aldrich) in toluene at room temperature overnight. After cleaning in toluene and ethanol, samples were cured at 110°C for 1h. Subsequently, aminosilanised Ti samples were spin coated with 3% solution of polyethyleneglycol diglycidylether (PEGDE; Sigma Aldrich) in 50 mM carbonate-buffer (pH 9), using the following parameters: 1000 rpm, 30s. The excess solution was removed by repeated rinsing with

water. After the deposition of the polyethyleneglycol diglycidylether films, the substrate was heat treated at 80°C for 2h in an oven with a heating and cooling rate of 2°C/min. RGD immobilisation was then immediately performed by spin coating with 0.5 mg/mL RGD peptide (c-RGDFV peptide, Cyclic Calbiochem) in carbonate-buffer with the same parameters presented before (see Scheme 1).
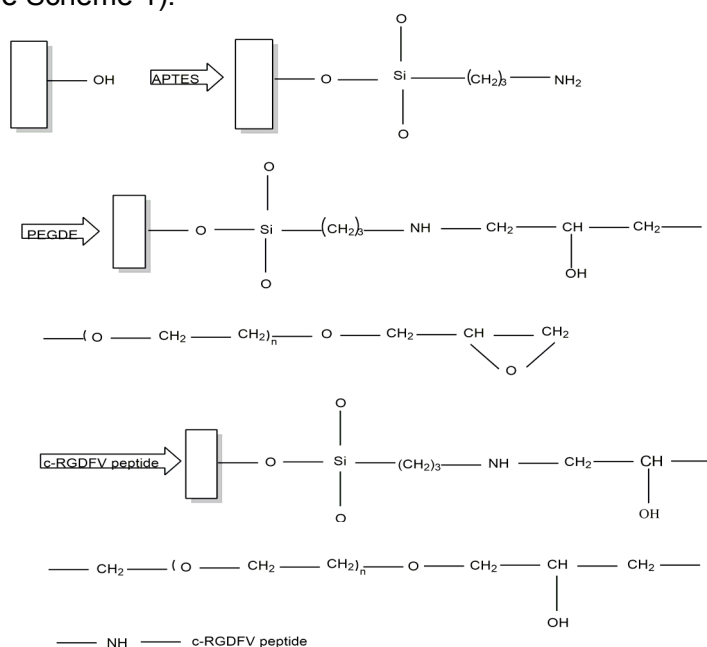
Scheme 1. Reaction schematic diagram for the functionalization and c-RGD peptide grafting onto anodized porous titanium: (I) APTES treatment; (II) bifunctional cross-linker (PEGDE) connection; (III) c-RGD peptide grafting.

FTIR-ATR was used to investigate the structure of APTES, PEGDE, and c-RGD films and the modification of porous titanium surface by a Perkin-Elmer FTIR model equipped with ATR accessory (PIKE MIRacle™) with diamond crystal plate.

Cell culture

Human osteoblasts at passage eight, isolated and characterized as described by Tomuleasa et al. [26] were cultured in Dulbecco's modified Eagle's medium (DMEM) / F-12HAM (Sigma) containing 10% foetal calf serum (FCS), 2mM L-Glutamine, 1% antibiotics, 1% non-essential aminoacids (NEA) (all reagents from Sigma). Test samples were placed in 12 well plates (Nunc); 1.2×10^5 cells were seeded in each well.

Cell membrane fluorescent labelling

Fluorescent marking of osteoblasts was performed using PKH26 Red Fluorescent Cell Linker Kits (Sigma-Aldrich). This staining ensures maintenance of fluorescence of live cells for a longer period of time. After trypsinization, $1x10^6$ cells were washed twice with PBS by centrifugation at 1000 rpm, 5 min and the cell pellet was resuspended in 1ml Diluent C and 1ml of Dye Solution (4µl of PKH26/ml) was added, followed by gentle pipetting. The staining was stopped after 5 min by adding 2 ml of complete medium containing 10% foetal calf serum and cells were centrifuged for 10 min at 1000 rpm. Another two washing steps were performed with 10 ml of complete medium and then cells were counted, resuspended in complete medium and seeded in 12 well plates on the surface of titanium samples.
The samples were formerly sterilized by immersion in 70° alcohol and exposing 3 hours to UV radiation.

Cell adhesion

After 1 hour, adherent cells were visualized by fluorescence microscopy (Zeiss Axiovert D1), using filters of 546 nm and the fluorescence intensity was measured using a BioTek Synergy 2 plate reader (excitation 540 nm, emission 620 nm). We used the option of area scan in BioTek measurements that offers multiple values (13 readings) of fluorescence obtained by scanning the whole specimen surface. This is the procedure by which we obtained the final graphical representation.

Cell proliferation

Cell proliferation was quantified using two methods: counting PKH26 stained cells on captured images in 3 different microscopic fields, randomly selected, and by fluorescence intensity measurements with BioTek Synergy 2 plate reader. Readings were performed at 4 days and 14 days.

Statistical analysis

Statistical analysis of cell counts was performed using a GraphPad Prism 5 software, Bonferroni Multiple Comparison post-test. Statistical significance was set at $p < 0.05$.

SEM morphological analysis

The cells were studied after 29 days of culture. Specimens were sputter coated with a gold layer using a Desk V coating device. The surface morphology of the samples with or without seeded cells was studied by scanning electron microscopy (JEOL 5600 LV).

A.-M. SALANTIU, O. SORITAU, N. DIRZU, F. POPA, L. MURESAN, V. POPESCU, P. PASCUTA, C. POPA

ACKNOWLEDGMENTS

REFERENCES

1. S. Nayak, T. Dey, D. Naskar, et al., *Biomaterials*, **2013**, 34, 2855.
2. N.A. Al-Mobarak and A.A. Al-Swayih, *Int. J. Electrochem. Sci*., **2014**, 9, 32.
3. T. Marcu, A.M. Salantiu, I. Gligor, et al., *J. Optoelectron. Adv. Mater*, **2013**, 15**,** 847.
4. I. Gligor, T. Marcu, M. Todea, et al., *J. Optoelectron. Adv. Mater,* **2011**, 13, 879.
5. B. Dabrowski, W. Swieszkowski, D. Godlinski, et al., *J Biomed Mater Res B Appl Biomater* **2010**, 95, 53.
6. L.M. Reis de Vasconcellos, D. Oliveira Leite, F. Nascimento de Oliveira, et al., *Braz Oral Res,* **2010**, 24, 399.
7. D. Arya, S. Tripathi and R Bharti, *J Dent Implant,* **2012**, 2, 93.
8. A.B. Novaes Jr, S.L. Scombatti de Souza, R.R. Martins de Barros, et al., *Braz. Dent. J* , **2010**, 21, 471.
9. H.S. Kim, Y. Yang, J.T. Koh, et al., *J Biomed Mater Res Part B: Appl Biomater*, **2009**, 88B**,** 427–435.
10. S.Oh,K.S. Moon, S.H. Lee, *J. Nanomater,* **2013***,* doi.org/10.1155/2013/965864.
11. S.Y. Park, H.S. Kim, J.H. Kim et al., *J.Tissue Eng Regener. Med*., **2012**, 9, 194.
12. M.L. Schwarz, M. Kowarsch, S. Rose, et al., *J.Biomed Mater Res A.,* **2009**, 89, 667.
13. E.S. Gawalt, M.J. Avaltroni, M. Danahy, et al., *Langmuir,* **2003**, 19, 200.
14. G. Tan, L. Zhang, C. Ning, et al., *Thin Solid Films,* **2011**, 519, 4997.
15. E.C. Pegg, G.S. Walker, C.A. Scotchford, et al., *J. Biomed Mater Res A,* **2009**, 90, 947.
16. P. Renoud, B. Toury, S. Benayoun, et al., *PLoS ONE* 7(7): e39367.2012, **2012**, doi: 10.1371/journal.pone.0039367.
17. N. Aissaoui, L. Bergaoui, J. Landoulsi, et al., *Langmuir,* **2012**, 28, 656.
18. G. Forget, L. Latxague, V. Héroguez, et al. In: *Conf. Proc. IEEE Eng Med Biol Soc.* **2007**, 5107.
19. P.W. Kämmerer, M. Heller, J. Brieger, et al., *Eur Cell Mater* **2011**, 21, 364-372.
20. M. Dettin, T. Herath, R. Gambaretto, et al., *J.Biomed Mater Res A*., **2009**, 1, 463.
21. H. Huang, Y. Zhao, Z. Liu, et al., *J Oral Implantol.* **200**3, 29, 73.
22. J. Kim, P. Seidler, L.S. Wan, et al., *J. Colloid Interface Sci.,* **2009**, 329, 114-119.
23. J.P. Matinlinna, S. Areva, L.V.J. Lassila, et al., *Surf. Interface Anal*., **2004**, 36, 1314-1322.
24. T.T. Nguyen, M. Raupach and L.J. Janik, *Clays Clay Miner,* **1987**, 35, 60-67.
25. J. Zhu, C. Tang, K. Kottke-Marchant, et al., *Bioconjug Chem*., **2009**, 20, 333-339.
26. C.I. Tomuleasa, V. Foris, O. Soritau, et al., *Rom. J. Morphol. Embryol.,* **2009**, 50, 349-355.

COMPARATIVE EVALUATION OF THE APICAL SEALING ABILITY OF FOUR DENTAL MATERIALS USED IN ENDODONTIC SURGERY – AN *IN VITRO* STUDY

ANDREEA IULIANA GULIE (căs. KUI)[a,*], GHEORGHE ZSOLT NICULA[b], CODRUTA POPESCU[c], EUGEN MIRONESCU[d], MANDRA BADEA[e]

ABSTRACT. The aim of this in vitro study was to assess dye microleakage and sealing ability of four dental materials: a polycarboxilate cement (Adhesor Carbofine® - Spofa Dental), a glass ionomer cement (Kavitan Plus®- Spofa Dental), a composite resin (Core-It®- SpiDent) and a MTA based cement (MTA Fillapex®- Angelus). Forty, extracted, human teeth with single root canals were selected for this study. The teeth were randomly divided into four study groups and one control group. The root canals were instrumented and filled with gutta-percha and sealer. Root-ends were resected and 3 mm deep cavities were prepared. Root-end cavities were filled, each with a type of material. Methylene blue dye was used for determination of dye leakage. Afterwards, Scanning Electron Microscopy was used to evaluate the sealing ability of each material. Kolgorow-smirnow z test was used to determine the type of data distribution. One-way analysis of variance (ANOVA) followed by a Tukey test were used to determine the statistical difference between groups, with $P < 0.05$ set as significant. All the four sealers produced apical leakage to a certain extent and there was no statistically significant difference between the five experimental groups. For SEM evaluation, the results showed that there is a statistically significant difference between the control group and the Adhesor Carbofine group. MTA based cement provides leakage results comparable to other commonly used root-end filling materials.

Keywords: Electronic microscopy, Composite cements, Cement paste, MTA

---

[a] *University of Medicine and Pharmacy "Iuliu Hatieganu", Faculty of Dentistry, Department of Prosthodontics, Cluj-Napoca, Romania*
[b] *University of Medicine and Pharmacy "Iuliu Hatieganu", Faculty of Medicine, Dept. of Cell and Molecular Biology, Pasteur St. No. 6, Cluj-Napoca, Romania*
[c] *University of Medicine and Pharmacy "Iuliu Hatieganu", Faculty of Medicine, Department of Socio-Humanistic Sciences – History of Medicine, Cluj-Napoca, Romania*
[d] *University of Medicine and Pharmacy "Iuliu Hatieganu", Faculty of Medicine, Dept. of Cell and Molecular Biology, Pasteur St. No. 6, Cluj-Napoca, Romania*
[e] *University of Medicine and Pharmacy "Iuliu Hatieganu", Faculty of Dentistry, Department of Dental Prevention, Cluj-Napoca, Romania*
* *Corresponding author: guile.andreea@umfcluj.ro*

INTRODUCTION

In endodontic therapy, non-surgical treatments and re-treatments are indicated and are considered a first option in the presence of persistent apical periodontitis. When optimal results cannot be achieved by a non-surgical orthograde re-treatment, then endodontic surgery is indicated. [1]

Apicoectomy (apicectomy/root-end resection) with retrograde obturation is a widely applied procedure in endodontics, when all efforts for the successful completion of orthograde endodontic therapy have failed. The main purpose of endodontic treatment is to eliminate micro-organisms from the root canal systems and prevent its re-infection. [2] In vitro studies suggest that a root-end filling is essential to prevent leakage from root canal space and dentinal tubes.

Placing a root-end filing material during periapical surgery should guarantee the complete sealing of the root canal. A correct apical sealing avoids recontamination and leads to a reduction of microorganisms, therefore to a successful treatment. [3]

Several materials have been indicated as root-end filling materials, though each of these materials has its own limitations. Different materials have been used in this direction, such as amalgams, ZOE cements, glass ionomer cements, composites. [5]

Zinc polycarboxylate cement consists of a powder which contains zinc-oxide, magnesium oxide, bismuth, aluminium oxides and stannous fluoride. The bond strength to enamel is greater than to dentin. The sealing ability of policarboxylate cement, using dye penetration methods is inferior to amalgam. [6]

Glass ionomer cement was introduced in the early 1970's as a new restorative material. The sealing ability of light-curing glass ionomer cements was significantly better than amalgam and also slightly better than conventional glass ionomer cements. [6]

The use of composite resin in addition to bonding agents is likely to produce a leak-resistant seal. There are studies showing an excellent long term success of composites along with dentin bonding agent, but presence of a dry field during placement is important. In addition, some components found in conventional composite resins, like inorganic fillers and silane coupling agent may be the reason why the materials presents anti-bacterial effects against bacteries like *P. gingivalis, P. intermedia, E. foecalis and P. endodontalis*. [6]

Mineral Trioxide Aggregate (MTA) has shown excellent seal and hard tissue repair compared with other root-end filling materials. Its main advantages are osteogenic and regenerative potential, biocompatibility and also anti-bacterial properties against *E. foecalis, S.aureus, P. aeruginosa,* especially when used after mixing with 0, 12% clorhexidine. [6]

It is a real challenge to design and test in laboratory a reliable experimental procedure that can be easily repeated and be clearly in explaining the results. Therefore, as an attempt to solve this problem, different methods, such as dye bacterial leakage or microscopy analysis, were suggested in order to assess the sealing ability of different root-end filling materials. [3] Our study aims a comparative evaluation of dye leakage and apical sealing ability for a polycarboxilate cement (Adhesor Carbofine® - Spofa Dental), a glass ionomer cement (Kavitan Plus® - Spofa Dental), a composite resin (Core-It® - SpiDent) and a MTA based cement (MTA Fillapex® - Angelus).

RESULTS AND DISCUSSION

For the dye-leakage evaluation, linear dye penetration was measured independently by two observers at two different times under same conditions; the mean value of the recorded measurements was chosen as the extent of dye penetration into each specimen. For each image, two measures were made, annotated with "Dim L" and "Dim R"; the annotation reveals the side of the root-canal where the measures were made, respectively left and right. All the four sealers produced apical leakage to a certain extent. The teeth in the control group showed maximum penetration. There was no statistically significant difference between groups (Dim.R) regarding apical leakage as determined by one-way ANOVA (F (4, 40) = 2.009, p = .115). Also, there was no statistically significant difference between groups (Dim.L) regarding apical leakage as determined by one-way ANOVA (F (4, 40) = 1.58, p = .201). (Table 1)

For the SEM evaluation the measures were made on the calibrated images obtained. The measures were made by two observers at two different times under same conditions; the mean value of the recorded measurements was chosen as the extent of the gap size for each specimen. There were chosen four points to measurement for each root, two different points for each side (left and right) of the root-canal filling (first point at the bottom and the second point at the top of the root-end filling). (Figure 1)

Table 1. Results of micro-leakage assessment of the five experimental groups

	Group	Dye penetration length Mean (μm) ±SD	Nr. Teeth	F	p	p1	p2	p3	p4	p5
Dim.R	CG	1.58±0.77	8			-	.579	.885	.983	.921
	PC	1.07±0.96	8			.579	-	.136	.877	.166
	GI	1.37±0.46	8	2.009	.115	.885	.136	-	.591	1.00
	MTA	1,32±0.46	8			.983	.877	.591	-	.653
	CR	1.94±0.82	8			.921	.166	1.00	.653	-

	Group	Dye penetration length Mean (μm) ±SD	Nr. teeth	F	p	p1	p2	p3	p4	p5
Dim.L	CG	1.52±0.77	8			-	.730	.993	.980	.771
	PC	1.07±0.96	8			.730	-	.924	.960	.138
	GI	1.37±0.46	8	1.58	.201	.993	.924	-	1.00	.516
	MTA	1.32±0.46	8			.980	.960	1.00	-	.431
	CR	1.94±0.82	8			.771	.138	.516	.431	-

Dim.R and Dim.L – the places where the measures were made for the apical leakage test, SD – standard deviation; CG – control group, PC – polycarboxylate cement, GI – glass ionomer cement, MTA – MTA based cement, CR – composite resin; F and P – values by one-way ANOVA; p1 – compared with CG; p2 – compared with PC; p3 – compared with GI; p4 – compared with MTA; p5 – compared with CR
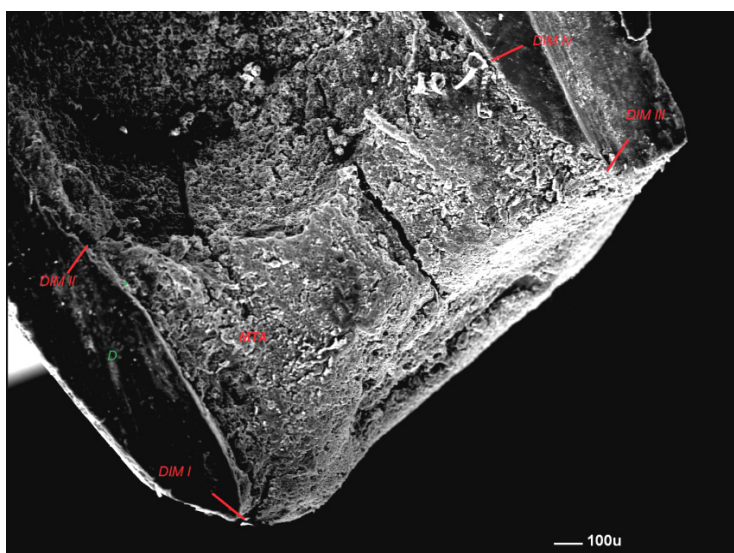
Figure 1. - SEM image in sagittal view, showing retrofilling material/dentin interface. D - dentin, MTA – MTA based cement; DIM. I to IV – the points where the measures were made for each sample SEM – Scanning Electron Microscopy (magnification 45x)

There was a statistically significant difference between groups as determined by one-way ANOVA ($F_{(4, 40)}$ = 3.28, p = .015). A Tukey post-hoc test revealed that dim.I was statistically significantly lower in CG (13.45±5.99μm, p= .006) comparing to PC group (51.90±25.41μm), as well as the dim.II was statistically significantly lower in CG (9.75±4.27μm, p= .020) comparing to PC group (41.86±24.53μm). A Tukey post-hoc test revealed that dim.III was

statistically significantly lower in CG (9.99±3.98µm, p= .041) comparing to PC group (39.02±29.23µm). Also dim. IV was statistically significantly lower in CG (7.33±5.31µm, p= .019) comparing to PC group (47.98±41.11µm).

There was also a statistically significant difference in CR group (9.23±6.61µm, p=.028) comparing to PC group (47.98±41.11µm) regarding just dim.IV. There were no statistically significant differences between GI and MTA groups (p = .538) and between PC and MTA groups (p=.466). (Table 2)

Table 2. Results of SEM evaluation of sealing ability for the five experimental groups

	Group	The gap size Mean(µm)±SD	Nr. teeth	F	P	p1	p2	p3	p4	p5
Dim.I	CG	13.45±5.99	8	4.61	.004	-	.006	.096	.653	.979
	PC	51.90±25.41	8			.006	-	.773	.146	.024
	GI	39.97±31.73	8			.096	.773	-	.742	.279
	MTA	27.45±18.94	8			.653	.146	.742	-	.928
	CR	19.21±8.25	8			.979	.024	.279	.928	-
		The gap size Mean(µm)±SD	Nr. teeth	F	P	p1	p2	p3	p4	p5
Dim.II	CG	9.75±4.27	8	4.76	.004	-	.020	.057	.603	1.00
	PC	41.86±24.53	8			.020	-	.993	.388	.017
	GI	37.63±23.86	8			.057	.993	-	.647	.048
	MTA	24.04±26.97	8			.603	.388	.647	-	.559
	CR	9.06±5.90	8			1.00	.017	.048	.559	-
		The gap size Mean(µm)±SD	Nr. teeth	F	P	p1	p2	p3	p4	p5
Dim.III	CG	9.99±3.98	8	3.36	.020	-	.041	.052	.858	.859
	PC	39.02±29.23	8			.041	-	1.00	.302	.302
	GI	38.08±28.72	8			.052	1.00	-	.350	.350
	MTA	19.70±12.52	8			.858	.302	.350	-	1.00
	CR	19.70±8.58	8			.859	.302	.350	1.00	-
		The gap size Mean(µm)±SD	Nr. teeth	F	P	p1	p2	p3	p4	p5
Dim.IV	CG	7.33±5.31	8	3.28	.015	-	.019	.433	.503	1.00
	PC	47.98±41.11	8			.019	-	.538	.466	.028
	GI	28.73±17.02	8			.433	.538	-	1.00	.525
	MTA	27.28±32.09	8			.503	.466	1.00	-	.598
	CR	9.23±6.61	8			1.00	.028	.525	.598	-

Dim. I to IV – the points where the measures were made for each sample; SD – standard deviation; CG – control group, PC – polycarboxylate cement, GI – glass ionomer cement, MTA – MTA based cement, CR – composite resin; F and P – values by one-way ANOVA; p1 – compared with CG; p2 – compared with PC; p3 – compared with GI; p4 – compared with MTA; p5 – compared with CR

The present study compared the sealing ability of four root-end filling materials (Adhesor Carbofine®, Kavitan Plus®, MTA Fillapex® and Core-It®). This research compared these four different materials under the same conditions, which represents a novelty for the experimental studies regarding root-end fillings. Also, the materials were compared using two methods of evaluation in order to determine more accurate results.

For the evaluation of apical leakage, the results failed to demonstrate any significant difference between the four root-end fillings materials used. This method, using dye penetration, has been chosen in order to assess microleakage. We used methylene blue because it is not expensive, has a high degree of staining and has a lower molecular weight than bacterial toxins. The limitation of dye leakage studies is that they measure the degree of leakage in only one dimension, which makes it impossible to evaluate the total amount of leakage. [14, 15, 16, 17]

Figure 2. - SEM image in sagittal view, showing retrofilling material/dentin interface. D- dentin, PC – polycarboxylate cement; SEM – Scanning Electron Microscopy (magnification 200x)

For Scanning Electron Microscopy (SEM) evaluation the results demonstrate a significant difference in sealing abilities between the control group and the first group (Adhesor Carbofine®). Polycarboxylate cement has not a specific indication when used as a root-end filling material, studies showing that it leaks at level significantly greater than amalgam or gutta-percha.

Significant differences were found between the control group and poycarboxylate cement, meaning that policarboxilate cement showed a lower sealing ability than the sealer used in control group. (Image 2) [18]

In our study, MTA Fillapex® was used as a MTA based cement. This material was developed as a paste/paste sealer in a formulation that allows its appropriate insertion into the root canal. [22] MTA contains tricalcium silicate, tricalcium aluminate, tricalcium oxide, silicate oxide and other mineral oxides forming a hydrophilic powder which sets in presence of water. Several studies have indicated that MTA exhibits significantly lesser leakage than other materials. [5, 18, 20, 21] The results found in this research showed a good sealing ability for MTA Fillapex, but not significantly different when compared with the other materials studied. (Image 3)

Figure 3. - SEM image in sagittal view, showing retrofilling material/dentin interface. D- dentin, MTA – MTA based cement; SEM – Scanning Electron Microscopy (magnification 45x)

Glass ionomer cements can be used for repairing perforated root canals or as retrograde root fillings. [19] Sealing ability of glass ionomer cements was adversely affected when the root end cavities were contaminated with moisture at the time of placement of cement. [18] Although in our study the root end cavities were completely dry before applying the glass ionomer cement, the sealing ability of Kavitan Plus® was poor. (Image 4) In our study, there was no statistically significant difference between the sealing ability of glass ionomer cement and the other three materials used.

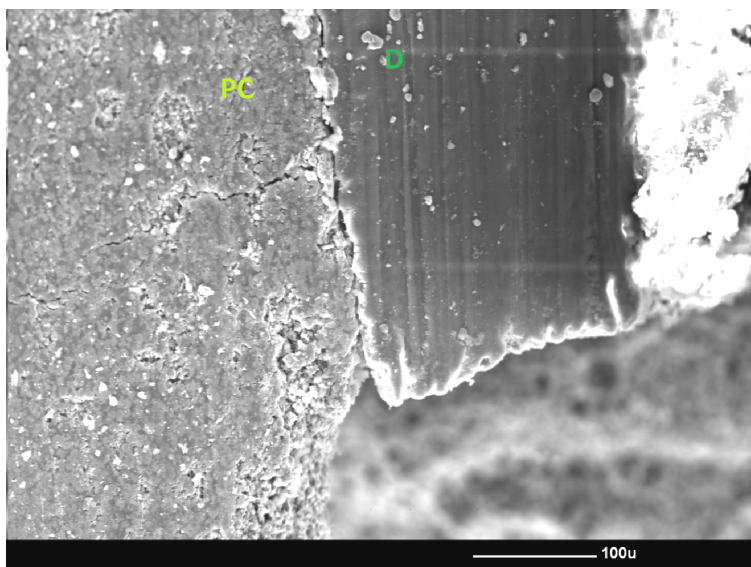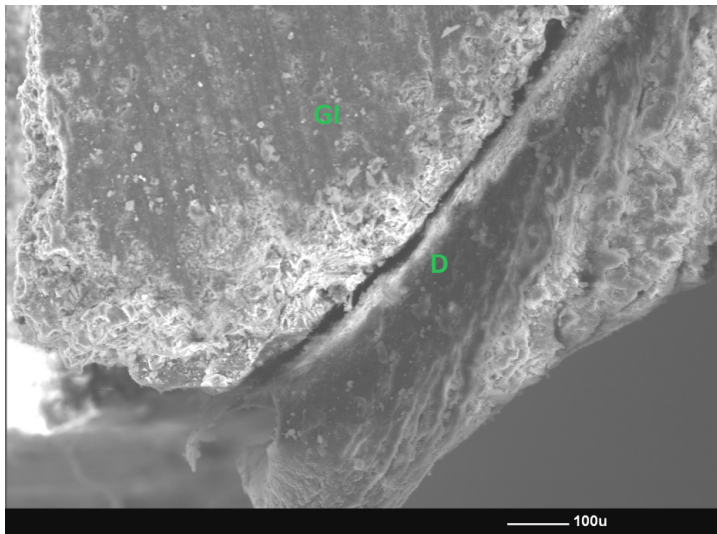**Figure 4.** - SEM image in sagittal view, showing retro-filling material/dentin interface. D- dentin, GI– glass ionomer cement; SEM – Scanning Electron Microscopy (magnification 100X)

Figure 5. - SEM image in sagittal view, showing retrofilling material/dentin interface. D- dentin, CR – composite resin; red arrows showing the cracks in the material; SEM – Scanning Electron Microscopy (magnification 45X)

The composite resin has a good sealing ability, which was proven also in this study. In clinics, the composite resin presents difficulties in endodontic surgery, because the presence of a dry field during placement is mandatory. [6,18] In our study, composite resin (Core-It®) showed a good sealing ability, in association with a bonding agent, but the SEM images revealed cracks in the material. (Image 5)

CONCLUSIONS

Within the limitations of this study the results in the present study revealed no difference in microleakage between all four materials used as root-end fillers.

Scanning Electron Microscopy (SEM) evaluation showed a significant difference between the sealing ability of polycarboxylate cement versus the control group. No statistically significant difference was observed between the four materials used in this experimental study. However, further *in vitro* and *in vivo* investigations should be conducted to assess the sealing ability of each material used in this study.

EXPERIMENTAL SECTION

Forty, extracted, human teeth with single, straight root canals were selected for this *in vitro* experimental study. The teeth were extracted for different periodontal problems and stored in distilled water and thymol (0, 2%) until use. The study was approved by the Ethics Committee of the University of Medicine and Pharmacy "Iuliu Hațieganu", Cluj Napoca (Protocol No. 805/ 25.06.2013).

Teeth surfaces were scaled in order to remove calculus and were immersed in NaOCl 5,25% in order to remove organic tissue. After 1 h of immersion in NaOCl, an orifice was created inside each tooth's crown, as an access for the root canal, using a high speed hand piece under continuous water spray.

A #15 K-file (Dentsply®) was used to establish the working length for each root canal. Crown-down root canal preparation was performed using a 0.06 ProTaper (Dentsply®) rotary instruments to the size of #40. During mechanical preparation, 5ml of 5,25% NaOCl was used for irrigation and at the end of the chemo-mechanical preparation, as the final flush, 5 ml of sterile saline were used. Root canals were dried with paper points (Gapadent®) and obturated with gutta-percha (Gapadent®) and sealer AH26 sealer (Dentsply, DeTrey, Konstanz, Germany) by the lateral condensation method. IRM cement was used to fill the coronal cavities. Afterwards, the sealer set completely for 24h.

From each root, a 3mm apical region was removed perpendicular to the long axis of root, under continuous water irrigation. The teeth were then divided into five groups, first group being the control group. In the control group we included 8 teeth with the apicoectomy made and for the other 4 groups of teeth, using a 008 diamond root bur; the root-end cavities were prepared, to a depth of 3 mm. For the second group the root-end cavity was filled with Adhesor Carbofine®, for the third group the cavities were filled with Kavitan Plus®, for the teeth in the forth group it was used MTA Fillapex® and for the fifth group a composite resin, Core-It® it was used, after applying etching gel and a bonding. For the last group, the material was immediately light cured for 40 seconds. All materials were prepared according to the manufacturer's directions. After the set of the materials, all specimens were stored in distilled water at 37^0C at 100% humidity for 72h.

Study A: Evaluation of apical leakage

All the external surfaces were coated with two layers of nail polish except the sectioned apical region. [8] All the teeth were afterwards immersed in methylene blue 1% for 24h. The samples were then taken out of the methylene blue and sectioned longitudinally by grooving the roots with a diamond disk in the bucco-lingual direction and splitting them with a chisel. All sections were photographed under a light microscope at 10X magnification using a digital camera and the images were analyzed using Cell D (Olympus) program. Afterwards, for each sample it was measured the length of dye penetration. Linear dye penetration was measured independently by two observers at two different times under same conditions; the mean value of the recorded measurements was chosen as the extent of dye penetration into each specimen. [9]

Study B: SEM evaluation

The sections obtained from the teeth were immersed in 6 mol LHCl for 30s, for acid dissolution (inorganic part), and 1% NaOCl for 30 min (organic part) and dried for 24h. Afterwards, the samples were mounted on aluminium stubs, gold sputtered in a Polaron E-5100 plasma-magnetron sputter coater (Polaron Equipment Ltd., Watford, Hertfordshire, UK) in argon atmosphere [10] of about 20 nm and then examined under Scanning Electron Microscopy (SEM) (*Jeol JSM 25S - Jeol, Japan*) at different magnifications (45X, 70x, 100x, 200x, 300x and 700x) for adaptation of each root-end material into the canal walls and the findings were measured, for each sample choosing 4 points to measure. All the images were captured using image processor Deben Pixie–3000 (Deben UK Ltd., Debenham, Suffolk, UK) [11] and then calibrated for measuring using a Cell^*D* software (Olympus Imaging Software Solutions, Germany) [12] Sagital

examination was performed, as the roots were sectioned longitudinaly. The Image tool programe includes functions as dimensional (distance, angle, perimeter, area) and gray scale measurement. The gap size was measured at four points in the longitudinal section. [13]

Statistical analysis was performed by SPSS software package, Version 21.0 for Windows (SPSS Inc. Chicago, IL, USA). Quantitative values are presented as mean ± standard deviation (SD). Kolgorow-smirnow z test was used to determine the type of data distribution. One-way analysis of variance (ANOVA) followed by a Tukey test were used to determine the statistical difference between groups, with $P < 0.05$ set as significant.

ACKNOWLEDGMENTS

<div align="center">

REFERENCES

</div>

1. Ashraf H., Faramarzi F., Paymanpour P., *Iranian Endodontic Journal*, **2013**, *8*, 177.
2. Moradi S., Ghoddusi J., Forghani M., *Journal of Endodontics*, **2009**, *31*, 1563.
3. Kazem M., Mahjour F., Dianat O., Fallahi S., Jahankhah M., Root-end filling with cement-based materials: *Dental Research Journal* (*Isfahan*), **2013**, *10*, 46.
4. Friedman S., *Journal of Endodontics*, **2011**, *37*, 577.
5. Torabinejad M., Ford P., Rooi T.R., *Endodontics and Dental Traumatology*, **1996**, *12*, 161.
6. Priyanka S.R., *Journal of Medical and Dental Sciences*, **2013**, *9*, 20.
7. Castelucci A., Endodontics, Second edition. Il Tridente, **2003**, 548.
8. Kumar N.S., Palanivelu A., Narayanan L.L., *Journal of Conservative Dentistry*, **2013**, *16*, 449.
9. Shahi S., Yavari H.R., Rahimi S., Eskandarinezhad M., Shakouei S., Unchi M., *Journal of Oral Sciences*, **2011**, *53,* 517.
10. G. Nicula, St. Balici, A. Florea, E. Mironescu, R. Munteanu, P. Murea, Gh. Benga, *Annals of the Romanian Society for Cell Biology*, **2010**, *15,* 22.
11. Flegler S.L., Heckman J.W., Komparens K.L., Scanning and transmission electron microscopy: an introduction, W.H. Freeman and Comp., New York, **1993**, 151.
12. Dudea D., Florea A., Mihu C., Câmpeanu R., Nicola C., Benga Gh., *Romanian Journal of Morphology and Embryology,* **2009**, *50*, 435.
13. Khalid, Al-Garawi Z., Al-Hezaimi K., Javed F., Al-Shalan T., Rotstein I., *International Journal of Oral Sciences*, **2012**, 202.

14. Ahlberg K.M., Assavanop P., Tay W.M., *International Endodontic Journal*, **1995**, *28*, 30.
15. Tamse A., Katz A., Kablan F., *International Endodontic Journal*, **1998**, *31*, 333.
16. Wu M.K., Wesselink P.R., *International Endodontic Journal*, **1993**, *26*, 37.
17. Ozata F., Erdilek N., Tezel H., *International Endodontic Journal*, **1993**, *26*, 241.
18. Vasudev S.K., Goel B.R. TS, ABSTRACT. *Endodontology*. **2003**, *15,* 12.
19. Kamel F.M., *Saudi Dental Journal*, **1994**, *6*, 107.
20. Torabinejad M., Higa R.K., McKendry D.J., Pitt Ford T.R., *Journal of Endodontics*, **1994**, *20*, 159.
21. Tang H.M., Torabinejad M., Kettering J.D., *Journal of Endodontics*, **2002**, *28*, 5.
22. Yoshino P., Nishiyama C.K., Modena K.C.D.S., Santos C.F., Sipert C.R., *Brazilian Dental Journal*, **2013**, *24,* 111.

THE STUDY OF NEW COMPOSITES WITH GRAPHENE USED IN DENTISTRY

SORINA SAVA[a,*], CODRUTA SAROSI[b], BOBOIA STANCA[b], ANDRADA TONEA[a], CAMELIA ALB[a], DIANA DUDEA[a]

ABSTRACT. The development of graphene nanopowder in a polymer matrix has opened, in recent years, a new and exciting area in the science of dental materials. Physico-chemical and mechanical properties of these materials are improved at a very low filler loading in the polymer matrix. The novelty of this study is the utilization of graphene-silver nanopowder as filler in new dental composites to improve the physico-mechanical properties. Three experimental composites, two with different percent in graphene-silver nanopowder and one commercial nanohybrid composite Herculite XRV Ultra (Kerr) were investigated by water absorption and solubility in distilled water and artificial saliva (1, 7, 14 and 21 days), respectively flexural strength and Young's modulus properties. One-way analysis of variance (ANOVA) test, for multiple comparisons between means to determine significant differences was used at a significance level set at $p \leq 0.05$. The experimental results show that composite with a greater amount of graphene (G2) present better results of water absorbtion and flexural strength.

Keywords: graphene, dental composites, water sorbtion, flexural strength

INTRODUCTION

The development of graphene nanopowder in a polymer matrix has opened, in recent years, a new and exciting area in the science of dental materials. These nanohybrid materials show a significant improvement in physico-chemical and mechanical properties that cannot normally be achieved using conventional composites, especially for dental composites. The extent of the improvement is related directly to the degree of nanofillers dispersion

[a] *Univestity of Medicine and Pharmacy Iuliu Hatieganu, Faculty of Dental Medicine, 32 Clinicilor Str., RO-400006, Cluj-Napoca, Romania.*
[b] *Babeş-Bolyai University, Raluca Ripan Chemistry Research Institute, 30 Fantanele Str., RO-400294, Cluj-Napoca, Romania.*
* *Corresponding author: savasorina@yahoo.com*

in the polymer matrix. The most important aspect of composites with graphene-silver nanopowder is that all these improvements are obtained at very low filler loading in the polymer matrix [1-4]. There have been studied most graphene composites according to the type of the processing method, the polymer matrix and fillers, but none is being used in dentistry. The interaction mechanism in (polymer/graphene/nanofiller of glasses) composites used in dentistry depends on: polarity, molecular weight, hydrophobicity, particles size and shape, reactive groups, etc., present in the polymer, graphene and nanofiller [5-7]. Composites used in dentistry are available as hybrid types, containing milled glass fillers and discrete nanoparticles (40–50 nm) and as nanofill types [8,9]. They containing both nano-sized filler particles, called nanomers, and agglomerations of these particles described as "nanoclusters". Polymer composites absorb water and release unreacted monomers in an aqueous oral environment. The water ingress into dental composites in the oral cavity can, over time, lead to deterioration of the physical/mechanical properties. There are studies on water absorption [10-13] or ethanol/water solution [11] or ethanol [12] for experimental and commercial light-cured dental composites.

The novelty of this study is the utilization of graphene-silver nanopowder as filler in new dental composites to improve the physico-mechanical properties.

In this study we have three experimental composites, two with different percent of graphene-silver nanopowder, comparing with commercial nanohybrid composite Herculite XRV Ultra (Kerr), in determination of water absorption and solubility in distilled water and artificial saliva (1, 7, 14 and 21 days), respectively flexural strength and Young's modulus properties. The values reported in tables and figures represent mean values and standard deviation of replicates. One-way analysis of variance (ANOVA) test, for multiple comparisons between means to determine significant differences was used at a significance level set at $p \leq 0.05$.

RESULTS AND DISCUSSION

Studies determining the water sorption and solubility of composite materials used in dentistry are especially important for their relative values, while numerical comparisons are not always possible.

The preparation, characterization and properties of graphene as filler in different composites for a large number of polymers are discussed in most papers [14,15,16]. Most of the properties of polymer/graphene composites were superior to the base polymer matrix as well as other carbon filler (carbon nanotubes, carbon nanofiber, and graphite) based composites. These improved properties of the composites are obtained at very low graphene contents (≤2 wt%).

Water sorption is different in many studies [17] and there are several factors influencing water uptake values. Water sorption is a diffusion-controlled process that occurs in the organic matrices, but the kinetics of water sorption is slower for some resins and may not have reached equilibrium even after several days [18]. In these study composites with greater amount of grapheme presented low solubility in saliva and higher solubility in water. The composite experimental without graphene is maintained at constant value in both water and saliva, in solubility and absorption.

Figure 1. The statistical parameters from testing ANOVA at water sorption in distilled water when the comparison has been done for the same day (1, 7, 14, 21) so that it can be seen if is a statistically significant difference between the type the sample for the same day. The statistical parameters obtained through ANOVA test, when comparisons has been done for the same group (G2, G4, G6, H) such that it can be seen that there is no a statistically significant difference between days at same sample type.

Considering only the same day (Figure 1) as a factor, we can say that the studied composite materials G2, G4, G6 and H have a different evolution of water absorption over time, depending on the immersion solution used in the study (Figure 1, 2). In the case of samples immersed in water statistically significant differences were found between measurements made on 7 and 21 days, not identifying significant pairs. For samples in artificial saliva significant differences could not be identified (Figure 2). Water absorption material was identified as having significant values in the case of samples immersion in

water. Immersion in artificial saliva does not seem to determine significant differences in absorption between materials. Comparing the studied composites can be seen (Figure 1) that G2 and G4 had statistically significant differences compared to the Herculite, for water immersion. There were no significant pairs on the artificial saliva immersion studies.
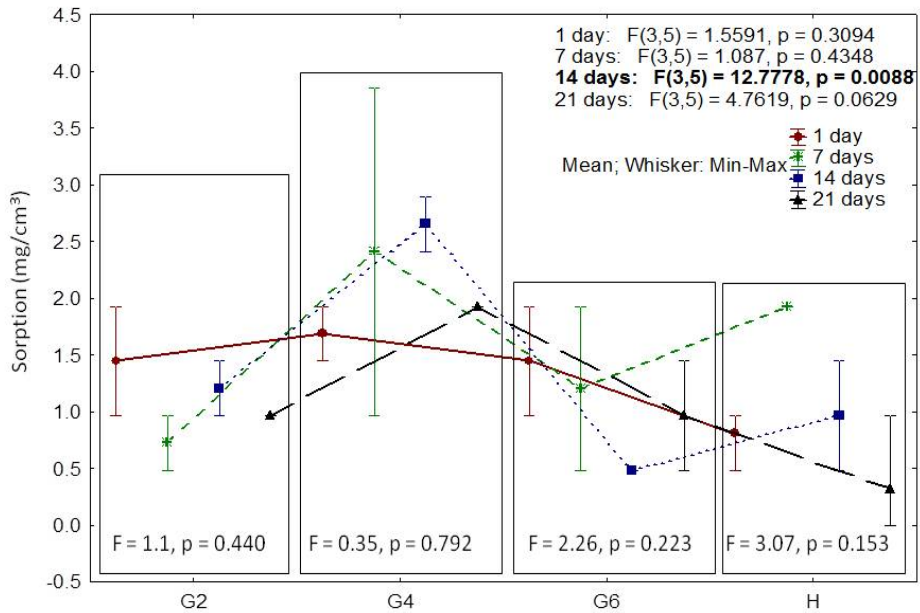
Figure 2. The statistical parameters at water sorption in artificial saliva, when the comparison has been done for the same day (1, 7, 14, 21) so that it can be seen if is a statistically significant difference between the type the sample for the same day. The statistical parameters at water sorption in artificial saliva, when comparisons has been done for the same group (G2, G4, G6, H) such that it can be seen that there is no a statistically significant difference between days at same sample type.

It shows a trend of water absorption increasing for G4 material; a final value at the end of the study relatively equal with the beginning value of the study for the G2 and G6 experimental materials and a slight decline for Herculite. Even if the differences of absorption values can be seen during the experiment, the final value is close to the initial measured value.

Taking into account only the time as a factor, we can say that the studied materials have different solubility evolution (figure 3, 4) in time, regardless of the immersion solution used in the study. A pair wise comparisons material has highlighted that G4 material presented statistically significant differences compared to other materials in both immersion solutions.
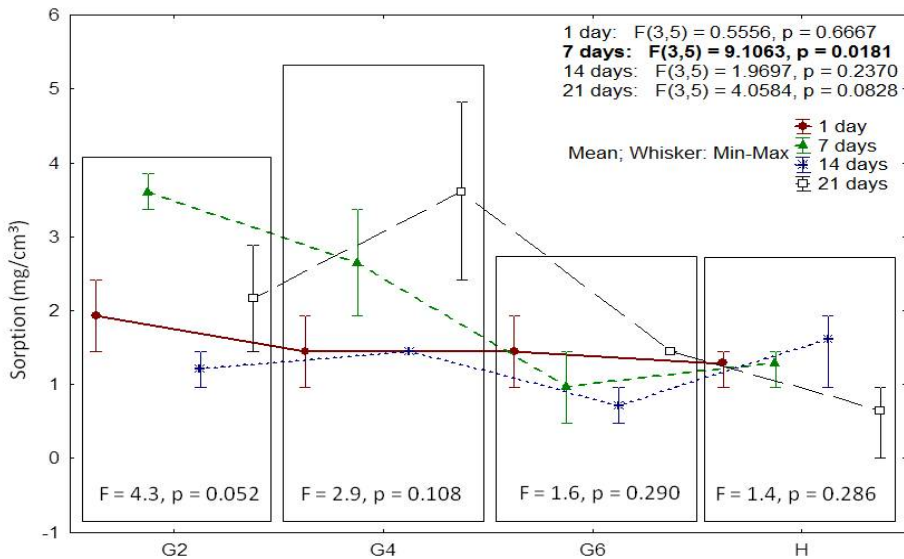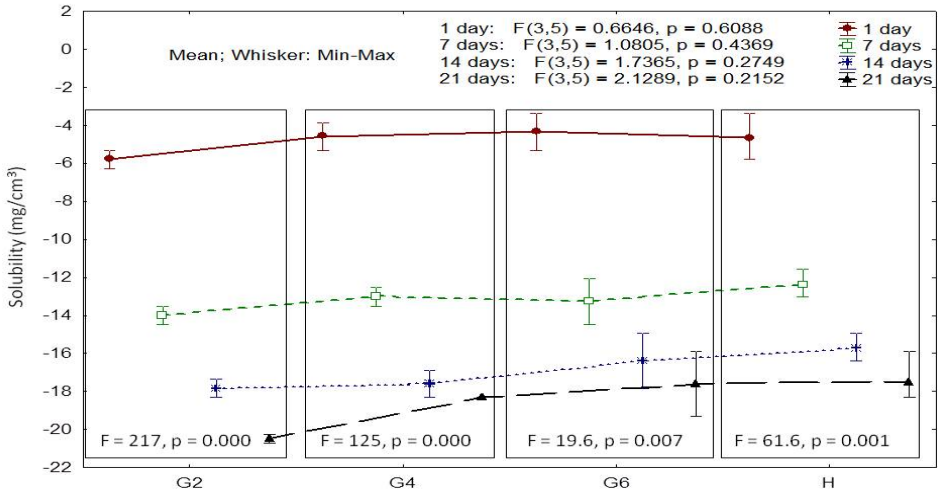
Figure 3. The statistical parameters from testing ANOVA at solubility in distilled water when the comparison has been done for the same day (1, 7, 14, 21) so that it can be seen if is a statistically significant difference between the type the sample for the same day. The statistical parameters obtained through ANOVA test, when comparisons has been done for the same group (G2, G4, G6, H) such that it can be seen that there is no a statistically significant difference between days at same sample type.
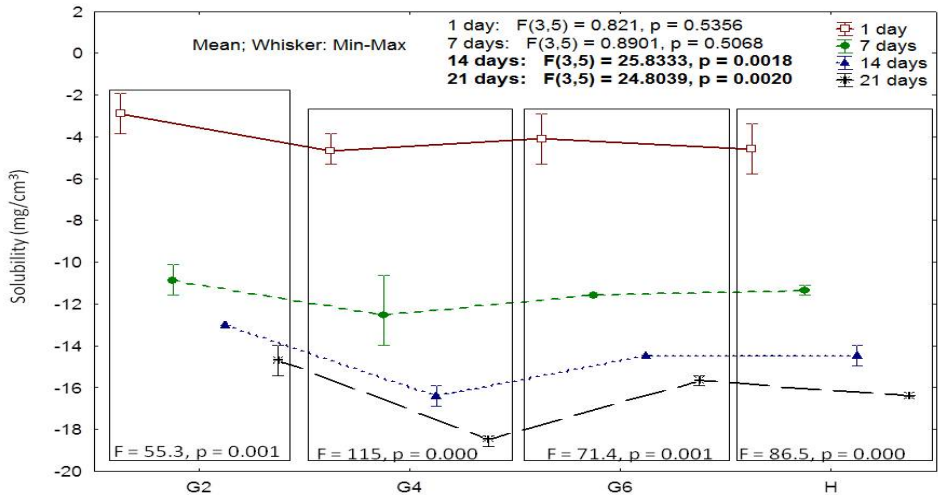
Figure 4. The statistical parameters from testing ANOVA at solubility in artificial saliva, when the comparison has been done for the same day (1, 7, 14, 21) so that it can be seen if is a statistically significant difference between the type the sample for the same day. The statistical parameters obtained through ANOVA test, when comparisons has been done for the same group (G2, G4, G6, H) such that it can be seen that there is no a statistically significant difference between days at same sample type.

Evolution water solubility (figure 3) of the four materials studied it is considered significantly different only between G2 and G4 composites respectively G4 and Herculite. For solubility in artificial saliva (figure 4) it is considered significantly different only between G2 and H composites, respectively G4 and G2. Comparing these two charts remark that the solubility in artificial saliva (figure 4) is lower than solubility in water (figure 3) of experimental materials, while for Herculite composite the values is similar in both medium.

Differences in the chemical composition of the composites considerably influence the degradation behavior of the resins [19]. This is attributed to the different chemistry of their organic matrix. The organic matrix of experimental and commercial composites consists of Bis-GMA and TEGDMA, aromatic and aliphatic dimethacrylate monomers, and show that the aromatic content is higher than that of the aliphatic [20]. Artificial saliva or water uptake in the organic matrix of polymer composites causes generally two opposing processes. The solvent will extract unreacted components, mainly the residual monomer, loss of weight and reduction in mechanical properties [21, 22].

The results obtained for the flexural strength and flexural modulus of the studied composites after immersion in water 37 ± 1^0C for 24 hours are shown in figure 5.
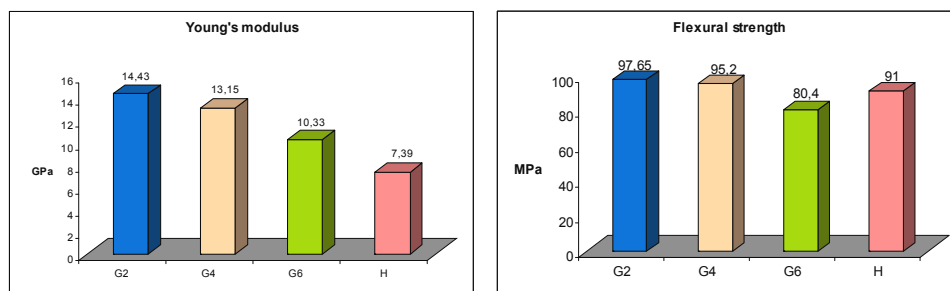
Figure 5. The average values for: a) Young's modulus and b) Flexural strength recorded after 24 hours in distilled water at 37^0C for two composite G2 and G4 with the graphene, two composite, without the graphene, G6 and H

After immersion in distilled water for 24 hours at 37ºC of the four materials studied (G2, G4, G6 and Herculite), G2 showed the greatest flexural strength, and followed by Herculite. This result shows that the flexural strength depends not only on the filler content but also on the filler chemistry. The composite G2 have in composition 10 wt % nanopowder with graphene (HA-Ag graphene). The flexural modulus of composites after immersion for 24 hours day follows the order H < G6 < G4 < G2. Comparison of flexural strength after immersion for 24 hours in water showed the values obtained are comparable and no significant difference was observed for the other

composites. Comparison of flexural modulus after immersion in water did not show any significant difference (p< 0.05) for 24 hours at 37^{0}C. Several researchers [23] have determined the intrinsic mechanical properties of the single, bi- and multiple layers of graphene. After polymerization the composites were immersed in water and artificial saliva. Water or artificial saliva uptake in the polymeric phase of dental composites causes generally two opposing processes. The solvent will extract unreacted components, mainly the residual monomer which leads to loss of weight and reduction in mechanical properties.

CONCLUSIONS

Correlating the results for sorption in water and artificial saliva with mechanical properties (flexural strength and Young's modulus) we can conclude that the experimental composites with a greater amount of graphene (G2) shows better results. After carbon nanotubes, graphene has been reported to have the highest elastic modulus and strength.

EXPERIMENTAL SECTION

Materials

One commercial and three experimental restorative materials were selected for evaluation from physico-mechanical point of view (Table 1).

Table 1. Description of materials used in this study

Material	Organic Phase	Inorganic phase	Company
Experimental nanocomposite G2	Bis-GMA TEGDMA	HA-Ag graphene 10% (%wt) Sr-Zr glass Quartz	ICCRR Cluj-Napoca
Experimental nanocomposite G4		HA-Ag graphene 5% (%wt) Sr-Zr glass Quartz	ICCRR Cluj-Napoca
Experimental nanocomposite G6		Sr-Zr glass Quartz HA	ICCRR Cluj-Napoca
Herculite XRV Ultra (H)	Bis-GMA TEGDMA	Barium glass filler Colloidal silica Prepolymerized filler	Kerr

Bis-GMA - 2,2-bis(4-(2'-hydroxy-3'methacryloyloxy-propoxy)phenyl)propane; **HA** - hydroxylapatite (synthetized in *ICCRR Cluj-Napoca* laboratory); **TEGDMA**- triethyleneglycol- dimethacrylate (Aldrich); **DMAEM**-2-dimethyl(aminoethyl)methacrylate (Aldrich); **Cq-** camphorquinone (Aldrich).

The inorganic filler consists of silanizated powders based on mixture of colloidal silica - SiO_2 (Degussa), hydroxyapatite (HA) with 15% graphene-silver nanoparticles and Sr-Zr bioglass (35-SiO_2, 20-SrO, 10-ZrO_2 10-Al_2O_3, 13-B_2O_3, 6-NaF, 6-CaF_2, wt.%), obtained as a mass through the conventional melting method in ICCRR laboratory. Surface treatment of the fillers was made by γ-methacriloyloxypropyl-trymethoxysilane (A174) (Aldrich).

Graphene-silver nanoparticles (Gr-Ag) composite were synthesized by the Radio-Frequency catalytic Chemical Vapor Deposition (RF-CCVD) method [12] using silver nanoparticles distributed over magnesium oxide (Ag_x/MgO, where x = 3 wt.%). The synthesis was performed using a methane flow rate of 80 mL/min and a reaction time of 60 minutes [24].

The *HA- graphene-silver* nanoparticles (Gr-Ag) were synthesized by precipitation of HA in presence of graphene-silver. The starting materials were CaO, H_3PO_4 (Aldrich) for synthesis of HAP. The mixed sols were subjected to heat treatment at 120°C and 400°C for 2 h.

The organic matrix- monomers mixture consists of: Bis-GMA/TEGDMA in 65/35 ratio. Bis-GMA was synthesised in ICCRR laboratory.

The experimental composites **G2**, **G4**, **G6** were prepared as monopaste, by dispersing in the organic matrix the silanizated bioactive inorganic fillers, in ratio 20/80 wt.%. The comercial composite Herculite XRV Ultra (**H**), in ratio 21/79 wt.%, was used as a reference material. In order to initiate the photochemical curing, there have been introduced in the monomer mixture an initiator system consisting of: *photosensitizer* - camphorquinone (Aldrich) 0.5% relative to the liquid mixture and a *polymerization accelerator* 2-dimethyl (aminoethyl)methacrylate (Aldrich) 1%.

Methods

A total of four groups were formed. For the water sorption and solubility measurements, ten disc specimens were prepared for each material. A mold for the preparation of a disc specimen 15+1 mm in diameter and 1 mm thickness was used. Sorption and solubility tests were determined according to the method described in ADA Specification No. 27-1993/ISO 4049/2000 regarding filling materials.

The specimens were light-cured, under a glass microscope slide, with an activated light source (Woodpecker®Dental Curing Light LED.B lamp) polymerization unit. The samples were irradiated in different positions for 40 s until the entire area was exposed. The discs removed from the mould were dried in the desiccator in the presence of calcium chloride at 37 ± 1° C for 24 hours. Before being weighed, the specimens are kept in the desiccator at 23° C. Weighed discs are divided into 2 groups, prior to be immersed in

distilled water and artificial saliva respectively, at 37 ± 1°C and maintained for 1:7:14:21 days (during which theirs weight was measured daily). After this time, discs were removed from water or artificial saliva with tweezers, wiped with paper, air-dried for 15 seconds and 1 minute after removal samples are weighed. The extent of absorption in water and artificial saliva for each disc was calculated using the formula:

$$Wsp = (m_2 - m_3) / V$$

where: m_2 - mass of the sample after immersion in water for 24 h (µg)
m_3 - mass of the sample kept in desiccator until constant mass (µg)
V - volume of the sample (mm^3)
Solubility tests were performed on the same composites (G2, G4, G6, H). Solubility tests were completed using the same samples as for absorption test, by maintaining the discs in water and artificial saliva at 37°C and values were recorded at 1, 7, 14 and 21 days Experimental values for solubility are expressed in µg/ mm^3 using the formula:

$$SL = (m_1 - m_3)/V$$

Where: m_1 – constant weight of the sample before water immersion (µg)
m_3 – constant weight of the sample maintain in the desiccator (µg)
V – Sample volume (mm^3)
The specimens for the mechanical tests, flexural strength (FS), were performed at 23°C, according to ISO 4049/2000. The samples were prepared using teflon molds with 2x2x25mm which did not offer resistance to the displacement of the specimen, minimizing the formation of cracks and flaws within the bulk material and surface during their preparation. After 24 ± 1 h , the specimens were loaded at a crosshead speed of 0.5 mm/min until fracture with a Lloyd Instruments-LR5k Plus mechanical testing machine controlled, using the Nexygen Software on a Windows PC.

ACKNOWLEDGMENTS

REFERENCES

1. V. Singh, D. Joung, L. Zhai, S. Das, S. I. Khondaker, S. Seal, *Progress in Materials Science*, **2011**, *56*, 1178
2. Z.-S. Wu, W. Ren, L. Gao, B. Liu, C. Jiang, H. M. Cheng, *Carbon,* **2009**, *47*, 493
3. C. Lee, X. Wei J. W. Kysar, J. Hone, *Science*, **2008**, *321*, 385
4. S. Stankovich,D.A. Dikin, G.H.B. Dommett, K.M. Kohlhaas, E. J. Zimney, E. A. Stach, *Nature*, **2006**, *442*, 282
5. Z. Fan, J. Wang, Z. Wang, H. Ran, Y. Li, L. Niu, P. Gong, B. Liu, S. Yang, *Carbon*, **2014**, *66*, 407
6. A. Cândido dos Reis, D. Tornavoi de Castro, M. A. Schiavon, L. Jardel da Silva, J.A. Marcondes Agnelli, *Brazilian Dental Journal*, **2013**, *24*, 599
7. S. Thomaidis, A. Kakaboura, W. D. Mueller, S. Zinelis, Dental Materials, **2013**, *29*, 132
8. M. O. Daltoé, C. P. Lepri, J. G. Wiezel, D. C. Tornavoi, J. A. M. Agnelli, A. C. Reis, *Minerva Stomatol*, **2013**, *62*, 63
9. C. P. Turssi, J. L. Ferracane, K. Vogel K, *Biomaterials*, **2005**, *26*, 4932
10. N. Martin, N. Jedynakiewicz, *Biomaterials*, **1998**, *19*, 77
11. E. Mortier, D. A. Gerdolle, A. Dahoun, M. M. Panighi, American Journal Dentistry, **2005**, *18*, 177
12. D. L. Leonard, D. G. Charlton, H. W. Roberts, M. E. Cohen, *Journal of Esthetic Restoration Dentistry,* **2002**, *14*, 286
13. J. A. von Fraunhofer, P. Jr. Curtis, *Dental Materials*, **1989**, *5*, 365
14. S. Stankovich, D. A. Dikin, R. D. Piner, K. A. Kohlhaas, A. Kleinhammes, Y. Jia, *Carbon,* **2007**, *45*, 1558.
15. J. I. Paredes, S. Villar-Rodil, A. Martinez-Alonso, J. M. D. Tascon, *Langmuir,* **2008**, *24*, 10560.
16. Y. Xu, Z. Liu, X. Zhang, Y. Wang, J. Tian, Y. Huang, *Adv Mater,* **2009**, *21*, 1275
17. I. Sideridou, S.A. Dimitris, C. Spyroudi, M. Karabela, *Biomaterials*, **2004**, *25*, 367
18. D. Dudea, M. Moldovan, L. Silaghi-Dumitrescu, H. Colosi, A. Botos, A. Irimie, C. Alb, *Studia UBB Chemia*, **2010**, *LV 1*, 66
19. S.B. Berger, A.R. Muniz Palialol, V. Cavalli, M. Giannini, *Brazilian Dental Journal*, **2009**, *20*(4), 314
20. C. Sarosi, A. Antoniac, C. Prejmerean, O. Pastrav, D. Patroi, G. Popescu, M. Moldovan, *Key Engineering Materials,* **2014**, *614*, 113
21. C. Lee, X.D. Wei, Q.Y. Li, R. Carpick, J.W. Kysar, J. Hone, *Physica Status Solidi*, **2009**, *246*, 2562
22. I.D. Sideridou, M.M. Karabela, E. Ch. Vouvoudi, *Dental Materials*, **2011**, *27*, 598
23. H. Porwal, S. Grasso, M.J. Reece*, Advances in Applied Ceramics*, **2013**, *12*(8), 443
24. A.R. Biris, S. Ardelean, M.D. Lazar, E. Dervishi, F. Watanabe, A. Ghosh, A. Biswas, A.S. Biris, *Carbon*, **2012**, *50*, 2252

THE USE OF BIODENTINE™ AS A ROOT-END FILLING MATERIAL

ANDREEA IULIANA GULIE (căs. KUI)[a,*], MÎNDRA BADEA[b]

ABSTRACT. Biodentine™ is a calcium silicate based cement and it was released in January 2011 by Septodont (France). The purpose of this study was to evaluate the literature regarding the use of Biodentine™ in order to emphasize the performances and effectiveness of this product in comparison with other dental materials used as retrograde filling materials and also to help clinicians make an informed choice about which dental material should use in periapical surgery. According to the published literature, Biodentine™ could be an efficient alternative to mineral trioxide aggregate or other dental cements to be used as a root-end filling material because of its physical, biological and handling properties. Although it seems it has a good behaviour in clinical practice, more clinical studies are required in order to support the indication as a root-end filling material.

Key words: *Biodentine™, root-end filling, tricalcium silicate cement*

INTRODUCTION

Apicoectomy, followed by a retrograde obturation, is a surgical technique applied in endodontics, when all the efforts for a successful orthograde endodontic therapy have failed. The purpose of the retrograde filling is to seal the root canal and prevent passage of bacteria or their toxins from the canal space into periradicular tissues. A root-end filling material is placed in direct contact with periapical tissues and it should have several qualities as it influences the tissue response and the outcome of surgical endodontic treatment. [1]

An ideal root-end filling material should adhere to the root canal walls and seal the root-end three-dimensionally. It should not promote (preferably it should inhibit) the growth of pathogenic microorganism, be well tolerated

---

[a] *Department of Prosthodontics, Faculty of Dentistry, Iuliu Hatieganu University of Medicine and Pharmacy, Cluj-Napoca, Romania*
[b] *Department of Dental Prevention, Faculty of Dentistry, Iuliu Hatieganu University of Medicine and Pharmacy, Cluj-Napoca, Romania*
* *Corresponding author: guile.andreea@umfcluj.ro*

by periradicular tissues with no inflammatory reactions and stimulate the regeneration of normal periodontium. A root-end filling material should also be dimensionally stable and unaffected by moisture in either the set or unset state; it should be easily distinguished on radiographs and be easy to handle. [2]

Biodentine™ is a calcium silicate based cement and it was released in January 2011 by Septodont (France). According to the manufacturer it can be used for crown and root dentin repair treatment, repair of perforations or resorbtions, apexification and root-end fillings. [3]

The purpose of this study was to evaluate the literature regarding the use of Biodentine™ in order to emphasize the performances and effectiveness of this tricalcium silicate in comparison with other dental materials used as retrograde filling. This will help clinicians make an informed choice about which dental material should use in periapical surgery.

RESULTS AND DISCUSSION

According to the manufacturer, Biodentine™ has large range of applications including endodontic repair (root perforations, apexification, resorptive lesions), as a retrograde filling material in endodontic surgery and as a pulp capping. This calcium silicate cement is performed using the MTA-based cement technology but with some improved properties, such as physical qualities and handling. This material has been frequently studied in recent literature and serves as an important representative of tricalcium silicate based cements; we believe that a review of these researches regarding the properties of Biodentine™ as a root-end filling material is contributory in generating a clearer picture about the general characteristics.

Two independent reviewers (A.G. and M.B.) conducted a literature search for publications from 2004 to November the 1st 2014 in Medline (PubMed) Embase, Web of Science, CENTRAL (Cochrane), Scopus, SciELO and clinicaltrials.gov. The search terms used were "biodentine", "tricalcium silicate", "root-end filling" and "endodontic surgery" (Image 1). The electronic search resulted 1766 articles.

For this review we considered clinical trials, case reports, in vitro studies, in vivo studies and other reviews, all written in English language. We excluded articles written in other languages, short communications and non-topic related articles or articles with no abstract available; from the total of 1766 articles, 52 formed the basis of the present review. Most of the articles were in vitro studies and written between 2012 and 2014. (Image 1)

We organized the present paper in several categories as fallows. In section 1 the mechanical and chemical properties, in section 2 dimensional stability, solubility and push-out bond strength, sealing ability in section 3, section 4 biocompatibility and antibacterial effect and in section 5 radioopacity.
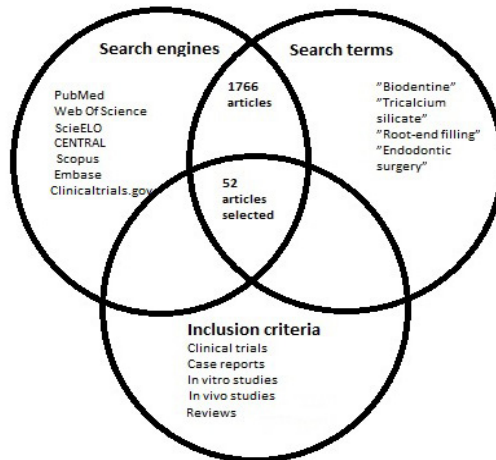
Figure 1. – Overview of the search methodology and selection criteria used in this literature review

1. Composition, mechanical and chemical properties

Biodentine™ is dispensed in a fixed powder: liquid proportion, providing a shorter setting time of 12 min (manufacturer's data sheet). The powder contains a main component (tricalcium silicate), a filler material (calcium carbonate), a radioopacifier (zirconium oxide) and traces of dicalcium silicate, calcium oxide and iron oxide. The liquid is an aqueous solution of a hydrosoluble polymer (water reducing agent) combined with calcium chloride which decreases the setting time. [4,5] Septodont is using a new technological platform named „Active Biosilicate Technology"™ in order to control the purity of the raw materials. This fact is proved also by Camilieri et al. in their study, when they could not found minor elements in the composition of Biodentine™, which can be beneficial for producing dental cements.

The calcium carbonate is used in the powder of Biodentine™ for its biocompatibility and its calcium content. The hydrosoluble polymer in the liquid is based on polycarboxilate and maintains a balance between low water content and consistency of the mixture. [6]

Although setting reaction is not fully investigated it is believed that Biodentine[TM] sets through a hydration reaction. In addition, researchers found a type of interfacial interaction called "the mineral infiltration zone" for calcium-silicate-based cements, including Biodentine[TM]. [7]

When compared to other root-end filling materials (Bioaggregate[TM] or IRM[TM]) Biodentine[TM] proved to have a shorter setting time, a higher compressive strength and micro-hardness and low fluid uptake. The addition of a water-soluble polymer in the liquid allows a higher strength, micro-hardness and very low water-cement ratios. [5]

J. Camilleri evaluated in several studies the properties of Biodentine[TM], especially its porosity. Porosity of tricalcium silicate-based cements occurs as a result of the spaces between the un-hydrated cement grains. [8] After the hydration, these spaces will be filled with water. When used as a root-end filling material, the porosity of Biodentine[TM] is affected by ambient conditions and material additives. Biodentine[TM] is less porous than other tricalcium silicate-base materials. In their study, Camilleri et al. concluded that Biodentine[TM] demonstrated cracks at the interface between root-dentine and the material interface, but also within the bulk of the material.

Biodentine[TM] also demonstrated leakage when used in a sandwich restoration overlaid with composite, both when the material was left unprepared and when it was etched. [9] Apparently, the etching created surface changes for Biodentine[TM] that might have the potential to enhance bonding of resinous materials. [10]

2. Push-out bond strength, solubility and dimensional stability

In case of a periapical surgery, a dental material should provide a strong bond with the canal walls, but also resist to the dislodgement during function. This is why the push-out bond strength is an important quality for a root-end filling. In our search, we found several articles about the push-out bond strength of Biodentine[TM] and other calcium silicate cements.

Aggarwal et al. studied the push-out bond strength of three cements (Biodentine[TM], MTA[TM] and MTA Plus[TM]) when used as a furcation repair material. They used 120 extracted molar, which were divided in groups according to the type of material used, blood contamination and setting time (24 hours and 7 days). The results showed that Biodentine[TM] has a better push-out bond strength than MTA after 24 hours and blood contamination has no effect in the perforations repaired with Biodentine[TM]. [11]

Alhodiry et al. also studied the effect of saliva and blood contamination on bi-axial flexural strength and setting time of Biodentine[TM] and Portland cement[TM]. They confirmed a shorter setting time for Biodentine[TM], than Portland

cement™. The setting time of Biodentine™ was less affected by contaminants when compared to Portland cement™. The authors found no significant difference in bi-axial flexural strength between Biodentine™ and Portland cement™. [12]

Guneser et al. evaluated the effect of various endodontic irrigants on the push-out bond strength of Biodentine™ compared to MTA™, amalgam and Dyract AP™. But after being exposed to various endodontic irrigants, Biodentine™ showed considerable performance as a perforation repair material compared to the other dental materials. [13] Elnaghy obtained similar results when exposed Biodentine™ under the effect of QMix™ and other conventional endodontic irrigants. QMix™ did not affect the bond strength of Biodentine™ and MTA™; Biodentine™ showed higher resistance than MTA™ to dislodgement forces from root dentin. [14]

The push-out bond strength of Biodentine™ and other silicate cements is apparently affected by the presence of smear layer on the canal walls and is also influenced by acidic environment. [15,16]

Few studies were found regarding other mechanical properties: dimensional stability and solubility. Caronna et al. studied the micro-hardness of three dental materials (MTA™, EndoSequence™ and Biodentine™) after setting in moist or dry conditions. They concluded that Biodentine™ setting was unaffected by the artificial periodontal conditions, but ProRoot wMTA™ showed greater hardness than Biodentine™ and EndoSequence™ in either environment tested. [17]

When used as a posterior restoration material Biodentine™ can be used for up to six months, at this time it suffers abrasion but without any marginal discoloration. In a case report published by Sihha et al. Biodentine™ was used as an apical barrier for the apexification of a maxillary right central incisor. After 12 month follow up, the tooth presented no clinical symptoms and on the XRay they observed a progressive involution of periodontal radiolucency and healing with a calcified barrier at the apex. The authors concluded that more clinical studies are needed in order to validate Biodentine™ as a suitable material in apexification, but they suggested that it can be a good alternative to MTA™, as Biodentine™ is simpler to be placed in the root-canal. [18] We also found that another two case reports studies confirm the successful use of Biodentine™ in apexification. [19,20]

3. Sealing ability

The sealing ability is, in fact, the capacity of adherence of a dental material to the canal dentine walls. It is imperative for a root-end filling material to have a good sealing ability, in order to prevent leakage between the root canal and periodontal space. We found only two in vitro studies regarding the sealing ability of Biodentine™ used as a root-end filling. (Table 1) We decided to include in our review another 3 studies where Biodentine™ is used

as a furcation repair material, as the clinical conditions are not very different. Another three clinical studies were found regarding the use of Biodentine[TM] as a root-end filling material.

Ravichandra et al. investigated the marginal adaptation of glass-ionomer cement, MTA[TM] and Biodentine[TM] as a root-end filling material. [21] In another study, Soundappan et al. investigated IRM[TM], MTA[TM] and Biodentine[TM] for their apical seal ability. [22] Both studies used for evaluation transversal sections of the resected roots which were examined by Scanning Electron Microscopy (SEM). In the first study, the authors concluded that Biodentine[TM] had a better marginal adaptation than the other two materials used in the study (MTA[TM] and a glass-ionomer cement). In the second study, Soundappan et al. concluded that Biodentine[TM] had a lower sealing ability at 2 mm depth of the root-end obturation, while MTA[TM] had the best results. Similar results were obtained, within the limits of their study, by Ozbay et al., were Biodentine[TM] exhibited a lower sealing ability than MTA[TM], on a dye penetration test. [23]

When used as a furcation repair material, Biodentine[TM] demonstrated lower sealing capacity than Micro-Mega MTA[TM], Pro-root MTA[TM] or MTA Angelus[TM]. [24,25,26]

Three case reports studies were found, in which Biodentine[TM] was used as a root-end filling material in apicoectomy. In the first study, Caron et al. presented two case reports, both in which they used Biodentine[TM] as a root-end filling material. [27] The follow up was made until 24 months and the authors concluded that although Biodentine[TM] has a low radioopacity, because of its biological properties and its clinical setting time it may be suitable for surgical endodontics. Pawar et al. obtained similar results when using Biodentine[TM] as a root-end filling material, after a periodontal surgery for two teeth that were previously traumatized and with a large periapical lesion. [28]

In the other clinical study, Biodentine[TM] was used successfully as a root-end filling material in the management of a palatogingival groove, because of its good mechanical properties and biocompatibility. [29]

Table 1. – Overview of sealing ability of Biodentine[TM] compared with other materials

Type of study	Evaluation Technique	Follow up	Clinical Aplications	No. of teeth	Materials Tested	Reference
1	2	3	4	5	6	7
In vitro study	Dye penetration	X	Interradicular Furcation	40	MICRO-MEGA MTA[TM]; Endosequence[TM]; Biodentine[TM]	Jeevani et al. (2014) [25]
In vitro study	Dye penetration	X	Interradicular Furcation	84	MTA Angelus[TM]; Biodentine[TM] GC Fuji lining LC[TM]; Aquafix Portland cement[TM]	Nikoloudaki et al. (2014) [26]
In vitro study	SEM evaluation	X	Root-end filling	30	MTA[TM]; Biodentine[TM] IRM[TM]	Soundappan et al. (2014) [22]

Type of study	Evaluation Technique	Follow up	Clinical Aplications	No. of teeth	Materials Tested	Reference
1	2	3	4	5	6	7
In vitro study	Dye penetration	X	Interradicular Furcation	30	Biodentine™; Pro-root MTA™; Calcium Phospfate cement™	Sanghavi et al. (2013) [24]
In vitro study	Dye penetration	X	Root-end filling	21	MTA Angelus™; Biodentine™	Ozbay et al. (2014)[23]
Case report	Xray	24 months	Root-end filling	2	Biodentine™	Caron et al. (2014) [24]
Case report	Xray	24 months	Root-end filling	1	Biodentine™	Johns et al. (2014) [29]
Case report	Xray	18 Months	Root-end filling	2	Biodentine™	Pawar et al. (2013) [28]

4.a. Biocompatibility

Biocompatibility refers to the ability of a material to perform with an appropriate host response in a specific situation. [30] This allows to a biomaterial to perform its desired function with respect to a medical therapy, without eliciting any undesirable local or systemic effects in the recipient or beneficiary of that therapy, but generating the most appropriate beneficial cellular or tissue response in that specific situation, and optimising the clinically relevant performance of that therapy. [31]

We found numerous studies regarding the biocompatibility of Biodentine™. In vitro studies evaluated cytotoxicity on different types of human cells, like osteoblasts, dental pulp cells, fibroblasts, mesenchymal stem cells and monicytes or even murinae odontoblastic cells. (Table 2)

In several studies, the authors mention a good biocompatibility of Biodentine™, which is comparable with MTA–based products (Ortho-MTA™, ProRoot MTA™, MTA Angelus™). However, in their study, Samyuktha et al. concludes that MTA™ had a lower cytotoxicity on human periodontal ligament fibroblasts than Endosequence™ and Biodentine™. [32] Similar results obtained Jung et al. who compared cytotocicity of Biodentine™, MTA™ and Bioaggregate™ on human dental pulp cells. They concluded that both, Biodentine™ and Bioaggregate™ are biocompatible, but Biodentine™ had a relative higher cytotoxicity than MTA™. [33]

We found 2 in vivo studies on animals who evaluated biocompatibility of Biodentine™. The first study, evaluated the effect of Biodentine™ on dog pulp cells. [34] The authors applied Biodentine™ and MTA™ for pulp capping and pulpotomy. There was no statistically significant difference between the two materials. In another in vivo study, the researchers evaluated the subcutaneous tissue reaction of rats in the presence of Biodentine™, MTA™ and zinc oxide eugenol cement. [35] After 14 days, the histological analyses showed good results for Biodentine™ as well as for MTA™.

Nowicka et al evaluated Biodentine[TM] and MTA[TM] as pulp capping materials on teeth scheduled for extraction (orthodontic reasons). After 6 weeks the extractions were made and histological analyses showed a good biocompatibility both for MTA and Biodentine[TM]. [36]

Lee et al. investigated in their study the effect of 3 endodontic bioactive cements (MTA[TM], Biodentine[TM], Bioaggregate[TM]) on the differentiation of mesenchymal cells. Within the limitations of their study, the authors concluded that all three cements induced the differentiation of mesenchymal cells into osteoblasts. [37]

Table 2. - Overview on biocompatibility studies over Biodentine[TM]

Type of study	Type of cells/tissues	Evaluation technique	Materials	Reference
1	2	3	4	5
In vitro study	MG63 osteoblast-like cells	Cytotoxicity using MTT assay; Protein quantification analysis; SEM analysis.	Biodentine[TM]; MTA[TM]	Attik et al. 2014 [42]
In vitro study	Immortalized human dental pulp cell line	Cytotoxicity using3-(4,5-dimethylthiazolyl-2-yl)-2,5-diphenyltetrazolium Bromide Assay; Effect of Materials on Odonto-blastic Differentiation; Signal Pathways of Materials	Biodentine[TM]; MTA Angelus[TM]; Ortho-MTA[TM];IRM[TM]	Chang et al. 2014 [43]
In vitro study	Fibroblast 3T3 cells	Cell Viability Assay; SEM analysis; Measurement of Citokine Expression at the mRNA Level	Biodentine[TM];MTA[TM]; GC Fuji IX[TM]	Corral Nunez et al. 2014 [44]
In vitro study	Human gingival fibroblasts	Flow Cytometry; Cell Adhesion Assay	Biodentine[TM];Pro-root MTA[TM]; GC Fuji IX[TM]	Zhou et al. 2013 [45]
In vitro study	Human periodontal ligament fibroblasts	Cytotoxicity evaluation with trypan blue	Biodentine[TM]; MTA[TM]; Endosequence[TM]	Samyuktha et al. 2014 [32]
In vitro Study	Rat odontoblast cells	Cytotoxicity using MTT assay; Antibacterial effect	Dycal[TM];Calcicur[TM]; Calcimol LC[TM]; TheraCal LC[TM];MTA Angelus[TM];Biodentine[TM]	Poggio et al. 2014 [38]
In vitro study	Murinae odonto-blast cell line	Cytotoxicity evaluation; Confocal Laser Scanning Microscope	Dycal[TM];ProRoot MTA[TM];MTA Angelus[TM]; Biodentine[TM]	Poggio et al. 2014 [47]
In vitro study	MDPC-23 and Od-21 cell lines	Spheroid (3D) formation Real time PCR; Scanning electron microscopy	Biodentine[TM];MTA[TM]	Perard et al. 2013 [48]
In vitro study	Human dental pulp cells	Alkaline Phosphatase Staining and Activity Analysis; Alizarin Red Staining and Quantifi-cation; Quantitative Real-time Reverse-transcrip-tase Polymerase Chain Reaction	Biodentine[TM]	Luo et al. 2014 [49]

Type of study	Type of cells/tissues	Evaluation technique	Materials	Reference
1	2	3	4	5
In vitro study	Mesenchymal stem cells	Cell Viability Assay; Reverse-transcription Polymerase Chain Reaction and Quantitative Real-time Polymerase Chain Reaction; ALP Staining	Biodentine™ MTA™; Bioaggregate™	Lee et al. 2014 [37]
In vitro study	Human dental pulp cells	Direct pulp capping with Biodentine; TGF-b1 secretion by pulp cells	Biodentine™	Laurent et al. 2012 [50]
In vitro study	Human monocytes	Cytotoxicity assay	ProRoot MTA™; Biodentine™; CEM cement™; Tech Biosealer™	Khedmat et al. 2014 [51]
In vitro study	Human dental pulp cells	Cell viability assay; Reverse transcription-polymerase chain reaction; Alizarin red S staining; Western blot analysis	Biodentine™; MTA™; Bioaggregate™	Jung et al. 2014 [33]
In vitro study	Human dental pulp cells	Cell proliferation assay; Migration assay; Adhesion assay; Quantitative real-time reverse-transcriptase polymerase chain (qRT-PCR)	Biodentine™	Luo et al. 2014 [53]
In vitro study	Human dentin	Hydroxyproline Assay; Transmission Electron Microscopy	Biodentine™; MTA Plus™	Leiendecker et al. 2012 [54]
In vivo study	Dogs pulp cells	Qualitative and quantitative histopathologic analyses	ProRoot MTA™; Biodentine™	Rossi et al. 2014 [34]
In vivo study	Rats subcutaneous tissue	Histopathologic analyses	Zinc oxide eugenol™; MTA Angelus™; Biodentine™	Mori et al. 2014 [35]
In vivo study	Human dental pulp	Clinical examination; Histopathologic analyses	Biodentine™; MTA™	Nowicka et al. 2013 [36]

4.b. Antibacterial effect

A biocompatible dental material should not only promote tissue repair reaction, but it should have antibacterial and healing induction properties. [38] This is why Poggio et al. found necessarily to test the antibacterial effect of several cements used in endodontics (Dycal™; Calcicur™; Calcimol LC™; TheraCal LC™; MTA Angelus™ and Biodentine™). The results showed that Biodentine™ had antibacterial effect on *Streptococcus sanguis* and on *Streptococcus salivarius*. When testing antibacterial effect on *Streptococcus sanguis* and *Streptococcues mutans*, Biodentine™ had a lower value than other cements, like Dycal™. The authors concluded that tricalcium silicate cements showed a better antibacterial activity and a lower cytotoxicity, unlike other cements investigated.

Nikhil et al. also investigated the antibacterial effect of Biodentine[TM] on *Staphylococcus aureus, Enterococcus faecalis, Candida albicans* and *Streptococcus mutans.* [39] Another aim of the present study was to explore the effect of adding one of these substances, chlorhexidine and doxycycline, to Biodentine[TM] as root-end filling material. The authors found a clear antibacterial effect of Biodentine[TM] alone on all the tested bacteria and fungi. Adding 2% clorhexidine enhanced the antibacterial activity of Biodentine[TM] alone, but 10% of doxycycline added decreased the antibacterial activity of Biodentine[TM] alone.

5. Radioopacity

An ideal repair material should be sufficient radio-opaque in order to be easily discerned from the other structures. [40] For retrograde fillings this property is very important so that the radiograph taken post-operatively confirm that the material is within the cavity, well placed and it is easy discerned from the other tissues (dentine and bone trabeculae). [41]

Biodentine[TM] exhibits a radioopacity value higher than 3 mm according to ISO 6786(2001). In the study presented by Grech et al. Biodentine[TM], as well as other materials tested (MTA[TM], Bioaggregate[TM] and IRM[TM]), lost its radioopacity over time, but with no statistically significant difference. [5] Camilleri et al. concluded in their study that Biodentine[TM] contains only 5% zirconium oxide and this is why it has lower radioopacity than MTA Angelus[TM]. [4]

CONCLUSIONS

According to the published literature Biodentine[TM] could be an efficient alternative to mineral trioxide aggregate or other dental cements to be used as a root-end filling material because of its physical, biological and handling properties.

However, in order to draw definitive conclusions about the use of Biodentine[TM] in periodontal surgery are necessary more prospective clinical studies and randomised control trials with a long term follow up.

ACKNOWLEDGEMENTS

REFERENCES

1. Saxena P., Gupta S.K., Newaskar V., *Restorative Dentistry & Endodontics, 2013, 38, 119.*
2. Chong B.S., Pitt Ford T.R., *Endodontic Topics,* **2005**, *11*, 114.
3. Septodont - France. Biodentine™ (Brochure), **2011**.
4. Camilleri J., Sorrentino F., Damidot D*., Dental Materials*, **2013**, *29, 580*.
5. Grech L., Mallia B., Camilleri J., *Dental Materials,* **2013**, *29, 20*.
6. Camilleri J., Kralj P., Veber M., Sinagra E., *International Endodontic Journal,* **2012**, *45*, 737.
7. Festy F., Watson T.F., *Biomaterials and Bioengineering*, **2012**, *91*, 454.
8. Camilleri J., *Dental Materials*, **2014**, *30, 709*.
9. Camilleri J., *Journal of Denstistry,* **2013**, *41, 600*.
10. Kayahan M.B., Nekoofar M.H., Kazandağ M., Canpolat C., Malkondu O., Kaptan F. et al., *International Endodontic Journal*, **2009**, *42,* 1004.
11. Aggarwal V., Singla M., Miglani S., Kohli S., *Journal of Conservative Dentistry*, **2013**, *16*, 462.
12. Alhodiry W., Lyons M..F, Chadwick R.G., *European Journal of Prosthodontics and Restorative Dentistry*, **2014**, *22,* 1.
13. Guneser M.B., Akbulut M.B., Eldeniz A.U., *Journal of Endodontics*, **2013**, *39,* 380.
14. Elnaghy A.M*., Journal of Adhesive Dentistry*, **2014**, *16,* 277.
15. El-Ma'aita A.M., Qualtrough A.J.E., Watts D.C., *Dental Materials*, **2013**, *29*, 797.
16. Elnaghy A.M., *Journal of Endodontics*, **2014**, *40, 953*.
17. Caronna V., Himel V., Yu Q., Zhang J.-F., Sabey K., *Journal of Endodontics*, **2014**, *40*, 986.
18. Sinha N., Singh B., Patil S*., Journal of Conservative Dentistry*, **2014**, *17*, 285.
19. Khetarpal A., Chaudhary S., Talwar S., Verma M., *Indian Journal of Dental Research*, **2014**, *25,* 513.
20. Nayak G., Hasan M.F., *Restorative Dentistry and Endodontics*, **2014**, *39*, 120.
21. Ravichandra P.V., Vemisetty H., Deepthi K., Reddy S.J., Ramkiran D., Krishna M. JN et al., *Journal of Clinical and Diagnostic Research*, **2014**, *8*, 243.
22. Soundappan S., Sundaramurthy J.L., Raghu S., Natanasabapathy V., *Journal of Dentistry of Tehran University of Medical Sciences,* **2014**, *11*, 143.
23. Ozbay G., Kitiki B., Peker S., Kargul B., *ACTA Stomatologica Croatica,* **2014**, 132.
24. Sanghavi T., Shah N., Shah R.R., *National Journal of Medical Research,* **2014**, *4*, 56.
25. Jeevani E., Jayaprakash T., Bolla N., Vemuri S., Sunil C.R, Kalluru R.S., *Journal of Conservative Dentistry*, **2014**, *17*, 340.
26. Nikoloudaki G.E., Kontogiannis T., Meliou H.A., Kerezoudis N.P., *Open Journal Stomatology*, **2014**, *4*, 402.
27. Caron G., Azérad J., Faure M.-O., Machtou P., Boucher Y., *International Journal of Oral Sciences,* **2014**, *2, 1*.
28. Pawar A.M., Kokate S.R., Shah R., *Journal of Conservative Dentistry*, **2013**, *16, 573*.

29. Johns D.A., Shivashankar V.Y., Shobha K., Johns M., *Journal of Conservative Dentistry*, **2014**, *17, 75.*
30. Black J., Biological Performance of Materials: Fundamentals of Biocompatibility, Fourth Edn CRC Press, **2006**.
31. Williams D.O., *Biomaterial*, **2008**, *2,* 2,941.
32. Samyuktha V., Ravikumar P., Nagesh B., Ranganathan K., Jayaprakash T., Sayesh V., *Journal of Conservative Dentistry*, **2014**, *17,* 467.
33. Jung J.-Y., Woo S.-M., Lee B.-N., Koh J.-T., Nör J.E., Hwang Y.-C., *International Endodontic Journal*, **2015**, *48,* 178.
34. Rossi A. De, Assed L., Silva B., Nelson-Filho P., Assed R., Queiroz A.M. De, *Journal of Endodontics*, **2014**, *40,* 1362.
35. Mori G.G., Teixeira L.M., Oliveira D.L. De, Jacomini L.M., *Journal of Endodontics*, **2014**, *40,* 1485.
36. Nowicka A., Lipski M., Parafiniuk M., Sporniak-Tutak K., Lichota D., Kosierkiewicz A. et al., *Journal of Endodontics*, **2013**, *39,* 743.
37. Lee B.-N., Lee K.-N., Koh J.-T., Min K.-S., Chang H.-S., Hwang I.-N. et al., *Journal of Endodontics*, **2014**, *40,* 1217.
38. Poggio C., Ceci M., Beltrami R., Dagna A., Colombo M., Chiesa M*., Annals of Stomatology (Roma),* **2014**, *4,* 69.
39. Nikhil V., Madan M., Agarwal C., Suri N., *Journal of Conservative Dentistry*, **2014**, *17,* 271.
40. Tagger M., Katz A., *International Endodontic Journal,* **2004**, *37,* 260.
41. Tanalp J., Karapınar-Kazandağ M., Dölekoğlu S., Kayahan M.B., *Scientific World Journal,* **2013**; DOI.org/10.1155/2013/594950.
42. Attik G.N., Villat C., Hallay F., Pradelle-Plasse N., Bonnet H., Moreau K. et al., *International Endodontic Journal,* **2014**, *12*, 1.
43. Chang S.-W., Lee S.-Y., Ann H.-J., Kum K.-Y., Kim E.-C*., Journal of Endodontics,* **2014**, *40*, 1194.
44. Corral Nuñez C.M., Bosomworth H.J., Field C., Whitworth J.M., Valentine R., *Journal of Endodontics,* **2014**, *40,* 406.
45. Zhou H., Shen Y., Wang Z., Li L., Zheng Y., Häkkinen L. et al., *Journal of Endodontics,* **2013**, *39,* 478.
46. Zanini M., Sautier J.M., Berdal A., Simon S., *Journal of Endodontics*, **2012**, *38,* 1220.
47. Poggio C., Arciola C.R., Beltrami R., Monaco A., Dagna A., Lombardini M. et al., *Scientific World Journal,* **2014**, *2,* 1819.
48. Pérard M., Le Clerc J., Meary F., Pérez F., Tricot-Doleux S., Pellen-Mussi P., *Journal of Materials Sciences*, **2013**, *2,* 1527.
49. Luo Z., Kohli M.R., Yu Q., Kim S., Qu T., He W., *Journal of Endodontics*, **2014**, *40,* 937.
50. Laurent P., Camps J., About I., *International Endodontic Journal,* **2012**, *45,* 439.
51. Khedmat S., Dehghan S., Hadjati J., Masoumi F., *Restorative Dentistry and Endodontics,* **2014**, *7658*, 149.
52. Jang Y.-E., Lee B.-N., Koh J.-T., Park Y.-J., Joo N.-E., Chang H.-S. et al., *Restorative Dentistry and Endodontics,* **2014**, *39,* 89.
53. Luo Z., Li D., Kohli M.R., Yu Q., Kim S., He W.-X., *Journal of Dentistry*, **2014**, *42,* 490.
54. Leiendecker A.P., Qi Y.-P., Sawyer A.N., Niu L.-N., Agee K.A., Loushine R.J. et al., *Journal of Endodontics,* **2012**, *38,* 829.

IMMUNOMODULATORY POTENTIAL OF PALLADIUM(II) COMPLEXES WITH (1E,6E)-1,7-BIS (3,4-DIMETHOXYPHENYL) HEPTA-1,6-DIENE-3,5-DIONE

EVA FISCHER-FODOR[a,c,*], ROMAN MIKLÁŠ[b], LUDOVIC TIBOR KRAUSZ[c,d], PIROSKA VIRAG[a], DANIELA CRISTINA MOLDOVAN[e], MARIA PERDE SCHREPLER[a], IOANA BERINDAN-NEAGOE[c], FERDINAND DEVÍNSKY[b], NATALIA MIKLÁŠOVÁ[b*]

ABSTRACT. In the cancer chemotherapy the metal-based cytotoxic drugs are invariable components of therapeutic protocols, despite the biologic drugs expansion. A current tendency is to design metal-based drugs with highest efficacy and limited toxicity on normal human cells implicated in immune response. Therefore we synthesized and characterized two palladium(II) complexes with (1*E*,6*E*)-1,7-bis(3,4-dimethoxypenyl)hepta-1,6-diene-3,5-dione, a curcuminoid like ligand; their cytotoxicity towards tumor cells was tested, and their expected impact on T and B lymphocytes was measured *in vitro*. The lymphocytes treatment with the free ligand, and with the two complexes **1** and **2**, increased significantly the proportion of the T helper CD4 positive cell population, concomitant with the decrease of T effector CD8 positive cells. The B cells were not affected by **1**, but **2** has a minor inhibitory effect on CD19+ and CD45RA+ cells. The cells function was tested through the compounds modulator effect on membrane markers CD25 and GITR, both being slightly down regulated by **2**, compensating of CD4+ overexpression and CD8+ down regulation. Moreover, complex **1** displayed minimal interferences with the cellular antitumor immunity, acting as a selective inhibitor of cancer cells growth.

Keywords: *(1E,6E)-1,7-bis(3,4-dimethoxyphenyl)hepta-1,6-diene-3,5-dione, palladium complex, cancer therapy, immune response*

[a] *Research Department, Institute of Oncology "Prof. Dr. I. Chiricuta", 34-36 Republicii Str., RO-400015, Cluj-Napoca, Romania*
[b] *Department of Chemical Theory of Drugs, Faculty of Pharmacy, Comenius University in Bratislava,8 Kalinčiakova Str., 83232 Bratislava, Slovakia*
[c] *Faculty of Medicine, Iuliu Hatieganu University of Medicine and Pharmacy Cluj Napoca, 8, Babes Str, RO-400012, Cluj-Napoca, Romania*
[d] *Public Health Center, 1 Miko Str., RO-530174, Miercurea Ciuc, Romania*
[e] *Regional Blood Transfusion Center, 19 Nicolae Balcescu Str, RO-40000, Cluj-Napoca, Romania*
* Corresponding authors: Eva Fischer-Fodor: fischer.eva@iocn.ro;
   Natalia Miklasova: miklasova@fpharm.uniba.sk.

INTRODUCTION

Several metal-based drugs were introduced in the clinical practice; among them the platinum complexes having cytotoxic properties are drugs of choice for systemic therapy of cancer [1]. When using cytotoxic drugs against different cancer localizations, besides the beneficial effect of tumor cell destruction, the normal cells are damaged as well, but more hazardous is the human immune systems damaging, because it cuts the human body self-defense mechanism.

A new tendency in the drug discovery encourages the development of drugs which exhibit cytotoxicity and stimulate the antitumor immunity; in the case of metal compounds, a possible approach is the employment of appropriate ligands. The natural compound curcumin displayed anticancer properties [2] selectively against tumor cells [3] and it is immunostimulatory [4]. The metal complexes of curcumin exhibit as well antitumor properties [5, 6], palladium being one of the central metals which form biological active compounds with curcumin analogues [7,8].

In the present study the curcuminoid (1*E*,6*E*)-1,7-bis(3,4-dimethoxyphenyl)hepta-1,6-diene-3,5-dione, and its palladium(II) complexes were synthesized and characterized. T and B lymphocytes are implicated in the adaptive immunity, being the basis of cell-mediated antitumor immunity in humans [9, 10], responsible for the quality of the cellular immune response. We estimated *in vitro* the Pd(II) complexes capacity to influence the lymphocytes activation processes, in order to establish weather they will hinder the immune response of the host organism.

RESULTS AND DISCUSSION

The curcuminoid (1*E*,6*E*)-1,7-bis(3,4-dimethoxypenyl)hepta-1,6-diene-3,5-dione was synthesized following a former procedure [11]. Complexes **1** and **2** (Scheme 1) as well as the precursor palladium complexes were synthesized based on a procedure reported in our previous studies [8,9].

The curcuminoid and the complexes **1** and **2** were tested *in vitro* on two human tumor cell lines: A2780 ovary and the HT-29 colon carcinoma, and on a primary culture of normal lymphocytes. Cytotoxicity was expressed as the half inhibitory concentration (IC50), the concentration which reduce with 50% the amount of living cells. IC50 values were obtained using the sigmoidal dose-response relation, and they reflect the compounds cytotoxicity against tumor and normal cells (Table 1). The curcuminoid, **1** and **2** exhibit *in vitro* cytotoxicity against the tumor cells and they have a milder effect on normal human lymphocytes.

Scheme 1. Synthesis of palladium(II) complexes **1** and **2.**
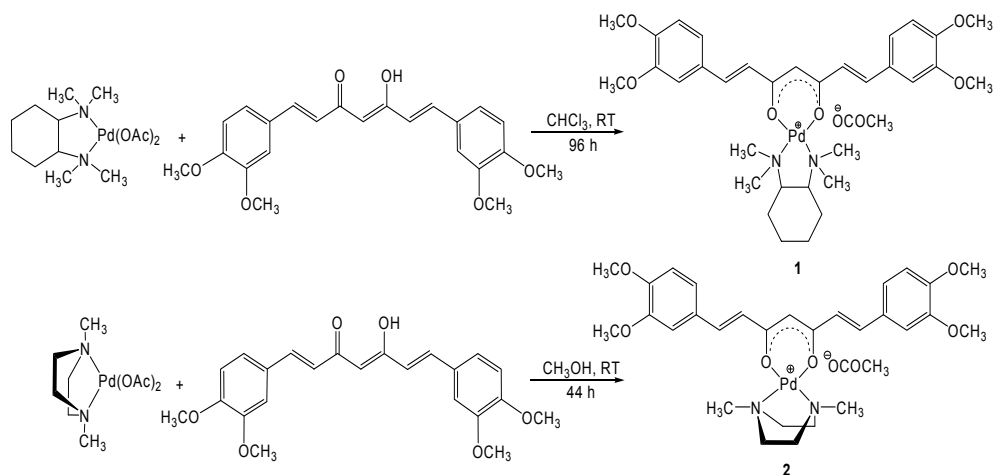
Table 1. Half inhibitory concentrations IC50 of curcuminoid and palladium(II) complexes (SD standard deviations).

Cell type	A2780 ovary cancer cells		HT-29 colon cancer cells		Normal lymphocytes	
IC50 values (mM)	Median values	SD	Median values	SD	Median values	SD
Curcumin	2.082	0.240	4.325	0.248	6.375	0.419
Complex **1**	1.522	0.141	0.767	0.099	3.857	0.307
Complex **2**	0.944	0.091	0.577	0.027	5.512	0.071

The treatment with curcuminoid, **1** and **2** increases significantly the number of CD4 positive cells in the population (Figure 1), but the standard drug oxaliplatin raise even more the CD4+ cells percent. In CD8 positive population a significant decrease occurred in the cell number after the treatment with all compounds ($p < 0.01$), related to untreated cells. Complex **2** diminish at a lower extent the CD8+ population, and its effect is milder as of oxaliplatin.

No significant difference was observed in CD19 cells expression between the untreated cells and curcumin ($p > 0.5$) and **1**, and **2** cause a decrease with limited importance, as depicted in Figure 2 (not significant in 95% confidence interval). GITR-positive lymphocytes proportion decreases when treated with **2**, which has a weak effect (p 0.0498, significant decrease in 95% confidence interval), while curcumin (p 0.0844) and complex **1** (p 0.0823) show no significant effect on these population. The same tendency was observed in CD25 positive population.

CD45R transmembrane signaling molecule [13] is characteristic for mature B cells and also for some T cell populations. CD25 is a transmembrane protein present on activated T and B cells; CD4+CD25+ suppressor cells and CD8+CD25+ T regulatory cells are critical in clearance of tumor cells. GITR is the glucocorticoid-induced tumor necrosis factor related protein; its expression increase upon T-cell activation and is implicated in programmed cell death and stimulates the antitumoral responses [14].
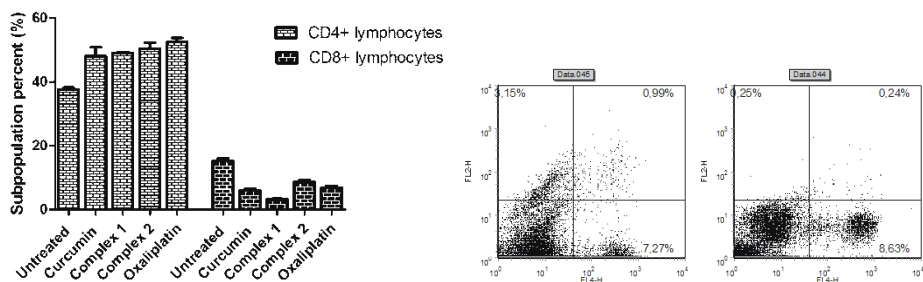
Figure 1. The effect of the complexes effect on CD4+ and CD8+ lymphocytes (left image) and histograms corresponding to flow cytometry measurements for complexes **1** (center) and **2** (right).
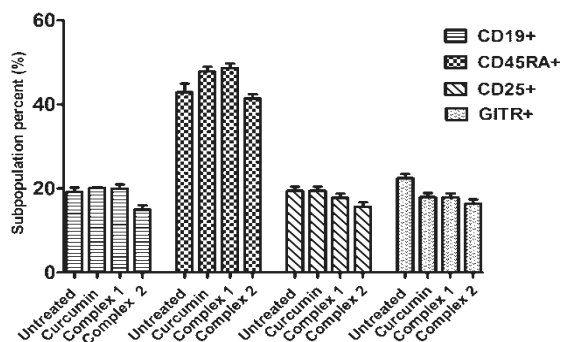
Figure 2. Modulation of CD19, CD45R, CD25 and GITR lymphocyte populations by the treatment with palladium (II) complexes.

The compounds stimulate the survival of the T helper CD4-positive cells in the whole population, and the 24-hours treatment of lymphocytes with the curcumin or his palladium complexes: **1** and **2** give rise to CD4+ enriched cell population.

Cytotoxic CD8-positive T cells are depleted as a consequence of the same treatment, but it is compensated by the enrichment in CD4+ (proportion of CD8 depletion and CD4 enrichment are interrelated). Therefore if non-self

cells destruction mechanism could be affected by novel compounds, the antibody recognition and antigen-presenting mechanisms will work better. The inhibitory effect against CD8+ lymphocyte have highest degree in complex **1** treatment, while the best proliferation in CD4+ lymphocytes is provided by **2**.

Only **2** decreases the survival of CD19 lymphocytes, curcumin and **1** does not interfere with B cells survival, therefore they will not influence the production of antibodies. **2** slightly inhibit B cells survival, but, the proportion of mature CD45R-expressing cells remains unaltered, therefore it couldn't significantly affect the immunoglobulin-secretor function of the B cells.

The activated lymphocytes proportion remains unchanged following the treatment with all compounds, CD25+ and GITR-expressing cells will be not affected, but **2** inhibit somewhat the GITR expression. The novel compounds will not influence lymphocyte activation, an important step in antitumor immune response of the host. Moreover, CD25+ proportion being unchanged and CD4+ increasing, it is obvious that among CD4 population the CD4+CD25+ suppressor cells involvement decreased which could enforce the antitumor response, and will lead to the amplification of effector function. Only in complex **2** effect it is observed a simultaneous increase in CD4+expression concomitant with CD25+ steadiness.

The patterns of CD19+ and CD45R+ cells modulation through curcumin compounds are similar; none of the compounds exert a significant effect on CD19, or CD45RA markers. CD8+CD45R+ cells are suppressor effectors cells [15]; it is very likely that their activity is amplified, because even if CD8+ population drop off, CD45RA+ cells are not affected, thus the proportion of CD8+CD45R+ suppressor effector cells ponder does not modify significantly, and despite the overall CD8 positive population depletion, the cytotoxic effect will be preserved a certain extent. GITR activate the CD4+ and CD8+ T cells [16], and induces tumor rejection [17]. Since curcumin and **1** does not affect GITR expression, and GITR+ cell survival exhibit a moderate decrease due to **2** action, the antitumor immune mechanisms involving CD4+ T cells and B cells will enhance, and the effect of CD8+ drop will be compensate once again by the reliability of GITR expression on the different cell populations, including CD8+ T-cells.

CONCLUSIONS

The curcuminoid and complexes **1** and **2** exhibit a very moderate toxicity against normal human lymphocytes; they do not inhibit the main cell subsets implicated in the signaling pathways of the antitumor response. The curcuminoid inhibits only the CD8+ cells, helps the CD4+ cells survival and it causes no impairment in the other epitopes expression in lymphocytes.

The immune response pathways are not affected by the treatment with the free ligand. Complex **1** action overall on the studied lymphocytes subsets indicates that he has many compensatory effect on the effector cells of the immune system, despite his inhibitory effect on CD8+ cluster, and we anticipate a positive modulation on immunity following *in vivo* administration. Complex **2** inhibitory effects on CD8+ cells and the slight decrease in CD19+ cell expression and GITR, can be a source of moderate immunodepression of the host organism *in vivo*. Overall, the curcuminoid and its palladium(II) complexes will be no source of severe side effects in a potential application as anticancer drugs.

EXPERIMENTAL SECTION

All chemicals for syntheses were of reagent grade and were used as they received; Pd(OAc)$_2$ was purchased from Sigma Aldrich.

All NMR spectra were measured on a Varian Gemini 2000 spectrometers at working frequencies 300 MHz (for ^{1}H-NMR) and 75 MHz (for ^{13}C-NMR). Spectra were measured in CD3OD, using as internal standard TMS. Infrared spectra were recorded on a FT-IR Impact 400 D spectrophotometer on KBr disks. Column chromatography was performed on silica gel (silica 0.035-0.070 mm 60 Å, Acros).

The measurements for biologic effect were made using FACSCalibur flowcytometer (Becton Dickinson, USA) and Synergy2 multiplate reader (BioTek, USA). A2780 and HT-29 tumor cell lines were from ECACC; lymphocytes were isolated on Histopaque separation media from the whole blood of a 42-years old female healthy donor following her informed written consent. We used RPMI-1604 and McCoy's5 cell culture media supplemented with 2mM glutamine, 10% fetal bovine serum, and penicillin-streptomycin solution for cell cultures, all media and supplements were provided by Sigma Aldrich Chemicals. Oxaliplatin was acquired from Actavis Pharma.

Syntheses: Complex **1**: 0.126 mmoles (0.05 g) of (1*E*,6*E*)-1,7-bis(3,4-dimethoxyphenyl)hepta-1,6-diene-3,5-dione were dissolved in 5 mL of dry chloroform. To this solution was added dropwise 0.126 mmoles (0.05 g) of Pd(II) complex containing (*R,R*)-*N,N,N',N'*-tetramethylcyclohexane-1,2-diamine dissolved in 5 mL of CHCl$_3$. Then, 30 μL of NaOH (1M) were added to the reaction mixture. After 96 hours of stirring at room temperature, the reaction mixture was checked by TLC and no unreacted starting curcuminoid was observed. Complex **1** was isolated as a yellow powder (0.06 g; 55%).

^{1}H-NMR (CD$_3$OD, 300 MHz) δ (ppm) 1.29-1.39 (m, 2H) 1.48-1.59 (m, 2H) 1.81 (m, 2H) 1.89 (s, 3H) 2.20 (m, 2H) 2.85 (s, 6H) 2.87 (s, 6H) 3.25 (m, 2H) 3.87 (s, 6H) 3.89 (s, 6H) 5.89 (s, 1H) 6.75(d, 2H) 6.98 (d, 2H) 7.21 (d, 2H) 7.25 (s, 2H) 7.47 (d, 2H). ^{13}C-NMR (CD$_3$OD, 75 MHz) δ (ppm) 25.89 (1C) 26.77 (2C) 27.36 (2C) 45.49 (4C) 58.25 (2C) 58.35 (2C) 70.90 (2C) 75.05 (2C) 113.28 (2C) 114.51 (2C) 125.83 (2C) 125.95 (2C) 131.49 (2C) 131.70 (2C) 143.49 (2 C) 152.67 (2C) 181.88 (2C). IR (KBr) v_{max} (cm^{-1}) 3436, 2931, 2860, 1728, 1620, 1597, 1508, 1465, 1400, 1268, 1139, 1025, 997, 845, 697, 585.

Complex **2**: 0.20 mmoles (0.08 g) of (1*E*,6*E*)-1,7-bis(3,4-dimethoxyphenyl)hepta-1,6-diene-3,5-dione were dissolved in 10 mL of dry methanol. To this solution was added 0.20 mmoles of Pd(II) complex containing 1, 4-dimethylpiperazine dissolved in 5 mL of MeOH. The final product was isolated as a yellowish powder (0.05 g; 62.5%).

^{1}H-NMR (CD$_3$OD, 300 MHz) δ (ppm) 1.90 (s, 3H) 2.64 (s, 6H) 2.75 (d, 4H) 3.86 (s, 6H) 3.88 (s, 6H) 3.90 (d, 4H) 5.89 (s, 1H) 6.72 (d, 2H) 6.96 (d, 2H) 7.16 (dd, 2H) 7.21 (s, 2H) 7.49 (d, 2H). ^{13}C-NMR (CD$_3$OD, 75 MHz) δ (ppm) 24.98 (1C) 46.72 (2C) 56.45 (2C) 56.56 (2C) 59.62 (4C) 106.11 (1C) 111.40 (2C) 112.71 (2C) 123.92 (2C) 124.00 (2C) 129.77 (2C) 141.93 (2C) 150.87 (2C) 152.69 (2C) 179.94 (2C). IR (KBr) v_{max} (cm^{-1}) 2929, 1618, 1597, 1580, 1503, 1451, 1393, 1257, 1136, 1021, 997, 996, 834, 797, 697.

Biologic activity: The cytotoxicity was assessed with the MTT (3-(4,5-dimethylthiazol-2-yl)-2,5-diphenyltetrazolium bromide, from Sigma Aldrich) colorimetric method, as described earlier [18]. The treated lymphocyte subpopulations were analyzed using flow cytometry, before and after 24 hours incubation with 0.5 mM curcumin, **1** or **2**. We analyzed the proportion of different cell types among the whole lymphocyte population as described before [19] using antibodies conjugated with fluorochromes: CD4 FITC, CD8 APC, CD25 FITC, CD19PE, CD45R FITC and GITR FITC. The biostatistical analysis was performed with the Graph Pad Prism5 software (GraphPad, USA).

ACKNOWLEDGMENTS

REFERENCES

1. S. Dasari, P.B. Tchounwou, *European Journal of Pharmacology*, **2014**, *740*, 364.
2. N. Hashima, B.B. Aggarwal, *International Journal of Biochemistry and Molecular Biology*, **2012**, *3*, 328.
3. S.C. Gupta, S. Prasad, J.H. Kim, S. Patchva, L.J. Webb, I.K. Priyadarsini, B.B. Aggarwal, *Natural Products Report*, **2011**, *28*,1937-55.
4. Z.C. Ding, G. Zhou, *Clinical and Developmental Immunology*, **2012**, *2012*, 890178.
5. A. Valentini, F. Conforti, A. Crispini, A. De Martino, R. Condello, C. Stellitano, G. Rotilio, M. Ghedini, G. Federici, S. Bernardini, D. Pucci, *Journal of Medicinal Chemistry*, **2009**, *52*, 484.
6. L. Baum, A. Ng, *Journal of Alzheimer's Disease*, **2004**, *6*, 367.
7. N. Miklášová, R. Mikláš, F. Devínsky, *Palladium complexes of curcumin and its analogues and methods of preparation of the same*, Patent WO 2014/175841 A1, **2014**.
8. N. Miklášová, E. Fischer-Fodor, R. Mikláš, L. Kucková, J. Kožíšek, T. Liptaj, O. Soritau, J. Valentová, F. Devínsky, *Inorganic Chemistry Communications*, **2014**, *46*, 229.
9. G. Karp. *Cell and Molecular Biology- Concepts and Experiments*, John Wiley & Sons, Hoboken, USA, ISBN-13 978-0-470-48337-4, 6th Ed, **2010**, Chapter 17.
10. V.C. Liu, L.Y. Wong, T. Jang, A.H. Shah, I. Park, X. Yang, Q. Zhang, S. Lonning, B.A. Teicher, C. Lee, *Journal of Immunology*, **2007**, *178*, 2883.
11. P.J. Roughley, D.A. Whiting, *Journal of the Chemical. Society Perkin Transactions 1*, **1973**, *2379*.
12. A. Kessel, T. Haj, R. Peri, A. Snir, D. Melamed, E. Sabo, E. Toubi, *Autoimmunity Reviews*, **2012**, *11*, 670.
13. J.A. Ledbetter, N.K. Tonks, E.H. Fischer, E.A. Clark, *Proceedings of the National Academy of Sciences of the USA*, **1988**, *85*, 8628.
14. G. Nocentini, C. Riccardi, *European Journal of Immunology*, **2005**, *35*, 1016.
15. C. Morimoto, T. Takeuchi, S.F. Schlossman, *Clinical and Experimental Rheumatolology*, **1989**, *7*, S3.
16. T. Ramirez-Montagut, A. Chow, D. Hirschhorn-Cymerman, T.H. Terwey, A.A. Kochman, S. Lu, R.C. Miles, S. Sakaguchi, A.N. Houghton, M.R. van den Brink, *Journal of Immunology*, **2006**, *76*, 6434.
17. A.L. Côté, P. Zhang, J.A. O'Sullivan, V.L. Jacobs, C.R. Clemis, S. Sakaguchi, J.A. Guevara-Patiño, M.J. Turk, *Journal of Immunology*, **2011**, *186*, 275.
18. E. Fischer-Fodor, A.M. Vălean, P. Virag, P. Ilea, C. Tatomir, F. Imre-Lucaci, M. Perde Schrepler, L.T. Krausz, L.B. Tudoran, C.G. Precup, I. Lupan, E. Hey-Hawkins, L. Silaghi-Dumitrescu, *Metallomics*, **2014**, *6*, 833.
19. J. Ceballos-Torres, P. Virag, M. Cenariu, S. Prashar, M. Fajardo, E. Fischer-Fodor, S. Gómez-Ruiz. *Chemistry - A European Journal*, **2014**, *18*, 10811.

PROGNOSTIC FACTORS IN LIVER FAILURE IN CHILDREN BY DISCRIMINANT ANALYSIS OF CLINICAL DATA. A CHEMOMETRIC APPROACH

HORIA F. POP[a], COSTEL SÂRBU[b,*], ANA ŞTEFANESCU[c], AUREL BIZO[c], TUDOR LUCIAN POP[c]

ABSTRACT. Discriminant analysis was applied as an efficient method to identify an objective score concerning liver failure in children using clinical data. Discriminant analysis was not only used for classifying the patients according to the survival status, but also for detecting the most important factors that discriminate between surviving and deceased patients. Based on the considered factors, we were able to compute a complete separation between surviving and deceased patients. The factors responsible for the separation were age, K and total bilirubin (3rd sampling day). The smallest contribution was obtained for aspartate aminotransferase (3rd sampling day), hemoglobin, thrombocytes, albumin. The obtained results confirm that clinical analysis combined with the multidimensional analysis of data gives an interesting and very useful way for correlations, interpretations, problem solving and cost effectiveness.

Keywords: Chemometrics, clinical data, discriminant analysis, liver failure prognosis

INTRODUCTION

Liver failure in children could have acute or chronic evolution. Acute Liver Failure (ALF) is a relatively rare but often fatal event in children [1]. Definition of ALF is hepatic necrosis resulting in loss of liver function within few months of the onset of clinical liver disease. Acute liver failure accounts

[a] *Babeş-Bolyai University, Faculty of Mathematics and Computer Science, 1 M. Kogălniceanu St., Cluj-Napoca, RO-400084, Romania*
[b] *Babeş-Bolyai University, Faculty of Chemistry and Chemical Engineering, 11 Arany Janos St., Cluj-Napoca, RO-400028, Romania*
[c] *Iuliu Haţieganu University of Medicine and Pharmacy, 8 Victor Babeş St., Cluj-Napoca, RO-400012, Romania*
* *Corresponding author: csarbu@chem.ubbcluj.ro*

for 10-15% of liver transplantation in USA [2]. The mortality without treatment, including liver transplantation, in ALF patients is over 70%. There are few patients with spontaneous regeneration of the liver with excellent long-term evolution [1].

It is very important to have an accurate evaluation of the prognosis of the patients with ALF in order to select the patients that will need liver transplantation in order to survive.

There are few reliable criteria for determination of the prognosis in ALF in children. Many attempts have been made to correlate clinical and laboratory data in order to establish the prognosis. Pediatric Acute Liver Failure (PALF) Study Group is a multicenter and multinational consortium created for this kind of studies with the most important results in children with ALF. Overall prognosis in children with ALF is variable with the etiology of the disease, between 68% survival in acute hepatitis A and 12% in drug toxicities [1]. Other parameters analyzed were age, degree of hepatic encephalopathy, severity of coagulopathy, bilirubin level [3]. In a British study of ALF due to acetaminophen intoxication prothrombin time, hypoglycemia, serum creatinine, acidosis and grade III encephalopathy were factors with poor prognosis [4].

Liver transplantation is the ultimate solution for patients with liver failure, acute or acute on chronic liver disease. King's College Criteria (using biochemical and clinical parameters available on admission: age, etiology, pH, prothrombin time, serum bilirubin, serum creatinine, encephalopathy) are widely used for selection of the patient with ALF for liver transplantation but they have not been validated in a large pediatric cohort [5].

The current prognostic score in use for organ allocation and the stratification of the need for liver transplantation is the MELD score (Model for End-Stage Disease), with its pediatric variant, the PELD score. The scores were developed in the early years of this century to improve organ allocation, discarding the "waiting time" on the transplant list as not being a good indicator of medical urgency [6-8]. The MELD score included creatinine, bilirubin and International Normalized Ratio measuring blood coagulability (INR) as parameters in the calculation formula, while the team designing PELD chose albumin, INR, total bilirubin, age (with more points attributed to children under the age of one) and evidence of failure to thrive. It proved to be a more efficient system, with fewer deaths while on the waiting list, despite the still high rate of mortality in the under two years of age group [9]; in this particular study, the change in PELD score proved to be an important predictor of outcome for children on the list. However, after the tempered enthusiasm of the first success, with higher rates of survival [10], criticisms ensued: the scoring system underestimated the near-term risk of death and subjected

children to several serious complications while "waiting", which forced health-care professionals and patients to resort to the "exception" mechanism that enabled the access to graft in spite of lower score. Further studies raised suspicions on the objectivity of the system, claiming inter-laboratory variability in the determination of INR [11], and in 2010 a modified PELD was proposed as a means of correcting and improving its efficacy [12].

Although the access to liver transplantation in children is rather limited in our country, the importance of a better risk stratification for children with liver failure remains unquestionable. Our goal is to analyze the PELD parameters as well as other factors of possible influence on morbidity and survival (sodium, ammonia, creatinine, and lactate) of patients with acute or acute-on-chronic liver failure and propose an alternate scoring system, based on their survival rates. In this order, the discriminant analysis (DA) has successfully been applied.

RESULTS AND DISCUSSION

The computed data set included 49 patients and the following 31 factors (variables or characteristics): age, leucocytes, hemoglobin, thrombocytes, C reactive protein, Aspartate aminotransferase (1st sampling day, AST_1), Alanine aminotransferase (1st sampling day, ALT_1), Aspartate aminotransferase (2nd sampling day, AST_2), Alanine aminotransferase (2nd sampling day, ALT_2), Aspartate aminotransferase (3rd sampling day, AST_3), Alanine aminotransferase (3rd sampling day, ALT_3), total bilirubin (1st sampling day, TB_1), Direct bilirubin (1st sampling day, DB_1), Total bilirubin (2nd sampling day, TB_2), Total bilirubin (3rd sampling day, TB_3), protein, albumin, pediatric end-stage liver disease (PELD), International Normalized Ratio measuring blood coagulability, value on the first day (INR_1), Na, K, glycaemia, urea, creatinine, worst creatinine level (V52_A), QT level on hospitalization day 1 (TQ_1), QT level on hospitalization day 2 (TQ_2), QT level on hospitalization day 3 (TQ_3), International Normalized Ratio measuring blood coagulability (INR), worst prothrombin index level (IP). We have to mention that the majority of measured variables (age, leucocytes, hemoglobin, thrombocytes, protein, albumin, Na, K) have a normal distribution according to the Kolmogorov-Smirnov statistical test. The chemometric analysis has been performed by using Statistica 7.1 software (StatSoft, Inc., Tulsa, USA).

After application of the stepwise DA to the matrix data (49 x 31) the factors (variables) presented in Table 1 were retained in the model. The statistics from this table illustrates the contribution to the patients discrimination of the considered factors (clinical data) according to different parameters.

Knowing that Wilks' lambda (λ^*) describes the unique contribution of each variable to the discriminatory power of the model (the smaller the value of λ^*, the more the model is discriminating and the larger the lambda λ^*, the more likely it is significant) and large values for F and close to 0 for λ^* shows that the variable has a significant contribution, the following statements may be retained.

It is easy to observe that the greatest contribution is given by age ($\lambda^* = 0.831$; F = 6.524). The next highest are K ($\lambda^* = 0.834$; F = 6.352) and BT_3 ($\lambda^* = 0.0843$; F = 5.958). The smallest contribution was obtained for AST_3 ($\lambda^* = 1.000$; F = 0.002), hemoglobin ($\lambda^* = 0.993$; F = 0.223), thrombocytes ($\lambda^* = 0.984$; F = 0.509), albumin ($\lambda^* = 0.981$; F = 6.33). Also a small contribution brings the protein ($\lambda^* = 0.958$; F = 1.387).

We performed also a canonical correlation analysis that determined the successive functions and canonical roots (the term root refers to the eigenvalues that are associated with the respective canonical function). The maximum number of functions will be equal to the number of groups minus one, or the number of variables in the analysis, whichever is smaller.

The corresponding standardized canonical discriminant function coefficients (c) corresponding to the single eigenvalue (4.126) are also showed in Table 1.

Table 1. Statistic results concerning discriminant analysis of clinical data

Factor in the model	Wilks' λ	λ*	F	p-level	c	r
INR	0.208	0.936	2.195	0.148	0.366	0.294
Albumin	0.199	0.981	0.633	0.432	-0.227	-0.257
AST_3	0.195	1.000	0.002	0.963	0.018	0.271
K	0.234	0.834	6.352	0.017	0.561	0.285
Hemoglobin	0.196	0.993	0.223	0.640	-0.183	-0.132
Age	0.235	0.831	6.524	0.016	-0.697	-0.174
Thrombocytes	0.198	0.984	0.509	0.481	-0.207	-0.107
V52_A	0.222	0.878	4.453	0.043	0.612	0.141
BT_3	0.231	0.843	5.958	0.020	0.903	0.160
Leukocytes	0.221	0.882	4.298	0.046	-0.737	0.004
ALT_3	0.205	0.950	1.682	0.204	0.539	0.205
TQ_3	0.208	0.937	2.145	0.153	0.328	0.224
Urea	0.215	0.908	3.224	0.082	-0.585	0.084
AST_1	0.222	0.878	4.457	0.043	-0.685	0.096
AST_2	0.214	0.911	3.127	0.087	0.569	0.251
Protein	0.204	0.958	1.387	0.248	-0.289	-0.216

As we know the higher the discriminant coefficient (absolute value) and the closer the correlation coefficient (r) is to 1 respectively, the more the variable importance for the separation of patients in defined groups.

The highest standardized discriminant coefficients correspond to BT_3 (0.903), leukocyte (0.737), age (0.697), AST_1 (0.685), K (0.561).

A common result that one looks at in order to determine how well the current classification functions predict group membership of cases is the classification matrix.

The classification matrix shows the number of cases that were correctly classified (on the diagonal of the matrix) and those that were misclassified.

The classification matrix presented in Table 2 indicates a complete separation of patients in a good agreement to their behavior.

Table 2. Matrix classification of patients

Group	Percent Correct	Yes p=.5102	No p=.4898
Yes	100.00	25	0
No	100.00	0	24
Total	100.00	25	24

We can also visualize how the functions discriminate between groups by plotting the individual scores for the discriminant function. The Figure 1 supports the excellent separation of the patients and their (dis)similarities according to scores obtained as linear combinations of the variables (factors) retained in the model.
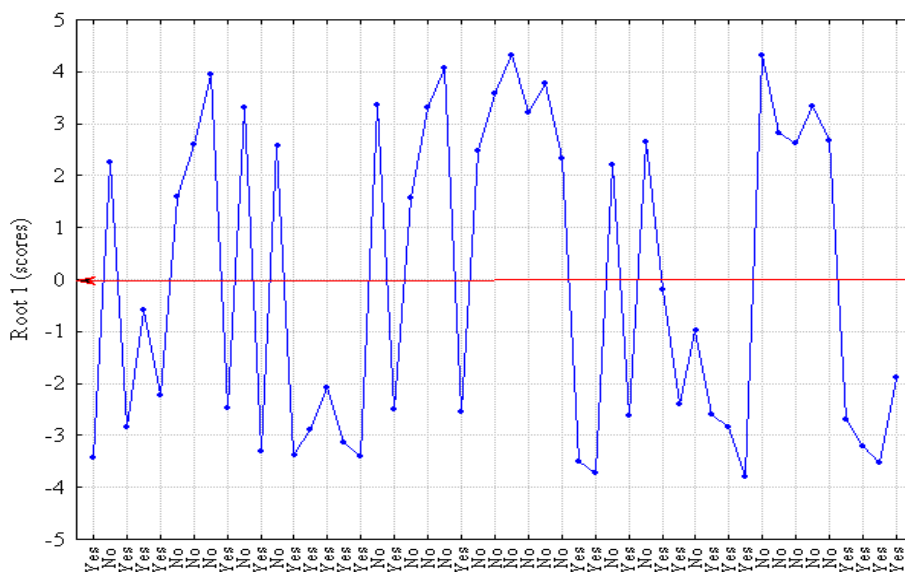

Figure 1. Graphic representation of scores corresponding to the 49 analyzed patients

CONCLUSIONS

Generally, Discriminant Analysis is a very useful tool for (1) detecting the variables that allow the researcher to discriminate between different (naturally occurring) groups, and (2) classifying cases into different groups with a better than chance accuracy.

Discriminant analysis was used not only for classifying the patients according to their disease but also for detecting the most important factors (variables) that discriminate between the groups.

This study illustrates two features of DA: the ability to determine the factor making the most important contribution to the difference between the two groups, and the ability to make an important contribution in the clinical setting. When support for a positive or negative diagnosis is required, DA may be able to provide such a binary decision, based on the multiple factors already available.

Clinical analysis combined with the multidimensional interpretation of data gives an interesting and very useful way of disease correlations, interpretations, problem solving and cost effectiveness.

DISCRIMINANT ANALYSIS

Discriminant Analysis (DA) was introduced and discussed in 1936 by R.A. Fisher [13], as a supervised classification method with large applications even today.

The method's main purpose is to predict class membership from a set of predictor variables by creating a function to produce the maximum between-group variance and the minimum intra-group variance. The predictor variables are related to these classes and the constructed memberships are then compared to the groups memberships indicated *a priori* by the user. This enables the user to test the grouping validity based on actual data, to test the created groups, or to assign groups membership to objects.

DA assumes the calculation of linear discriminant functions of independent variables starting from a qualitative dependent variable and two or more quantitative independent variables [14-17]. This is a parametric method, which means that it is based on certain statistical assumptions. The equality between the variance-covariance matrices of the groups to be separated and normal distribution of data are two of requirements for optimal application of DA. However, the difficulties due to the unfavourable statistical characteristics only influence the boundaries and therefore the classification by DA, but not the determination of the discriminant functions [18].

The contribution of the independent variables to the discrimination of groups can be appreciated either by the assay of the classes homogeneity using statistics F, like in the case of analysis of variance method, or by using Wilks' lambda for each variable. Wilks' lambda is the standard statistics used to express the significance of the overall discriminatory power of the variables in the model, where the value 1.0 indicates no discrimination power, while the value 0 indicates a perfect discrimination power. The partial Wilks' lambda describes the unique contribution of each variable to the model's discrimination power. The closer the partial lambda is to 0, the better the discrimination force of the variable is. In addition, the tolerance value illustrates the redundancy of the variable in the model. It is defined as the proportion of the variance contributed by respective variable, and is computed as 1 minus R-square of the respective variable, with all other variables included in the model. If the variable is completely redundant, the squared tolerance value approaches zero.

This information can also be obtained from the discriminant coefficients associated to the descriptive variables, and from the correlation coefficients between the descriptive variables and the scores. The higher the discriminant coefficient is in absolute value, and the closer the correlation coefficient is to one, the higher the variable importance for the cases separation into groups is. As well, the standardized discriminant coefficients, like, for example, the beta weights in regression methods, are used to asses the relative classification importance of the independent variables.

Multivariate analysis methods, including DA, have successfully been applied for the prognosis of liver failure and liver diseases using different clinical data [19, 20].

ACKNOWLEDGMENTS

REFERENCES

1. P.F. Whitington, E.M. Alonso, R.H. Squires, *Acute liver failure.* In: Kelly D. (editor). *Diseases of the liver and biliary system in children*, Third Ed., Wiley-Blackwell, Oxford, **2008**, pp.169-188.
2. E.M. Alonso, R.H. Squires, P.F. Whitington, *Acute liver failure in children*. In: F.J. Suchy, R.J. Sokol, W.F. Balistreri WF (editors). *Liver disease in children*. Trd. Ed., Cambridge University Press, New York, **2007**, pp. 71-96.
3. R.H. Jr. Squires, B.L. Shneider, J. Bucuvalas, *J. Pediatr.*, **2006**, *148*, 652.

4. S.B.K. Mahadevan, P.J. McKiernan, P. Davies, D.A. Kelly, *Arch. Dis. Child.*, **2006**, *91*, 598.
5. J.G. O'Grady, G.J.M. Alexander, K.M. Hayllar, *Gastroenterol.*, **1989**, *97*, 439.
6. R.H. Wiesner, S.V. McDiarmid, P.S. Kamath, *Liver Transpl.*, **2001**, *7*, 567.
7. R.B. Jr. Freeman, R.H. Wiesner, A.M. Harper, *Liver Transpl.*, **2002**, *8*, 851.
8. R.B. Jr. Freeman, *Transplantation Proceedings*, **2003**, *35*, 2425.
9. R.B. Jr. Freeman, R.H. Wiesner, J.P. Roberts, *Am. J. Transplant.*, **2004**, *9,* 114.
10. S.V. McDiarmid, R.M. Merion, D.M. Dykstra, A.M. Harper, *Liver Transpl.*, **2004**, *10*, S23.
11. R. Arjal, J.F. Trotter, *Clin. Liver Dis.*, **2009**, *13*, 67.
12. J. Seda Neto, E. Carone, *Liver Transpl.*, **2010**, *16*, 426.
13. R.A. Fisher, *Ann. Eugenic.*, **1936**, *7*, 179.
14. W.R. Klecka, *Discriminant Analysis*, Sage Publications, Iowa, **1980**.
15. G.H. McLachlan, *Discriminant Analysis and Statistical Pattern Recognition*, Wiley, New York, **2004**.
16. C. Sârbu, H.F. Pop, R.S. Elekes, G. Covaci, *Rev. Chim.*(Bucharest), **2008**, *59*, 1237.
17. H.F. Pop, C. Sârbu, *MATCH*, **2013**, *69*, 391.
18. D.L. Massart, B.G.M. Vandeginste, S.N. Deming, Y. Michotte, L. Kaufman, *Chemometrics, a Textbook,* Elsevier Science Publishers, Amsterdam, **1988**.
19. M. Hamilton, *J. Clin. Path.*, **1977**, *30*, 454.
20. R.T. Russell, I.D. Feurer, P. Wisawatapnimit, E.S. Lillie, E.T. Castaldo, C. Wright Pinson, *HPB*, **2008**, *10*, 30.

FATTY ACIDS DETERMINATION IN TROUT PLASMA AND MEAT BY GC-MS

SONIA SUVAR[a], ELENA HORJ[a], PAULA PODEA[b], ANDREEA IORDACHE[c], DANIEL COCAN[d], MONICA CULEA[a*]

ABSTRACT. The aim of this study was to develop a simple and reliable GC-MS method to compare the fatty acids in trout plasma and meat. The lipids were extracted from 0.5 mL of plasma and 1 g of meat using chloroform: methanol 1:2 (v:v) and then derivatized into fatty acids methyl esters (FAMEs) by esterification with methanol: acetyl chloride 4:1 (v:v). For FAMEs quantitation, undecaenoic acid (C11:1) was used as internal standard. High proportions of unsaturated fatty acids (UFAs) were found both in plasma and in meat samples. The highest proportion of UFAs in meat samples (53%) was represented by the ω-3 fatty acids.

Keywords: DHA, EPA, essential fatty acids, FAME, GC-MS, SFA, UFA.

INTRODUCTION

Gas chromatography coupled to mass spectrometry (GC-MS) is the method of choice for fatty acids identification and quantitation [1-3]. Fatty acids methyl esters (FAMEs) are the most widely used derivatives for GC analysis due to their easy derivatization procedure, volatility and good chromatographic separation [4].

In the vast family of fatty acids, only the polyunsaturated fatty acids (PUFAs) are essential nutrients. They were named *essential fatty acids* (EFA) and divided in two main categories: ω-6 fatty acids and their homologous and ω-3 fatty acids. Unlike the linear and rigid chemical structure of the saturated fatty acids (SFA), the structure of PUFAs is bended, twisted and flexible [5].

---

[a] *Babeş-Bolyai University, Faculty of Physics, 1 Kogălniceanu str., 400084 Cluj-Napoca, Romania.*
[b] *Babeş-Bolyai University, Faculty of Chemistry and Chemical Engineering, 1 Kogălniceanu str., 400084 Cluj-Napoca, Romania.*
[c] *National R&D Institute for Cryogenics and Isotopic Technologies, 4 Uzinei str., 240050 Râmnicu Vâlcea, Romania.*
[d] *University of Agricultural Sciences and Veterinary Medicine, 3-5 Mănăştur str., 400372 Cluj-Napoca, Romania.*
[*] *Corresponding author: culea.monica@phys.ubbcluj.ro*

The ω-3 fatty acids get into our diet through a food chain that starts from the algae – the richest ω-3 fatty acids sources – which are consumed by small aquatic animals, and ends with the fish, which eat them. Other sources of dietary ω-3 fatty acids, but with a shorter carbon chain, are the flaxseeds and the walnuts. The sources of ω-6 fatty acids in our diet are mostly the vegetable and seed oils [6].

Once consumed and absorbed into the body, the ω-3 and ω-6 fatty acids are incorporated into the cell membranes. Then, they are converted into intermediate molecules and finally, into hormone-like substances named *eicosanoids*. Among the *eicosanoids*, the most important are the *prostaglandins* – cellular signaling molecules that mediate the inflammatory process, fighting against infections and performing multiple roles within the immune and cardiovascular systems, and even within the brain [5, 6]. Recent studies have confirmed that mankind has evolved due to a balanced diet in ω-3 and ω-6 fatty acids. The ideal ω-3/ω-6 ratio, established by nature, is 1:1, while, in the modern world, in the typical American diet, this ratio has reached 1:20 [6].

Docosahexaenoic acid (4,7,10,13,16,19-DHA; $C_{22}H_{32}O_2$) is an ω-3 PUFA. Highest body concentrations of DHA are found in retinal membranes [5].

Eicosapentaenoic acid (5, 8, 11, 14, 17 -EPA; $C_{20}H_{30}O_2$) is the other major dietary ω-3 PUFA. EPA is present in blood components [5] and when working in tandem with DHA, the EPA eicosanoids derivatives maintain control over DHA eicosanoids derivatives [6].
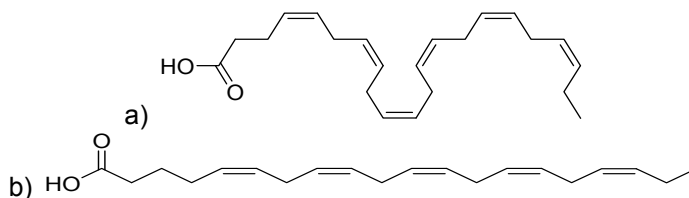
Figure 1. The ω-3 fatty acids chemical structures: a) DHA (C22:6 ω-3); b) EPA (C20:5 ω-3).

The nutritional quality of fish species can be evaluated from the fatty acids profile and by determining the EPA and DHA proportions [7].

The purpose of this research was to develop and validate a GC-MS method in order to investigate the essential fatty acids composition of rainbow trout (*Oncorhynchus mykiss*) plasma and meat.

RESULTS AND DISCUSSION

The fatty acids profile of freshwater fish is unique in variety and degree of unsaturation [8-16]. Their nutritional role is recognized. The two main omega-

3 fatty acids eicosapentaenoic acid and docosahexaenoic acid appear to decrease the risk of cancer [17-18]. Seasonal variation of these nutrients study is also very much studied [19-21].

Therefore, it is essential to have a simple and rapid method for qualitative and quantitative characterization of less common fatty acids (e.g. long-chain polyunsaturated fatty acids). The sensitivity and selectivity of GC-MS make it a powerful tool for the analysis of FAMEs [3].

Figure 2 presents the total ion current chromatogram of a mixture of trout plasma fatty acids. The FAMEs were identified using the NIST Mass Spectral Library.
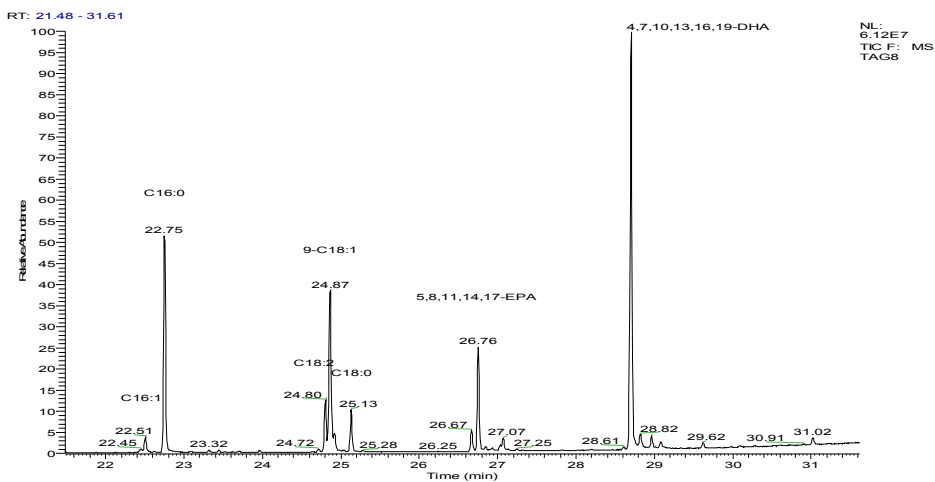
Figure 2. TIC chromatogram of trout plasma FAMEs obtained from GC-MS analysis.

The method was validated using fatty acids standards of 20 μg/ml. The limit of detection (LOD) was 1ng and precision and accuracy gave values lower than 20%.

Table 1 shows the fatty acids composition (weight% of total fatty acids) of trout plasma and meat. Saturated fatty acids represent only 25.61% (in plasma) and 31.04% (in meat) of the total fatty acids, palmitic acid (C16:0) having the highest concentration. Stearic acid (C18:0) is present in relatively smaller proportions (5.42% and 6.27%).

The unsaturated fatty acids (UFAs) constitute more than half of the total fatty acids found in plasma and meat samples (74.39% and 68.95%, respectively). The major monounsaturated fatty acids (MUFAs) were: C16:1, C18:1n-7, C18:1n-9, oleic acid (C18:1n-9) being the most abundant. Linoleic acid (C18:2 ω-6) represents 19% (in plasma) and 11.3% (in meat) of the total UFAs. The ω-3 PUFAs (the sum of EPA and DHA) represent approx. 26% and 36.6% respectively, of the total FAs found in trout plasma and meat.

Table 1. Fatty acid concentrations (%) in trout plasma and meat n = 5
(R_t – retention time; SFA – saturated fatty acids, UFA – unsaturated fatty acids;
SFA = C16:0 + C18:0; UFA = C16:1 + C18:2 + 9-C18:1 + C18:1 + EPA + DHA)

		Fatty acids (%)	
	R_t (min)	Plasma	Meat
hexadecenoic acid (C16:1)	22.51	2.86	2.19
hexadecanoic acid (C16:0)	22.75	20.18	24.78
9,12 octadecadienoic acid (C18:2)	24.80	14.13	7.81
9-octadecenoic acid (C18:1)	24.87	27.79	18.91
octadecenoic acid (C18:1)	24.93	3.62	3.43
octadecanoic acid (C18:0)	25.13	5.42	6.27
5,8,11,14,17 eicosapentaenoic acid (C20:5)(EPA)	26.76	5.41	8.51
4,7,10,13,16,19 docosahexaenoic acid(C22:6)(DHA)	28.71	20.59	28.11
SFA		25.61	31.04
UFA		74.39	68.95
EPA		5.41	8.51
DHA		20.59	28.11

The representatives mass spectra of DHA and hexadecanoic acid (palmitic acid) as FAMEs are shown in figures 3 and 5.

In the mass spectrum of DHA methyl ester the molecular ion is missing but it presents the specific ions M-15 (m/z 313), M-101 (m/z 227) of small intensity, indicating the molecular mass (M=328) and also high intensity ions, specific for alkyl group with double bonds, as m/z 55, 67, 79, 91 etc.
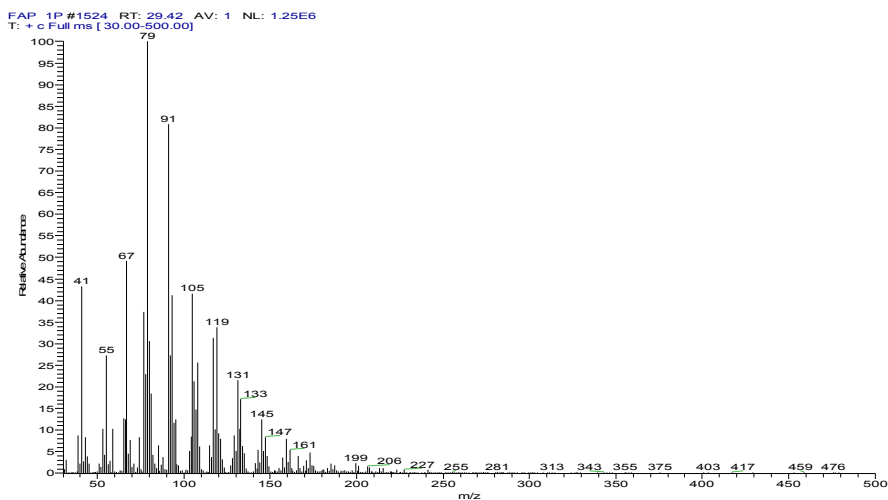
Figure 3. Representative mass spectrum of 4,7,10,13,16,19 DHA
methyl ester (M=328) in trout meat.

In figure 5, the ion m/z 270 represents the molecular ion peak of palmitic acid methyl ester. The ion m/z 239 [M-31]$^+$ representing loss of a methoxy group confirming a methyl ester compound. m/z = 227 [M-43]$^+$ represents loss of a C_3 unit (carbons 2 to 4), via a complex rearrangement, and m/z = 74 is the McLafferty rearrangement ion, also a specific ion confirming that the spectrum is that of a methyl ester. The series of ions m/z = 87, 101, 115,129, 143, 157, 199, etc., of general formula [$CH_3OCO(CH_2)_n$]$^+$, is a series of related ions formed by losses of neutral aliphatic radicals14 amu, of which that at m/z = 87 is most abundant.
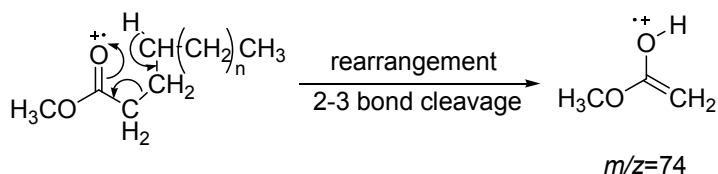
Figure 4. McLafferty rearrangement ion m/z 74 [9]

In the rearrangement ion m/z 74, a hydrogen atom from position 4 of the aliphatic chain migrates to the carbo-methoxy group, through a six-membered transition state, which is sterically favoured. If one of the hydrogen atoms on carbon 4 is substituted, the McLafferty ion will be lower in intensity, as appears in the mass spectra of derivatives of unsaturated fatty acids with increasing numbers of double bonds. The ion m/z = 227 [M-43]$^+$ is formed by a loss of a propyl radical. The ion at [M-29]$^+$ results by a cleavage between carbons 3 and 4 [9].
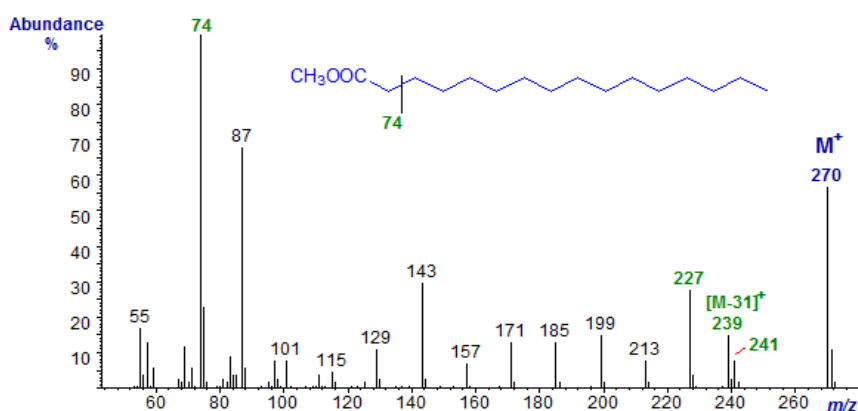
Figure 5. The mass spectrum of hexadecanoic acid methyl ester
(palmitic acid, M=270) [9]

Fig. 6 shows the considerable proportion of UFAs in comparison with SFAs, both in plasma and in meat. It should be noted that in meat samples, the ω-3 PUFAs represent 53% of the total UFAs.
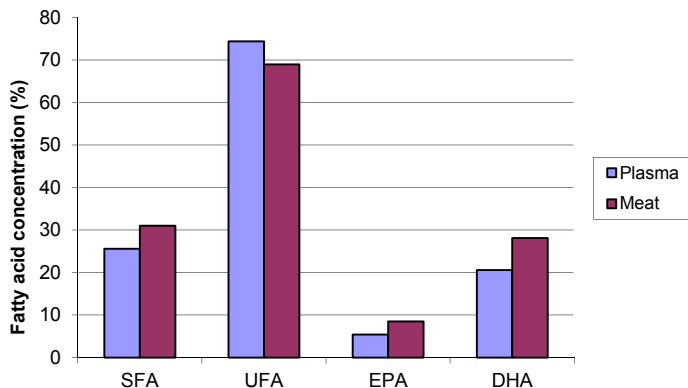
Figure 6. Fatty acids content of plasma and meat trout samples.

In plasma, the ω-3/ω-6 ratio was 1.84, while in meat, 4.68. The DHA/ EPA ratio was 3.8 in plasma and 3.3 in meat. This result can be explained by the fact that EPA is not found in great amounts in tissues as it is quickly used in DHA and eicosanoids biosynthesis [5].

CONCLUSIONS

The GC-MS method developed here for determining the fatty acid profile of trout plasma and meat samples is simple and reliable. Good validation parameters were obtained.

The PUFAs concentration found in trout plasma and meat was higher than that of the other FAs, in the following order: PUFA>MUFA>SFA. Our results proved that trout meat is a valuable source of essential fatty acids.

EXPERIMENTAL SECTION

Materials and methods

Acetyl chloride was purchased from Fluka (Germany) while all the other chemicals were from Merck (Darmstadt, Germany).

To quantify the FA concentrations by GC-MS, undecaenoic acid (C11:1) was used as internal standard.

The fatty acids (FA) were determined from trout plasma and meat samples. The FA were extracted from 0.5 mL of plasma by adding 0.5 mL chloroform: methanol 2:1 (v:v). The solution was shaken vigorously for 30 s, at room temperature.

1 g of trout meat was crushed with 1 g of quartz sand in a ceramic dish and homogenized with 5 mL distilled water. After a 5 min centrifugation, the supernatant was collected and the FAs were extracted by using the same solvent extraction conditions as for plasma. The samples were centrifuged for 5 min (5800 rot/min) and the upper methanol - water phase was removed. The lower chloroform phase containing the extracted fatty acids was then dried in a nitrogen flow, at 60°C.

The lipids were converted to corresponding FAMEs (fatty acids methyl esters) by esterification of the carboxylic functions with 200 µL methanol: acetyl chloride 4:1 (v:v), 20 min, 80°). The derivatives were evaporated to dryness by a nitrogen stream, at 60°C, and then dissolved in 500 µL dichloromethane. 10 µg of C11:1 was added to each sample for GC-MS quantitation.

GC – MS apparatus

The fatty acids were separated and identified using a Gas chromatograph Trace GC equipped with an Rtx-5MS capillary column (30m x 0.25mm I.D., 0.25 µm film thickness) and coupled to a quadrupole mass spectrometer Trace DSQ (Thermo Finnigan). The temperature program for FAMEs separation was: 50°C for 2 min rising with a rate of 8°C/min at 310°C (8 minutes). Helium was used as carrier gas at a flow rate of 1 mL/min. 1µL of each sample was injected into the GC-MS using the split mode (10:1) and a TriPlus autosampler. The mass spectrometer operated in electron impact (EI) mode at 70 eV. The following conditions were ensured: the transfer line temperature was set at 250°C, the injector temperature, at 200°C and the ion source temperature, at 250°C. The emission current was 100µA. The qualitative analysis was carried out in the 50-500 a.m.u. mass range.

GC – MS quantitation

The quantitative analysis was performed with respect to the internal standard (C11:1), by using the following formulas:

$$F_i = \frac{\dfrac{A_i}{A_j}}{\dfrac{m_i}{m_j}} \tag{1}$$

$$m_i\left(\mu g\right) = m_j\left(\mu g\right)\frac{A_i}{F_i \cdot A_j} \tag{2}$$

where F_i is the response factor of the compound i, m_i is the quantity of compound i, m_j is the internal standard quantity; A_i and A_j are the peak areas of the compounds (i and j).

ACKNOWLEDGMENTS

REFERENCES

1. E.D. Dodds, M.R. McCoy, L.D. Rea, J.M. Kennish, *Lipids*, **2005**, *40*, 419.
2. R.C. Murphy, S.J. Gaskell, *J. Biol. Chem.*, **2011**, *286*, 25427.
3. E.O. Abu, I. Oluwatowoju, *Prostaglandins, Leukotrienes and Essential Fatty Acids,* **2009**, *80*, 189.
4. N. Dubois, G. Barnathan, J.-P. Gouygou, J.-P. Bergé, *Eur. J. Lipid Sci. Technol.,* **2009**, *111*, 688.
5. J.P. SanGiovanni, E.Y. Chew, *Progr. in Retinal and Eye Research*, **2005**, *24*, 87.
6. S.L. Andrew, *"The omega-3 connection: the groundbreaking omega-3 antidepression diet and brain program*", Elena Francisc Publishing, Bucharest, **2005**, chapter 2.
7. M.D. Huynh, D.D. Kitts, *Food Chem.,* **2009**, *114*, 912.
8. U. Chukwuemeka, G.I. Ndukwe, T.O. Audu*, Internet J. Food Safety*, **2008**, *10*, 9.
9. http://lipidlibrary.aocs.org/ms/ms03/index.htm
10. N.M. Arat, I.H. Haliloğlu, Ö. Ayik, *Turkish J. Vet. Animal Sci.*, **2003**, *27*, 311.
11. R.K. Booth, R.S. McKinley, J.S. Ballantyne, *J. Fish Biol.,* **1999**, *55*, 260.
12. C. Cahu, J.Z. Infante, T. Takeuchi, *Aquaculture J.,* **2003**, *227*, 254.
13. I.H. Haliloğlu, N.M. Aras, *Turkish J. Vet. Animal Sci.*, **2002**, *26*,1097.
14. R.J. Henderson, *Arch. Anim. Nutr.*, **1996**, *49*, 5.
15. C. Ugoala, G.I. Ndukwe, T.O. Andu, *Internet J. Food Safety*, **2008**, *10*, 9.
16. A.P. Simopoulos, *Eur. Heart J.Suppl.*, **2001**, *3*, 8.
17. A. Hjartåker, *Scandinavian Journal of Nutrition*, **2003**, *47*(3), 111-122.
18. N. Kaba, Y. Sennan, B. Birol, *Journal of Animal and Veterinary Advances*, **2009**, *8*(3), 541-544.
19. T. Kandemir, N. Polat, *Journal of Fisheries and Aquatic Sciences*, **2007**, *7*, 27-31.
20. C. Stripp, K. Overvad, J. Christensen, L.B. Thomsen, A. Olsen, S. Møller, A. Tjønneland, *The Journal of Nutrition*, **2003**, *133*, 3664-3669.
21. D.R. Tocher, *Journal of Fisheries Science*, **2003**, *11*(2), 107-184.

ASSESSEMENT OF TRIAZINE HERBICIDES CONTENT IN HONEY SAMPLES BY SOLID-PHASE EXTRACTION AND HPLC ANALYSIS

ANDREEA DRĂGUŞ[a], MIHAIL SIMION BELDEAN-GALEA[a*]

ABSTRACT. Triazines are a group of compounds used as selective pre-emergence herbicides in different types of crops, such as corn, soybean, as well as orchards and vineyards. Due to their large use in the agricultural sector triazines have been detected in different types of food matrices. In the present study, the triazines content in different honey samples collected directly from private producers in various countryside areas from Romania is evaluated. The clean-up and extraction procedure was carried out by solid phase extraction and further analysis and quantification undertaken with high performance liquid chromatography. In the analyzed samples, the presence of triazine herbicides was detected. Their concentrations ranged between 4.97 and 997.5 µg/kg honey, exceeding in almost all analyzed samples the EU MRLs requirements for triazines in honey.

Keywords: triazine herbicides, honey, solid phase extraction, high-performance liquid chromatography

INTRODUCTION

The agricultural sector is the most significant user of pesticides. In the long term, these chemicals can cause deleterious effects upon the environment [1]. Contamination of different matrices allows pesticides to spread through the food chain, thus impacting human health [2, 3]. Therefore, the European Union has established Maximum Residue Levels (MRLs) in order to meet food safety requirements, the maximum residual levels of pesticides being established in Regulation (EC) No. 396/2005, the lowest limit being 0.01 mg/kg and the highest 1 mg/kg.

Triazines represent a class of compounds used as selective pre-emergence herbicides in different types of crops, such as corn, soybean, as well as orchards and vineyards Their persistence in soil has been shown to

[a] *Babeş-Bolyai University, Faculty of Environmental Science and Engineering, 30 Fântânele Street, RO-400294, Cluj-Napoca, Romania.*
[*] *Corresponding author: simion.beldean@yahoo.com*

have a DT_{50} (half-life) of 40 days and can reach up to 166 weeks, depending on the soil type [4, 5].

Different studies showed the presence of triazine herbicides in various matrices such as water [6-10], soil [4, 5] agricultural products [11], seaweeds [12] food samples [13-15] etc. which suggest that these chemicals are mobile in the environment.

Taking into account that triazine compounds can act as endocrine disruptors, mimicking hormonal activity [16], in the last period different methods for the analysis of these compounds in various matrices have been developed.

The most employed techniques involved in the quantification of triazine herbicides are gas and liquid chromatography [6-18].

For the extraction, different methods, such as liquid phase extraction (LPE) [8, 9, 11, 13, 14], solid phase extraction (SPE) [10, 12, 17] or supercritical fluid extraction (SFE) [18, 19] have been used.

Since LPE requires the use of significant volumes of toxic organic solvent and SFE involves an expensive instrumentation, SPE remains the most suitable method for the analysis of triazine herbicides in liquid samples.

Honey is a staple product consumed by a large percentage of society due to its beneficial properties on human health. One of the most important checked parameter from honey samples is the pesticides residue.

Pesticides residue can get into honey via spraying the crops during the collection of pollen and nectar [20]. Due to this reason the assessment of pesticides pertaining to this matrix presents importance for quantifying their risk to human health.

In this paper, the assessment of triazine herbicides content in honey samples collected directly from private producers in various countryside areas from Romania located in Transylvania, Moldova and Dobrogea is reported. The analysis of triazines was performed by solid-phase extraction followed by high performance liquid chromatography analysis. The results of the analyzed samples showed the presence of triazine herbicides in concentrations ranging from tens to hundreds µg/kg honey.

The novelty of this work consists in the assessment of triazine content in matrices that is not subjected to routine monitoring. Thus, the risk associated with their consumption is difficult to predict.

RESULTS AND DISCUSSION

1. Analytical performance of the analysis method

The performance of the HPLC method used for the analysis of triazine herbicides in honey samples was expressed by precision, linearity, limit of detection (LOD) and limit of quantification (LOQ) (Table 1).

Precision was expressed as intra-day precision (repeatability) by means of five replicates (n = 5) of a triazine standard mixture in concentration of 1.25 μg/mL. The obtained results were situated under 3% which prove a good repeatability of the method.

Table 1. Analytical performances of HPLC method

Compound	Linear curve equation (linear range 0.62-10 ng)	R^2	Slope	SD	LOD (μg/L)	LOQ (μg/L)	RSD %
Simazine	y = 49916x - 3596.3	0.996	49916	379	0.023	0.076	1.24
Prometon	y = 46067x - 782.58	0.992	46067	542	0.035	0.118	1.75
Atrazine	y = 42868x - 3430.5	0.999	42868	797.9	0.056	0.186	2.98
Ametryn	y = 43269x + 1969.7	0.998	43269	452	0.031	0.104	1.55
Propazine	y = 43269x + 1969.7	0.999	43269	586.1	0.041	0.135	1.98
Prometryn	y = 37949x + 2154.8	0.996	37949	441.9	0.035	0.116	1.67
Terbutryn	y = 37711x + 3049.9	0.999	37711	673.0	0.054	0.179	2.64

R^2 - coefficient of determination; SD - standard deviation; LOD - limit of detection, LOQ - limit of quantification, RSD - relative standard deviation for (n = 5);

The quantification of the target compounds in real samples was made using the calibration curve method. The data from Table 1 shows a good linearity for all target triazines and the R2 values ranging from 0.992 to 0.999. LOD and LOQ of studied triazines were determined using the standard deviation and the slope of each calibration curve. LODs were situated in the range of 0.076 - 0.056 μg/L and LOQs in the range of 0.076 – 0.18 μg/L, respectively.

2. Accuracy of SPE procedure

Because for the extraction of the triazines from honey samples a slightly modified Albero et al. [21] method was used, the accuracy of the extraction procedure was tested.

The accuracy was expressed by extraction recovery (ER) and was calculated using the follow equation:

$$ER\,(\%) = \frac{(amount\,found - initial\,amount)}{spiked\,amount} \, x\,100$$

The results presented in Table 2 show good recoveries of the studied compounds, the values being situated over 80%. Thus the SPE protocol has been used for the extraction of the triazine herbicides from collected honey samples.

Table 2. Recoveries of the triazine herbicides in honey samples

Compound	Initial Amount (ng)	Spiked amount (ng)	Amount found[(*)] (ng)	ER ± SD (%)
Simazine	-	500	446	89.2 ± 0.70
Prometon	-	500	446	89.2 ± 1.50
Atrazine	-	500	483	96.6 ± 1.53
Ametryn	-	500	480	96 ± 2.08
Propazine	-	500	437	87.4 ± 2.52
Prometryn	-	500	439	87.8 ± 3.51
Terbutryn	-	500	460	92 ± 3.56

[(*)] - mean value of three replicates

3. Analysis of honey samples

The analyses employed in the present study demonstrate the presence of triazines in the honey samples. In Figure 1 it is shown a juxtaposed chromatogram of a honey sample and a standard mixture where the presence of the triazines can be observed.
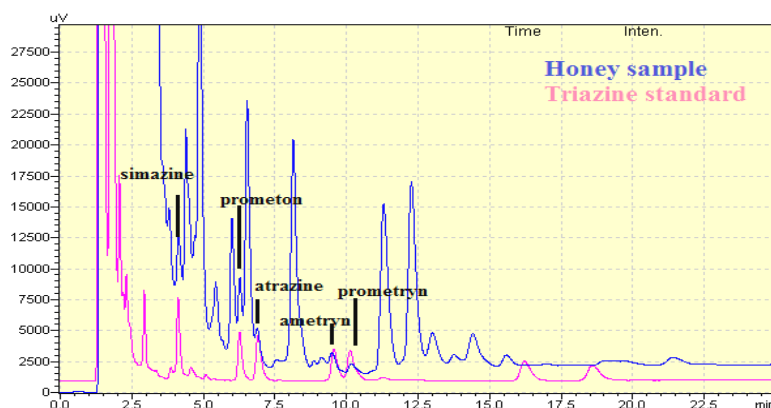
Figure 1. Chromatogram of tested triazines in honey sample (honey sample – upper chromatogram; triazine standard mixture (1.25 µg mL^{-1}) – lower chromatogram)

The results of the analyzed samples showed that the concentrations of triazine herbicides from the honey samples are dependent on the sampling area (Table 3).

Thus, the highest amounts of triazine herbicides were found in the samples collected from Dobrogea and Moldova areas, where modern agriculture is practiced which involves the use of pesticides for plant treatments. The found concentrations ranged between 50.2 and 102.11 µg/kg in Tulcea County (sample 4T, 5T) and 80.67 and 997.54 µg/kg in Vaslui County (samples 7V, 8V, 9V, 10V, 11V, 12V, 13 V).

Table 3. The occurence of triazine herbicides in analyzed honey samples

Sample code	Concentration (μg/kg)							
	Simazine	Prometon	Atrazine	Ametryn	Propazine	Prometryn	Terbutryn	Total
2 C	nd	nd	1.19	nd	5.65	nd	nd	6.84
3 C	nd	nd	4.97	nd	nd	nd	nd	4.97
4 T	50.20	nd	nd	nd	nd	nd	nd	50.20
5 T	34.59	26.08	11.18	16.34	13.92	nd	nd	102.11
7 V	80.49	nd	nd	nd	nd	nd	34.58	115.07
8 V	58.56	54.96	nd	nd	nd	nd	nd	113.52
9 V	3.80	7.80	75.97	60.29	88.74	nd	15.00	251.6
10 V	116.05	31.66	nd	nd	20.04	nd	nd	167.75
11 V	82.05	17.15	nd	nd	4.78	nd	nd	103.98
12 V	32.73	nd	nd	nd	nd	nd	47.94	80.67
13 V	490.0	507.5	nd	nd	nd	nd	nd	997.5
14 B	nd	nd	nd	nd	nd	nd	nd	-

nd- not detected

The lowest concentrations ranged between 4.97 and 6.84 μg/kg were found in samples collected from Cluj County (sample 2 C and 3 C), while in the sample collected from Bistrita-Năsăud County (sample 14 B) triazines did not occur. In these two regions usually traditional agriculture is practiced and the amount of pesticides use for plant treatments is low or entirely missing.

The high concentrations of triazine herbicides found in acacia honey samples (sample 8V, 9V, 11V,) could be explained by the fact that the flowering of acacia tree corresponds to the period in which these herbicides have been applied on the corn crop.

It is also observed that the most prevalent herbicides are simazine and prometon while prometryn was not found in any samples.

If it is taken into consideration that atrazine, simazine and terbutryn have been recently introduced on the list of priority substances regarding the Water Framework Directive (WFD) (2000/60/EC) their use in agriculture should be limited.

Moreover, analyzing the obtained results and taking into consideration that the MRLs for simazine in honey established by the EU is 0.01 mg/kg it can be observed that in the analyzed samples the total content of triazine exceeds the regulatory framework for those samples collected from Moldova and Dobrogea areas.

CONCLUSIONS

This study showed the presence of triazine herbicides in honey samples in concentrations which are dependent on the sampling zone.

The highest content of triazines which exceeds the EU regulatory framework was found in the samples collected from Moldova and Dobrogea, areas where modern agriculture is practiced.

In Transylvania area where usually traditional agriculture is practiced the content of triazines does not exceed EU requirements.

The presence of triazine herbicides in honey sample obtained from tree flowers and poly-flora proves the mobility of these chemicals in environmental compartments.

EXPERIMENTAL SECTION

1. Reagents and solutions

A standard mixture of seven triazine herbicides (simazine, prometon, atrazine, ametryn, propazine, prometryn and terbutryn) with a concentration of 100 μg/mL each herbicide, dissolved in methanol was purchased from Sigma-Aldrich (USA). The working solution with a concentration of 10 μg/mL for each herbicide was obtained by dilution of the standard mixture in methanol. Acetonitrile and methanol (HPLC grade) were obtained from Merck (Germany). Milli-Q water was prepared using a Milli-Q Plus water system from Millipore (USA). Potassium dihydrogen phosphate (KH_2PO_4) with a purity of 99% was purchased from Sigma-Aldrich.

2. Instrumentation and chromatographic conditions

Chromatographic separation and determination of the triazine herbicides were carried out on a Shimadzu high performance liquid chromatograph, equipped with a 10 LC pump, 10 LSD UV-Vis detector and a manual injection valve with a loop of 5 μL. A NovaPak-C18 column (30 cm × 3.9 mm, 4 μm, Waters, USA) was used for the separation of the compounds.

Separation of the analytes was performed by isocratic elution with a mixture of acetonitrile:phosphate buffer (25 mM) (40:60, *v/v*) at a flow rate of 1.2 mL/min. The detection wavelength was set at 220 nm.

The quantification of the target compounds in real samples was made by means of the calibration curve. For this purpose five standard solutions in concentration of 0.625; 1.25; 2.5; 5 şi 10 μg/mL were prepared by dilution of the standard mixture with methanol. The calibration curves were built using the chromatographic peak area and the concentration of each triazine herbicide.

3. SPE procedure

Isolation and preconcentration of the target compounds from the honey samples were carried out on a SPE device (Supelco) using C18 EC (end capping) cartridges purchased from Phenomenex, USA. Before extraction

the SPE cartridges were conditioned in three steps using 5 mL Milli-Q water, followed by 5 mL MeOH and again by 5 mL Milli-Q water.

For the extraction of the triazine herbicides from the honey samples it was employed a slightly modified version of Albero et al. [21] as follows: 10 g of honey were dissolved in 40 mL mixture of Milli-Q water:methanol (70:30 *v/v*) and subjected to sonication for 15 minutes. The obtained solution was passed through the extraction cartridge at a flow rate of 2 mL/min for the retention of the herbicides. After that, the cartridge was washed by passing 5 mL of Milli-Q water through the cartridge in order to remove the interferences. Finally, the target compounds were eluted with 3 mL of methanol and evaporated to dryness under nitrogen. The residue was diluted in 0.5 mL methanol and then injected into the chromatographic system for the analysis of target compounds.

To study the accuracy of the SPE procedure 10 g of honey dissolved in 40 mL mixture of Milli-Q water:methanol (70:30 *v/v*) were spiked with 500 ng of each herbicide and extracted by SPE according to the protocol described above.

4. Sampling points

In order to have a better assessment of the triazine herbicides use in agriculture over their content in honey, three areas from Romania were taken into account. One area is situated in Transylvania (Cluj County and Bistriţa-Năsăud County), where traditional agriculture is practiced, and another two situated in Moldova (Vaslui County) and Dobrogea (Tulcea County) respectively, where modern agriculture is practiced (Figure 2).

The honey samples were collected in sterilized polyethylene bottles with a volume of 100 mL and kept at room temperature until analysis. Four types of honey were taken into consideration; acacia flower (sample 3C, 8V, 9V and 11V), sun flower (sample 5T, 7V and 10V), colza (sample 4T and 12V) and poly-flora (sample 2C, 13V and 14B).

Figure 2. The map of honey sampling areas

ACKNOWLEDGEMENTS

REFERENCES

1. Y. Guo, X.Y. Meng, H.-L. Tang, E.Y. Zeng, *Environmental Pollution*, **2008**, *155(1)*, 150.
2. L. Ferencz, A. Balog, *Carpathian Journal of Earth and Environmental Sciences,* **2010***, 5(1)*, 111.
3. A.F. Hernandez, T. Parron, A.T. Tsatsakis, M. Requena R. Alarcon, O. Lopez-Guarnido, *Toxicology,* **2013**, *307*, 136.
4. C. Yanze-Kontchou, N. Gschwind, *Journal of Agricultural and Food Chemistry*, **1995**, *43*, 2291.
5. K.H. Bowmer, *Australian Journal of Soil Research*, **1991**, *29(2)*, 339.
6. A. Drăguş, M.S. Beldean-Galea, R. Mihăiescu, T. Mihăiescu, D. Ristoiu, *Environmental Engineering and Management Journal*, **2012**, *11(2)*, 319.
7. D. Vonberg, J. Vanderborght, N. Cremer, T. Putz, M. Herbst, H. Vereecken, *Water Research*, **2014,** *50*, 294.
8. X. Liu, Z. Shen, P. Wang, C. Liu, Z. Zhou, D. Liu, *Journal of Chromatography A*, **2014**, *137*, 58.
9. Q.-X. Zhou, Y.-Y. Gao, *Chinese Chemical Letters*, **2014**, *25(5)*, 745.
10. J.J. Berzas Nevado, C. Guiberteau Cabanillas, M.J. Villaseñor Llerena, V. Rodríguez Robledo, *Microchemical Journal*, **2007**, *87,* 62.
11. P. Li, X. Yang, H. Miao, Y. Zhao, W. Liu, Y. Wu, *Analytica Chimica Acta*, **2013**, *781*, 63.
12. N. Rodríguez-González, M.J. González-Castro, E. Beceiro-González, S. Muniategui-Lorenzo, D. Prada-Rodríguez, *Talanta*, **2014**, *121*, 194.
13. Y. Wang, J. You, R. Ren, Y. Xiao, S. Gao, H. Zhang, A. Yu, *Journal of Chromatography A*, **2010**, *1217*, 4242.
14. X. Yang, R. Yu, S. Zhang, B. Cao, Z. Liu, L. Lei, N. Li, Z. Wang, L. Zhang, H. Zhang, Y. Chen, *Journal of Chromatography B*, **2014,** *972*, 111.
15. K.C. Zacharis I. Rotsias, P.G. Zachariadis, A. Zotos, *Food Chemistry,* **2012**, *134(3)*, 1665.
16. M. Suzawa, H.A. Ingraham, *PLoS ONE,* **2008**, *3*, e2117. DOI:10.1371/journal.pone.0002117
17. P. Önnerfjord, D. Barceló, J. Emnéus, L. Gorton, G. Marko-Varga, *Journal of Chromatography A*, **1995**, *737,* 35.
18. M.A. Garcia, M.I. Fernandez, M.J. Melgar, *Bulletin of Environmental Contamination and Toxicology*, **1995**, *54*, 825.
19. S.R. Rissato, M.S. Galhiane, F.R.N. Knoll, B.M. Apon, *Journal of Chromatography A*, **2004**, *1048(2)*, 153.
20. K.A. Stoner, B.D. Eitzer, *PLoS ONE*, **2013**, *8(10)*, e77550. DOI:10.1371/journal.pone.0077550
21. B. Albero, C. Sanchez-Brunete, J.L. Tadeo, *Journal of Agricultural and Food Chemistry,* **2004**, *52*, 5828.

COMPARATIVE STUDY OF POLYPHENOLS FROM PROPOLIS EXTRACTS OF DIFFERENT ORIGIN

**ADRIANA DĂRĂBAN[a], NELI KINGA OLAH[a,b,*],
RAMONA FLAVIA CÂMPEAN[b], FLAVIA FURTUNA[b], CODRUTA COBZAC[c,*],
GHEORGHE DEHELEAN[a], MARIUS BOJIȚĂ[d], DANIELA HANGANU[d]**

ABSTRACT. The propolis, a resinous substance produced by bees, was used from ancient times as one of the best general panaceea. The main active compounds known in propolis are the phenolic acids and flavonoids from the class of polyphenols. This paper presents the flavonoids and phenolic acids evaluation by chromatographic (TLC and HPLC) methods of some propolis samples originating from Arad (4 samples) and Bihor (3 samples) counties, from west of Romania. There were identified the caffeic, ferulic and gallic acids respectively the chrysine and kaempferol. The chrysine content ranges from 0.15 to 1.95 mg/ml and the kaempferol from 0.07 to 8.88 mg/ml. The caffeic acid content ranges from 0.05 to 0.70 mg/ml and the ferulic acid from 0.01 to 1.39 mg/ml.

Keywords: propolis, polyphenols, flavonoids, phenolic acids, TLC, HPLC.

INTRODUCTION

Propolis means, in greek language, some that defend the city or the hive. The propolis is a resinous product, made by the honey bees (*Apis mellifera* L.) from the waxes and resinous compounds collected from the trees and other plants. The propolis can have different aspects, generally it is a solid product with gumy aspect, with a color from ocker yellow to red, brown, light brown or greenish [1]. The bees use the propolis to protect the hive against infections, bacterias or fungus.

[a] *"Vasile Goldis" Western University of Arad, Faculty of Medicine, Pharmacy and Dental Medicine, 86 Rebreanu Street, Arad, Romania*
[b] *SC PlantExtrakt SRL, 407059 Rădaia. Cluj, Romania*
[c] *Babes-Bolyai University, Faculty of Chemistry and Chemical Engineering, Cluj-Napoca, Romania*
[d] *Iuliu Hațieganu University of Medicine and Pharmacy, Faculty of Pharmacy, Cluj-Napoca, Romania*
* *Correspondent authors: olahdr@aol.com, neliolah@yahoo.com, codruta.cobzac@yahoo.com*

The propolis has been used since ancient times because of its therapeutic effects. It can be used for the treatment of many diseases, because it shows antibacterial, antiseptic and detoxifying effects. It is a basic product used in apitherapy, an alternative medicine very popular in the antic Egypt, Greece and China.

The composition of propolis depends on various factors such as season and vegetation of the area. The chemical analysis of raw propolis show the presence of resins, waxes, essential oil, polyphenols, sugars, aminoacids, vitamins, enzymes, mineral salts, pollen and other solid impurities [2]. The recent studies do not have quantified more than 2-3 % of essential oil represented by aromatic compounds like benzyl-derivatives, vanilin, eugenol in European propolis, sesquiterpenes in Asian propolis and monoterpenes in South American propolis [3]. An other active compound class that is quantitatively important in propolis is the polyphenols represented by flavonoids, mostly aglyka of the glycosidic flavonoids from the plant species from that the bees collect the substances, respectively phenolic acids, mostly hydroxybenzoic derivatives like caffeic acid, ferulic acid or gallic acid [4].

European, Chinese and Argentinian propolis are characterized by the presence of phenolic acids and flavonoids, the most abundant being chrysin (2–4%) [5]. The total phenolic compound content found in ethanolic extract of red propolis (232 mg/g) was higher than that ever found for Brazilian propolis samples [6,7]. These values were similar to those find in temperate climate propolis originating from the species *Populus* sp., a resin-producing plant rich in polyphenols [7,8]. The low flavonoid concentration (43 mg/g) observed in ethanolic extract was similar to that normally found for Brazilian green propolis [8].

Due to its complex chemical composition, a lot of benefic effects of propolis and its extracts were identified. Recent studies highlighted the beneficial effect of hive products on health as they improve circulation, reduce inflammation and stimulates immunity. Propolis is known as one of the most powerful natural antibiotic. The presence of polyphenols and essential oil impart antimicrobial, antifungal, antitumoral, anti-inflammatory, hepatoprotective, antidiabetic, cardioprotective, antiangiogenic and immunomodulatory properties. Moreover, it was proved that propolis contains compounds which regenerate the damaged tissues, improve the liver and pancreas functions and have epithelisant, anti-edematous, radioprotective and antiasthmatic effects [9-11].

Due to its complex composition and special powerful therapeutic effects propolis was used to prepare several medicinal products, administered internally or applied externally and special cosmetic products – shampoo, creams, etc. This wide range of uses is based on its antioxidant effect conferred by the high content of polyphenols belonging mainly to flavonoids and caffeic acid derivatives.

In Romania the apiculture is a wide spread agricultural activity. The bee products were used and studied from long time. Mărghitaș et al. have studied the propolis from Transylvania, Cluj, Hunedoara, Brașov counties from agricultural, chemical and therapeutic point of view. They found that the Transylvanian propolis contains 0.55 – 3.91 mg/g chrysin, 0.56 – 2.66 mg/g galangine and 0.46 – 1.49 mg/g caffeic acid [12,13]. The Moldavian propolis was studied by Croci et al., finding in three different origin samples high quantities of phenolic acid, mainly caffeic acid, ferulic acid, 3,4-dimethoxycinnamic acid and protocatehic acid and also a high content of total flavonoids, around 25 % expressed in quercetine [14,15]. Coneac et al. [16,17] have studied the propolis from Timiș county, Banat, west part of Romania. The aim of their research was to optimize the extraction conditions of polyphenols from propolis and to standardize the hydroalcoholic extract. They have found in the three studied samples important quantities of quercetine (0.386 – 13.2 mg/g), apigenine (0.213 – 13.8 mg/g), kaempferol (0.137 – 3.198 mg/g), rutoside (0.496 – 37.184 mg/g), chrysin (0.638 – 31.9 mg/g) respectively caffeic acid (0.316 – 19.365 mg/g). The qualitative and quantitative analyzes were performed by chromatographic (TLC, HPLC) and spectral methods [12-17], being employed also image analysis combined with appropriate fuzzy clustering method [18].

This study presents the evaluation of the chemical quality of propolis from west part of Romania.

RESULTS AND DISCUSSION

The first step of monitoring of polyphenols from propolis was made by TLC. This analysis show the polyphenol fingerprint of studied samples and can be evaluated the similarities and the differences. In figure 1 and 2 are presented the TLC chromatogram of the studied propolis samples.

The TLC chromatogram show the presence of more polyphenols in the samples originating from Covăsânț, Dorgos and Ștei respectively Livada Beiuș. Caffeic acid and chrysine were identified in all samples; Covăsânț, Dorgos, Ștei and Livada Beiuș samples having the highest concentrations. The less concentrated in polyphenols is the sample from Lipova. It can be observed a lot of similarities and differences between the studied samples, both from qualitative and quantitative point of view. The similarities are due probably by the collection of the pollen and waxes from the same species, the differences are due by the specific species from the bees harvesting areas. In the sample from Dorgos can be seen some special compounds colored in red that are not present in other studied propolis samples.
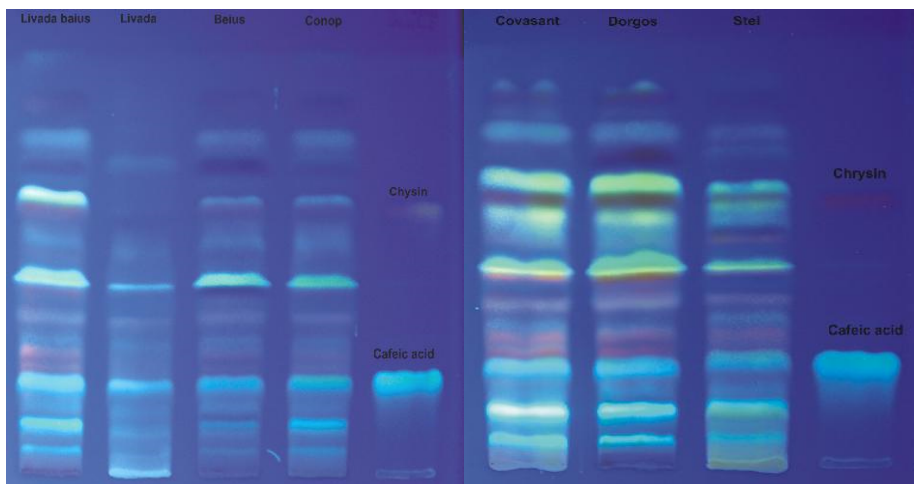
Figure 1. TLC chromatogram in fluorescence at 365 nm,
after spraying with Neu-PEG reagent
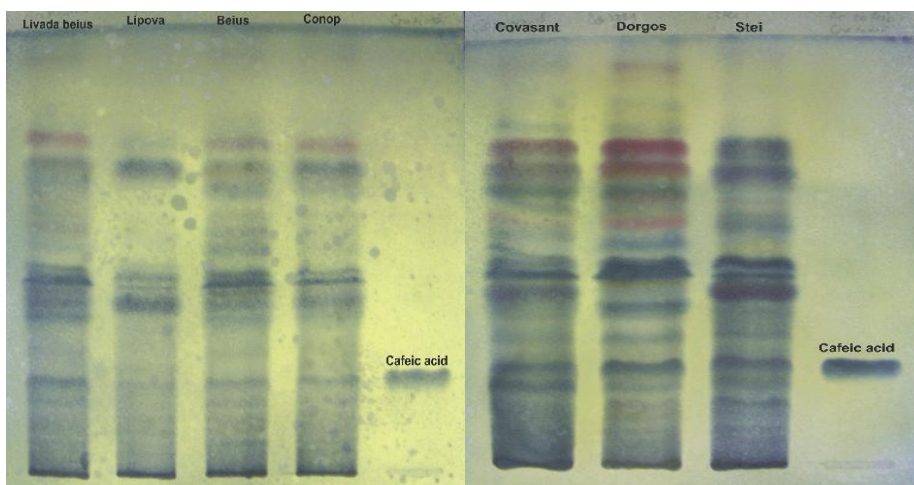
Figure 2. TLC chromatogram in visible light, after spraying
with anisaldehyde and phosphomolibdenic reagents

To determine more accurately and to quantify individualy some of polyphenols HPLC analysis was performed. In figures 3-5 are presented the obtained HPLC chromatograms. In table 1 are presented the retention times and the wavelength corresponding to the maximum absorbance from UV-VIS spectra for standards and the separated compounds from the

studied propolis samples. The identification of the individual compounds is based on the comparison of retention times, maximum wavelength values and UV-Vis spectra shapes of the standards and the separated compounds.

It can be observed the presence of caffeic acid in all studied samples, the ferulic acid in the samples originating from Conop, Arad county respectively in all 3 samples from Bihor county. The gallic acid was found just in the sample from Ștei. As flavonoids, kaempferol was found in the samples from Covăsânț, Dorgos, Ștei and Beiuș, respectively chrysine in the samples from Conop, Covăsânț and Ștei.

In figure 6 are presented the calibration curves for the identified compounds (caffeic acid, ferulic acid, gallic acids, chrysine and kaempferol). In table 2 are presented the equations for the calibration curves, correlation factors and the concentrations determined in the propolis extracts.

It can be observed also some peaks that cannot be identified due to lack of standards. So, the compound separated at 1,7 minutes is present in all samples (less Beiuș); 7,6-7,8 minutes in all samples; 10,2-10,9 minutes respectively 22,2-23,4 minutes in all samples (less Ștei); 39,5-41,0 minutes is present just in the samples from Bihor county. These similarities can be explained based on the similar species from the bees harvesting area, while the differences appear probably because of some species specific only for that area.
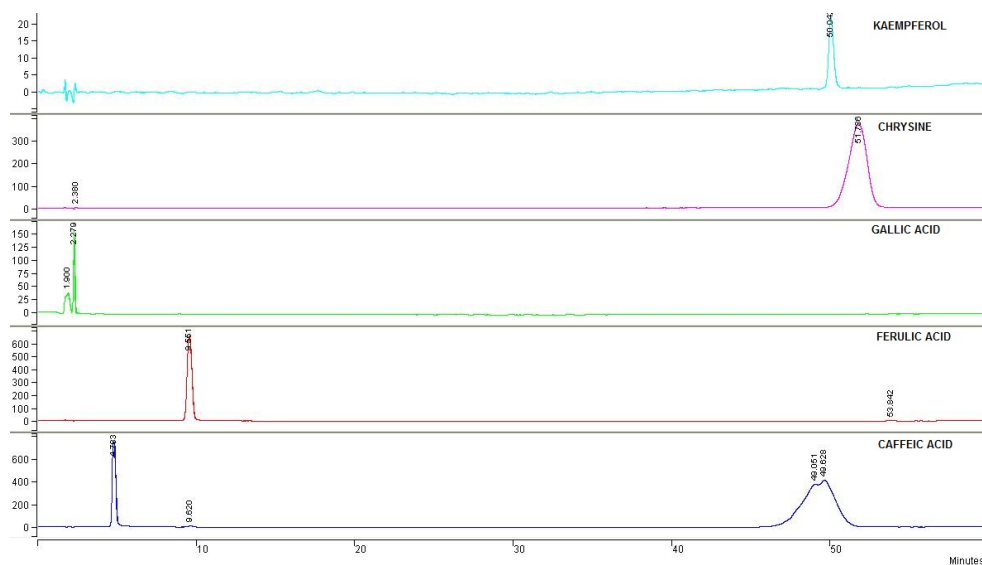
Figure 3. The HPLC chromatogram of standards
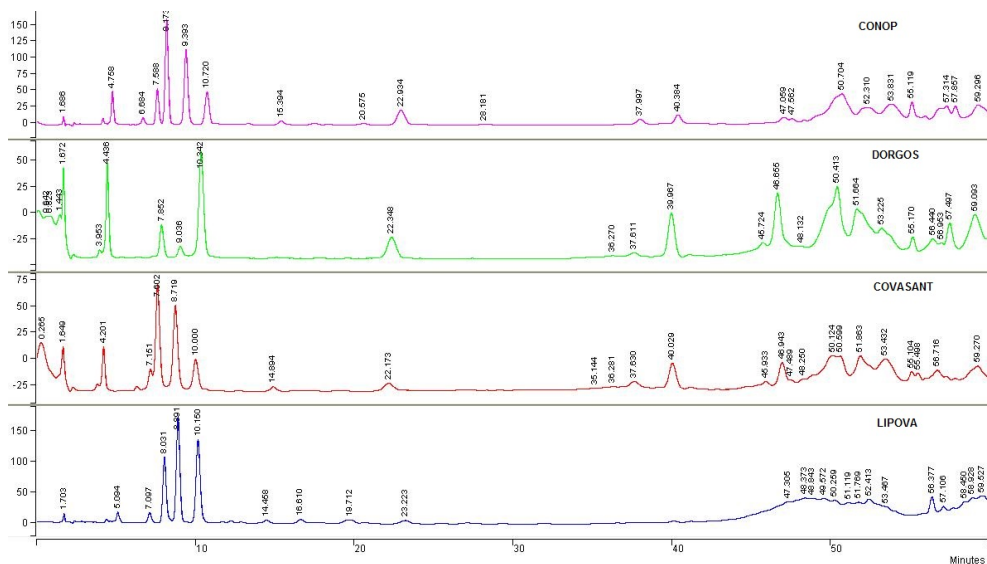
Figure 4. The HPLC chromatogram of the samples from Arad county
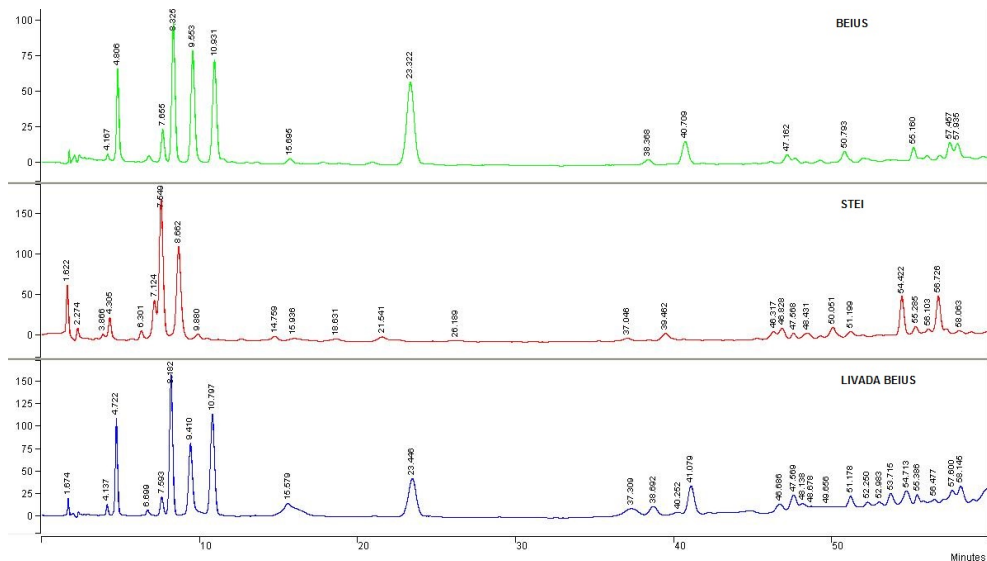
Figure 5. The HPLC chromatogram of the samples from Bihor county

The HPLC results confirm those obtained in the first TLC monitoring step.

HPLC quantitative assessment reveals a high content of flavonoids and phenolic acids in the Dorgos (Arad) sample and less in the Lipova (Arad). These results confirm also the TLC analysis findings.
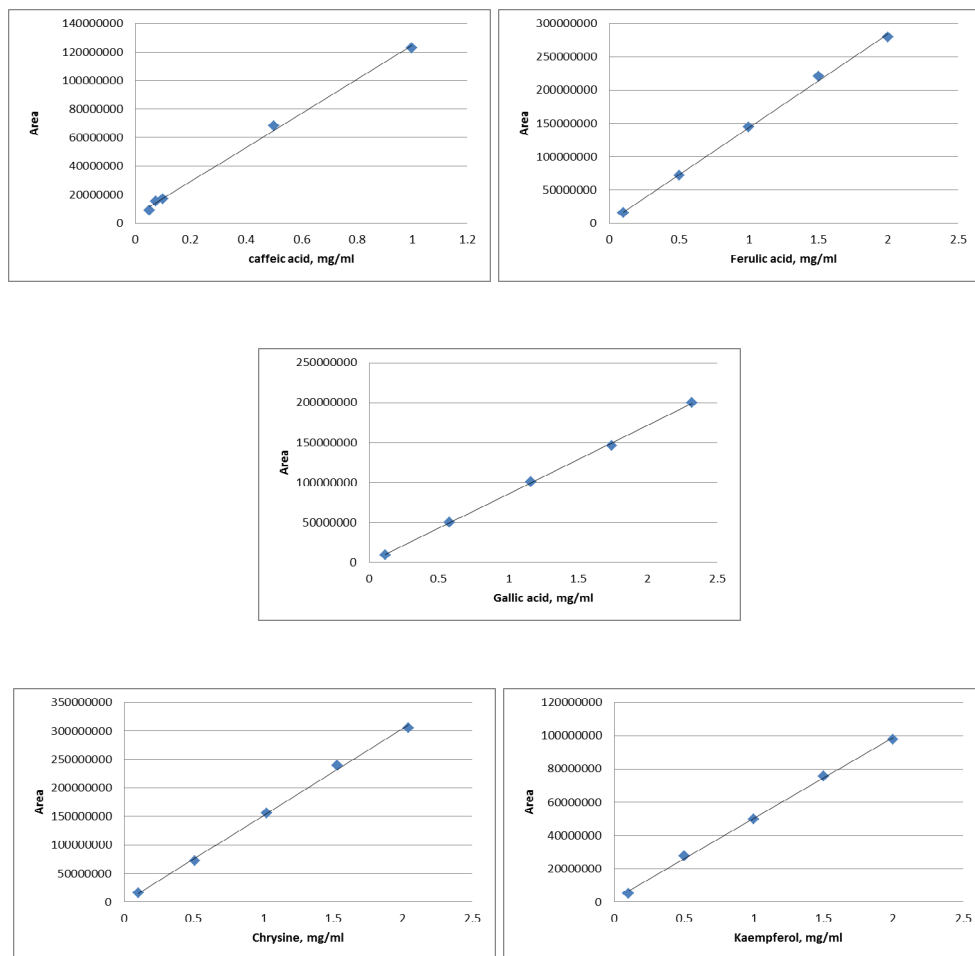
Figure 6. The HPLC standards calibration curves

Table 1. Retention times and maximum wavelength from UV-Vis spectra

Samples		Caffeic acid	Ferulic acid	Gallic acid	Kaempferol	Chrysine
Standards	RT, min	4.9	9.6	2.3	50.0	51.8
	UV-Vis max. abs., nm	238 322	236 321	270	265 365	267 311
Conop	RT, min	4.8	9.4			50.7
	UV-Vis max. abs., nm	240 322	237 320			267 311
Lipova	RT, min	5.1				
	UV-Vis max. abs., nm	238 322				
Covăsânţ	RT, min	4.2			50.0	51.9
	UV-Vis max. abs., nm	237 322			267 366	267 312
Dorgos	RT, min	4.4			50.4	
	UV-Vis max. abs., nm	238 322			266 366	
Ştei	RT, min	4.3	9.6	2.3	50.0	51.2
	UV-Vis max. abs., nm	239 322	237 321	271	266 366	266 310
Beiuş	RT, min	4.8	9.6		50.8	
	UV-Vis max. abs., nm	239 322	237 321		264 364	
Livada Beiuş	RT, min	4.7	9.4			
	UV-Vis max. abs., nm	238 321	237 321			

If we compare our results with the results obtained for European, Chinese and Argentinian propolis we can observe that the sample from Conop has a comparable chrysine content (1.95 mg/ml in 1:10 extract respectively 1.95 % in raw propolis).

Table 2. HPLC quantitative determinations

Samples	Caffeic acid (mg/ml)	Gallic acid (mg/ml)	Ferulic acid (mg/ml)
Calibration curves equation	$A = 10^8 \cdot c + 5 \cdot 10^6$	$A = 9 \cdot 10^7 \cdot c - 128491$	$A = 10^8 \cdot c + 3 \cdot 10^6$
Correlation factor	0.9979	0.9995	0.9986
Conop	0.05		1.68
Lipova	0.04		
Covăsânț	0.09		
Dorgos	0.70		
Ștei	0.20	0.16	0.01
Beiuș	0.40		1.09
Livada Beiuș	0.65		1.39
	Kaempferol, mg/ml	Chrysine, mg/ml	
Calibration curves equation	$A = 5 \cdot 10^7 \cdot c + 2 \cdot 10^6$	$A = 2 \cdot 10^8 \cdot c - 851324$	
Correlation factor	0.9985	0.9995	
Conop		1.95	
Lipova			
Covăsânț	0.36	0.87	
Dorgos	8.88		
Ștei	0.36	0.15	
Beiuș	0.07		
Livada Beiuș			

Comparing the obtained results with the literature data of Romanian propolis we can observe that the chrysin and caffeic acid contents are similar with those from Timiș county and higher that those from Transylvania samples. The kaempferol content of Dorgos sample from Arad county being much higher that was found in the samples from Timiș county.

CONCLUSIONS

Even that Romania was one of the first countries that promoted the propolis study, this paper is one of the first that report the chemical characteristics of the propolis originating from the west part of country, namely from Arad and Bihor counties. This paper present a comparative study of more samples from most important apicultural centers from these counties with the purpose to can have also statistically clear image of the propolis quality of the region.

This study highlight that the propolis from west of Romania have a high polyphenols, flavonoids (chrysine and kampferol) and phenolic acids (caffeic acid, ferulic acid), content that can lead us to presume that it will have also an

important antioxidant capacity. The results shown higher values as those reported for propolis originating from China, Europe or Brasilia and similar or higher than that reported from Timiș county, west of Romania or other regions from Romania. These results propose the propolis collected from this part of Romania to be used in food, cosmetic and pharmaceutical fields, to be raw material for safe and efficient medicinal products, cosmetics or food supplements.

Because the propolis is a natural product obtained by bees from the resins collected from different species, the vegetation from the bees harvesting areas influenced the chemical composition of propolis samples originating from different places. The used chromatographic methods (TLC and HPLC) showed these differences and highlight also the similar compounds.

The used chromatographic methods can be used for the quality evaluation of propolis.

EXPERIMENTAL SECTION

The propolis samples origin and preparation for study

The studied propolis were collected from various beekeepers from west part of Romania, Arad respectively Bihor counties. There were collected 4 samples from Arad county: Conop, Lipova, Covăsânț and Dorgos respectively 3 samples from Bihor county: Beiuș, Livada Beiuș and Ștei (figure 7).

To prepare the propolis for analysis the samples were extracted by grinding the samples and than mixed with 70 % vol. ethanol. The extraction was performed by maceration (cold extraction) using 10 g of propolis and 100 ml solvent. The mixtures were well shaken, and then 48 hours kept in dark, during which were occasionally shaked. At the end, each mixture was filtered. For each sample were prepared three extracts [19].

The TLC analysis

The flavonoides and phenolic acids were determined by thin layer chromatography using a silica chromatographic plate with fluorescence indicator at 254 nm. The mobile phase was toluene (Merck) – diethyl ether – acetic acid 10% (Merck), in proportion of 50:50:10 v/v. The used standards were caffeic acid and chrysin, each having a concentration of 1 mg/mL in methanol. It was applied 15 µL from the samples and 10 µL from each standard. After drying the plate at room temperature, the first chromatogram was observed in the fluorescence at 365 nm, after which the plate was sprayed with Neu-PEG reagent and observed in fluorescence at 365 nm. The second chromatogram was sprayed with a 10% phosphomolybdenic acid solution in methanol, followed by anisaldehyde reagent; the plate was heated at 105-110°C for 5-10 minutes and the chromatograms were observed in visible light [20]. The chromatograms were observed under a Camag reprostar lamp and documentation system equipped with a HP digital camera.

Figure 7. The collection places of studied propolis samples

The HPLC analysis

The determination was carried out on a Varian Star HPLC system. It was used a silica C18 column (Phenomenex, Luna C18, 150 x 4.6 mm, 5 µm). Like mobile phase was used a tertiary gradient prepared from 0.1% (v/v) phosphoric acid (Merck) in water, methanol and acetonitrile (Merck). The elution started with a linear gradient, beginning with isocratic elution followed for the next 30 minutes with 75 % phosphoric acid 0,1%, then for 5 minutes with 69 % phosphoric acid 0,1%, then for 5 minutes with 67 % phosphoric acid 0,1% and at the end for 20 minutes with 54 % phosphoric acid. The flow rate was 1 mL/min [21]. The DAD detector was operated at 280 and 340 nm and the

injection volume was 10 µL for each sample and standard. As standards were used chrysin (1.02 mg/mL), caffeic acid (1 mg/mL), ferulic acid (1 mg/mL), gallic acid (0,116 mg/mL), kaempferol (1 mg/mL), in methanol. For quantitative determination were used different concentrations of standards: caffeic acid (0.05 – 1 mg/ml), ferulic acid (0.1 – 2 mg/ml), gallic acid (0.116 - 2.32 mg/ml), chrysine (0.102 – 2.04 mg/ml) respectively kaempferol (0.1 – 2 mg/ml).

REFERENCES

1. A. Salatino, E. Weinstein Teixeira, G. Negri, *Evid. Based Complement. Alternat. Med.*, **2005**, *2(1)*, 33.
2. E.L. Ghisalberti, P.R. Jefferies, R. Lanteri, J. Matisons, *Experientia*, **1978**, *34*, 157.
3. V. Bankova, M. Popova, B. Trusheva, *Chem. Cent. J.,* **2014**, *8*, 28.
4. M.B. Abubakar, W.Z. Abdullah, S.A. Sulaiman, B.S. Ang, *Evid. Based Complement. Alternat. Med.*, **2014**, *2014*, 371730.
5. C. Gardana, M. Scaglianti, P. Pietta, P. Simonetti, *J. Pharm. Biomed. Anal.*, **2007**, *45(3)*, 390.
6. R.G. Woisky, A. Salatino, *J. Apicult. Res.,* **1998**, *37*, 99.
7. M.R. Ahn, S. Kumazawa,T. Hamasaka, K.S. Bang, T. Nakayama, *J. Agric. Food. Chem.*, **2004**, *52*, 7286.
8. S. Kumazawa, T. Hamasaka, T. Nakayama, *Food Chem.*, **2004**, *84*, 329.
9. P. Premratanachai, C. Chanchao, *Asian Pac. J. Trop. Biomed.*, **2014**, *4(5),* 377.
10. V.C. Wagh, *Adv. Pharmacol. Sci.*, **2013**, *2013*, 308249.
11. J.B. Daleprane, D.S. Abdalla, *Evid. Based Complement. Alternat. Med.*, **2013**, *2013*, 175135.
12. L.A. Mărghitaș, D. Dezmirean, F. Drâglă, O. Bobiș, *Bull.USAMV Anim. Sci. Biotechn.*, **2014**, *71 (2),* 111.
13. L.A. Mărghitaș, D. Dezmirean, O. Bobiș, *Evid. Based Complement. Alternat. Med.*, **2013**, *2013*, 159392.
14. A.N. Croci, B. Cioroiu, D. Lazăr, A. Corciova, B. Ivanescu, M.I. Lazăr, *Farmacia*, **2009**, *57 (1)*, 52.
14. A.N. Croci, B. Cioroiu, D. Lazăr, A. Corciova, B. Ivanescu, M.I. Lazăr, *Farmacia*, **2009**, *57 (1)*, 52.
15. A.N. Croci, D. Lazăr, L. Potorac, A. Corciova, B. Ivanescu, M.I. Lazăr, *Farmacia*, **2009**, *57 (1)*, 104.
16. G.H. Coneac, L. Vlaia, I. Olariu, V. Vlaia, D. Lupuleasa, C. Popoiu, *Farmacia*, **2014**, *62 (2)*, 400.
17. G. Coneac, E. Gafițeanu, D.I. Hădărugă, N.G. Hădărugă, I.A. Pînzaru, G. Bandur, L. Urșica, V. Păunescu, A. Gruia, *Chem. Bull. Politehnica Univ. (Timișoara)*, **2008**, *53 (67) (1-2)*, 56.
18. C. Sârbu, A.C. Moț, *Talanta*, **2011**, *85 (2),* 1112.
19. ***, European Pharmacopoeia, 8th edition, EDQM, **2015**.
20. ***, Homoopathisches Arzneibuch 2013, Deutscher Apotheker Verlag, Stuttgart, **2013**.
21. R. Yan, Y. Cao, B. Yang, *Molecules*, **2014**, *19*, 4409.

ANALYTICAL CAPABILITY AND VALIDATION OF A METHOD FOR TOTAL PETROLEUM HYDROCARBON DETERMINATION IN SOIL USING GC-FID

MARIN ŞENILĂ[a,*], ERIKA LEVEI[a], LĂCRIMIOARA ŞENILĂ[a], OANA CADAR[a], MARIUS ROMAN[a], MIRELA MICLEAN[a]

ABSTRACT. The paper presents the analytical capability and validation of a method for quantitative determination of total petroleum hydrocarbons in soil by gas chromatography with flame ionization detector (GC-FID). In order to validate the method, the main figures of merit such as limit of detection and limit of quantification, working range, precision and recovery were studied and the measurement uncertainty was estimated based on the bottom-up approach according to the international guidelines of ISO/IEC 17025. Limit of detection, estimated from chromatograms measured for spiked blank at low level mass concentration, was 8.3 mg/kg, while limit of quantification was 25 mg/kg. Precision was studied in terms of repeatability and reproducibility for the concentration range of 25 – 1000 mg/kg. Standard deviation of repeatability (sr) was 6.3% (n=10 parallel samples), while standard deviation of reproducibility (sR) was 9.9 % (n=10 parallel samples). Recovery (%) estimated using a certified reference material (CRM), was 93 ± 7.0 %, while the estimated expanded relative uncertainty was 17.2 %. This paper offers all the steps necessary to validate the determination method for total petroleum hydrocarbons in soil applied according to the standard ISO 16703 and to evaluate the measurement uncertainty for this method. The obtained figures of merit fulfil the requirements of the standardized method and also of the Romanian legislation, and demonstrate that the laboratory can properly apply the method in order to achieve accurate results. The paper represents a model for the method validation in analytical laboratories in order to check the fit for purpose of analytical methods.

Keywords: *GC-FID, total petroleum hydrocarbons, validation, measurement uncertainty, soil, fit for purpose*

---

[a] *INCDO-INOE2000, Research Institute for Analytical Instrumentation, Donath Str. No. 67, RO-400293, Cluj-Napoca, Romania.*
[*] *Corresponding author: marin.senila@icia.ro.*

INTRODUCTION

All over the world there are numerous sites polluted with petroleum products that may have adverse effects on living organisms' health [1, 2]. Petroleum products results from crude oil by fractional distillation. In a simplified scheme of petroleum refining, crude oil is first distilled into different boiling range fractions. A processed petroleum product contains a complex mixture of many different organic substances counting paraffinic, naphthenic, olefinic, aromatic and polycyclic aromatic hydrocarbons, as well as heteroatoms (N, O, S) containing organic compounds. Also, it may contain traces of metals and organometallic compounds [3, 4].

The persistence and toxicity of different pollutants, between them petroleum hydrocarbons [5-7], created an imperative need for developing reliable methods for their qualitative and quantitative determination in environmental samples. The reliability of a measurement can be expressed by method validation as well as by stating the uncertainty of the measurement result [8-11]. However, the evaluation of measurement uncertainty pose a great challenge for analytical chemists due to the need for a complete understanding of the whole analysis steps and of the method performance parameters.

There are several techniques used for the determination of petroleum hydrocarbon content in soils [12]. Among them, the most known are those based on gravimetry, infrared spectroscopy and gas chromatography with different detection modes (FID, MS), applied subsequent to extractions in different organic solvents [12, 13].

Even if there are numerous instrumental techniques that can be used for petroleum hydrocarbon quantification, the consistent analysis of petroleum products contaminated soil is a complicated task, both due to the complex composition of petroleum products and also due to the complex matrix of soil [3]. Prior to the instrumental determination, the extraction of analyte can be an important uncertainty source. Consequently, the identification and quantification of major sources of uncertainty in the petroleum hydrocarbon determination sequence is necessary. By finding the main sources of uncertainty and critical steps of the determination, the decrease of the uncertainty related to petroleum hydrocarbon determination is possible.

The standardized GC-FID method [14] can be applied for samples with total petroleum hydrocarbon (TPH) (mass fraction) between 100 mg/kg and 10 000 mg/kg soil, expressed as dry matter, but can be adapted to lower concentrations. The method allows the determination of hydrocarbons with a boiling range of 175 °C to 525 °C (n-alkanes from C10 to C40, isoalkanes, cycloalkanes, alkylbenzenes, alkylnaphthalenes and polycyclic aromatic

compounds) [14]. Comparing to the gravimetric or IR methods, gas chromatographic determination offers qualitative information about the components of the sample.

When presenting the measurement results it is necessary to evaluate their confidence intervals [15, 16]. The International Organization for Standardization (ISO) guide [17] recommends the calculation of uncertainty using a model equation, based on evaluation of its uncertainty components, and by using the law of propagation of uncertainty.

There are several options to evaluate the measurement uncertainty existing in the literature [18]. The main ways to assess uncertainty are based on the top-down or bottom-up approaches. In the top-down approach the major sources of uncertainty are considered and estimated, while in the bottom-up approach all the uncertainty sources are thoroughly estimated and only those with significant contributions are used to calculate the measurement uncertainty. The top-down approach is time-consuming and requires a very good understanding of the analytical procedure, but it enables identification of major uncertainty sources and consequently reduction of total measurement uncertainty [16, 19].

The aim of this study was to perform a detailed validation for TPH determination in soil by GC-FID applied according to the standard ISO 16703 and to evaluate the measurement uncertainty for this method. The validation steps taken into account the guidelines of the international standard ISO/IEC 17025 [20]. The measurement uncertainty was calculated using modelling approach following the estimation of combined uncertainty. This paper represents a model for the method validation in analytical laboratories in order to check the fit for purpose of analytical methods.

RESULTS AND DISCUSSION

Method validation

The validation of the analytical procedure for quantitative determination of TPH in soil was performed by evaluating the main figures of merit: limit of detection (LoD), limit of quantification (LoQ), working and linear range, trueness/accuracy and precision (both repeatability and reproducibility) according to the EURACHEM guide requirements [21].

A specific chromatogram for a standard solution used in TPH determination is presented in Figure 1. In the chromatogram, the total peak area is that delimited by the retention times of n-decane and n-tetracontane. Therefore, only semi-volatile (>C10-C16) and non-volatile hydrocarbons (>C16-C40) [22] are included in the TPH parameter measured by this method.
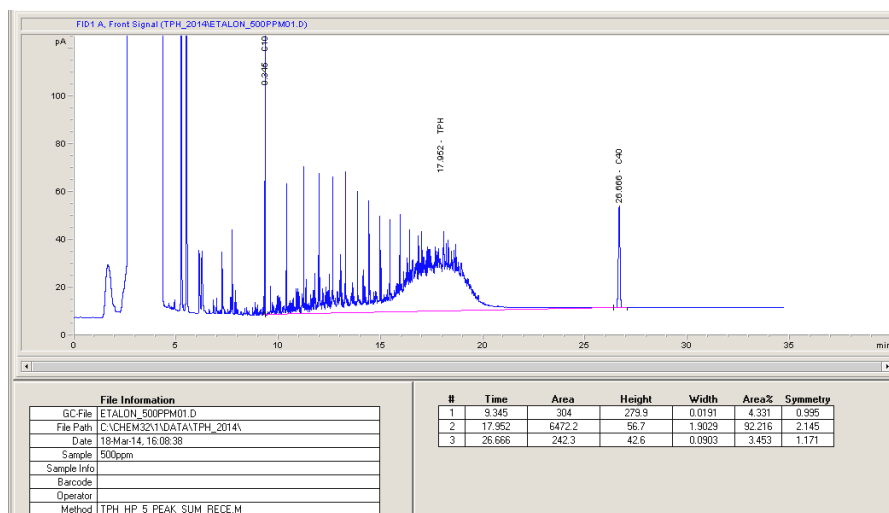
Figure 1. *GC-FID chromatogram of TPH standard (500 mg/kg). The first and the last identified peaks (C10 and C40, respectively) delimitate the retention time window (RTW)*

LoD and LoQ

In order to estimate LoD and LoQ, chromatograms of 10 independent spiked blank solutions at low level mass concentration (10 mg/L) were measured and the standard deviation of signal area was calculated. LoD was estimated for an area equal to the net signal of spiked blank and three times its standard deviation, while LoQ was estimated for a signal equal to the area signal of spiked blank and nine times its standard deviation [20]. The target was to obtain a value for LoQ of at least 25% from alert level for TPH in soil (200 mg/kg) established by Ministerial Order 756 [23] which means a value for LoQ of maximum 50 mg/kg. Data in Table 1 showed that the performance target was achieved by our method.

Table 1. LoD and LoQ for the determination of TPH in soil

Stdev (s) blank signal (signal area)	LoD (3s/b) (mg/kg)	LoQ (9s/b) (mg/kg)
39.5	8.3	25

Ten standard solutions at the calculated LoQ concentration (25 mg/L) were prepared and analysed for its confirmation by evaluation of precision (repeatability) and trueness (recovery). The targeted repeatability expressed as relative standard deviation (RSD) was 20 %, while targeted recovery was 90-115 %.

Working and linear range

At the lower end of the range, the restrictive factor is LoQ, while, at the upper end, limitations are imposed by various effects depending on the instrument response. Linearity was evaluated from the regression function of calibration using 7 standards (25, 50, 100, 250, 500, 750, and 1000 mg/L TPH). The fit for purpose linear range was selected to be between LoQ and 1000 mg/L.

Ten replicates of the 25 mg/L and ten of the 1000 mg/L calibration standards were measured. To check homogeneity of variances, the standard deviations (s_1) and (s_7) of the lowest and the highest concentrations from calibration curves, and the PG ratios (s_1^2/s_7^2 or s_7^2/s_1^2) were calculated and compared with the Fischer value $F_{9;9;0.99} = 5.35$. The values for intercept (a), slope (b), determination coefficient (r^2), and PG ratio are presented in Table 2.

Table 2. Calibration curves for working range LoQ – 1000 mg/L

Parameter	a	b	r^2	PG
TPH	-197.78	14.34	0.9994	4.96

a – intercept; b – slope; r^2 – determination coefficient, PG – test value factor for significant differences of variances at the limits of the linear range

The experimental data showed that variances are homogenous, therefore linear regression curve can be used [24].

Trueness / accuracy

Trueness was studied by evaluating the recovery of a soil CRM (Sandy Loam CRM). Thus, 6 parallel samples of soil CRMs were analysed in order to determine the methods trueness, and the results are presented in Table 3. Average recovery for soil TPH Sandy Loam CRM was 93% with relative expanded uncertainty of 7.0% (n = 6 parallel samples). In addition, trueness was evaluated using the recovery for real soil samples spiked with known content of TPH. To the each 100 g soil sample (6 parallel samples) amounts of 27.8 mg BAM K008 standard were added. Hence, the added THP concentrations were 278 mg/kg. The recovery rate was calculated by taking into account the found concentrations in the enriched samples and the added concentration.

The average recovery for spiked soil samples was 88% with a relative expanded uncertainty of 7.5% (n = 6 parallel samples), which conforms satisfactory performance according to the requirements of ISO 16703 standard (the recovery shall be more than 80% [14]). The possible factors that contribute to the recoveries below 100% may be the loss of parts of analyte during the sample preparation step, due to the volatility of some compounds from TPH class. Thus, when calculate the final result, the average recovery for spiked samples should be considered.

Table 3. Results of analysis of TPH Sandy Loam CRM (mean ± expanded uncertainty, n = 6 parallel samples) and certified value ± expanded uncertainty

Parameter	Measured value (mg/kg)	Certified value (mg/kg)
TPH	3395 ± 238	3650 ± 270

The results showed that the confidence interval of the measured value was within the confidence interval of the certified value.

Precision

Commonly, the precision is estimated in terms of repeatability and reproducibility, and, in our case, were estimated considering within and between days variation, respectively. For the repeatability study the results were obtained by analysing 10 parallel samples by a single operator using the same equipment. The target was to obtain a limit of repeatability (r) below 8.3% (according to the precision data given in ISO 16703). For the reproducibility study, a real soil sample was measured in 10 different days by different operators using the same equipment. The target was to obtain a limit of reproducibility (R) below 28.5% (according to the precision data given in ISO 16703), which mean a standard deviation of reproducibility (s_R) below 10.2 %. According to the obtained results, r was 6.3 %, while s_R was 9.9 % (R = 27 %), which conforms satisfactory performance.

In Table 4 is presented a summary of the results of method validation.

Table 4. Results of method validation for the measurement of TPH in soil by using GC-FID method

Validation parameter	Results
Limit of detection	8.3 mg/L
Limit of quantification	25 mg/L
Linear range	25 – 1000 mg/L
Trueness (recovery)	93% for CRM; 88% for spiked samples
Precision (limit of repeatability, r)	6.3% (n=10 parallel samples)
Precision (limit of reproducibility, R)	27% (n=10 parallel samples)

Measurement uncertainty evaluation

Measurement uncertainty was estimated based on the bottom-up approach [18]. All the contributions were obtained from calibration certificates (volumetric flasks, pipettes, reference materials, etc.) and from statistical analysis of repeated measurements (CRM analysis, precision experiments) through the method validation study performed in the laboratory. In brief, the steps of the method are as shown in Figure 2.
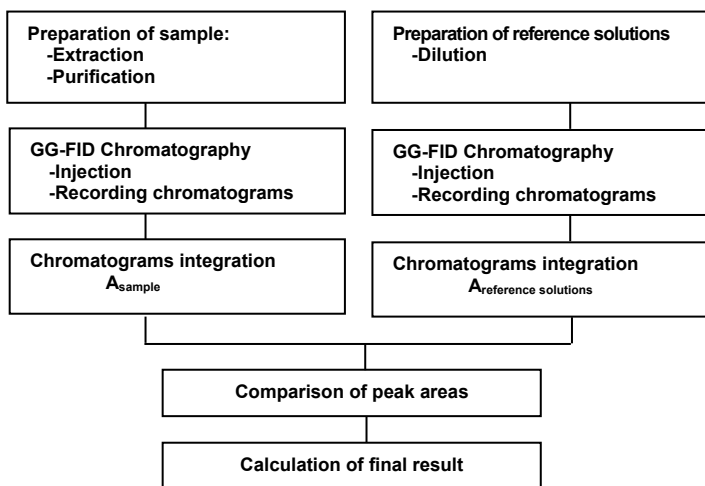
Figure 2. Experimental procedure for the measurement
of mass concentration of TPH in soil by GC-FID

The identified main sources of measurement uncertainty were uncertainty of calibration reference materials (Ci), uncertainty of delivered volumes, uncertainty of signal area of the reference solutions, and recovery of the method, as presented in Figure 3 – cause and effects diagram.

Figure 3. Cause and effects diagram of uncertainties in measurement
of mass concentration of TPH by using GC-FID

Uncertainties of GC-FID and analytical balances were calculated from data obtained from calibration certificates (declared uncertainty). After estimation, all sources of uncertainty were combined according to the law of propagation of uncertainties, obtaining the combined standard uncertaint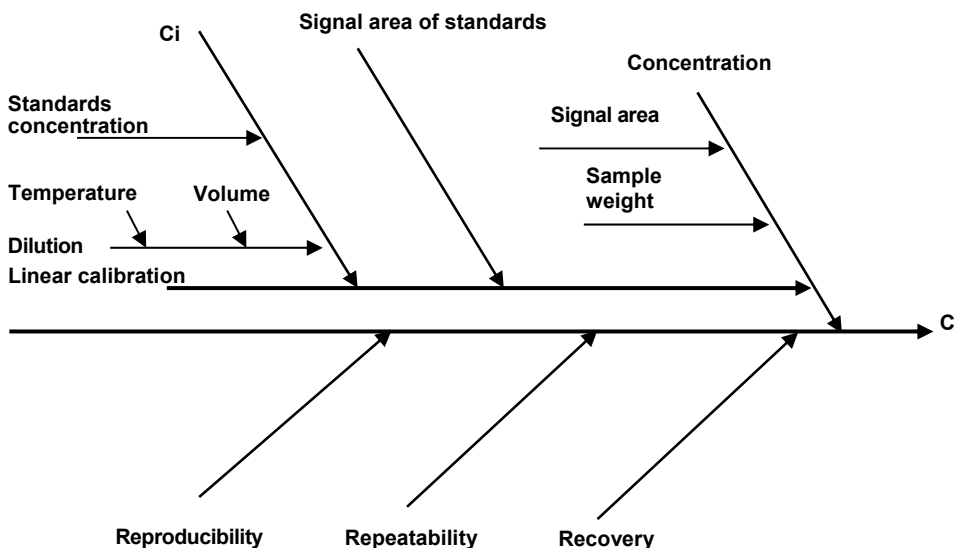y (Uc). The final result was reported as expanded uncertainty (U_E), calculated as $U_E = k \times U_c$, where k is the coverage factor, corresponding to a 95 % confidence level.

Table 5. Uncertainty components of mass concentration of TPH in soil by using GC-FID method

Source	Unit	Value	Standard uncertainty	Interventions	Total standard uncertainty	Relative uncertainty
Concentration of standard	g/g	0.967	0.009	1	0.009	0.0090
Weight of standard	g	0.10	0.0001	1	0.0001	0.0010
Volumetric flask	mL	10	0.033	7	0.231	0.0230
Pipette	µL	1000	4.60	1	4.60	0.0046
Pipette	µL	750	4.20	1	4.20	0.0056
Pipette	µL	500	3.90	1	3.90	0.0078
Pipette	µL	250	3.70	1	3.70	0.0015
Pipette	µL	100	0.590	1	0.590	0.0059
Pipette	µL	50	0.540	1	0.590	0.0110
Pipette	µL	25	0.520	1	0.540	0.0210
Weight of sample	g	10	0.001	1	0.0001	0.00001
Equipment	g/g	1	0.01	1	0.010	0.0100
Calibration	mg/L	382	14.2	1	14.2	0.0370
Reproducibility	mg/L	404	25.4	1	25.4	0.0630
Dry mass	%	70.0	1.50	1	1.50	0.0210

The combined relative uncertainty was calculated to be 8.6 %. The biggest contribution to combined uncertainty was represented by method reproducibility (28% of the total uncertainty), but also the calibration curve (16% of the total uncertainty) and the use of low volume pipettes (e.g. 9% of the total uncertainty is given by the delivered volume of 25 µL). To calculate the expanded uncertainty of the result of a measurement at the 95 % confidence level, the result for the combined uncertainty was multiplied by a coverage factor of 2. Thus the expanded uncertainty of the TPH determination in soil by FT-IR method is 17.2 %.

Relative uncertainty contributions are used to illustrate the relative impact of different uncertainty components. As presented in Table 5, method reproducibility has the highest contribution to the combined uncertainty, while the weighting of sample has an insignificant contribution to the method uncertainty.

CONCLUSIONS

The paper presents all the steps necessary to evaluate the measurement uncertainty and validate the standardized method for TPH determination in soil according to the ISO 16703 standard in a laboratory in order to demonstrate its

fit for purpose. The studied figures of merit fulfil the requests in terms of LoD and LoQ, accuracy, and precision set out in the ISO 16703 standard. Gas chromatographic determination provides low LoQ, which make it suitable to measure the TPH concentrations at the limits imposed by environmental legislation. Trueness was studied by evaluating the recovery of a soil CRM and also by evaluating the recovery for spiked soil samples. The recovery for spiked samples was in the target imposed by ISO 16703 (higher than 80%). However, since it was well below 100% (only 88%) it should be taken into account when calculate the final result. Also, particular attention should be paid to sample preparation in order to avoid analyte loss during this step. It was demonstrated that that the method can be applied in the testing laboratory for the designed purpose, determination of TPH in soil by GC-FID.

EXPERIMENTAL SECTION

All reagents were of p.a. quality, purchased from Merck (Darmstadt, Germany). Sandy Loam soil (CRM358, Sigma-Aldrich, USA), diesel oil BAM-K008, Federal Institute for Materials Research and Testing, Germany) and 1/1 diesel oil/ lubricating oil mixture (BAM-K010e, Federal Institute for Materials Research and Testing, Germany) certified reference materials (CRMs) were used for the validation procedure. The volumes were measured using calibrated glassware (Hirschmann, Germany).

The method consists in the mixing of 20 g of well homogenized soil with 40 mL of acetone and 20 mL heptane containing n-decane and n-tetracontane to establish the Retention Time Window (RTW), removal of acetone by extraction with water followed by removal of polar substances using Florisil columns and recording of the GC chromatogram.

Standard solutions (25, 50, 100, 250, 500, 750, and 1000 mg/L TPH) prepared from a mixture of 1/1 diesel oil/lubricating oil CRM (BAM-K010e) were used for the external calibration of the instrument. Measurements were carried out using an Agilent Technologies 6890N gas chromatograph (GC) with flame ionization detector (FID). The used capillary column was a 30 m L×0.32 mm ID×0.25 μm, HP-5 95% dimethylpolysiloxane (Agilent J&W). High purity helium (Linde Gas, Romania) was used as carrier gas.

The GC-FID was operated in split mode and the oven temperature was: initial temperature 40°C, held for 6 min, then ramped to 315°C at 20°C/min and held for 15 min. Detector temperature was set at 330°C and the injector temperature was set at 300°C.

ACKNOWLEDGMENTS

REFERENCES

1. Y. Zhang, M. Liu, H. Chen, G. Hou, *Ecotoxicology and Environmental Safety,* **2014**, *102*, 160.
2. H. Wang, T. Fischer, W. Wieprecht, D. Möller, *Environmental Science and Pollution Research,* **2015**, DOI 10.1007/s11356-014-4049-3.
3. E. Saari, "Towards minimizing measurement uncertainty in total petroleum hydrocarbon determination by GC-FID", dissertation thesis, Faculty of Science of the University of Oulu, *Acta University Oulu A*, 544, **2009**.
4. J.G. Speight, "Handbook of Petroleum Product Analysis", **2002**, John Wiley & Sons, Inc. publication.
5. J. Bramley-Alves, J. Wasley, C.K. King, S. Powell, S.A. Robinson, *Journal of Environmental Management,* **2014**, *142*, 60.
6. C.M. Reddy, T.I. Eglinton, A. Hounshell, H.K. White, L. Xu, R.B. Gaines, G.S. Frysinger, *Environmental Science & Technology*, **2002**, *36*, 4754.
7. S. Chakraborty, D. Weindorf, B. Li, A.A. Ali Aldabaa, R.K. Ghosh, S. Paul, M.N. Ali, *Science of the Total Environment,* **2015**, *514,* 399.
8. T. Frentiu, M. Ponta, R. Hategan, *Chemistry Central Journal*, **2013**, *7*, 43.
9. M. Senila, E. Levei, L. Senila, O. Cadar, G. Oprea, C. Roman, *Studia UBB Chemia*, **2011**, *56*, 27.
10. A. Drolc, A. Pintar, *Accreditation and Quality Assurance*, **2012**, *17*, 323.
11. M. Ponta, T. Frentiu, *Studia Universitatis Babes-Bolyai Chemia*, **2012**, *57*, 7.
12. R.N. Okparanma, *Applied Spectroscopy Reviews*, **2013**, *48*, 458.
13. L. Senila, A. Gog, M. Senila, C. Roman, L. Silaghi-Dumitrescu, *Revista de Chimie*, **2012**, *63*, 557.
14. ISO 16703, 2004, Soil quality – Determination of content of hydrocarbon in the range C10 to C40 by gas chromatography, *International organization for standardization, Geneva, Switzerland*.
15. W. Kessel, *Thermochimica Acta*, **2002**, *382*, 1.
16. A. Drolc, A. Pintar, *Accreditation and Quality Assurance*, **2011**, *16*, 21.
17. JCGM 100:2008, 1995, Guide to the Expression of Uncertainty in Measurement (GUM), *International organization for standardization, Geneva, Switzerland*.
18. S.L.R. Ellison, M. Rosslein, A. Williams, EURACHEM/CITAC, "Quantifying uncertainty in analytical measurement", 3nd edn. LGC, Teddington, **2012**.
19. M. Senila, A. Drolc, A. Pintar, L. Senila, E. Levei, *Journal of Analytical Science and Technology,* **2014**, *5*, 37.
20. ISO/IEC 17025, 2005, General requirements for the competence of testing and calibration laboratories, *International organization for standardization, European Committee for Standardization, Brussels.*
21. EURACHEM, 1998, The fitness for purpose of analytical methods, Eurachem LGC, Teddington European Environment Agency, http://www.eea.europa.eu/data-and-maps/indicators/progress-inmanagement-of-contaminated-sites/progress-in-management-of-contaminated-1.
22. W. Chang, M. Dyen, L. Spagnuolo, P. Simo, L. Whyte, S. Ghoshal, *Chemosphere*, **2010**, *80*, 319.
23. Ministerial Order 756, 1997, Official Gazette of Romania, 303/bis/06.11.1997.
24. ISO 8466-1, 1990, Water Quality – Calibration and evaluation of analytical methods and estimation of performance characteristics - Part 1, *International organization for standardization, Geneva, Switzerland*.

REMOVAL OF Zn(II) IONS FROM AQUEOUS SOLUTION BY ADSORPTION ON MUSTARD HUSKS

DUMITRU BULGARIU[a,b], DORU TOADER JURAVLE[a], LAURA BULGARIU[c,*]

ABSTRACT. Removal of Zn(II) ions by adsorption on a low-cost material, namely mustard husks, was examined in this study. The batch experiments were performed as a function of initial solution pH, adsorbent dose, initial Zn(II) concentration and contact time, at room temperature ($25 \pm 0.5°$C), in order to establish the optimum conditions of adsorption process. The experimental results have shown that 5.0 g/L of mustard husks is sufficient to remove 73.16% of 54.20 mg/L Zn(II) from 25 mL of aqueous solution, in 60 min of contact time and at initial solution pH of 5.5. The adsorption data fitted well the Langmuir isotherm model, with a maximum adsorption capacity of 12.99 mg/g, while the kinetics of adsorption process is described by pseudo-second order model. The results of this study highlight that the mustard husks can become an efficient and economical alternative for the removal of Zn(II) ions from aqueous effluents.

Keywords: adsorption, Zn(II) ions, mustard husks, isotherm, kinetics

INTRODUCTION

Pollution of environment with heavy metals is an important issue in many industrialized regions around the world. Their large utilization and industrial importance have determined the serious pollution of many ecosystems with such pollutants, that unlike organic pollutants are not biodegradable, tend to accumulate in living organisms, and many of them are known to be toxic or carcinogenic.

[a] *"Al.I. Cuza" University of Iaşi, Faculty of Geography and Geology, 20A Carol I str., RO-700506, Iaşi, Romania.*
[b] *Romanian Academy, Branch of Iaşi, Collective of Geography, 18A Carol I str., RO-700506, Iaşi, Romania.*
[c] *Technical University "Gheorghe Asachi" of Iaşi, Faculty of Chemical Engineering and Environmental Protection, 71A D. Mangeron str., RO-700050, Iaşi, Romania*
[*] *Corresponding author: lbulg@tuiasi.ro*

Zinc is an important element for many growing industrial sectors, such as metallurgical industry, electroplating industry, mine drainage, galvanization industry, wood preservative industry, alloy industry, ceramics, batteries manufacturing, etc. [1, 2]. The rapid development of these economical activities have increase the quantities of waste water that contains significant amounts of Zn(II) ions that are directly or indirectly discharged into environment, and that drastically affects its quality. It is well known that zinc is a trace element that is essential for human health, due to its importance in psychological function of living tissues and many biological processes. Nevertheless, too much zinc can cause several serious health problems, such as gastric cramps, skin irritation, vomiting, nausea and anemia [3]. This is the reason why the permissible limit for Zn(II) ions in drinking waters is only 0.5 mg/L [4].

The most common methods involved in the removal of Zn(II) ions and other heavy metals from various types of industrial effluents include chemical precipitation [5, 6], membrane filtration [6, 7], ion exchange [8, 9], electrochemical techniques [10], etc. Unfortunately, most of these methods have several important limitations, such as generation of high quantities of toxic sludge that required further treatments, high cost of operation, high energy consumption, long treatment time and poor selectivity.

Among the conventional methods, the adsorption of heavy metal ions can be considered an inexpensive, eco-friendly and efficient method that have received a special attention during of last years, mainly because is effective in recovery and recycling of retained metal ions, have a low sludge production and is easy to operate. Activated carbon is a well-known conventional adsorbent hat has been widely employed in the wastewater treatment. Unfortunately, its utilization is not feasible due to high price and costs associated with the regeneration as a result of high-degree losses in decontamination processes [11].

Adsorbent materials derived from agricultural wastes have been intensively used as substitutes for such conventional adsorbent. These wastes are usually composed by polymers, especially different types of lignino-celluloses, and are particularly attractive for the removal of environmental contaminants because are cheap, available in large quantities and contains in their structure numerous functional groups that could represent binding sites for metal ions [12]. From these reasons, many studies from literature have reported the utilization of various agricultural wastes, such as: jack fruit peel, mango bark sawdust [13, 14], sawdust [15], rice straw [16], lemon shells [17], etc., for the removal of Zn(II) ions, in various experimental conditions.

The mustard is an annual plant that is intensively cultivated in many regions of the world, mainly due to their widely utilizations in food industry, and recently for the biodiesel production. After harvesting, the mustard seeds are

peeled and selected, and the obtained husks together with low quality seeds are considered a non-value waste that is discharged or incinerated. However, various functional groups, such as carboxyl, hydroxyl, carbonyl, amine, etc. [18] are present in the structure of this low-cost material, suggesting that mustard husks can be a potential adsorbent for the removing of metal ions. In recent studies, we report the ability of such adsorbent material to remove Pb(II) and Cd(II) ions from aqueous solution [18, 19]. The mustard husks were assessed as adsorbent for the removal of some toxic metal ions (such as Cd(II), Pb(II), Cr(VI), Cu(II)) [20-22]), but to the best of our knowledge, this is the first report on the removal of Zn(II) on mustard husks.

In this study, the removal of Zn(II) ions from aqueous solution using mustard husks as low-cost adsorbent was investigated. The influence of the most important experimental parameters that affects the efficiency of adsorption process (initial solution pH, adsorbent dose, initial Zn(II) concentration and contact time) has been examined in batch experiments. Two adsorption isotherm models (Langmuir and Freundlich) and two kinetic models (pseudo-first order and pseudo-second order models) have been used to determine the best fitting model for experimental data. The parameters for each model have been also calculated for the adsorption of Zn(II) onto mustard husks.

RESULTS AND DISCUSSION

In order to characterized the adsorptive performances of mustard husks for Zn(II) removal from aqueous solution, three aspects must be considered, namely: (a) optimization of process parameters; (b) modeling of adsorption isotherms and (c) modeling of adsorption kinetics.

1. Optimization of adsorption process parameters: Many studies from literature have shown that the adsorption of metal ions occurs with maximum efficiency only in well defined experimental conditions [23 24]. Therefore, the first goal of batch adsorption experiments should be to establish the optimum values of most important parameters that affect the adsorption process, such as initial solution pH, adsorbent dose, initial Zn(II) concentration and contact time.

1.1. Effect of initial solution pH: The initial solution pH significantly affects both the dissociation degree of functional groups from adsorbent surface and the speciation and solubility of metal ions in aqueous solution. From this reason, the value of this parameter should be optimized first.

In this study, the influence of initial solution pH on Zn(II) adsorption efficiency onto mustard husks was examined in the pH range between 1.0 and 6.5, and the obtained results are presented in Fig. 1. It can be observed that at initial solution pH higher than 3.5 the removal percent attain the maximum value and remains almost constant (69 – 73%) on entire pH range.

This represents an important advantage in the utilization of mustard husks for removal of Zn(II) ions from aqueous solution, since it does not require a rigorous correction of solution pH in order to attain a high efficiency of adsorption process. In addition, the experimental results illustrated in Fig. 1 indicate that Zn(II) adsorption on mustard husks occurs predominantly by ion exchange interactions. In these interactions are involved the mobile ions from adsorbent structure (Ca^{2+} or Mg^{2+}) and these do not depend by the dissociation degree of functional groups from adsorbent structure. In consequence, the maximum adsorption efficiency is obtained in a wide range of initial solution pH.
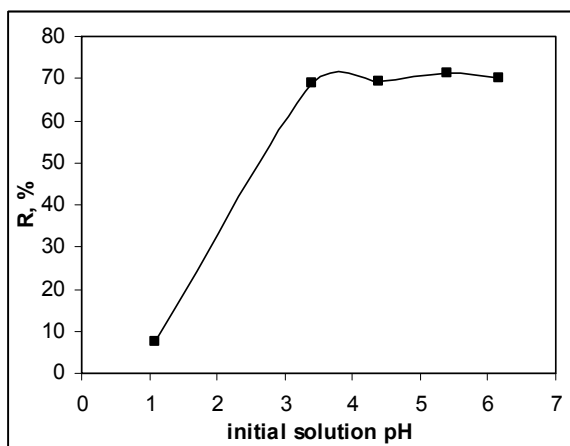

Figure 1. Effect of initial solution pH on Zn(II) adsorption onto mustard husks (c_0 = 54.19 mg/L, adsorbent dose = 5 g/L, contact time = 24 h, t = 25°C).

In strong acid media (pH = 1.5) the adsorption of Zn(II) ions is poor (7.65%), and this is probably due to the fact that the high proton concentration in aqueous solution drastically restricted the interactions between Zn(II) ions and functional groups of adsorbent.

Based on these observations, the optimum initial solution pH for Zn(II) adsorption onto mustard husks was considered to be 5.5 (when 73.16% of Zn(II) ions are removed from aqueous solution), and all further experiments were performed at this pH value.

1.2. Effect of adsorbent dose: The influence of adsorbent dose on the Zn(II) adsorption efficiency was studied using different amounts of mustard husks, in the range of 4.0 – 40.0 g/L, and experimental results (Fig. 2) showed that the adsorption process is highly dependent on this parameter.

Therefore, by increasing the adsorbent dose from 4.0 to 40.0 g/L, the adsorption capacity of mustard husks drastically decrease from 8.23 to 1.09 mg/g. In the same adsorbent dose range, a relatively slow increase in the percent of Zn(II) removal (R,%) from 79.19 to 96.14% was also obtained. Further increase in the adsorbent dose does not change significantly the values of adsorption parameters.

The observed variation is a typical one and can be explained by the increase of the binding sites number as the adsorbent dose rise, until a saturation point is reached, after which no further Zn(II) adsorption occurred [24].
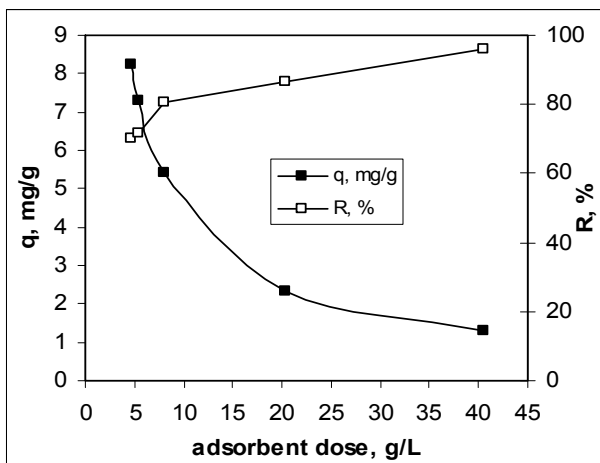

Figure 2. Effect of adsorbent dose on Zn(II) adsorption onto mustard husks (c_0 = 54.19 mg/L, initial solution pH = 5.5, contact time = 24 h, t = 25°C).

Therefore, the optimum adsorbent dose was selected to be as 5.0 g/L, and was used for further experiments.

1.3. Effect of initial Zn(II) concentration: The influence of initial Zn(II) concentration on its adsorption onto mustard husks is presented in Fig. 3. The increase of the initial Zn(II) ions concentration from 13.54 to 189.69 mg/L increased the adsorption capacity of mustard husks from 2.11 to 12.72 mg/g. In the same concentration range, the values of removal percent decrease from 81.26 to 33.68%, with increase of initial Zn(II) concentration.

The opposite variation of the adsorption parameters (q and R) was previously reported [3, 11, 12, 25] and seems determined by the fact that an increase of initial metal ions concentration provide higher driving forces to overcome all mass transfer resistances between solid adsorbent and aqueous solution, and this make that the values of q parameter to increase. However, at higher initial concentration of metal ions, the superficial functional groups of adsorbent are already occupied, and consequently the diffusion of Zn(II) ions appear to be inhibited. In consequence the values of Zn(II) removal percent (R, %) will decrease with increasing of initial metal ions concentration.
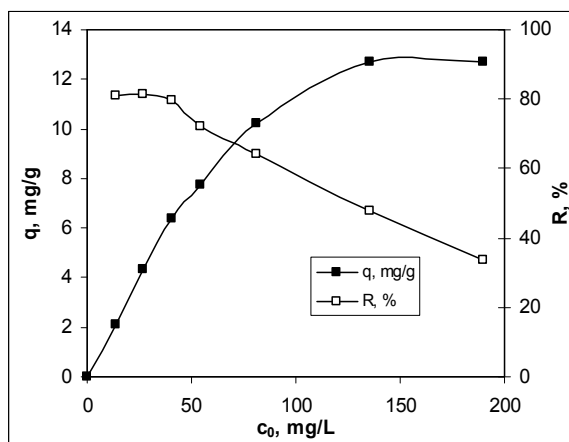

Figure 3. Effect of initial Zn(II) concentration on its adsorption onto mustard husks (initial solution pH = 5.5, adsorbent dose = 5.0 g/L, contact time = 24 h, t = 25°C).

The obtained experimental results have shown that the most efficient removal of Zn(II) ions onto mustard husks occurs when initial Zn(II) concentration is lower than 20 mg/L. In this concentration range (0 – 20 mg/L), the Zn(II) concentration in effluent solution is lower than the value of maximum permissible limit (1.0 mg/L) [26] and mustard husks can be considered an efficient adsorbent in the treatment of wastewater. When initial Zn(II) concentration is higher than 20 mg/L, in order to reduce the metal ions concentration below the permissible limit, are necessary two or more adsorption steps.

1. 4. Effect of contact time: The experimental results (Fig. 4) showed that the adsorption capacity of mustard husk for Zn(II) increase with increasing of contact time. Initially the adsorption process occurs very fast, therefore in the first 30 min more than 63% of Zn(II) ions were retained, after that the rate becomes slower near to equilibrium, which is obtained after 60 min. Once the equilibrium state was reached, the adsorption of Zn(II) ions onto mustard husks did not change significantly.
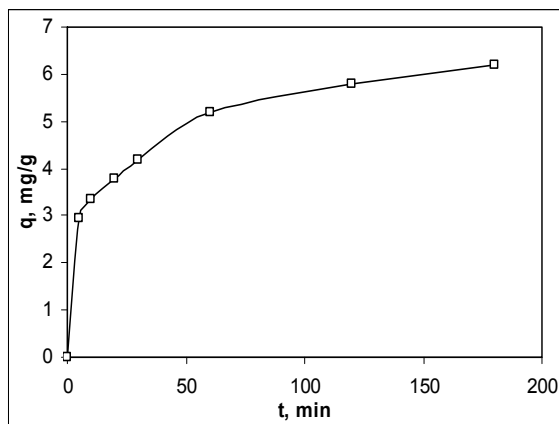
Figure 4. Effect of contact time on Zn(II) adsorption onto mustard husks
(c_0 = 54.19 mg/L, initial solution pH = 5.5, adsorbent dose = 5.0 g/L, t = 25°C).

The shape of dependence illustrated in Fig. 4 suggest that the adsorption process of Zn(II) ions from aqueous solution onto mustard husks is the result of two successive stages: (a) first stage where the adsorption rate is very high (first 30 min) which is predominantly determined by the easy of interaction between Zn(II) ions and adsorbent sites that are available in high number, and (b) second stage where the adsorption capacity is almost constant and corresponds to the equilibrium of adsorption process. In the second stage, the number of available sites from adsorbent surface is more reduced, and the diffusion process becomes more important in the binding of Zn(II) ions.

Therefore a contact time of at least 60 min is necessary for the efficient removal of Zn(II) ions from aqueous solution using mustard husks, in mentioned experimental conditions.

2. Adsorption isotherm modeling: Adsorption isotherms are essential for practical design of adsorption system, because their parameters express the surface properties and affinity of adsorbent for a given metal ion. In order to estimate the potential utilization of mustard husks for Zn(II) ions removal from aqueous solution, two isotherm models (Langmuir and Freundlich) were employed to evaluate the adsorption properties of this low-cost adsorbent.

The Langmuir model is the most widely applied model for monolayer adsorption, and is based on the following assumptions: (i) the number of adsorption sites is fixed, (ii) all sites are equivalent, (iii) each site can retain only one metal ion until a complete coverage of adsorbent surface, and (iv)

the retained metal ions do not interact after adsorption [27, 28]. Unlike Langmuir model, the Freundlich isotherm model is used to describe the multi-layers adsorption on heterogeneous surfaces or surfaces supporting sites of different affinities [27, 29]. The linear mathematical equations of these two isotherm models are presented in Table 1.

Table 1. Quantitative characterization of Zn(II) adsorption of mustard husks on the basis of Langmuir and Freundlich isotherm models

Isotherm model	Mathematical equation	Calculated parameters
Langmuir model [27, 28]	$$\frac{c}{q} = \frac{1}{q_{max} \cdot K_L} + \frac{c}{q_{max}}$$	$R^2 = 0.9939$ $q_{max} = 12.9907$ $K_L = 0.0301$
Freundlich model [27, 29]	$$\log q = \log K_F + \frac{1}{n}\log c$$	$R^2 = 0.9141$ $1/n = 0.5283$ $K_F = 9.9186$

Notation: q_{max} – maximum adsorption capacity (mg/g); K_L – Langmuir constant; K_F and n – constants of Freundlich isotherm model.

The parameters of Langmuir and Freundlich isotherm models have been evaluated from the slopes and intercepts of corresponding linear plots (c/q vs. c for Langmuir model, and log q vs. log c for Freundlich, model respectively – Fig. 5), and the obtained values for Zn(II) ions adsorption onto mustard husks are also summarized in Table 1.

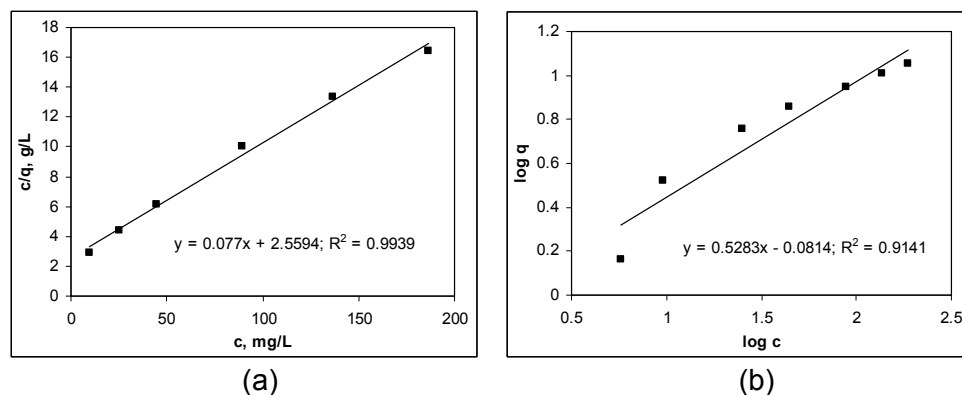(a)   (b)

Figure 5. Graphical representation of Langmuir model (a) and Freunslich model (b) for the adsorption of Zn(II) ions onto mustard husks.

The values of correlation coefficients (R^2) shows that the equilibrium isotherm data obtained in case of Zn(II) ions removal onto mustard husks are very well represented by Langmuir isotherm model. In consequence, the

surface of mustard husks is considered to present made up of homogeneous adsorption and demonstrate the formation of monolayer coverage of Zn(II) ions on the other surface of adsorbent. The maximum adsorption capacity (q_{max}, mg/g) calculated from this model, is comparable with the Langmuir capacities of other agricultural wastes tested as low-cost adsorbents for Zn(II) ions removal from aqueous solution (Table 2).

Table 2. Comparative values of Langmuir adsorption capacities
for Zn(II) removal on various types of agricultural wastes

Adsorbent	pH	q_{max}, mg/g	Reference
Palm tree leaves	5.5	14.60	[30]
Maize cobs	7.5	5.77	[31]
Tea factory waste	5.5	8.9	[32]
Mango peel	-	28.21	[33]
Sugarcane bagasse	5.0	31.11	[34]
Lignin	5.5	11.25	[35]
Mustard husks	5.5	12.99	This study

The Freundlich isotherm model is employed to evaluate the adsorption intensity of Zn(II) ions onto mustard husks. The fractional value of 1/n parameter shows that the adsorption of Zn(II) is a favorable process. However, the value of R^2 coefficient obtained for this model is lower than that obtained in case of Langmuir model (Table 1), which indicate that Freundlich isotherm model is not so adequate to describe the adsorption of Zn(II) ions onto mustard husks.

3. Kinetic modeling: In order to analyze the kinetics of adsorption process of Zn(II) ions onto mustard husks, the pseudo-first order and pseudo-second order kinetic model were used. These models are based on the linear equations that are presented in Table 3.

Table 3. Kinetic characterization of Zn(II) adsorption onto mustard husks.

$q_{e, exp}$		6.4192
Kinetic model	Linear equation	Calculated parameters
Pseudo-first order model [36, 37]	$\log(q_e - q_t) = \log q_e - k_1 \cdot t$	$R^2 = 0.9734$ $q_e = 3.4127$ $k_1 = 0.0079$
Pseudo-second order model [36, 37]	$\dfrac{t}{q_t} = \dfrac{1}{k_2 \cdot q_e^{\,2}} + \dfrac{1}{q_e} t$	$R^2 = 0.9963$ $q_e = 6.4935$ $k_2 = 0.0237$

$q_{e, exp}$ – adsorption capacity at equilibrium, obtained experimentally (mg/g),
q_e and q_t - adsorption capacities of Zn(II) at equilibrium and at time t, respectively (mg/g), k_1 - the rate constant of pseudo-first order kinetics equation (min^{-1}), k_2 - the pseudo-second order rate constant (g/mg min).

The kinetics parameters of the pseudo-first order and pseudo-second order kinetics models, calculated from their linear representation ($\log(q_e-q_t)$ vs. t and t/q_t vs. t, respectively) (Fig. 6) are given in Table 3, together with corresponding correlation coefficients (R^2).

(a)   (b)
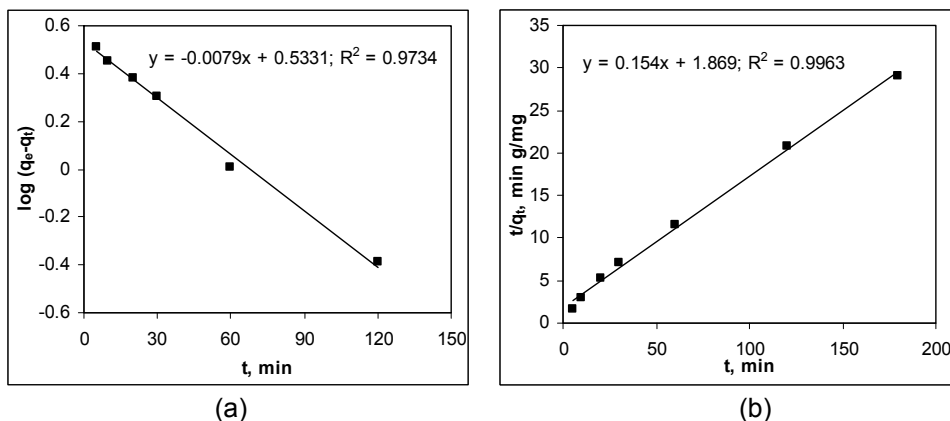
Figure 6. Linear representation of the pseudo-first order kinetic model (a) and pseudo-second order kinetic model (b) for Zn(II) adsorption onto mustard husks.

It can be observed that the correlation coefficient ($R^2 = 0.9963$) for the pseudo-second order kinetic model is higher in comparison with the value obtained form the pseudo-first order kinetic model, and the calculated value of adsorption capacity at equilibrium (q_e, mg/g) from the pseudo-second order kinetic model is very close to those obtained experimentally ($q_{e, exp} = 6.4192$ mg/g). These observations clearly indicate that the pseudo-second order kinetic model is more adequate to describe the adsorption kinetic of Zn(II) ions onto mustard husks.

The pseudo-second order kinetic model is based on the assumption that in adsorption process, the rate limiting step is the chemical interaction between metal ions from aqueous solution and functional groups from adsorbent surface [37]. Similar behaviors have been reported for the removal of Zn(II) ions on various types of agro-waste materials [30-34].

CONCLUSIONS

In this study, the removal of Zn(II) ions from aqueous solution by adsorption onto mustard husks was investigated. The experiments were performed in batch systems, as a function of several experimental parameters (such as initial solution pH, adsorbent dose, initial Zn(II) concentration and contact time), in order to establish the optimum experimental conditions.

The experimental results have shown that the highest adsorption capacity of mustard husks was obtained at initial solution pH of 5.5, 5.0 g/L adsorbent dose and a minimum 60 min of contact time, when for an initial Zn(II) concentration lower than 20 mg/L, this material can be considered an efficient adsorbent in the treatment of wastewater.

The Langmuir isotherm model best-fit the equilibrium data for the adsorption of Zn(II) ions onto mustard husks, and the maximum adsorption capacity was 12.99 mg/g. The analysis of kinetic data showed that the adsorption of Zn(II) ions onto mustard husks followed the pseudo-second order kinetic model, and this means that the rate controlling step is chemical interaction (most probable ion exchange type) between superficial functional groups of adsorbent and Zn(II) ions from aqueous solution.

The results presented in this study indicate that mustard husks can be an efficient alternative adsorbent for the removal of Zn(II) ions from aqueous media.

EXPERIMENTAL SECTION

1. Adsorbent material: The mustard husks used as adsorbent in this study was obtained from Faculty of Agriculture (USAMV Iaşi, Romania), from their own production. The agricultural waste was washed several times with double distilled water to remove impurities and dried in air at $65 - 70°C$ for 24 hours. The obtained material was crushed and sieved to a particle size of $1.0 - 1.5$ mm, stored in desiccators and was directly used as adsorbent, without any pre-treatment. The chemical composition of mustard husks was determined using a Bruker EDX spectrometer, and was found to be: 50.41% C, 41.25% O, 1.18% P, 2.23% S, 2.11% N, 1.53% Ca, 0.59% Mg and others 0.71%.

2. Chemical reagents: All chemical reagents were of analytical degree and were used without further purifications. In all experiments, diluted solutions were prepared using fresh double distilled water, obtained from a commercially distillation system.

A stock solution of 680 mg Zn(II)/L was obtained by dissolving zinc nitrate (purchased from Reactivul Bucharest) in double distilled water. All other concentrations, which varied between 13.54 and 189.69 mg/L were prepared by dilution from stock solution. The initial solution pH was obtained by adding small volumes of 0.1 M HNO_3 or NaOH solutions.

3. Adsorption experiments: The adsorption experiments were performed using by batch technique, adding a constant amount of mustard husks (0.125 g) to a volume of 25 mL of solution of known Zn(II) concentration in 150 mL conical flasks, with intermittent stirring for a required period of time.

The effect of initial solution pH was examined at room temperature ($25 \pm 0.5°C$), adjusting the pH values between 1.0 and 6.5. The influence of adsorbent dose on Zn(II) adsorption was also investigated by mixing adsorbent samples between 4.0 and 40.0 g/L with 25 mL of Zn(II) solution (54.20 mg/L) at pH 5.5. The effect of initial Zn(II) concentration on mustard husks adsorption efficiency was studied within 13.54 – 189.69 mg/L concentration range. In case of kinetics experiments, the same amount of adsorbent (0.125 g) was mixed with 25 mL of 54.20 mg/L Zn(II) solution at various time intervals, between 5 and 180 min.

After adsorption procedure was complete, the two phases were separated through filtration, and Zn(II) concentration in filtrate was analyzed spectrophotometrically using xylenol orange (Digital Spectrophotometer S104D, λ = 570 nm, 1 cm glass cell, against blank solution) [38].

The adsorption efficiency of mustard husks for Zn(II) ions from aqueous solution was quantitatively evaluated using the following parameters:

- adsorption capacity (q, mg/g):

$$q = \frac{(c_0 - c) \cdot (V/1000)}{m} \tag{1}$$

- percent of Zn(II) removed (R,%):

$$R = \frac{c_0 - c}{c_0} \cdot 100 \tag{2}$$

where: c_0, c are the initial and equilibrium concentration of Zn(II) ions from aqueous solution (mg/L); V is volume of solution (mL) and m is the mass of adsorbent material (g).

ACKNOWLEDGMENTS

REFERENCES

1. O. Abdelwaha, N.K. Amin, E.S.Z. Ashtoukhy, *Chemical Engineering Research and Design*, **2013**, *91*, 165.
2. K.S. Baig, H.D. Doan, J. Wu, *Desalination*, **2009**, *249*, 429.
3. F. Fu, Q. Wang, *Journal of Environmental Management*, **2011**, *92*, 407.
4. Directive 98/83 / EC on the quality of water intended for human consumption: http://europa.eu/legislation_summaries/environment/water_protection_management/l28079_en.htm

5. T.A. Kurniawan, G.Y.S. Chan, W.H. Lo, S. Babel, *Chemical Engineering Journal*, **2006**, *118*, 83.
6. D. Mohan, S. Rajput, V.K. Singh, P.H. Steele, C.U. Pittman, *Journal of Hazardous Materials*, **2011**, *188*, 319.
7. M.J. Rivero, O. Primo, M.I. Ortiz, *Journal of Chemical Technology and Biotechnology*, **2004**, *79*, 822.
8. J. Llanos, P.M. Williams, S. Chemg, D. Rogers, C. Wright, A. Perez, P. Canizares, *Water Research*, **2010**, *44*, 3522.
9. M.A. Barakata, E. Schmidt, *Desalination*, **2010**, *256*, 90.
10. A. Mittal, L. Krishnan, V.K. Gupta, *Separation and Purification Technology*, **2005**, *414*, 125.
11. J. Febrianto, A.N. Kosasih, J. Sunarso, Y.H. Ju, N. Indrawati, S. Ismadji, *Journal of Hazardous Materials*, **2009**, *162*, 616.
12. A. Demirbas, *Journal of Hazardous Materials*, **2008**, *157*, 220.
13. V. Mishra, C. Balomajumder, V.K. Agarwal, *Clean Soil Air Water*, **2010**, *38*, 1062.
14. V. Mishra, C. Balomajumder, V.K. Agarwal, *International Journal of Applied Chemical Science and Research*, **2011**, *2*, 179.
15. L. Agorboude, R. Navia, *Journal of Hazardous Materials*, **2009**, *167*, 536.
16. C.G. Rocha, A.M. Zaia, R.V.S. Alfaya, A.A.S. Alfaya, *Journal of Hazardous Materials*, **2009**, *166*, 383.
17. T.K. Naiya, P. Chowdhury, A.K. Bhattacharya, S.K. Das, *Chemical Engineering Journal*, **2009**, *148*, 68.
18. L. Bulgariu, R.M. Hlihor, D. Bulgariu, M. Gavrilescu, *Environmental Engineering and Management Journal*, **2012**, *11*, 1969.
19. L. Bulgariu, D.I. Tudorache Fertu, M. Gavrilescu, *Annals of the Academy of Romanian Scientists - Series on Chemistry*, **2014**, *1*, 5.
20. A.K. Meena, K. Kadirvelu, G.K. Mishraa, C. Rajagopal, P.N. Nagar, *Journal of Hazardous Materials*, **2008**, *150*, 619.
21. D. Swami, D. Buddhi, *International Journal of Environment and Pollution*, **2006**, *27*, 324.
22. D. Sud, G. Mahajan, M.P. Kaur, *Bioresource Technology*, **2008**, *99*, 6017.
23. A. Dabrowski, Z. Hubicki, P. Podkoscielny, E. Robens, *Chemosphere*, **2004**, *56*, 91.
24. U. Farooq, J.A. Kozinski, M.A. Khan, M. Athar, *Bioresources Technology*, **2010**, *101*, 5043.
25. R.K. Gautam, A. Mudhoo, G. Lofrano, M.C. Chattopadhyaya, *Journal of Environmental Chemical Engineering*, **2014**, *2*, 239.
26. NTPA 001 and 002 / 2005: Available to www.gnm.ro/otherdocs/nsbhrtjqp.pdf.
27. K.H. Chong, B. Volesky, *Biotechnology and Bioengineering*, **1995**, *47*, 451.
28. B.H. Hameed, A.A. Ahmad, N. Aziz, *Chemical Engineering Journal*, **2007**, *133*, 195.
29. L. Bulgariu, C. Cojocaru, B. Robu, M. Macoveanu, *Environmental Engineering and Management Journal*, **2007**, *6*, 425.
30. F.A.A. Al-Rub, *Separation Science and Technology*, **2006**, *41*, 3499.
31. I. Banu, *Revista de Chimie (Bucharest)*, **2008**, *59*, 1375.

32. K.L. Wasewar, M. Atif, B. Prasad, I. M. Mishra, *Desalination*, **2009**, *244*, 66.
33. M. Iqbal, A. Saeed, I. Kalim, *Separation Science and Technology*, **2009**, *44*, 3770.
34. D. Mohan, K.P. Singh, *Water Research*, **2002**, *36*, 2304.
35. X.Y. Guo, A.Z. Zhang, X.Q. Shan, *Journal of Hazardous Material*, **2008**, *151*, 134.
36. Y.S. Ho, G. McKay, *Water Research*, **2000**, *34*, 735.
37. C. Gerente, V.K.C. Lee, P. Lee, G. McKay, *Critical Reviews in Environmental Science and Technology*, **2007**, *34*, 41.
38. J.A. Dean, "*Handbook of Analytical Chemistry*", Mc-Grow Hill Inc., New York, **1995**, chapter 5.

GROUNDWATER CHEMISTRY RENDERING USING DUROV, PIPER AND ION BALANCE DIAGRAMS. STUDY CASE: THE NORTHERN PART OF SIBIU COUNTY

MARIA-ALEXANDRA HOAGHIA[a,b,*], CECILIA ROMAN[a], CLAUDIU TĂNĂSELIA[a], DUMITRU RISTOIU[b]

ABSTRACT. The chemical behaviours of groundwater are dynamic fields of research. Variations and changes of groundwater, as drinking water source composition impress negative effects on human health. In Romania, groundwater represents free and common fresh water. Chemistry and quality of groundwater is changed due to natural and anthropogenic factors. The aim of this study is to determine and evaluate the chemical composition of groundwater from the northern part of Sibiu County using Piper, Durov, and ion balance diagrams. The graphical representations show the type of waters based on the ion content. As results, high concentrations of major anions (SO_4^{2-}, Cl^-, NO_2^-, NO_3^-) and cations (Ca^{2+}, Mg^{2+}, Na^+, K^+) were found and according to Piper and ion balance diagrams, the prominent types of waters are Ca^{2+}-HCO_3^- type.

Keywords: groundwater, chemical composition, Durov diagram, Piper diagram, ion balanced diagram

INTRODUCTION

Water is a limited and vital resource for humans and nature. Water quality is significant, especially when it comes to anthropogenic and natural pollution. The importance of groundwater is given not only by its valuable mineral content, as drinking water, but also by its flow of pollutants.

Worldwide, countries face the same problems regarding the deterioration of groundwater quality. Natural pollution affects aquifers (China, India, European countries) composition with high concentrations of arsenic as natural enrichment

---

[a] *INCDO-INOE 2000, Research Institute for Analytical Instrumentation, 67 Donath, RO-400293, Cluj-Napoca, Romania.*
[b] *Babes-Bolyai University, Faculty of Environmental Science and Engineering, 30 Fantanele, RO-400294, Cluj-Napoca, Romania.*
[*] *Corresponding author: alexandra.hoaghia@icia.ro*

of groundwater [1, 2]. Metal pollution and high concentrations of varied chemical compounds (SO_4^{2-}, Cl^-, NO_2^-, NO_3^-) impress negative influences on groundwater and soil quality [3-6].

In Romania, groundwater resources present significant concentrations of NO_3^-, SO_4^{2-}, Cl^-, Ca^{2+}, Mg^{2+}, Na^+ and K^+ [7]. Dominant types of waters are Mg^{2+}-Ca^{2+}-HCO_3^- and Na^+-HCO_3^- types [8].

The objective of the current study is the determination of the physico-chemical composition of groundwater sources (water wells and streams) using Durov and Schoeller diagrams. The types of water are ascertained depending on the abundance of ions, using Piper and ion balanced diagrams.

RESULTS AND DISCUSSION

Table 1 presents the summary statistics of the physicochemical indicators (pH, EC-electrical conductivity, TDS-total dissolved solids, NO_2^-, NO_3^-, SO_4^{2-}, Cl^-, Na^+, Ca^{2+}, Mg^{2+}, K^+) along with the environmental quality standards according to Romanian legislation [9], World Health Organisation Guidelines for drinking water [10] and U.S. EPA National Primary and Secondary Drinking Water Regulations [11].

Table1. Summary statistics of the physicochemical parameters

Variable		Minimum	Maximum	Water quality standards*	Guidelines values**	MCL***
pH (pH units)		6.99	7.96	6.5-9.5	-	6.5-8.5
EC (µS/cm)		637	1572	2500	-	-
TDS	(mg/l)	319	786	-	-	500
NO_2^-		0.1	7.0	0.5	3.0	1.0
NO_3^-		7.7	252	50	50	10
SO_4^{2-}		30	252	250	-	250
Cl^-		7.9	78	250	-	250
Na^+		6.2	62	200	-	-
Ca^{2+}		51	129	200	-	-
Mg^{2+}		5.9	23	200	-	-
K^+		0.65	13	-	20	-
HCO_3^-		201	592	-	-	-

*According to Romanian Legislation [9], **according to the Guidelines for Drinking Water [10], ***according to U.S. EPA Legislation National Primary and Secondary Drinking Water Regulations [11].

The results show significant values for the indicators with higher values as the standards. Sample water S19 presents the higher value for the TDS (figure 1). Water wells samples S3, S4, S5, S6, S7, S17 and spring samples

S20, S21 present significant values for NO_2^-, while S7 is ten times higher as the MCL (maximum concentration level). Except samples S1, S6, S17, the rest of the water samples exceeds twice and more the NO_3^- MCL. Sample S15 exceeds the SO_4^{2-} MCL, while for the other samples the obtained values are lower as 250 mg/l (MCL).
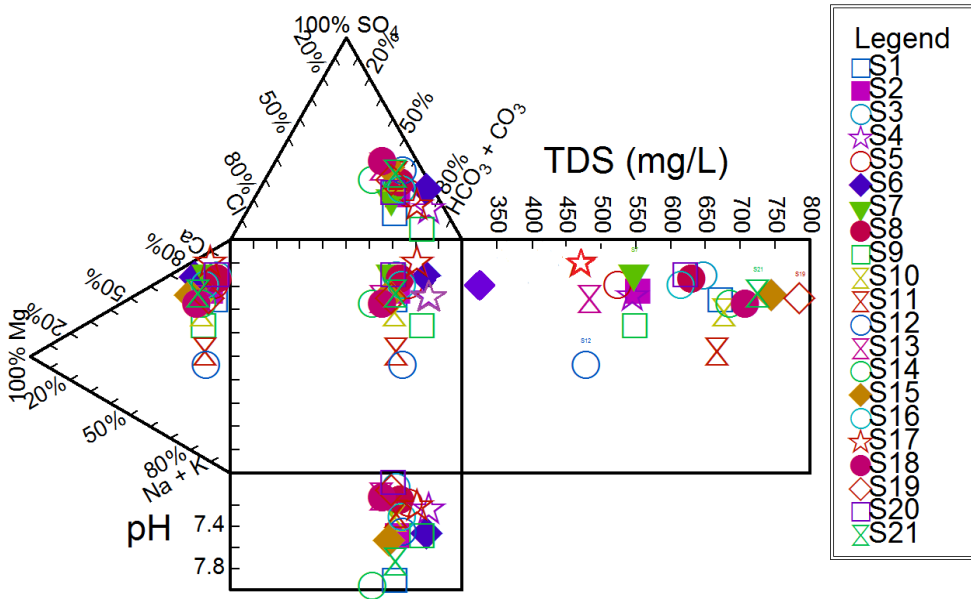

Figure 1. Chemical composition of water samples

The HCO_3^- values are ranging from 201 mg/l (F1) to 592mg/l (F4), with a 444 mg/l mean. The Durov diagram is used to graphically illustrate cations and anions concentrations, related to pH and TDS values (figure 1).

The relative ion concentrations (after the charge balancing) are represented graphically by the ion balanced diagrams.

According to ion balance diagrams, all nineteen well water samples and both public spring samples are Ca^{2+}-HCO_3^- type. Samples S1 and S6 present the lowest amount for the NO_3^- and SO_4^{2-} concentrations (figure 2).

Dispersion of ions is represented using Piper diagram. Largest anion dispersion is represented by HCO_3^- concentration, and the Ca^{2+} concentration has the largest cation dispersion. Pipere diagram shows the dominant water types, which is Ca^{2+}-HCO_3^- type for all water samples, which indicates that the hydrochemistry of the groundwater samples is characterized by alkaline earths which exceed alkali metals [12] (figure 3).
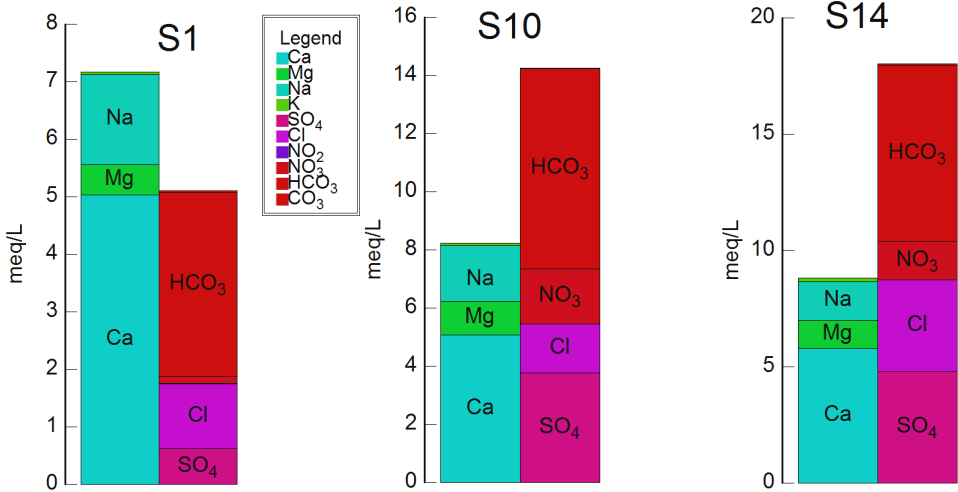
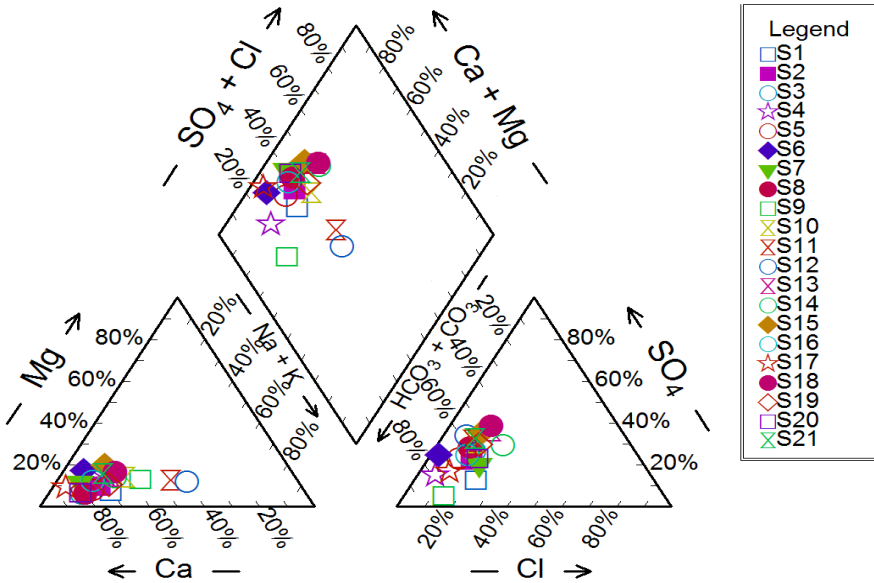**Figure 2.** Ion charge balancing representation for samples S1, S10, S14

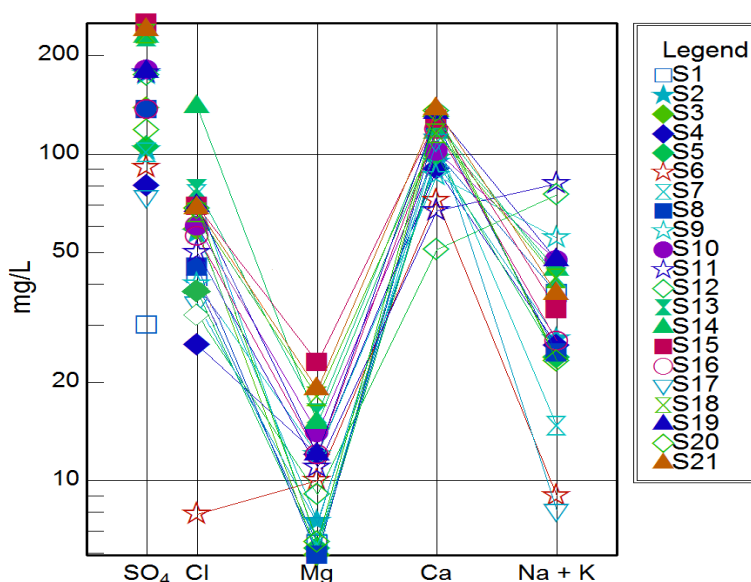**Figure 3.** Classification of groundwater types after the ion charge

Figure 4. Ion concentrations and the ratio among ions

Variations of the chemical parameters concentrations (SO_4^{2-}, Cl^-, Ca^{2+}, Mg^{2+}, Na^+, K^+) and the ratio among them are represented by Schoeller diagram in figure 4 [13, 14].

Higher concentrations for all water samples are SO_4^{2-} concentrations, while K^+ concentrations are the lower ionic concentrations.

Samples S3, S13, S15, S21 have the highest SO_4^{2-}, Cl^-, Mg^{2+} and Ca^{2+} concentrations, while S4, S6, S7, S17, S19 present the lowest values for same parameters, as Schoeller diagram illustrates.

CONCLUSIONS

The studied groundwater samples, from the northern part of Sibiu County, present significant chemical concentrations for major cations content (Ca^{2+}, Mg^{2+}, K^+, Na^+), main anions (SO_4^{2-}, Cl^-, NO_2^-, NO_3^-, HCO_3^-) and TDS values. Anions concentrations (SO_4^{2-}, NO_2^-, NO_3^-) exceed the MCLs from Romanian standards [8] and WHO Guidelines [9]. The TDS presents high values, while 50% of water samples show high concentrations of SO_4^{2-} (>120mg/l) and all water samples are contaminated with NO_3^- with concentrations among 50 mg/l and 150 mg/l (50 mg/l MCL).

According to Piper diagram and Ion balanced diagrams the water samples (water wells and streams) are classified as Ca^{2+}-HCO_3^- type. Using Piper diagram, the ion dispersion is represented and it indicates that the largest anion dispersion is represented by the HCO_3^- dispersions and the Ca^{2+} concentration has the largest cation dispersion.

EXPERIMENTAL SECTION

Short description of the study area

Well water (S1-S19) and stream (S20, S21) samples were collected from the northern part of Sibiu County, which is situated in the Tarnavelor Plateau. The area is characterized with a temperate continental climate. The annual average air temperature ranges between 7-8 ºC. Annual precipitation ranges from 600 to 700 mm, with monthly and annual variations [15, 16].

Aquifers can be found from 0 to 0.5 m at the minor bed level and from 4 to 5 m in the major bed level and 10 m at the versant level [17]. Groundwater and streams constitute the fresh and free drinking water resources used by the Medias inhabitants.

The quality of groundwater is decay because of the near localized of the water wells from the anthropogenic sources (point sources). Point sources are collecting tanks, dry toilets, stables, waste water and storm drainage system. This situation occurs at national level and in the studied area.

Sampling and sample preparation

Nineteen well water samples (S1-S19) and two spring samples (S20, S21) were collected in the rainy season of 2014 (March). The water samples were stored in 1000 ml pre-cleaned polyethylene-terephthalate (PET) bottles. Samples were kept in a freezer at 4 ºC. For major anions and cations measurements, water samples were filtered using plastic filter unit equipped with 0.45 µm disposable cellulose acetate filter membrane and for the cations samples were acidified using HNO_3^-(67%).

MATERIALS AND METHODS

Instrumentation

The physicochemical parameters (pH, TDS and EC) were measured using a multiparameter Multi 350i WTW (Germany). Using titration with HCl against methyl orange indicator, the HCO_3^- content was analysed

For the anion content (NO_2^-, NO_3^-, SO_4^{2-}, Cl^-), IC 761 Compact Methrom A.G. Switzerland ion chromatograph was used.

Mass spectrometry using a DRC II Perkin-Elmer Inductively Coupled Plasma-Mass Spectrometer (Perkin-Elmer, Canada), was used for the major cations (Mg^{2+}, Ca^{2+}, K^+ and Na^+) determination.

The graphical approaches represented by Piper, Durov, Schoeller and ion balanced diagrams were elaborated using AqQa 1.1 software.

ACKNOWLEDGMENTS

REFERENCES

1. Y. Deng, H. Li, Y. Wang, Y. Duan, Y. Gan, *Procedia Earth and Planetary Science,* **2014**, *10*, 100.
2. P. Ravenscroft, W.G. Burgess, K.M. Ahmed, M. Burren, J. Perrin, *Hydrogeology Journal,* **2005**, *13*, 727.
3. G.V. Lavrentyeva, *Journal of Environmental Radioactivity*, **2014**, *135*, 128.
4. J.V. Cruz, M.O. Silva, M.I. Dias, M.I. Prudencio, *Applied Geochemistry,* **2013**, *29*, 162.
5. A.G. Douagui, I.K. Kouame, K. Koffi, A.B.T. Goula, B. Dibi, D.L. Gone, K. Coulibaly, A.M. Seka, A.K. Kouassi, J.M. Mangoua, I. Savane, *Journal of Hydro-environment Research,* **2012**, *6*, 227.
6. M. Miclean, E. Levei, O. Cadar, M. Senila, I.S. Groza, *Carpathian Journal of Earth and Environmental Sciences*, **2013**, *5 (4)*, 93.
7. D.C. Weindorf, L. Paulette, T. Man, *Environmental Pollution,* **2013**, *182*, 92.
8. H.A.L. Rowland, E.O. Omoregie, R. Millot, C. Jimenez, J. Mertens, C. Baciu, S.J. Hug, M. Berg, *Applied Geochemistry,* **2011**, *26*, 1.
9. ***311 Law from 6rd June **2004** that improves and complement 458 Law from 29 July **2002** regarding the quality of drinking water. Official Gazette 2004, Part I, no. 582/30.06.2004 [In Romanian].

10. ***Guidelines for Drinking-water Quality,* Fourth Edition, World Health Organization, **2011**. Online source: http://www.who.int/water_sanitation_health/publications/2011/dwq_chapters/en/.
11. ***U.S. Environmental Protection Agency (EPA) National Primary and Secondary Drinking Water Regulations (NPDWRs and NSDWRs or secondary standards): Guidance for Nuisance Chemicals, **2006**. Online sources: http://water.epa.gov/drink/contaminants/#List.
12. P.J.S. Kumar, *Geoscience,* **2013**, *54*, 12208.
13. L. Barbiero, J.P. de Queiroz Neto, G. Ciornei, A.Y. Sakamoto, B. Capellari, E. Fernandes, V. Valles, *Wetlands*, **2002**, *3* (*22)*, 528.
14. R.A. Huizar, G.T. Mendez, R.R. Madrid, *Hydrological Science,* **1998**, *5 (43)*, 669.
15. L. Badea, M. Buza, Gh. Niculescu, M. Sandu, W. Schreiber, M. Serban, A. Kadar, "Relief units from Romania, Apuseni Mountains and Transilvaniei Plateau". ("Unităţi de relief din România. Munţii Apuseni şi Podişul Transilvaniei"), Ars Docendi Press, Bucureşti, **2006**.
16. F. Grecu, "Hârtibaciu hydrographic basin. Elements of morphology" ("Bazinul Hârtibaciu. Elemente de morfologie"), Academiei Press, Bucureşti, **1992**.
17. E.D. Horhoi, "Târnava Mare channel environmental quality: a geoecological study" ("Calitatea mediului înconjurător în Culoarul Tîrnavei Mari: studiu geoecologic"), Logos 1994 Press, Oradea, **2001**.

THERMAL BEHAVIOUR OF POLYURETHANE MATRIX COMPOSITE MATERIALS

ANCUŢA ELENA TIUC[a,*], OVIDIU NEMEŞ[a], IOANA PERHAIŢA[b], HORAŢIU VERMEŞAN[a], TIMEA GABOR[a], VIOREL DAN[a]

ABSTRACT. This paper describes the thermal behaviour of some composite materials, polyurethane foams reinforced with tire rubber waste and fir sawdust. According to experimental results, TG and DTG plots were drawn for finding the thermal stability domains, the partial and total weight loss and the temperature of the maximum weight loss. Composite materials have superior thermal stability of raw materials from which they were made. Increasing the percentage of polyurethane foam results in greater weight loss front of recycled rubber, but lower than fir sawdust and polyurethane foam.

Keywords: thermal analysis, fir sawdust, polyurethane foam, recycled rubber

INTRODUCTION

Thermogravimetric analysis (TGA) is a thermal analysis technique which measures the amount and rate of change in the weight of a material as a function of temperature, in static rate or under a temperature program, in a controlled atmosphere.

TGA technique is becoming increasingly used not only in determining the composition of materials but also to predict their thermal stability up to elevated temperatures. In TGA, typical weight loss profiles are analyzed for the amount or percent of weight loss at any given temperature, the amount or percent of non-combusted residue at final temperature, and the temperature of various degradation steps [1, 2].

In the last decade, the incorporation of reinforcements from natural resources such as jute, sisal, hemp, kenaf and wood fibers into polymeric materials to improve their performance has been widely studied [3–8].

[a] *Technical University of Cluj-Napoca, Faculty of Materials and Environmental Engineering, 103-105 Muncii Ave, Cluj-Napoca, Romania.*
[b] *"Raluca Ripan" Institute for Research in Chemistry, Babeş-Bolyai University, Cluj-Napoca, Romania.*
* *Corresponding author Ancuta.TIUC@imadd.utcluj.ro*

Polyurethane foams are used in many applications such as automotive, bedding and furniture industry. This is explained by their exceptional characteristics such as sound insulation, energy and shock absorption, consumer comfort and protection from impact. However, polyurethane foam also has some disadvantages, such as low thermal stability and low mechanical strength [9–12].

Thermal degradation of wood is highly dependent on its constituents [13, 14]. The complex structure of wood and the interaction between its components makes it difficult to differentiate the degradation of each component (cellulose, holocellulose, hemicelluloses and lignin) on heat treatment.

The thermal behavior of materials containing wood [15–18], rubber [18, 19] and polyurethane foam [20, 21] is strongly dependent on the composition and interfaces established between components.

The main aspects on the thermal stability of polyurethane foam, fir sawdust, particles of recycled rubber and composite materials obtained from these raw materials, are presented in this study.

RESULTS AND DISCUSSION

For a more complex characterization of the new composite materials based on recycled rubber, fir fibers and polyurethane foam, a thermogravimetric analysis was necessary. Thermal stability of raw materials used to obtain composite materials is an important aspect for their fabrication process; its highest processing temperature being known. Thermal analysis can offer useful information on stability or the temperature range in which the compounds can be used without changing their composition and properties [22], and therefore for possible applications.

Thermal degradation of fir sawdust is dependent on its constituents, the small weight loss before 100°C can be attributed to water evaporation; weight loss rate gradually increased above 200°C and a distinct weight loss appeared between 200–400°C [15]. It is known that the hemicelluloses decompose before lignin and cellulose [16]. Kim et al. confirmed that hemicelluloses degrade between 180–350°C, the lignin degrades between 250–500°C, and the degradation of cellulose takes place between 275–350°C [17].

Thermal decomposition of rubber derived from waste tires is characterized by three distinct decomposition regions: the degradation or volatilization of additives such as oils and stearic acid (200–300°C); the degradation of natural rubber (NR) and styrene–butadiene rubber (SBR), which are the main components of tire rubber (350–480°C) and the decomposition of butadiene rubber (BR) (450–500°C) [18, 19].

The polyurethane foam exhibited three thermal decomposition steps at onset temperatures: the vaporization of any volatiles and unpolymerized medium molecular weight units of the resin component (135°C); the faction of the polyol-

isocyanate bond formed during polymerization where the vaporized isocyanate component and liquid polyol remained (290°C) and char formation from the pyrolysis of the polyol component (450°C) respectively [20, 21].

The temperature domains of the decomposition stages, for new composite materials, starting temperature of weight loss steps, partial and total weight loss and temperature of the maximum weight loss for all samples, are presented in Table 1.

Analyzing the data in Table 1 we can observe that weight loss for the analyzed raw materials is quite different, 66.1% for recycled rubber (R), 83% for fir sawdust (FS) and 94.4% for polyurethane foam (PUF). This behavior is expected and can be explained by the fact that there are different materials. In terms of thermal stability, R has the highest stability (T_{max}=458°C) followed by PUF (T_{max}=381°C) and the last one is FS (T_{max}=359°C). It is expected that the thermal behavior of the raw materials influence the thermal behavior of composite materials of which they are part.

Table 1. Thermal degradation temperatures and weight loss of the investigated samples.

Sample	Temperature domain [°C]	T_{onset*} [°C]	T_{max} [°C]	Partial weight loss [%]	Total weight loss [%]
Polyurethane foam (PUF)	25 - 330	253	320	15.3	94.4
	330 - 800	350	381	79.1	
Fir sawdust (FS)	25 - 150	45	63	4.0	83.0
	150 - 800	250	359	79.0	
Recycled rubber particles (R)	25 – 430	299	372	49.2	66.1
	430 – 800	435	458	16.9	
Recycled rubber and 10% polyurethane foam (R-PUF10%)	25 – 320	244	305	9.2	67.2
	320 – 430	331	379	37.7	
	430 - 800	435	460	20.3	
Recycled rubber and 20% polyurethane foam (R-PUF20%)	25 – 320	247	308	9.8	69.3
	320 – 430	340	381	40.5	
	430 - 800	439	457	19.0	
Fir sawdust, recycled rubber and 15% polyurethane foam (R-FS-PUF15%)	25 – 320	250	310	10.5	69.8
	320 – 430	339	388	33.5	
	430 - 800	429	458	25.8	
Fir sawdust, recycled rubber and 25% polyurethane foam (R-FS-PUF15%)	25 – 320	252	320	10.4	73.5
	320 – 430	349	395	37.1	
	430 - 800	437	461	26.0	

T_{onset*} = *starting temperature of weight loss steps.*

Figure 1 shows the TG curves, for composite materials made from particles of recycled rubber and polyurethane foam in different proportion. Total weight loss increases with the increase in the percentage of polyurethane foam used as binder, from 67.2% for sample R-PUF10% to 69.3% for sample R-PUF20%, compared to R 66.1%. Comparing the two composites in terms of thermal stability with raw materials, the sample R-PUF10% has a better thermal stability decomposed at 460°C instead of 458°C, the decomposition temperature for R.
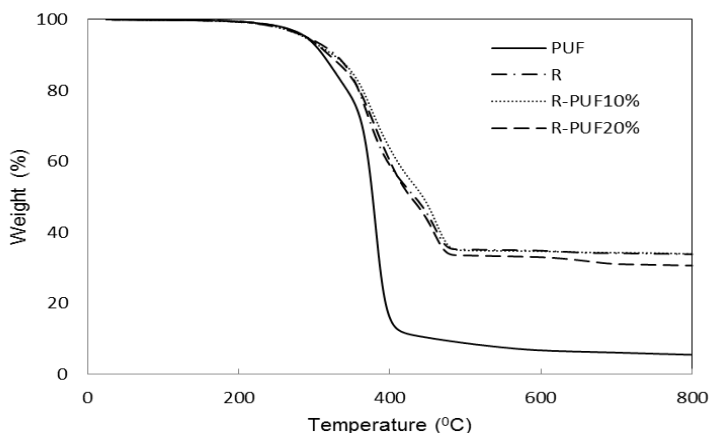

Figure 1. TG curves of the composite materials with rubber (R) and polyurethane foam (PUF)
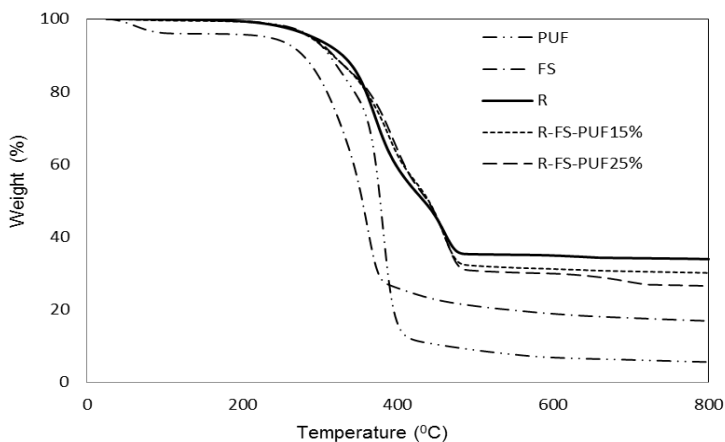

Figure 2. TG curves of the composite materials with rubber (R), fir sawdust (FS) and polyurethane foam (PUF)

For composite materials based on recycled rubber (25%) and fir sawdust (25%) and 15% respectively 25% polyurethane foam as binder, (Figure 2) total weight loss increases with the percentage of binder, from 69.8% to 73.5%, compared to the weight loss of the recycled rubber. The R-FS-PUF25% sample had a higher thermal stability, it decomposed at 461°C, with three degrees higher than major raw material R. In conclusion, the composite material has a better thermal stability than raw materials.

DTG curves, Figure 3, clearly showed that the recycled rubber had two distinct decomposition regions. The first weight loss (49.2%) was between 25–430°C, and was attributed to the degradation or volatilization of additives such as oils and stearic acid and to the degradation of natural rubber (NR) at 372°C. The final weight loss (16.9%) was 430–800°C and it appeared mainly due to the degradation of styrene–butadiene rubber (SBR) at 458°C, and butadiene rubber (BR) at 467°C. The observed degradation trend was in accordance with a former study which attributed the DTG peak temperature of 378°C to NR, 458°C to SBR and 468°C to BR [18].
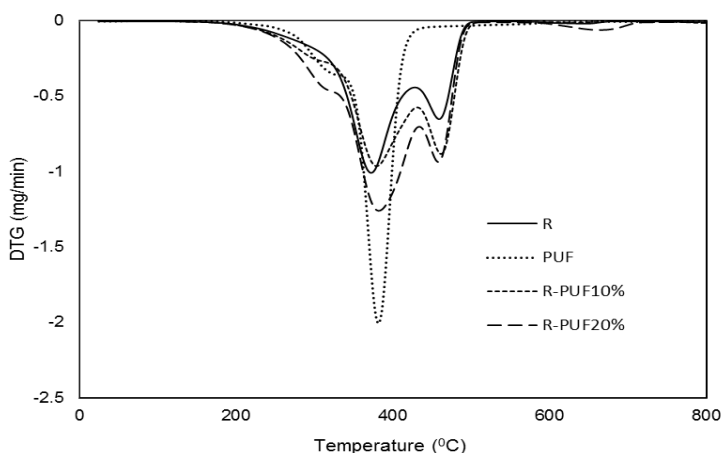

Figure 3. DTG curves of the composite materials with rubber (R)
and polyurethane foam (PUF)

In the cases of the composite materials, R-PUF10%, respectively R-PUF20%, if a mass loss occurs at around 247°C due to the scission of the polyol-isocyanate bond formed during polymerization, the weight loss of composite materials increases with the percentage of polyurethane foam used as binder (Figure 3).

On the decomposition curve of fir sawdust (Figure 4), the first peak appeared below 100ºC and can be assigned to the evaporation of water. The second peak at 359°C was broad, which means there was overlapping between the decomposition of hemicelluloses, cellulose, lignin and wood extractives.
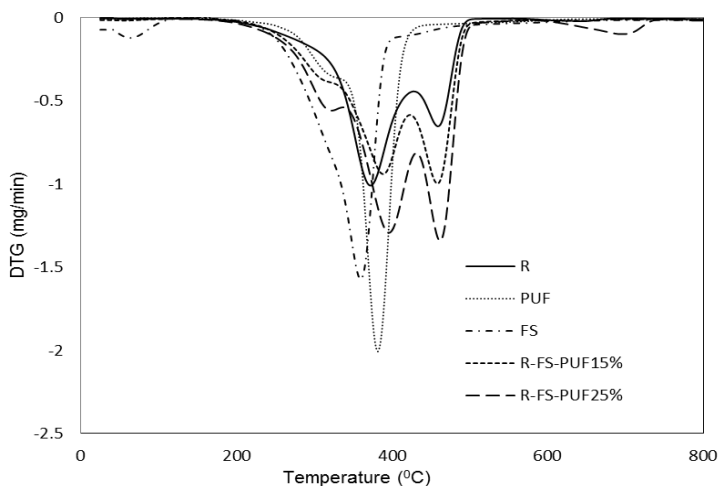
Figure 4. DTG curves of the composite materials with rubber (R),
fir sawdust (FS) and polyurethane foam (PUF)

The thermal stability of composite materials with fir sawdust added is better than that of the composite materials with recycled rubber and polyurethane foam only. In Figure 4 is observed that composite materials keep the shape of the recycled rubber decomposition curve, but with a greater weight loss and an increase in decomposition temperature.

CONCLUSIONS

The thermogravimetric plots show that basic research may be possible to describe the mechanisms of thermal decomposition of waste (fir sawdust and rubber from tires) and polyurethane foam, as raw materials.

Weight loss of analyzed raw materials is quite different, 66.1% for R, 83% for FS and 94.4% for PUF, because they are different materials but combined together in well-defined proportions give composite materials with superior properties.

Thermal stability of composite materials investigated are superior to any raw material use in this study and is clearly demonstrated by higher decomposition temperatures of composite materials: 461°C for R-FS-PUF25% and 460°C for R-PUF10% instead of 458°C for R 381°C for PUF and 359°C for FS, the decomposition temperatures of raw materials.

EXPERIMENTAL SECTION

Samples

Samples analyzed in this study are composite materials based on two types of raw materials (fir sawdust and recycled rubber particles from used tires) and polyurethane foam (flexible, with open cell) as binder.

Investigation methods

Thermogravimetric analysis (TGA) we performed on based composite materials with fir sawdust, polyurethane foam and recycled rubber particles, was performed using a Mettler-Toledo TGA/SDTA 851e, 1600°C, Analysis Thermal System.

Measuring conditions. Samples were placed in an alumina crucible and heated at 10°C/min over a temperature range of 25–800°C. The experiments were conducted under a nitrogen atmosphere at a flow of 50 mL/min. Samples weights of TGA were between 15–25 mg in their original state.

ACKNOWLEDGMENTS

REFERENCES

1. B. Sreedhar, M. Sairam, D.K. Chattopadhyay, P.A.S. Rathnam, D.V. Mohan Rao, *Journal of Applied Polymer Science*, **2005**, *96*, 1313.
2. P. Sukumar, V. Jayashree, M.R. Gopinathan Nair, M.N. Radhakrishnan Nair, *Journal of Applied Polymer Science,* **2009**, *111*, 19.
3. M. Jawaid, H.P.S. Abdul Khalil, *Carbohyd Polym,* **2011**, *86*, 1.
4. C.A. Cateto, M.F. Barreiro, C. Ottati, M. Lopretti, A.E. Rodrigues, M.N. Belgacem, *Journal of Cellular Plastics,* **2013**, *50*, 81.
5. J.M.F. De Paiva, E. Frollini, *Macromolecular Materials and Engineering*, **2006**, *291*, 405.
6. S.-P. Huo, M.-C. Nie, Z.-W. Kong, G.-M. Wu, J. Chen, *Journal of Applied Polymer Science*, **2011**, *125*, 152.
7. C.G. Silva, F. Oliveira, E.C. Ramires, A. Castellan, E. Frollini, *Tappi Journal,* **2012**, *11*, 41.
8. B.-L. Xue, J.-L. Wen, R.-C. Sun, *ACS Sustainable Chemistry & Engineering*, **2014**, *2*, 1474.
9. D. Randall, S. Lee, "The polyurethanes book", J. Wiley, **2002**, chapter 2.

10. Z. Wirpsza, T.J. Kemp, "Polyurethanes: chemistry, technology, and applications", E. Horwood, **1993**, chapter 3.
11. D.V. Dounis, G.L. Wilkes, *Polymer*, **1997**, *38*, 2819.
12. A.P. Mouritz, Z. Mathys, *Composite Science and Technology*, **2001**, *61*, 475.
13. H.L. Lee, G.C. Chen, R.M. Rowel, *Journal of Applied Polymer Science,* **2004**, *91*, 2465.
14. Q. Liu, C. Lv, Y. Yang, F. He, L. Ling, Journal of Molecular Structure*, *2005**, *733*, 193.
15. A.N. Shebani, A.J. van Reenen, M. Meincken, *Thermochimica Acta*, **2008**, *471*, 43.
16. M. Gröndahl, A. Teleman, P. Gatenholm, Carbohydrate Polymers, **2003**, *52*, 359.
17. H. Kim, S. Kim, H. Kim, H. Yang, *Thermochimica Acta,* **2006**, *451*, 181.
18. S. Seidelt, M. Müller-Hagedorn, H. Bockhorn, *Journal of Analytical and Applied Pyrolysis*, **2006**, *75*, 11.
19. G.-G. Choi, S.-H. Jung, S.-J. Oh, J.-S. Kim, *Fuel Processing Technology*, **2014**, *123*, 57.
20. C. Beyler, M. M. Hirschler, "Handbook of fire protection engineering*"*, National Fire Protection Association, **2002**, chapter 2.
21. D.U. Shah, F. Vollrath, D. Porter, *Polymer*, **2015**, *56*, 93.
22. A.M. Iurian, I. Perhaiţa, R. Şeptelean, A. Saponar, *Studia UBB Chemia*, **2013**, *LVIII, 1*, 141.

COIR EMPLOYED AS SOILLESS CULTIVATION SUBSTRATE AND ITS INTERFERENCE WITH NUTRIENT SOLUTION DURING TWO TOMATOES CROPPING PERIODES (CASE STUDY)

NIKOLAOS GOUGOULIAS[a],LIVIU GIURGIULESCU[b,*], DIMITRIOS KALFOUNTZOS[a], ALEXANDROS PAPACHATZIS[a], IOANNIS VAGELAS[a], DIMITRIOS FTAKAS[a], DIMITRIOS PATERAS[a], ADAMANTIA CHOULIARA[c]

ABSTRACT. The experiment was conducted in the glasshouse of TEI of Thessalia, for two growing periods, in soilless tomato cultivation, with coir substrate (open system). The electrical conductivity of the inflow solution to crops, fluctuated from 1.80 to 2.55 dS m-1 and pH values ranged from 5.5 to 6.8, while for the efflux solution from the crops, ranged from 2.00 to 3.50 dS m-1 for electrical conductivity, and from 5.5 to 6.9 for pH. On the coir substrate, the electrical conductivity ranged from 0.3 to 1.13 dS m-1 (water extract of 1 part of coir : 5 parts of H2O) and for pH from 5.87 to 6.83 during the first crop period; during the second cultivation, the electrical conductivity it fluctuated from 0.65 to 1.91 dS m-1 and for pH from 5.7 to 6.7. According to this study, 20% of substrate was decomposed, CEC increased, also the salinity status of the coir increased essentially during the second cultivation period, correlated with nitrate and phosphate forms enrichment of the substrate, while a slight negative affection to the crop production was observed; in generally, the coir substrate, is a good choice with excellent results for cultivation return.

Keywords: soilless cultivation, nutrient solution, coir substrate, tomato.

INTRODUCTION

In an efficient soilless cultivation (hydroponics), the plants are free from diseases, and grow faster than in the soil; naturally in hydroponics, nutrient solutions used, must be constantly controlled, as far as it concern their chemical composition and concentration as well as the chemical stability of the

---

[a] *Department of Agronomy Technology, Technological Educational Institute of Thessaly, 41110 Larissa, Greece.*
[b] *Department of Chemistry and Biology, Technical University of Cluj-Napoca, North Universitary Center of Baia Mare, 430122 Baia-Mare, Romania.*
[c] *Informatic's Scientist, data analysis.*
* *Corresponding author: giurgiulescu@gmail.com*

substrate employed must be assessed; adverse effects of soilless cultivations result concerning particularly the high cost of controlling systems provision and solution preparation; a significant factor affecting efficiency of nutrient solution in open hydroponic culture systems, is the observed loss of fertilizer and soil pollution, due to non-recycling of the liquids drained [1,2].The development of today's hydroponic's growing systems [3-7], is based on modern distribution systems of nutrient solution [8-12]. In the present study, the efficiency of used method for nutrient solution preparation is assessed, and as it concerns coir as substrate used in the present study, its alteration, during two crop periods, was evaluated [13].

RESULTS AND DISCUSSION

Nutrient solution: It was observed that in the inflow of the solution in two cropping periods, with regard to the electrical conductivity, it was produced a solution with slightly higher values of electrical conductivity (Figure 1). Also the runoff solution for both crops showed values of electrical conductivity, higher than the respective values of the influx solution, affected by the accumulation of salts in the substrate. In (Figure 2) is noted that during the inflow of the solution in both crops, with regard to the pH, it was produced a solution with slightly higher values; the runoff solution showed values of pH, also in generally higher values than the respective values of the influx solution.
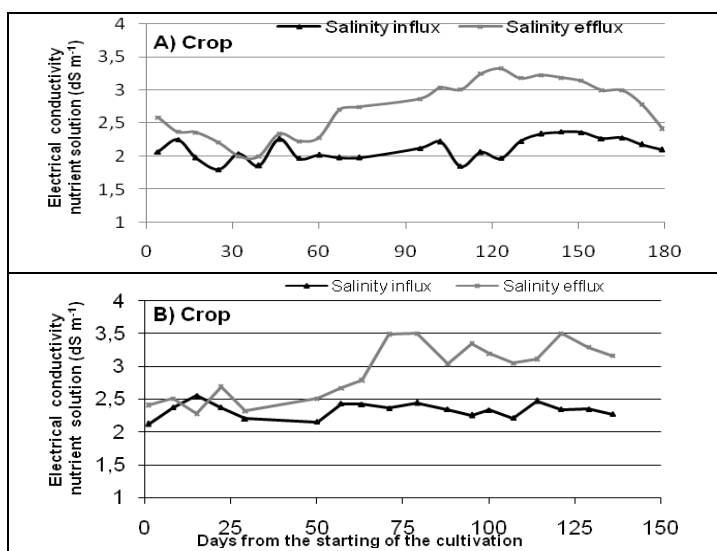

Figure 1. Fluctuations of electrical conductivity of influx and efflux of the nutrient solution of soilless tomato cultivation, during of two crops development
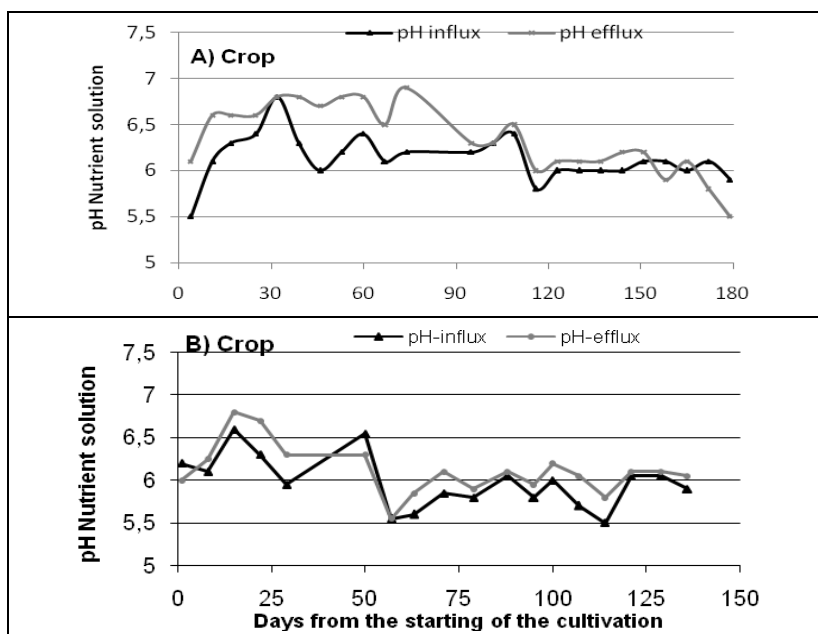
Figure 2. Fluctuations of pH values of the nutrient solution influx and efflux of soilless tomato cultivation, during the two crops development.

Substrate: The values of electrical conductivity were recorded concerning the substrate, during the development of two cultivation periods, as they were affected by the nutrient solution (Figure 3). In the first crop period, it was observed that during early days of cultivation, the electrical conductivity of the substrate was fluctuated, thereafter it was reduced and stabilized at the value of 0.63 dS m^{-1}, 90 days after the starting of the cultivation. At the second crop period, it was observed that for the early days of cultivation the electrical conductivity of the substrate was fluctuated, thereafter it was reduced and stabilized with low fluctuations at the value of 1.40 dS m^{-1}, 79 days after the starting of the cultivation. The values of pH were also recorded concerning the substrate during the two cultivation periods, as they were affected by the nutrient solution, (Figure 4). In the first crop period, the pH of the substrate during the cultivation was fluctuated from 5.87 to 6.83, while during the second crop, it was fluctuated from 5.7 to 6.7. Then, for the second cultivation period (B crop), it was revealed that the electrical conductivity was stabilized at higher values and for pH at lower values, in comparison to A crop; then a significant amount of salts was accumulated in coir during the second cultivation.
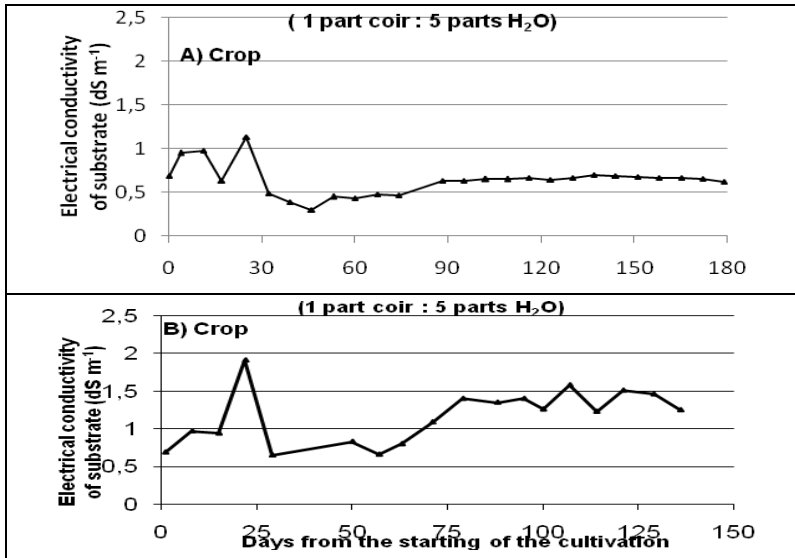
Figure 3. Fluctuations of electrical conductivity the coir substrate of soilless tomato cultivation, during the two crops development.
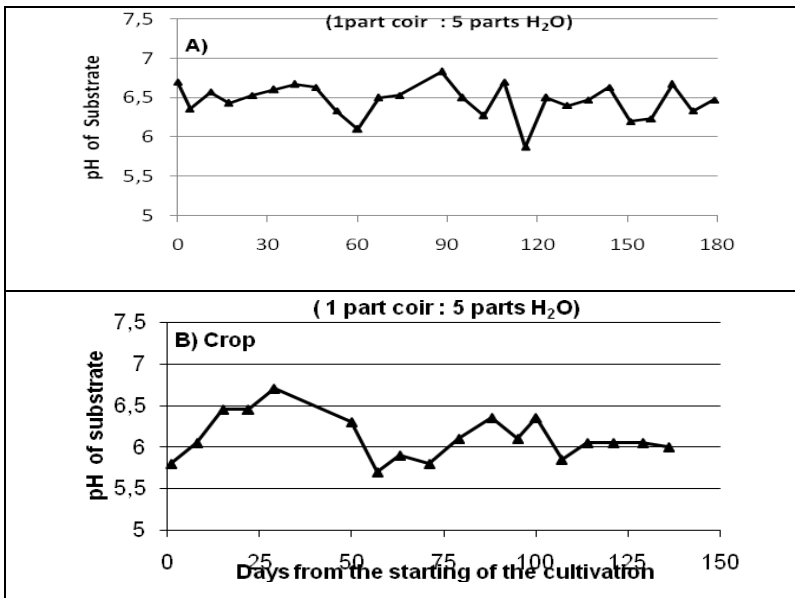

Figure 4. Fluctuations of pH values the coir substrate of soilless tomato cultivation, during of two crops development.

The increased values of electrical conductivity are accompanied by nitrate and P-Olsen forms accumulation in substrate particularly at the end of the B crop, compared with the respective values in the initial material (Table 1). In contrast, the values of pH of substrate resulted at the end of the B crop, decreased compared with the respective values of substrate, resulted at the end of the A crop and the initial substrate. The exchangeable - K forms of substrate resulted, at the end of the A and of the B crop, decreased compared to respective values of the initial substrate. In contrast, available forms Zn, Cu, Mn (extracted with DTPA) of substrate resulted, at the end of the A and of the B crops, increased compared with the respective values of the initial substrate.

Table 1. Chemical properties of the coir substrate used, before and after utilization.

Chemical Property	Initial Coir (since the starting of the crop)	Final Coir at the end of the A crop (or Initial Coir for the starting of the B crop)	Final Coir (at the end of the B crop)
	Commercial material	**wet basis**	
pH (1part substrate: 5parts H_2O)	6.7 ± 0.05	6.1 ± 0.05	5.75± 0.03
$CaCO_3$ (%)	0.13 ± 0.01	0.13 ± 0.01	0
Organic matter (%)	11.71 ± 1.1	8.39 ± 0.8	9.41± 1.0
CEC (cmol kg^{-1} substrate)	49.5 ± 5.7	75.2 ± 6.2	73.25± 6.3
Electrical conductivity, extract (1part substrate: 5 parts H_2O) (dS m^{-1})	0.68 ± 0.01	0.65 ± 0.01	0.94± 0.01
N -total (g kg^{-1})	0.333 ± 0.12	0,19 ± 0.05	0.56 ± 0.18
N-NH_4^+ (mg kg^{-1})	214 ± 14.5	22.6 ± 4.8	5.6 ± 1.7
N-NO_3^- (mg kg^{-1})	119 ± 11.3	167.6 ± 19.4	172,9± 18.6
Exchangeable-Na (mg kg^{-1})	402.5± 10.2	69.0 ± 3.6	92.0 ± 5.8
P -Olsen (mg kg^{-1})	14.73 ± 2.2	80.36 ± 9.8	145 ± 14.9
Exchangeable-K (mg kg^{-1})	2072.1 ± 101.2	733.2 ± 56.7	898.9 ± 44.8
Zn -Total (mg kg^{-1})	6.03 ± 0.5	24.59 ± 1.1	21.2 ± 1.2
Cu -Total (mg kg^{-1})	-	11.11 ± 0.8	24.1 ± 1.4
Mn -Total (mg kg^{-1})	-	-	31.1 ± 4.7
Zn -DTPA (mg kg^{-1})	1.66 ± 0.07	17.53 ± 2.4	12.66 ± 1.9
Cu -DTPA (mg kg^{-1})	0.56 ± 0.02	4.60 ± 0.8	0.67 ± 0.06
Mn -DTPA (mg kg^{-1})	1.7 ± 0.1	2.85 ± 0.2	2.13 ± 0.2
Moisture (%)	79.65	87.21	82.5

Data represent average means and SE deviation

In briefly, substrate after the second cultivation period utilization, is subjected to some alteration affected by salinity accumulation from nutrient solution, or by relative decomposition of that organic material; the CEC, nitrate forms and P available values of substrate increased but K available forms decreased.

Despite the variations in pH and electrical conductivity of the nutritive solution influxes [14], the plants showed a good development as well as the foliar chemical analysis of plants (Table 2), showed satisfactory nutritional status. The annual production of the first cultivation (A crop) was 100 tn/ha, with mean fruit weight 0.25 kg and of the second cultivation (B crop), 90 tn/ha, with mean fruit weight 0.23 kg.

Table 2. Foliar analysis of plants

	N (%)	P (%)	K (%)
A crop (120 days after the starting of the cultivation)	3.47	0.65	4
B crop (90 days after the starting of the cultivation)	3.22	0.63	3.90

CONCLUSIONS

The effectiveness of a soilless cultivation system in glasshouse conditions, with coir as substrate, was evaluated, in an experiment of two successive cultivations periods. In according to these results, the produced nutrient solution, showed several fluctuations, in comparison to the values expected, concerning electrical conductivity and pH values.A certain divergence upwardly was observed of the electrical conductivity values for produced nutrient solution; as for pH, it was found also higher values, for both growing periods (A crop & B crop). With regard to the runoff solution (efflux), which seeps of the substrate, also studied during of the two crops periods, the corresponding solution was found with higher values concerning electrical conductivity and pH, in comparison with influx**.** In both crops the coir substrate reached a stabilization status in salinity, after the middle of each cultivation period, but in significantly higher levels for the second cultivation period (B crop).

Particularly, as far as it concerns **coir substrate** evaluation, after two cropping periods utilization, a certain decomposition of the organic material was observed (≈ 20%), and an increase of salinity accumulation correlated with nitrate and phosphate forms enrichment of the substrate; the pH of the substrate was reduced and a significant accumulation of Zn amounts (total and available forms) was recorded.

Despite the marked adverse effects, crops returned satisfactory yields, but a reduction of tomato production about 10%, for B crop was remarked, and that could be attributed to substrate salinity increased values. Nevertheless, coir is estimated as an excellent substrate despite the certain alteration assessed after two periods of employment; the most important is to adopt the necessary recommendations, in order to be respected the necessary settings to the system irrigation-fertilization unity.

EXPERIMENTAL SECTION

In the glasshouse of TEI of Thessalia, situated in Larissa, an open hydroponic's system, with automatic control and production unit of nutrient solutions has been established. Tomato plants in an area of 100 m^2 were cultivated, the first period lasted (A crop) from 14-10-2010 to 11-04-2011 and the second period (B crop) from 17-10-2011 to 29-02-2012. The substrate used was pressurized packages of coir (Table 1); the unit contains three stock solutions, that are in three different barrels (photo:1). The necessary amounts of solution from each barrel come out automatically, by creating the final nutrient solution regulating the EC and pH values by the unit program. According with directives of the supplier, it is recommended for tomato a nutrient solution with pH:6 and electrical conductivity EC: 2 dS m^{-1}.

The content of the three parent nutrient solutions for the first and second crop were:

A´ Barrel: (Ca^{2+} = 507, NO_3^- = 680.6, K^+= 116.8, NH_4^+= 55, Fe^{2+} = 1.8) me/L H_2O.
B´ Barrel: (Mg^{2+}=195, K^+= 644.2, H^+= 286, SO_4^{2-} = 580, NO_3^- = 115.2, PO_4^{3-} = 430) me/L H_2O.
Γ´ Barrel: 6.6 mL concentrated HNO_3 / L H_2O.

Each watering had a duration of 3 min and the inflow of the nutrient solution was 58.9 mL/min. In the first crop, the first 60 days after the starting of the crop, three watering times were applied per day, the next 50 days 4 times and the next 69 days 5 times per day. In the second crop, the first 40 days of the start of the crop, three watering times were applied per day, the next 40 days 4 times, and the next 56 days, 5 times per day.

The purpose of the experiment is to assess the chemical stability of substrate used, to investigate the effectiveness of the system that ensures the desired pH (6) and electrical conductivity values (2dS m^{-1}),and to adopt efficiently the appropriate variations in that adjustment in the unity installed.

METHODS OF ANALYSES

Coir samples were analyzed using the following methods which are referred by [15,16]:

Organic matter was analyzed by chemical oxidation with 1 mol L^{-1} $K_2Cr_2O_7$ and titration of the remaining reagent with 0.5 mol L^{-1} $FeSO_4$.

Both ammonium and nitrate nitrogen were extracted with 0.5 mol L^{-1} $CaCl_2$ and estimated by distillation in the presence of MgO and Devarda's alloy, respectively.

Available P forms (Olsen P) was extracted with 0.5 mol L^{-1} $NaHCO_3$ and measured by spectroscopy.

Exchangeable forms of potassium ware extracted with 1 mol L^{-1} CH_3COONH_4 and measured by flame Photometer (Essex, UK).

Available forms of Mn, Zn, and Cu were extracted with DTPA (diethylene triamine pentaacetic acid 0.005 mol L-1 + CaCl2 0.01 mol L-1 + triethanolamine 0.1 mol L^{-1}) and measured by atomic absorption.

For the determination of total metals Mn, Cu and Zn, 1 g of wet material of coir, were analyzed by digestion at 350 ^0C. According to the method described by [17]., (1974) and [18] the sample containing 10 mL HNO_3 + 5 mL $HCLO_4$ were analyzed by Atomic Absorption (Spectroscopy Varian Spectra AA 10 plus, Victoria, Australia). The detection of Mn, Cu and Zn in coir was done with the use of flame of air-acetylene mixture.

Every value of the electrical conductivity or pH, corresponds to the mean of three replicates. Statistical analyses were performed by the use of statistical program MINITAB [19]. Data represent average means and SE deviation.

REFERENCES

1. Gül A., Tüzel I.H., Tuncay Ö., Eltez R.Z. & Zencirkiran E., *International Symposium Greenhouse Management for Better Yield & Quality in Mild Winter Climates*, **1997**, *491,* pp. 389-394.
2. Dasgan H.Y. & Ekici B., *In International Symposium on Soilless Culture and Hydroponics*, **2004**, *697,* pp. 399-408.
3. Manios, V.I., Papadimitriou, M.D. and Kefakis, M.D., *Acta Hort. (ISHS),* **1995**, *408*, 11.
4. Inden, H. and Torres, A., *Acta Hort. (ISHS)*, **2004**, *644*, 205.
5. Azad, A.K., Ishikawa, K., Diaz-Perez, J.C., Eaton, T.E.J. & Takeda, N., *Agricultural Sciences*, **2013**, *4*(07), 1.
6. Buwalda, F., van Os, E.A., Giacomelli, G., Samperio Ruiz, G., Vermeulen, T., van Weel, P.A. & Ruijs, M.N.A., *International Symposium on Growing Media and Soilless Cultivation*, **2013**, *1034*, pp. 201-207.

7. Rius-Ruiz, F.X., Andrade, F.J., Riu, J. & Rius, F.X., *Food chemistry*, **2014**, *147*, 92-97.
8. Sonneveld, C., Baas, R., Nijssen, H.M.C. and De Hoog, J., *Journal of Plant Nutrition*, **1999**, *22*(6): 1033.
9. Zekki, H., Gauthier, L. & Gosselin, A. *Journal of the American Society for Horticultural Science*, **1996**, *121*(6), 1082.
10. Bugbee, B., *Acta Horticulture*, **2004**, *648*, 99.
11. Bissonnette, W.M., Wainwright, R.E., Payne, C., Thompson, J., Bromley, R. and Morgan, C., U.S. Patent No. 8,261,486. Washington, DC: U.S. Patent and Trademark Office, **2012**.
12. Domingues, D.S., Takahashi, H.W., Camara, C.A. & Nixdorf, S.L., *Computers and Electronics in Agriculture*, **2012**, *84*, 53.
13. Furlani A.M.C., de Abreu M.F., de Abreu C.A., Furlani P.R. & Bataglia O.C., *International Symposium on Soilless Culture and Hydroponics*, **2004**, *697,* pp. 109-115.
14. Martínez-Cárdenas, L., Reed, D., Kent, M., Ramírez-Vallejo, P., Juárez-López, P., Cruz-Crespo, E., Bugarín-Montoya, R. and García-Paredes, J.D., *International Symposium on Growing Media and Soilless Cultivation,* **2013**, *1034*, pp. 501-504.
15. Hesse, P.R., *A Textbook of Soil Chemical Analysis*. John Murray, London, **1972**.
16. Page, A.L., Miller, R.H. and Keeney, D.R., "Methods of Soil Analysis Part 2: Chemical and Microbiological Properties. Agronomy, ASA and SSSA", Madison, Wisconsin, USA, **1982**.
17. Allen, S.E., Grimshaw, H.M., Parkinson, J.A. and Quarmby, C., "Chemical analysis of Ecological materials", Blackwell Scientific Publications, **1974**.
18. Varian, M., "Flama Atomic Absorption Spectroscopy. Analytical Methods", Varian Australia, **1989**, Publ. N0: 85-100009-00.
19. Ryan, B.F., Joiner, B.L. and Cryer, J.D., "MINITAB Handbook: Updated for release 14", **2005**, 5th edition.

IS STARCH ONLY A VISUAL INDICATOR FOR IODINE IN THE BRIGGS-RAUSCHER OSCILLATING REACTION?

LÉNÁRD-ISTVÁN CSEPEI[a,b,*], CSABA BOLLA[a]

ABSTRACT. In this work we studied the effect of malonic acid concentration on the Briggs-Rauscher oscillating reaction both in absence and in presence of starch, which acts as indicator for the iodine intermediate. For the starch free mixtures, the number of oscillations and the oscillation time increased with the increase of initial malonic acid concentration, while the period time showed the opposite trend. When starch was also present in the Briggs-Rauscher mixture, the number of oscillations, the oscillation time and period length were higher in comparison with the starch free mixtures with the same initial malonic acid concentration. In presence of starch, within one oscillation period, the iodine consumption segment was also longer compared to those measured for the starch free mixtures. This suggests that the starch is not only a simple visual indicator for the iodine intermediate, but it probably acts as a reservoir for iodine due to the starch-triiodide equilibrium during each oscillation cycle. As such, the starch may influence the kinetics of the reaction steps involving the iodine intermediate. Finally, we present a simple method for the treatment of the residual Briggs-Rauscher mixture which enables the removal of the strong acid, the oxidizing agents and the quantitative recovery of the Mn^{2+} catalyst in form of MnO_2. Thereby, this method enables to minimize the environmental effect of the residual mixture before disposing it.

Keywords: *Briggs-Rauscher oscillating reaction, malonic acid, iodine, starch, indicator, starch-triiodide complex, oscillation time, period time, apparent activation energy, nonlinear chemical dynamics, environmental awareness*

INTRODUCTION

The Briggs-Rauscher reaction is a prominent example of the liquid phase oscillating reactions. Although it was discovered more than four decades

---

[a] *Babeş-Bolyai University, Faculty of Chemistry and Chemical Engineering, Arany János Str., Nr. 11, RO-400084 Cluj-Napoca, Romania.*
[b] *Current adress: Fraunhofer Institute for Interfacial Engineering and Biotechnology IGB, Bio-, Electro- and Chemocatalysis BioCat, Straubing Branch, Schulgasse 11a, 94315 Straubing, Germany.*
* Corresponding author: cslenard@gmail.com*

ago [1], an intensified interest towards this reaction could be observed since the early 2000s.

The net chemical reaction is the iodination of an organic substrate by iodate ion and hydrogen peroxide, catalyzed by Mn^{2+} ion in acidic media [2, 3, 4]. In the first years after its discovery, thirty elementary steps were identified [3, 4] and it was found that a set of thirteen steps - known as skeleton mechanism - describes qualitatively well the nonlinear behavior of the reaction [5, 6]. This mechanism was further refined over the past one and a half decade [7-11].

The intermediates of the reaction (e.g. I_2, I^-, HOI, HIO_2, $IO_2\cdot$, $HOO\cdot$) show more than one extreme point – maximum and minimum – in time. The periodic changes of the iodine concentration can be seen visually: during the reaction colorless-brown-pale yellowish-colorless cycles can be observed. A few reports described that in presence of starch indicator the oscillations of iodine concentration are more visible because of the formation of the starch-triiodide complex: the color of the reacting mixture changes within one period from colorless to deep blue then to brownish and colorless again [1, 12, 13, 14, 15, 16, 17]. In some of these studies spectroscopic methods were applied to learn more details about the involvement of the iodine or starch-triiodide complex in the BR-reaction [15, 16]. Nevertheless, besides the more dramatic color change, no other differences were documented between the oscillations of the starch containing and starch free BR mixtures in the above literature sources.

It is also interesting to mention that the inorganic subset of the Briggs-Rauscher reaction is very similar to the well studied Bray-Liebhafsky oscillating reaction. The Bray-Liebhafsky reaction involves only hydrogen-peroxide, iodate ions and mineral acid. Although the iodine is an intermediate also in this chemical oscillator, up to our best knowledge the effect of starch was not studied yet on the Bray-Liebhafsky reaction.

In our previous studies we also used starch for qualitative observations concerning the iodine formation and consumption upon addition of several substances (ascorbic acid, tartaric acid, pyrogallol and salicylic acid) to the oscillating Briggs-Rauscher mixture [18, 19]. During these experiments, however, we have already noticed some quantitative differences between the oscillations of a starch free and starch containing mixture. As it is known that some organic compounds (such as ascorbic acid and other hydroxyl-group containing organics) interfere strongly with starch-iodine reaction [20], based on our experiments reported in [18, 19] it was not possible to establish what the reason for the observed differences was. These observations triggered a more systematic study on the effect of starch on the reaction [21]. We also varied the malonic acid concentration, because the iodine consumption rate within one oscillation

depends on the malonic acid concentration [13]. Therefore, our goal was also to check the complex interrelation between malonic acid, iodine and starch in this reaction. In the present work we report the phenomenological effect of starch on the oscillation parameters of Briggs-Rauscher reaction studied at different malonic acid concentrations. In the following paper we will report the effect of starch on the kinetics of iodine consumption within one period of oscillation.

RESULTS AND DISCUSSION

In the first series of experiment the initial concentration of malonic acid was varied from 0,031 to 0,199 M while keeping constant the initial concentration of potassium-iodate (0,0675 M), hydrogen peroxide (0,92 M), manganous sulfate (0,0065 M) and sulfuric acid (0,025 M) in absence of starch indicator. During the second series of measurement 0,48 mg/ml starch indicator was added, while keeping the other conditions the same as at the first series of runs. All these experiments were carried out at a temperature of 25ºC. Under every condition, the experiment was repeated typically three times in order to check for the reproducibility of the observed effects. More than that, the quantitative oscillating parameters were statistically analyzed.

The Figure 1 displays the reproducibility test at the lowest malonic acid concentration: three runs of the BR reaction recorded after each other using the same initial composition, in absence of starch. The reproducibility demonstrated on Figure 1 was typical also for measurements under every other condition.

The stock solutions A and B were mixed in the reactor; then the malonic acid and manganese sulfate containing solution C was injected by a rapid delivery piston pipette at the time indicated by the green arrow on Figure 1 (for the composition of the stock solutions A, B and C see the Experimental section).

The oscillation started immediately, without induction period after the injection of the solution C. However, the very first oscillation appearing right after the injection of the solution C was a first, incomplete oscillation, since it did not exhibit a minimum like the subsequent ones. In our previous studies [18, 19, 22, 23] we started to record the potential a few seconds after the mixing of all the three solutions, therefore the first, incomplete oscillation was not observable. After the first, incomplete oscillation there were regular oscillations, i.e. those three in the middle of the Figure 1, possessing well defined minima, maxima and similar shape. The very last oscillation was much broader and had significantly lower amplitude than the regular ones. However, when the malonic acid concentration was higher than 0,075 M, the last oscillation was also regular.
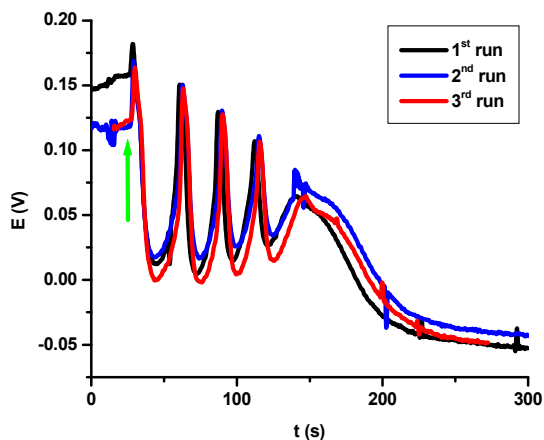
Figure 1. Reproducibility test of the oscillations in a starch free BR-mixture.
The malonic acid concentration was 0,031 M.

The following oscillating parameters are considered here:

1) oscillation time (s): the time elapsed from the maximum of the first, incomplete oscillation until the minimum of the last regular oscillation. At malonic acid concentrations higher than 0,075 M the last oscillation was also included in the length of the oscillation time
2) period time (s): the time elapsed between two consecutive oscillatory maxima,
3) amplitude (V): the potential difference between a maximum and minimum,
4) number of oscillations: only the regular oscillations were counted. The last broad oscillation observed at low malonic acid concentrations and the „two-third oscillation" were not taken into account.

As the Figure 1 demonstrates, the peak shapes and parameters are well reproducible. The high frequency potential fluctuations with minor amplitude appeared due to electric noise in the electronic recording system.

Qualitative comparison of the oscillations of starch free and starch containing BR-mixtures

In the followings, the qualitative features of the BR reaction are compared in absence and in presence of starch while keeping constant the initial concentrations of malonic acid, hydrogen peroxide, sulfuric acid and iodate-, manganous ion (Figure 2). It is notable that in presence of starch, the number of oscillations and the oscillation time is much higher than in the starch

free mixture. On the other hand, the period times are visibly longer and the amplitudes throughout the reaction are more uniform when starch is present in the reacting mixture.

As described earlier, one period of oscillation on the E(V) versus time plot consists of four distinct segments [19, 25]: two decreasing segments and two increasing segments with different slopes and lengths. The color changes of the oscillating mixture during one period are described below:

In the starch free mixture, brown coloration appeared during the steep decreasing segment, which indicates iodine formation. During the slightly increasing slope the brown color faded out gradually to pale yellow, indicating relatively slow reaction between iodine and the enolic form of the malonic acid. During the rapidly increasing segment, the mixture became transparent and remained transparent during the relatively slowly decreasing segment. Then the cycle repeated. After the last oscillation, the color of the mixture became deep brown, indicating strong iodine formation and accumulation.

In the starch containing mixture the color turned into deep blue during the fast decreasing segment and it faded out to slightly brownish during the slow increasing slope. During the fast increasing and the relatively slowly decreasing segment the mixture was colorless. At the end of the oscillations the mixture was deep blue because of the formed iodine.
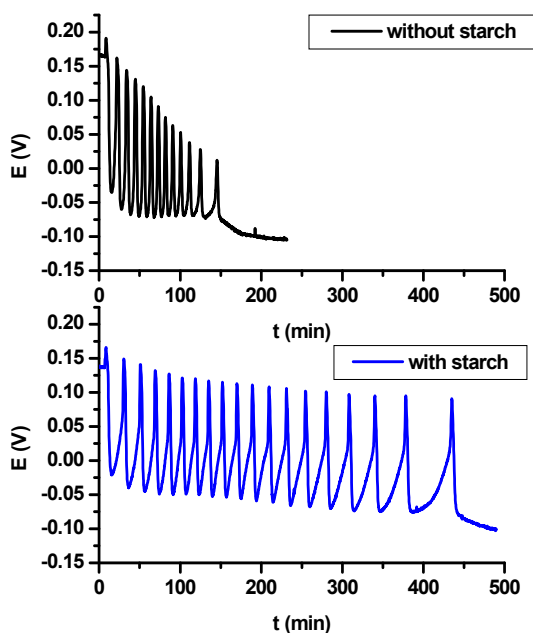

Figure 2. The oscillations recorded in a BR mixture containing 0,131 M malonic acid. The starch concentration: black – 0,00 mg/ml, blue – 0,48 mg/ml.

Quantitative comparison of the oscillations of starch free and starch containing BR-mixtures

The effect of malonic acid concentration on the quantitative parameters listed above is presented here.

First, the number of oscillations was plotted versus the initial malonic acid concentration for both the starch free and starch containing mixtures. A linear increase can be observed in each case (Figure 3, top). In presence of starch, the number of oscillations was approximately two times higher than in the case of starch free mixtures.

The oscillation time increased approximately linearly with the malonic acid concentration for the starch free mixture and apparently exponentially for the starch containing mixture (Figure 3, bottom).
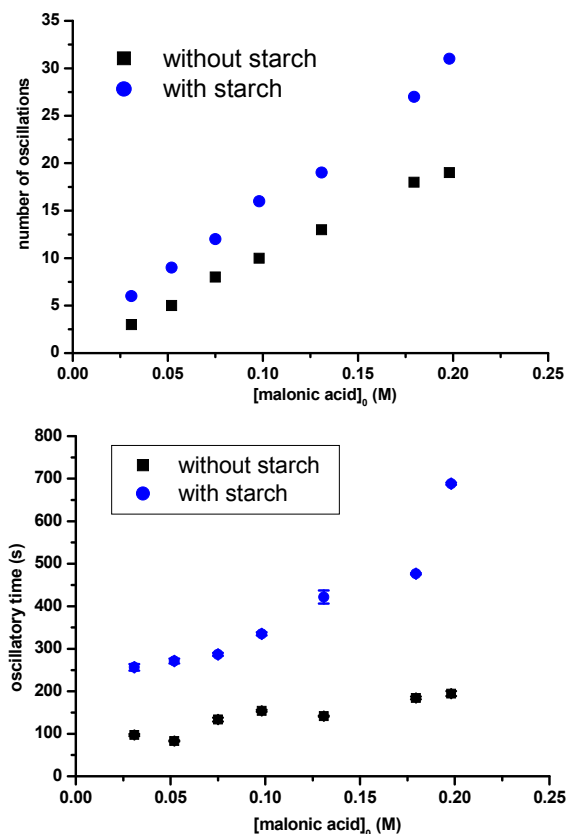

Figure 3. The effect of malonic acid concentration on the number of oscillations and the oscillation time.

In general, the length of the iodine consumption segment (which was evaluated by measuring the lenght of the slowly increasing segment after the potential minimum) was dominant within one cycle of oscillation. This observation is in agreement with the observation of Furrow [13]. In the case of starch free mixture, the iodine consumption segment was 38-45% of the period time. On the other hand, in presence of starch, the iodine consumption constitutes 48-60% of the period time.
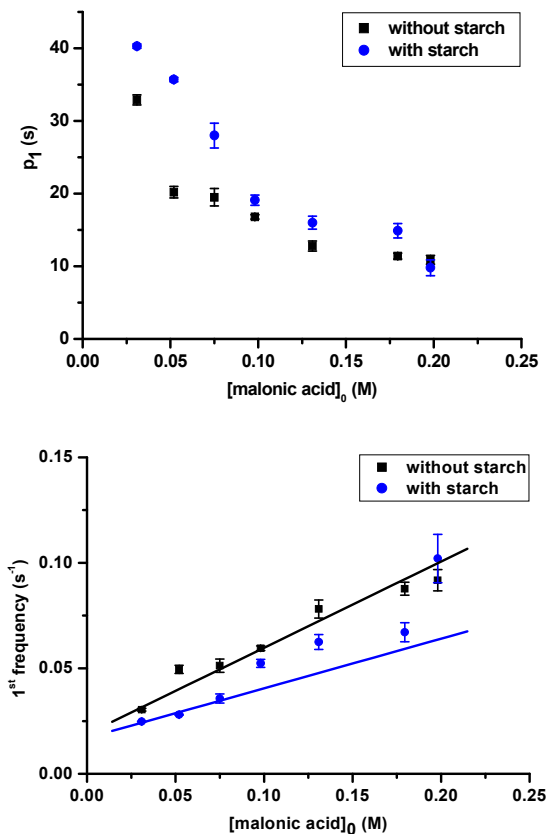

Figure 4. The effect of malonic acid concentration on the first period time and frequency, respectively.

The period time was decreasing with the increase of the malonic acid concentration. This trend was the same for both the starch free and starch containing mixture. However, in the starch containing the period times were higher (Figure 4, top).

Table 1. The dependence of the frequency (f) of the first oscillation
on the initial malonic acid concentration.

C_{starch} (mg/mL)	Equation	R^2
0,00	f = 0,02+0,41·[malonic acid]$_0$	0,9835
0,48	f = 0,02+0,19·[malonic acid]$_0$	0,9090

Similarly to the observation of Furrow, the reciprocal period time (that is equal to the frequency) increases approximately linearly with the substrate concentration [13]. This linear dependence is given on Figure 4 bottom, while the equations of the straight lines are in the Table 1.

Finally, no trend was found between the amplitude of the first three oscillations and the initial concentration of the malonic acid, irrespectively whether starch was present or absent in the mixture.

Determination of the apparent activation energy for the starch containing BR-mixture

In the third series of measurements the reaction temperature was varied between 26 and 52ºC for a BR mixture with 0,199 M malonic acid and 0,48 mg/ml starch. The apparent activation energies were evaluated.

The apparent activation parameters of the BR reaction are usually determined from the temperature dependence of the oscillation time [26, 27] and the period time [12, 25]. In the literature it was noted that both of these quantities decrease exponentially with the temperature. The dimension of the reciprocal oscillation time and period time is the same as the dimension of a first-order rate constant (second^{-1}).

The Arrhenius plot of the reciprocal oscillation time and period time, respectively lead to straight lines (Figure 5 and 6). From the slope of these lines the apparent activation energy of the reaction was calculated corresponding to the starch containing mixture. The values are compiled in Table 2, among the apparent activation energies reported in the literature. Due to the fact that the reaction mechanism is very complex – it consists of at least 30 elementary steps in absence of starch – the determined activation energy does not correspond to any of the elementary steps of the BR reaction, but it is „global" or apparent activation energy. In the presence of starch, there is at least one additional equilibrium reaction corresponding to the formation of the starch-triiodide complex. Therefore, due to the above described complexity, it is very difficult to draw conclusions on the effect of starch on the apparent activation energy.

On the other hand, because the reaction mechanism is so complex and the compositions of the BR mixtures reported in the literature are different (Table 2), the apparent activation energies are not comparable directly [27].

Figure 5. The effect of temperature on the oscillation time (black squares) and the corresponding Arrhenius-plot (blue dots). The malonic acid and starch concentration was 0,199 M and 0,48 mg/ml, respectively.
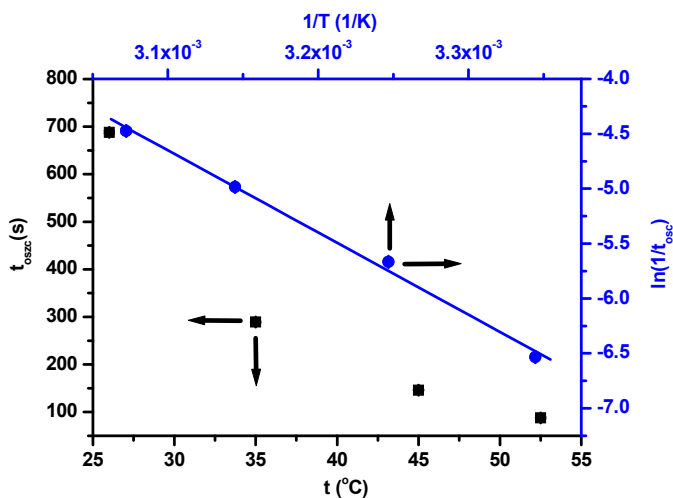

Figure 6. The effect of temperature on the first period time (black squares) and the corresponding Arrhenius-plot (blue dots). The malonic acid and starch concentration was 0,199 M and 0,48 mg/ml, respectively.
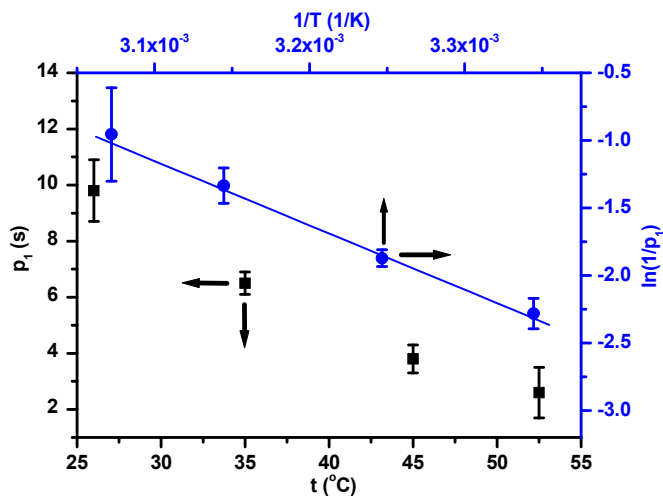
Table 2. The apparent activation energy of BR mixtures with different compositions. Ea (I.) – activation energy determined from the temperature dependence of the oscillation time. Ea (II.) – activation energy determined from the temperature dependence of the period time. (a) – this work, n.a. – data not available.

Ref. Comp.	(a)	23	25	26	27
$[H_2O_2]_0$ (M)	0,92	0,92	0,48	1,20	1,20
$[MA]_0$ (M)	$1,99 \cdot 10^{-1}$	$5,0 \cdot 10^{-2}$	$5,0 \cdot 10^{-2}$	$5,0 \cdot 10^{-2}$	$5,0 \cdot 10^{-2}$
$[KIO_3]_0$ (M)	$6,75 \cdot 10^{-2}$	$6,75 \cdot 10^{-2}$	$6,75 \cdot 10^{-2}$	$6,0 \cdot 10^{-2}$	$3,33 \cdot 10^{-2}$
$[H_2SO_4]_0$ (M)	$2,50 \cdot 10^{-2}$	$2,50 \cdot 10^{-2}$	$2,50 \cdot 10^{-2}$	$4,0 \cdot 10^{-2}$	$2,66 \cdot 10^{-2}$
$[MnSO_4]_0$ (M)	$6,50 \cdot 10^{-3}$	$6,50 \cdot 10^{-3}$	$6,50 \cdot 10^{-3}$	$6,0 \cdot 10^{-3}$	$6,67 \cdot 10^{-3}$
c_{starch} (mg/ml)	0,48	0,00	0,00	0,00	0,00
$E_a(I.)$ (kJ/mol)	62±3	38±2	n.a.	57	68±2
$E_a(II.)$ (kJ/mol)	42±1	51±1	61±7	n.a.	n.a.

CONCLUSIONS

The results of our experiments show that starch does not act only as a simple indicator of iodine intermediate in the oscillatory Briggs-Rauscher reaction. In the presence starch containing mixtures, the number of oscillations and also the period time of oscillations increased compared to the starch free mixture. Additionally, the reaction step involving the iodine and the malonic acid seems to be slowed down significantly in presence of starch in the reacting mixture. This may hint towards the fact the starch acts as a „reservoir" for iodine due to the starch-triiodide reaction, and it may change significantly the kinetics of the reaction steps in which the iodine (and in general, the triiodide anion) is involved. One of these steps is the iodination of the malonic acid, which produces the iodide ion. Another important step is the reaction of iodine with water which produces HOI, another key intermediate of the Briggs-Rauscher reaction. Last but not least, iodine may catalyze the decomposition of the diiodomalonic acid which accumulates gradually over the Briggs-Rauscher reaction [9]. Therefore, in presence of starch, the kinetics of the diiodomalonic acid decomposition step may also be slowed down.

EXPERIMENTAL SECTION

Two stock solutions were prepared according to the procedure described in our previous reports (solution A: 1,84 M hydrogen peroxide, and solution B: 0,27 M potassium iodate and 0,1 M sulfuric acid) [18, 19, 22, 23, 24]. The stock solution C contained 0,026 M manganese sulfate and different malonic acid

concentrations (0,124, 0,208, 0,300, 0,392, 0,542, 0,720, 0,793 M). Starch solution was prepared by dissolution of starch in water at 60ºC and cooled down to room temperature. All chemicals were used without any further purification: H_2O_2 (Merck, p.a), KIO_3 (AnalytiCals, p.a), H_2SO_4 (Riedel de Haen, p.a), $CH_2(COOH)_2$ (Reachim, p.a), $MnSO_4$ (Reactivul, p.a), starch (Reactivul, p.a). Doubly distilled water was used for the preparation of all the solutions.

The stock solutions were mixed in a double walled glass reactor connected to a thermostat. After mixing, the composition of the BR reaction mixture was the following: $[H_2O_2]_0$=0,92 M, $[H_2SO_4]_0$=0,025 M, $[MnSO_4]_0$ = 0,0065 M, $[KIO_3]_0$ = 0,0675 M, whereas the concentration of malonic acid was 0,031; 0,052; 0,075; 0,098; 0,131; 0,180; 0,199 M. A magnetic stirrer and a submersible magnetic bar were used for the thorough stirring of the BR mixture. The reaction was monitored employing an iodide ion selective electrode (Radelkis, Budapest) and a double junction saturated calomel electrode as reference electrode. The variation of the potential in time has been registered using a computer eqipped with a National Instruments® data acquisition card. Then the E(V) vs time plots along with the further data analysis were made in Origin program.

The first series of measurements was carried out without addition of starch, while the second in presence of 0,48 mg/ml starch. Both measurement series were done at 25 ºC. The third series of measurement consisted of temperature variation in four steps between 26 and 52 ºC, using the following BR composition: $[H_2O_2]_0$ = 0,92 M, $[H_2SO_4]_0$ = 0,025 M, $[MnSO_4]_0$ = 0,0065 M, $[KIO_3]_0$ = 0,0675 M, [malonic acid]$_0$ = 0,199 M, and starch concentration of 0,48 mg/ml. Three measurements were carried out under every condition. The parameters (oscillation time, period time, number of oscillations, amplitude) were averaged over the three measurements, and the standard deviation was calculated. The standard deviation was used as weighting factor for linear regression.

We present here also the treatment method that we developed for decreasing significantly the environmental impact of the residual reaction mixture. The residual BR mixture contains always unreacted hydrogen peroxide, sulphuric acid, manganese- and iodate ions and sometimes significant amounts of iodine from the decomposition of iodo-malonic acid. Since all of these compounds are of environmental concern, all the residual BR-mixture was collected in a larger beaker and treated in the following way: first sodium-tiosulphate was added which transformed the iodine into iodide ion. The iodide ion reacted with the residual iodate ion and produced iodine. Therefore, the sodium-tiosulphate was added until the iodine formation completely ceased – this signaled that all the residual iodate ions were completely consumed from the mixture. Then sodium carbonate was added in order to reduce the acidity of the mixture. At slightly basic pH the Mn^{2+} ion was oxidized to MnO_2 by the dissolved O_2 (the oxygen being a product of the BR-reaction as well) [29].

$$2 \, Mn^{2+} + 4HO^- + O_2 \rightarrow 2MnO_2 + 2H_2O \qquad \qquad (R1)$$
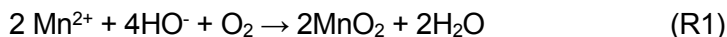
The formed MnO_2 decomposed catalytically the residual amounts of H_2O_2 to O_2 and H_2O. After sedimentation, the MnO_2 was separated by filtration. Therefore, by treating of the residual BR-mixture with two inexpensive chemicals such as sodium-tiosulphate and carbonate it was possible to remove all the strong oxidizing agents, the mineral acid and to recover quantitatively the heavy metal ion in form of MnO_2. At the end, the solution contained only sodium-, potassium-, iodide, sulphate- and residual tiosulphate ions which are environmentally much less harmful.

ACKNOWLEDGEMENT

REFERENCES

1. T.S. Briggs, W.C. Rauscher, *J. Chem. Educ.*, **1973**, *50*, 496.
2. D.O. Cooke, *Int. J. Chem. Kinet.*, **1980**, *12*, 683.
3. S.D. Furrow, R.M. Noyes, *J. Am. Chem. Soc.*, **1982**, *104*, 38.
4. S.D. Furrow, R.M. Noyes, *J. Am. Chem. Soc.*, **1982**, *104,* 42.
5. S.D. Furrow, R.M. Noyes, *J. Am. Chem. Soc.*, **1982**, *104*, 45.
6. P. De Kepper, I.R. Epstein, *J. Am. Chem. Soc.*, **1982**, *104*, 49.
7. S.D. Furrow, R. Cervellati, G. Amadori, *J. Phys. Chem. A*, **2002**, *106*, 5841.
8. G. Szabo, A. Csavdari, L. Onel, G. Bourceanu, Z. Noszticzius, M. Wittmann, *J. Phys. Chem. A*, **2007**, *111*, 610.
9. R. Cervellati, E. Greco, S.D. Furrow, *J. Phys. Chem. A*, **2010**, *114*, 12888.
10. R. Cervellati, S.D. Furrow, *Russ*. *J. Phys. Chem. A*, **2013**, *87*, 13, 2121.
11. G. Holló, K. Kály-Kullai, T.B. Lawson, Z. Noszticzius, M. Wittmann, N. Muntean, S.D. Furrow, G. Schmitz, *J. Phys. Chem. A,* 2014, 118, 26, 4670.
12. A.K. Dutt, R.S. Banerjee, *Z. Phys. Chem. Leipzig*, **1982**, *263*, 2, 298-304.
13. S.D. Furrow, *J. Phys. Chem.*, **1995**, *99*, 11131.
14. R. Cervellati, S.D. Furrow, S. De Pompeis, *Int. J. Chem. Kinet.*, **2002**, *34* (6), 357.
15. M.J. Mahon, A.L. Smith, *J. Phys. Chem.*, **1985**, *89*, 1215.

16. B.Z. Chowdry, A.P. Mendham, J. Tetteh, R. Withnal, *ChemPhysChem*, **2002**, *5*, 443.
17. S.D. Furrow, *J. Chem. Ed.*, **2012**, *89*, 1421.
18. L.I. Csepei, A Briggs-Rauscher reakció oszcillációinak leállitása (The Cessation of the Oscillations of Briggs-Rauscher Reaction), Bachelor Diploma Thesis, Babes-Bolyai University, Faculty of Chemistry and Chemical Engineering, **2005**.
19. L.I. Csepei, Cs. Bolla, *Studia UBB Chemia*, **2009**, *54*, 4, II, 249.
20. S.S. Sharma, S. Sharma, V.K. Rai, *Annals of Botany*, **1990**, *65*, 281.
21. L.I. Csepei, Cs. Bolla, I. Pontos, The Effect of Malonic Acid Concentration on the Briggs-Rauscher Reaction in Presence and Absence of Starch, 13th International Conference of Chemistry, Hungarian Technical Scientific Society of Transylvania, Cluj-Napoca, 8-11 November **2007**.
22. L.I. Csepei, Inhibiţia reacţiei oscilante Briggs-Rauscher cu acid salicilic (Inhibition of Briggs-Rauscher Reaction with Salicylic Acid), Master Diploma Thesis, Thesis, Babes-Bolyai University, Faculty of Chemistry and Chemical Engineering, **2006**.
23. L.I. Csepei, A hőmérséklet hatása a Briggs-Rauscher reakcióra (The effect of Temperature upon the Briggs-Rauscher Oscillating Reaction), 8th Scientific Conference on Technical Sciences, 7-9 April **2006**.
24. L.I. Csepei, Cs. Bolla, *Studia UBB Chemia*, **2011**, *55*, I, 285.
25. I. Pontos, Bachelor Thesis, Babes-Bolyai University, Faculty of Chemistry and Chemical Engineering, **1999**.
26. R. Ramaswami, N. Ganapathisubramanian, *J. Chem. Educ.*, **1979**, *56*, 321-325.
27. R. Cervellati, K. Höner, S.D. Furrow, F. Mazzanati, S. Costa, *Helv.Chim. Acta*, **2004**, *87*, 133-155.
28. J.A. Thoma, D. French, The Starch-Iodine-Iodide Interaction. Part I. Spectrophotometric Investigations, *J. Am. Chem. Soc.*, **1960**, *82 (16)*, 4144-4147.
29. D. Harvey, Modern Analytical Chemistry, McGraw Hill, **2000**, 345-346.

QUANTITATIVE ANALYSIS OF THE NONCOMPLIANT LANDFILL CONSTITUENTS

MICHAELA BIANCA SOPORAN[a,*], OVIDIU NEMEŞ[a]

ABSTRACT. In order to establish the nature and composition of the municipal wastes located in the municipal landfill Pata Rât, Cluj-Napoca, ten samples were collected in depth, every meter. Aiming the landfill characterization, the nature and the percentage composition of the materials was determinate.

Keywords: waste, landfill, material, composition.

INTRODUCTION

The aim of this work is to determine the landfill waste structure to further define the strategies concerning the waste selection and the obtained gas quantities. Studies were made on material degradation from noncompliant landfills, nearby Cluj-Napoca. We considered the analysis is influenced by waste composition distribution randomly deposited over time. The waste collection from an area of approximately 400.000 inhabitants was not done selective and the storage was mixed and uncontrolled. During the filling process, there was no plan for covering the storage and now, it is almost impossible to specify the time when the waste was disposed. The prolonged time of approximately 35 years of filling and the constituent layers resulted from the evolution of all materials and products that were stored indicate no periodicity in the composition of layers, by height. [1], [2]

This paper highlights the composition of waste stored in Pata Rât landfill. We mention that this study is the first which was achieved on this site.

RESULTS AND DISCUSSION

Knowing the waste nature and distribution is a very important way in determining the method of landfill operation [3-8]. In order to show the more precisely as possible the waste distribution in the Pata Rât landfill we

---

[a] *Technical University of Cluj-Napoca, Faculty of Materials and Environmental Engineering, Department Environmental Engineering and Sustainable Development Entrepreneurship, 103-105 Muncii Ave, Cluj-Napoca, Romania.*

[*] *Corresponding author: bianca.soporan@yahoo.com*

have analysed 10 samples collected as described. The composition variation of municipal waste is depicted in figure 1, from a to j.
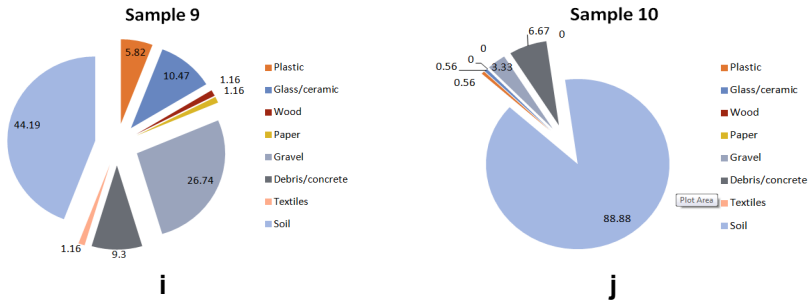

a

b

c

d

e

f

g

h
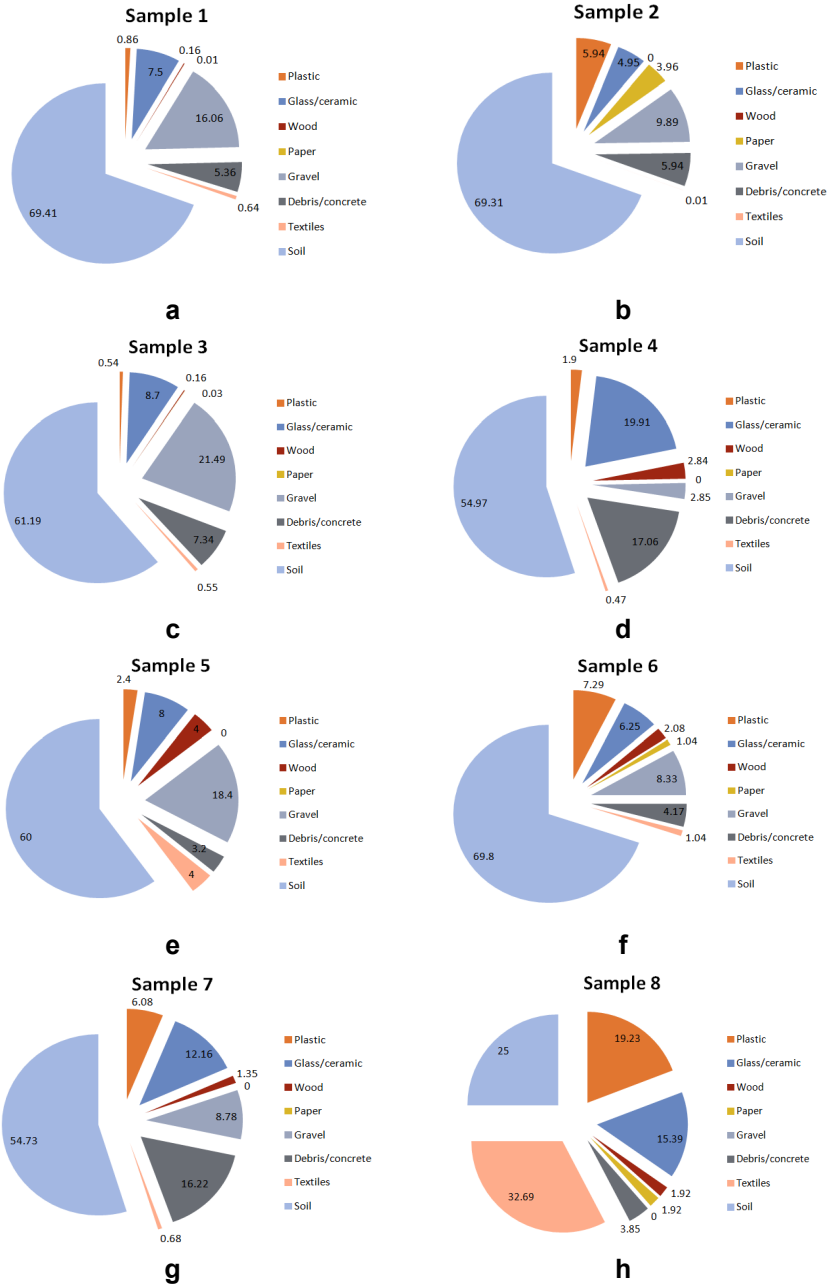
Figure 1. Material percentage variation in municipal waste samples

Analysis of samples has led to the establishment of their composition which varies as follows:

- plastic 0.56 ÷ 23% range;
- glass in 0.56 ÷ 19.91% range;
- wood in 0 ÷ 4% range;
- paper in 0 ÷ 3.96% range;
- textiles in 0 ÷ 32.69% range ;
- construction debris and concrete in 3.2 ÷ 17.06% range;
- soil in 25 ÷ 88% range.

In order to find the average composition of the waste layer, the following procedure was adopted: the minimum and the maximum values was removed from each category, then irrelevant results were excluded for establishing the results taken into account to determine the average composition and finally, averages values were calculated for each category of material. The irrelevant results had been considered as the highest maximum and the lowest minimum. [1]

After the plastic percentage from landfill was calculated, using data from Figure 1 and the above procedure, the following situation appeared: the maximum and minimum elimination (sample 3 and sample 8), the considered outcome (sample 1, sample 2, sample 4, sample 5, sample 6, sample 7, sample 9 and sample 10). The average balanced concentration is:

$$C_{A\ plastic}\ [\%] = 3.85625\% \cong 3.86\%.$$

Similarly, the average compositions of other components was calculated. Considering the results above, the following average composition of the analysed landfill area was calculated without minimum and maximum elimination).

The results of applying this methodology are shown in Table 1:

Table 1. The municipal waste average composition
in Pata Rât landfill, Cluj-Napoca

Concentration	UM	Balanced average	Average
Plastic	%	3.86	5.06
Glass/ceramics	%	9.18	9.39
Wood	%	1.21	1.37
Paper	%	0.52	0.81
Gravel	%	11.14	11.59
Debris/concrete	%	7.36	7.91
Textiles	%	1.07	4.12
Soil	%	60.45	59.75

The analysis made showed that the macroscopic recoverable materials (plastic, glass, wood, paper, textiles) has an approximate share of 20%. The inert material, (gravel and debris) has a share of approximately 20%, while the resulting waste degradation along with the soil have a share of 60%.

In this analysis, we have taken into account that the researches on municipal waste which contains also high quantities of construction and demolition waste and soil layers from the excavations and coatings. Therefore, we consider sampling in each layer cannot disregard this fact, so we propose a method to assess the potential recovery status of a non-compliant landfill.

Landfill materials can be grouped in three major parts: the recoverable component (macro); the inert component; the resulted component from biodegradable waste degradation.

In order to determine the components percentage, the following procedure was proposed: zoning the deposit according to historical known deposit activity; preliminary assessment of the areas according to their potential; establishment of potential components for analysis and evaluation at the macroscopic level; mapping of potential analysed areas; source and operating decisions analysis.

Excluding technological exploitation issues, we proposed a method for assessing the potential by determining the waste components. Considering that landfill was made randomly, the method for determining components should be based on vertical and horizontal sampling.

Vertical sampling step should be of 1-2 m and horizontal sampling step should be 10-15 m. The propose method is based on the experiment made to determine the landfill material degradation. The assumption made in the sense that there was a filling order and the corresponding specified time, was not checked by the measurements.

CONCLUSIONS

Analysing the results of municipal waste composition from noncompliant landfill nearby Cluj-Napoca, we found that we cannot draw a clear conclusion on the relationship between the values measured and the layer from which the sample had been taken. We believe that waste was not deposited successively, in an order from the bottom to the top. At the same time, the waste deposit randomly determined sequence of different compositions that cannot be characterized or assigned to a certain period of time.

We proposed a useful landfill characterization, knowing that the filling and the technological treatments were random and difficult to quantify. We made this analysis as a characterization of noncompliant landfill components.

EXPERIMENTAL SECTION

In order to determine the material composition of municipal waste from noncompliant Pata Rât landfill, Cluj-Napoca, a 10 m deep driller pit was realised and sampled every meter.

Drilling was made with a mobile drilling facility operated by SC Minesa - Research and Design Institute of Mining SA - Cluj-Napoca. [2]

Analyses were performed in the *Laboratory Testing of National Research and Development Institute for Industrial Ecology*, ECOIND, from Bucharest.

The tests made on samples for determining the composition of deposited materials were done in two stages: determination of macro characterization and the micro state of degraded waste.

ACKNOWLEDGMENTS

REFERENCES

1. M.B. Soporan, *Studies on municipal waste degradation and physical-chemical activity assessment in noncompliant landfill* - PhD Thesis, Technical University of Cluj-Napoca, Faculty of Materials and Environmental Engineering, Department of Environmental Engineering and Sustainable Development Entrepreneurship, Cluj-Napoca, Romania, **2012**, chapter 3.

2. ***, Protocol contract research type Partnerships, *VALENDEM* acronym, 2nd stage, 3rd phase, *Preliminary Experiments for Landfill Gas Characterization,* Technical University of Cluj-Napoca*,* **2011**, chapter 3.

3. M.B. Soporan, V.F. Soporan, G. Bătrînescu, E.A. Cociș, O. Nemeș, *Studia UBB Chemia*, **2012**, *3*, 5.

4. M.B. Soporan, V.F. Soporan, O. Nemeş, E.A. Cociș, *Reviews on opportunities of landfill gas recovery*, SIDOC Project – Doctoral students' session, SICOM, Technical University of Cluj-Napoca, Romania, 21 iunie **2012**.

5. M.T. Barral Silva, A.M. Menduina, Y.C. Seijo, F. Diaz-Fierros Viqueira, *Waste Management & Research*, **2007**, *25*, 99.

6. Y. Zhao, L. Song, R. Huang, L. Song, X. Li, *Waste Management & Research,* **2007**, *25*, 130.

7. ***, European Energy and Transport - Trends to 2030 - update 2007, http://ec.europa.eu/dgs/energy_transport/figures/trends_2030_update_2007/ energy_transport_trends_2030_update_2007_en.pdf;

8. ***, European Environment Agency, The road from landfilling to recycling: common destination, different routes, ISBN: 978-92-9167-930-0, http://www.eea.europa.eu/publications/brochure_2007_4;

9. ***, United States Environmental Protection Agency, Washington, D.C. 20460, Conducting Remedial Investigations/Feasibility Studies for Municipal Landfill Sites, http://www.epa.gov/superfund/policy/remedy/pdfs/540p-91001-s.pdf

ENVIRONMENTAL IMPLICATIONS CONCERNING THE CHEMICAL COMPOSITION AND PARTICLE DISTRIBUTION OF ANTI – SKID MATERIAL

DANA FLORINA MUNTEAN[a,*], ILARIE IVAN[b], LIANA MURESAN[a]

ABSTRACT. Anti skid material (AM) used to improve the traffic conditions could affect the particulate matter emissions during winter. The investigated AM sample contains silica particles to improve the friction coefficient between tires and road surface and crystalline sodium chloride as anti glaze agent. We found also some interesting rusty particles containing iron hydroxide (lepidocrocite and goethite) mixed with fine quartz sliver. Compression test shows that those particles have a low strength being able to be disintegrated in harsh traffic conditions. The powder resulted after crushing of rusty particles feature fine fractions with diameter in the range of 1 – 10 μm. Such fractions were found in the collected sedimenting particles (SP) proving their ability to be suspended in atmosphere. The monitoring performed with Automatic Monitoring Air Quality Stations shows the average values for $PM_{2.5}$; PM_{10} and SP are below the maximum accepted limit. However the registered values were high in days with intensive car traffic and lower in other days. The situation could be improved by a proper sorting of rusty particles from re-circulated anti skid material.

Keywords: anti - skid material, particulate matters, lepidocrocite, PM_{10}, $PM_{2.5}$

INTRODUCTION

Particulate matter (PM) monitoring is one of the main environmental issues in the European Union. Several regulations were adopted in order to develop a suitable management of such emissions [1, 2]. PM_{10} and $PM_{2.5}$ are the reference for particulate emissions from various urban activities [3, 4]. The health risk is increased for the monitored particulate matter emissions (e.g. $PM_{2.5}$ and PM_{10}) due to their ability to be inhaled. The risk depends on the aerosol size and the breathing air velocity [5], related to the possibly

[a] *Protection Agency Cluj, Calea Dorobanţilor Str., No. 99, RO-400609, Cluj-Napoca, Romania.*
[b] *Technical University of Cluj-Napoca, Muncii Ave. No. 103 -105, RO-400641, Cluj-Napoca, Romania.*
* *Correspondent author: muntean_nina@yahoo.com*

harmful components. Previous studies show a heterogeneous composition for PM_{10} and $PM_{2.5}$ which contains mainly minerals but also organic phases depending on the source. Anthropogenic activities, as well as acid rain and particulate emission, present erosive action on the environment being a major source of particulate matter [6, 7]. Another major anthropogenic source is the automotive traffic by combustion emission as well as floating mineral particles suspension due to the air currents.

For instance, automotive traffic PM emission measured in 2011 in Istanbul shows 28.5 % in winter and only 3.9 % in summer [8]. Why more PM emission in winter? It is an interesting subject to follow. The automotive traffic particulate emission have two major sources: combustion particles such as soot and organic aerosols (which depends on the each car combustion system and filters) [9, 10] and mineral fine fractions resulted from the tires interaction with the roads surface (which feature a strong dependence on the weather and precipitation level) [11, 12]. It was observed that soot and organic aerosols have small diameters in the range of PM2.5 meanwhile mineral particles are rather situated in PM_{10} range.

The road dust induces air floating particles due to the interaction with the moving cars [13, 14]. An important source of minerals in the dust is the asphalt and the road shoulder erosion at the contact with the car tires [12]. The breaking procedure enhances the abrasion, which increases with the friction coefficient. Anti – skid material is often used to adjust the road friction coefficient during the winter. This granular material acts as a rough dust between the tire and the road surface. It is subjected to an average grinding in such condition affecting its structure, certainly being able to release fine mineral fractions. These are incorporated into the road dust and further suspended in the air [12].

Similar study evidence the re-suspension tendency for the sedimenting particles on the adjacent snow layers due to their small size which are very sensitive to a significant modification of air velocity [14, 15]. The re-suspension process act mainly due to the lower cohesive forces observed for the fine particles which are lifted up by ascension force. Such mechanism could increase the PM_{10} and $PM_{2.5}$ air level during winter when is expected to be lower than in summer.

The anti skid material prove to be a major pollution source during winter. All mention aspects reveals that the mechanical behavior of the anti – skid material under traffic condition is the cause of pollution increasing. Such properties are directly influenced by the chemical composition and particle dispersion. The aim of present paper is to analyze the composition of anti-skid material used in Cluj-Napoca and to identify it's components in the PM_{10} and $PM_{2.5}$ emissions.

RESULTS AND DISCUSSION

AM contains two kinds of components: silica particles (mended to increase the friction coefficient between cars tires and road surface) and an anti – frost agent to prevent the glaze formation (usually sodium chloride is used).

The collected AM samples have a composition based on silica particles ranging from 1 to 10 mm. The total mineral amount represents 80 % and the rest of 20 % is the sodium chloride as anti – frost agent. A closer observation of the collected samples evidence silica particles having rounded shape and some intriguing brown particles (rusty like) having an unknown nature. They seem to be mineral conglomerates with a complex microstructure.

Sodium chloride particles are crystallized in cubic system featuring large crystals having cubic and octahedral particles as typical forms related to the BCC structure.

The mineral composition of AM sample was determined by XRD spectroscopy. The AM particles were grinded in a ball mill to obtain a powder suitable to be subjected at XRD investigation. The obtained diffractogram is presented in Figure 1a.
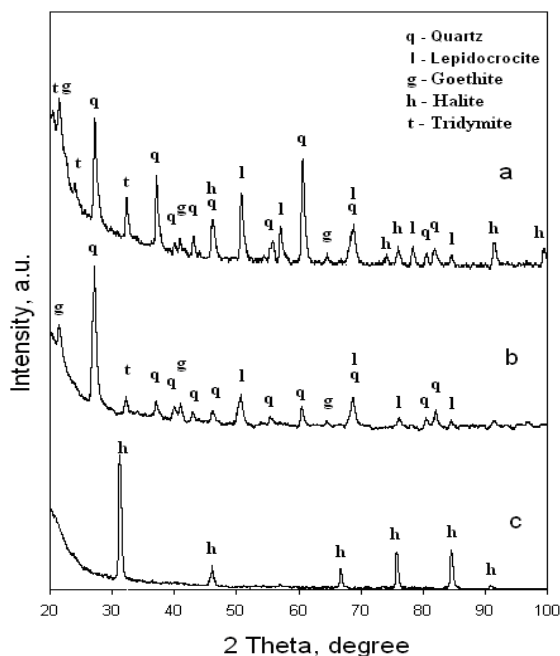

Figure 1. The X - ray diffraction spectrum for the investigated anti-skid material:
a) grinded non skid material, b) grinded iron hydroxide particles and c) halite particles.

It features well developed peaks related to the crystalline state of the sample. The dominant mineral found in the composition is quartz, having the most intense peaks. Sodium chloride was identified as crystalline halite. Each component amount was appreciated based on the XRD peaks relative intensities related to its structure factor. All identified components of AM sample are listed in Table 1 as well as their amount in the sample and their optical features in cross polarized light.

The significant presence of Tridymite (an allotrope of quartz) is sustained by it's presence in common river sand in Romania due to the sedimentation condition [16, 17]. Moderate quantities of tridymite found in silica granular material is a collateral evidence that the gravel used in the investigated anti skid material is dug up into a local gravel - plant (e.g. Harghita county – due to the proximity to the Sf. Ana volcano). Quartz has a hexagonal compact crystal lattice meanwhile trydimite is orthorhombic (it derives from quartz by intensive heat treatments as found in volcanic eruptions. Both quartz and tridymite particles feature a light green gray aspect in cross polarized light, Figure 2a. Their morphology is derived from broken silica spherical particles. It features several rounded particles mixed up with broken ones having sharp edges crossed at small angles.

Table 1. Components properties of AM sample

Component	Quartz	Lepidocrocite	Goethite	Halite	Tridymite	Total
Wt.%	60	10	8	10	12	100
Particle size range, μm	30 - 250	10 - 250	10 - 250	30 - 500	30 - 250	-
Color in cross polarized light	Green-gray	Reddish-brown	Reddish-brown	Pale white	Green-gray	-

The most interesting findings in AM are the iron hydroxides in crystalline form of: lepidocrocite and goethite. In figure 2a appears as brown particles having 30 – 50 μm. Their presence in AM sample proves to be related to the intriguing brown particles observed at macroscopic analysis. Therefore, we separated from the AM sample a significant number of rusty particles as well as a significant number of halite. Each category was crushed separately and resulted powders were investigated by XRD. The obtained spectra are presented in figure 1b and 1c.

Even more intriguing is the results of rusty particles composition. The major component over 65 % is the mixture of lepidocrocite (γ – iron hydroxide) accompanied by its allotrope goethite (α – iron hydroxide). The surprise is the evidence of quartz (35 %). It is really an interesting quest: how could be explained such composition revealed for the rusty particles. Some evidences to

reveal the mystery was found in the mineralogical microscopy performed with cross polarized light on the rusty particles powder, Figure 2b. It appear to be a refined mixture of quartz slivers having 20 – 30 µm (some of them presents rounded shape due to their log proliferation in open environment and some are fresh broken featuring sharp edges). The iron hydroxides act as a binder of quartz slivers. It is possibly in condition of road traffic.
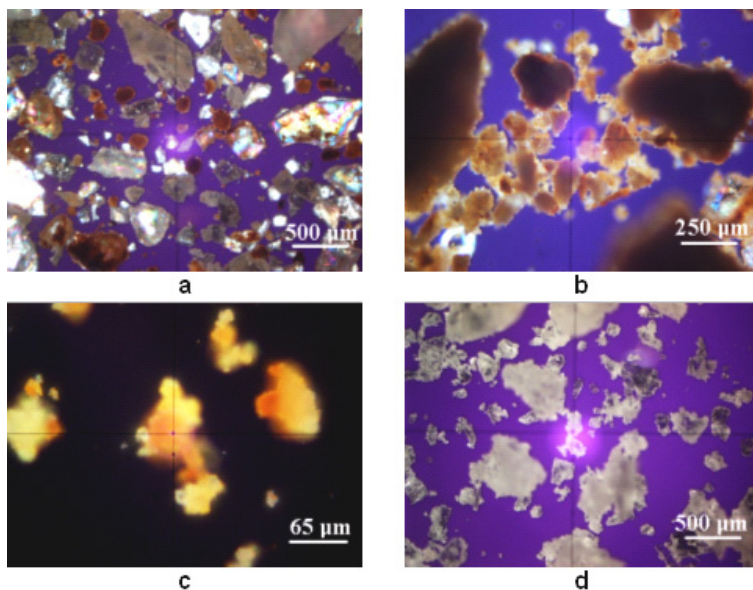

Figure 2. The cross polarized light microphotographs:
a) broken anti-skid material particles, b) broken iron hydroxide particles,
c) fine fractions of iron hydroxide particles, and d) halite particles.

A more detailed view catch some individualized iron hydroxide particles, figure 2c, having diameters between 10 – 50 µm. Their appearance is agglomerated, sustained the ability as mineral binder in relative humid environment.

The quartz particles from the street dust physical interacts with the car cassis rust in presence of anti skid material and relative humidity typical for winter and forms micro aggregates like those observed in Figure 2b. Considering several cycles of coalescence between micro aggregates finally results macroscopic particles such those observed in AM sample. This is a major fact which proves that AM sample contains re-circulated anti skid material re collected from the road sides. The implication for environment could be important even is able to become an environmental hazard.

Sodium chloride extracted from AM sample was also subjected to XRD. It reveals peaks only for halite, proving its high purity. The micro-structural aspect is presented in figure 2d, a fine mixture of cubs and octahedral crystal forming domains with polyhedron shape. Hence, sodium chloride is very solvable in aqueous or humid environment it is not a problem to interfere with air particulate matter suspensions.

The compression test results shows broking strength of 2054 MPa for silica particles and 840 MPa for iron hydroxide conglomerate. Silica particles compression strength strongly depends on the flawless structure. The values are in good agreement with the data in literature [18]. It proves that quartz particles have a good quality and are more resistant at mechanical solicitation than the other particles found in AM. Particularly, the iron hydroxide conglomerate feature small quartz slivers in composition, fact observed in Figure 2b. They act as cracking promoters reducing the compression strength as well as the particle cohesion.

Considering the interaction between car tires and road surface it exhibits local solicitation higher than 1000 MPa, fact which leads to the inevitable disintegration of rusty particles. Furthermore, the silica granules from anti – skid material acts as milling bodies refining the size of iron hydroxides as well as quartz slivers. Figure 2 b and 2c gives us some dimensional clues that fine particle could result after disintegration process. It needs to be considered diameters such 1, 2.5, 10, 20, up to 50 μm. All sizes range could be easy generated by automotive traffic.

The decaying of rusty particles in winter condition under pressure leads to the formation of fine particles below 10 μm diameter. The evidence of disintegration at microscopic level was traced out by dispersing the milled powder in deionized water under intensive agitation. Thin layer of particles were transferred on glass slide by immersion in the agitated dispersion for 30 seconds, followed by natural drying. The glass slide was microscopically inspected under cross polars and the resulted images are presented in Figure 3a. The iron hydroxide particles are very abundant, many of them features diameters around 20 μm but there are several finest particles in the range of 1 – 10 μm. All these fine micro - particles are able to be floated by air currents along the roads formed by automotive traffic [13, 14].

The thin layer was also subjected to XRD. Resulted a pattern is very similar with the one in Figure 1b. It proves that lepidocrocite, goethite and quartz slivers are able to form individualized PM_{10}; $PM_{2.5}$ and floating – sedimentable particles into the atmosphere. The data in literature state that any material particles spreaded or abandoned on the street are enclosed in the common street dust, and after is subjected to the air re-suspension [12, 15]. If so, we expect to found in winter atmosphere some other minerals belonging to the street adjacent environment decaying (e.g. clay mineral and perhaps calcite, very often found in the ground in Cluj-Napoca).
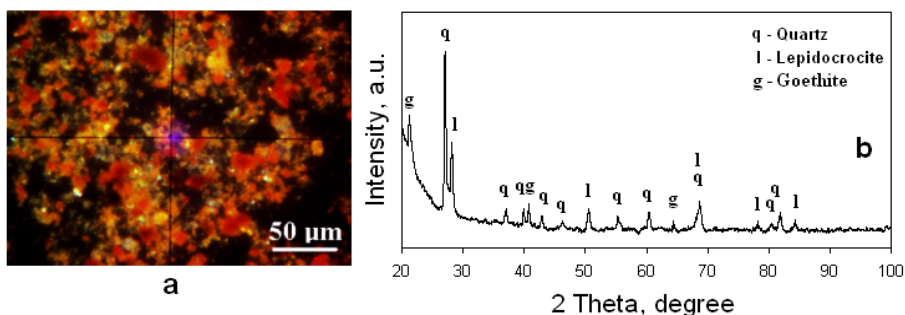
Figure 3. Thin layer of rusty particles powder transferred on glass slide via aqueous dispersion: a) cross polarized light microphotograph and b) XRD pattern.

Therefore, we collected particulate matter samples from atmosphere for the most representative winter months (December 2011, January 2012, and February 2012). The sedimenting particles (SP) collected were subjected to the XRD analysis. Resulted spectra are presented in Figure 4. Each of them present very well developed peaks proving the high crystalline state of the samples. The composition is the same for all three samples. The average characteristics are centralized in Table 2.
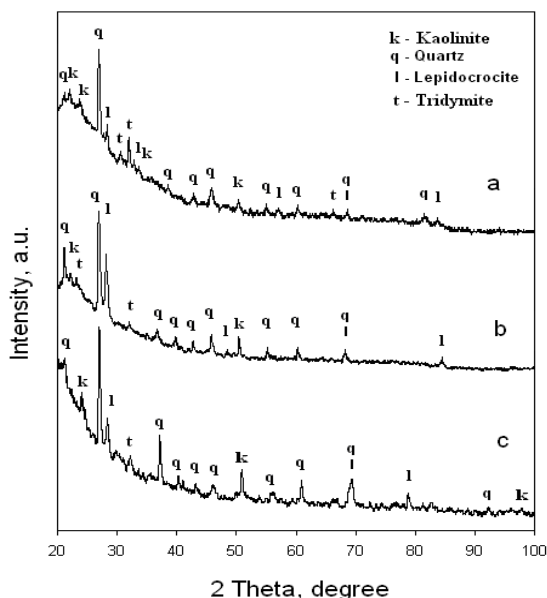

Figure 4. The X - ray diffraction spectrum for the sedimentable particles collected from air: a) December 2011, b) January 2012, and c) February 2012.

Table 2. Components properties of SP sample

Component	Quartz	Lepidocrocite	Kaolinite	Tridymite	Total
Wt.%	70	15	10	5	100
Particle size range, μm	1-30	1-30	1-10	1-30	-
Color in cross polarized light	Green-gray	Reddish-brown	Blue-white	Green-gray	-

Note: some isolated micro – particles could exceed 50 μm diameter

Microstructure of the sedimenting particles collected in December 2011 contains well dispersed fine microscopic particles. The cross polarized light inspection, Figure 5a, reveals a mixture of fine quartz particles together with lepidocrocite, kaolinite and tridymite. The detail at high magnification presented in Figure 5b, reveals better the shape and size of the minerals involved. The dimension ranges as well as mineral color in polarized light are centralized in Table 2. Similar observations were found for the SP samples collected in January 2012 and February 2012, the mineralogical microscopy results being displayed in Figure 5 c - f at average and high magnification.

Caolinite presence in the SP composition is interesting during winter because it is a clay mineral which belongs to the street adjacent areas. Its presence in the street dust is more signaled in summer [13]. The winter condition with snow and frost areas inhibits the decaying of street adjacent areas (the top ground is frost no particle is able to move under air currents). Still, a kaolinite amount of 10 % could be usual in winter considering the remains incorporated in street dust in autumn.

Quartz found in SP samples has two sources during winter: the soil decaying remains and the quartz slivers resulted from disintegration of rusty particles found in AM sample. It is the dominant mineral representing 70 % of SP average composition. But, the major prove of air disperse particulate maters generated by the anti – skid material is the presence of lepidocrocite at 15 % amount. Its particle size varies in a range of 1 – 30 μm as can be observed in Figure 5 b, d, and f. The evidenced range contains the most hazardous air particulate matters such $PM_{2.5}$ and PM_{10}.

The tridymite presence in SP samples as traces (over 5 %) also proves of particulate emissions caused by anti –skid material. In the real condition the multiple interactions between car tires and road surfaces intermediated by AS sample leads also to degradation of silica particles, some of them being crystallized as tridymite. The bilateral shock compression during car braking could promote cracks along silica crystal imperfection favoring the particle disintegration.

An amount of 15 % lepidocrocite was found in SP sample. It was induced in atmosphere by the same way as quartz slivers. Mineralogical microscopy evidence a lot of lepidocrocite particles in the range of 1-10 µm, sizes able to be incorporated in the $PM_{2.5}$ and PM_{10} emissions. It is interesting that goethite do not appear in SP sample. It is possible that goethite fine particles exposed for a long term to the winter environmental condition to transform themselves into lepidocrocite via natural decaying [19 – 20].
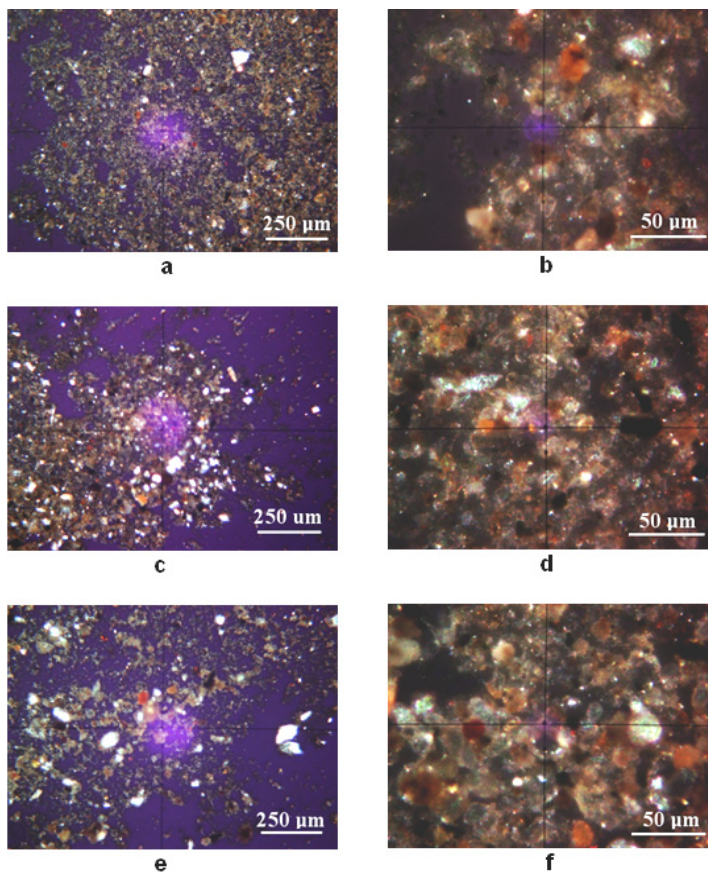

Figure 5. The cross polarized light microphotographs – different magnifications: a,b) December 2011, c,d) January 2012, and e,f) February 2012.

The particulate matter emissions were also quantitative measured using the Automatic Monitoring Air Quality Stations in the custody of Environmental Protection Agency of Cluj. Achieved data were centralized in Table 3.

Table 3. Particulate matter emissions data

Emission type		December 2011	January 2012	February 2012
PM$_{2.5}$, μg/m^3	min.	2.17	2.90	6.53
	max.	47.50	64.73	53.85
	average	28.19	23.50	35.23
PM$_{10}$, μg/m^3	min.	2.72	5.25	9.25
	max.	49.32	52.76	52.58
	average	27.37	19.95	31.33
SP, g/m^2/month	average	5.73	5.97	6.02

PM$_{2.5}$ emissions average value ranges from 23.50 to 35.23 μg/m^3 for all monitoring period. The risk level is low, because the average value is far away from the maximum limit. However, in days with high automotive traffic were signaled slightly exceeds of the limit: in 31 January 2012 was registered a peak of 64.73 μg/m^3 (an excess with 14.73 μg/m^3); and in 23 February 2012 was registered a peak of 53.85 μg/m^3 (an excess with 3.85 μg/m^3). The slightly exceeding mentioned is caused by the conjugated effect of intensive car traffic with presence of anti – skid material on the road surface.

The same variation could be observed for PM$_{10}$, Table 3, the average values are really lower than the accepted limit. The fact sustains that the environmental risk is low. However the PM$_{10}$ maximum registered exceeds the limit with: 2.76 μg/m^3 in January 2012, and with 2.58 μg/m^3 in February 2012 at the same days reported for PM$_{2.5}$. The SP emissions are in a good range, below the maximum limit of 17 g/m^2/month, no exceed were registered. Overall, the environmental risk is very low, because the average value is far away from the maximum limit.

A proper street management could reduce the effect of AS material related particulate matter emissions by an adequate sorting of re-circulated anti –skid material.

CONCLUSIONS

Anti – skid material investigated in present study contains silica particles (e.g. quartz and trydimite) to increase the friction coefficient between cars tires and road surface and halite (sodium chloride) as anti glaze agent. Some interesting rusty particles were found in the anti skid material used in Cluj-Napoca in the 2011 – 2012 winter. The XRD and mineralogical microscopy analysis found that their composition is a micro-structured mixture of iron hydroxides (e.g. lepidocrocite and goethite) with fine quartz slivers. Compression test shows a good strength of silica particles of AM and a low strength for rusty particles. These ones are mechanically disintegrated by the force action between

car tires and street surface. Silica particles having a higher strength act as milling bodies of the rusty particles. We milled some of rusty particles and the resulted powder was dispersed in deionized water. Aqueous dispersion evidences the formations fine fraction in the range of 1 – 10 μm. The particulate matter samples collected from air from December 2011 to February 2012 proves the incorporation of lepidocrocite and quartz slivers from anti skid material. Lepidocrocite amount reached in SP sample is situated at 15 %. The results of monitoring performed with Automatic Monitoring Air Quality Stations prove that the emissions are directly increased with the car traffic on the Aurel Vlaicu Street. The average values for PM2.5, PM10 and SP are below the maximum accepted limit, so the risk level is low. Finally, we can conclude that a better management of anti skid material could be improved to reduce the particulate matter emission during winter by a proper sorting of re-circulated anti skid material.

EXPERIMENTAL SECTION

Anti skid material samples were collected in the 2011 – 2012 winter from the distribution points around Aurel Vlaicu Street in Cluj-Napoca, Romania. Equal quantities of anti skid material were mixed together to obtain an average representative sample (AM). AM sample was further grinded in a ball mill to obtain a mixture of broken particles which are suitable for physic and chemical analysis.

The particulate emissions into the atmosphere were monitored with Aurel Vlaicu Air Station. There were collected from air monthly samples of sedimentable particles (SP) via wet deposition for December 2011, January 2012, and February 2012. The SP dispersion was dried by evaporation, resulted powder was considered for analysis in present paper. PM_{10} and $PM_{2.5}$ were also monitored for the area of interest using the Automatic Air Quality Monitoring stations driven by Environmental Protection Agency of Cluj.

Mineralogical composition was elucidated by XRD spectroscopy using a DRON 3 diffractometer equipped with data acquisition module and Matmec IV.0 soft. The XRD spectra were obtained using a Cu k_α radiation. Mineral were identified from XRD patterns using Match 1.0 identification soft powered by Crystal Impact Company and PDF2 (Powder Diffraction File database second edition).

Particles size and morphology were investigated using the mineralogical microscopy with cross polarized light, using a Laboval 2 microscope produced by Carl Zeiss Jena. Digital capture was performed with a Samsung Camera having 10 Mpx. The special microscopic interpretation and particles measuring were developed using Image J 1.40g soft as a free resource provided by National Institute of Health of USA.

Compression tests were performed on a standard compression machine registering the broken pressure at compression for some of the particles within the anti skid material.

REFERENCES

1. L. Gidhagen, H. Johansson, G. Omstedt, *Atmospheric Environment*, **2009**, *43*, 1029.
2. M. Gerboles, D. Buzica, R.J.C. Brown, R.E. Yardley, A. Hanus-Illnar, M. Salfinger, B. Vallant, E. Adriaenssens, N. Claeys, E. Roekens, K. Sega, J. Jurasovic, S. Rychlik, E. Rabinak, G. Tanet, R. Passarella, V. Pedroni, V. Karlsson, L. Alleman, U. Pfeffer, D. Gladtke, A. Olschewski, B. O'Leary, M. O'Dwyer, D. Pockeviciute, J. Biel-Cwikowska, J. Tursic*, Atmospheric Environment*, **2011**, *45*, 3488.
3. S. Vardoulakis, P. Kassomenos, *Atmospheric Environment*, **2008**, *42*, 3949.
4. T. Maté, R. Guaita, M. Pichiule, C. Linares, J. Díaz, *Science of the Total Environment*, **2010**, *408*, 5750.
5. C.C. Botar, *Studia UBB Chemia*, LVIII, **2013**, *4*, 23.
6. A.G. Hosu-Prack, I. Petean, G. Arghir, L.D. Bobos, I. Iurcut, M. Tomoaia-Cotisel, *Carpathian Journal of Earth and Environmental Sciences*, **2013**, *8, 4,* 75.
7. Y.F. Fan, Z.Q. Hu, Y.Z. Zhang, J.L. Liu, *Construction and Building Materials*, **2010**, *24*, 1975.
8. M. Koçak, C. Theodosi, P. Zarmpas, U.I., A. Bougiatioti, O. Yenigun, N. Mihalopoulos, *Atmospheric Environment*, **2011**, *45*, 6891.
9. Q. Yao, S.Q. Li, H.W. Xu, J.K. Zhuo, Q. Song, *Energy*, **2009**, *34*, 1296-1309.
10. F. Yan, E. Winijkul, S. Jung, T.C. Bond, D.G. Streets, *Atmospheric Environment*, **2011**, *45*, 4830.
11. H. Tervahattu, K.J. Kupiainen, M. Raisanen, T. Makela, R. Hillamo, *Journal of Hazardous Materials*, **2006**, *132*, 39.
12. J. Berger, B. Denby, *Atmospheric Environment*, **2011**, *45*, 3692.
13. A.G. Hosu-Prack, I. Petean, G. Arghir, L.D. Bobos, M. Tomoaia-Cotisel, *Studia UBB Chemia*, **2010**, *55*, 93.
14. M. Kauhaniemi, J. Kukkonen, J. Härkönen, J. Nikmo, L. Kangas, G. Omstedt, M. Ketzel, A. Kousa, M. Haakana, A. Karppinen, *Atmospheric Environment*, **2011**, *45*, 3646.
15. D. Martuzevicius, L. Kliucininkas, T. Prasauskas, E. Krugly, V. Kauneliene, B. Strandberg, *Atmospheric Environment*, **2011**, *45*, 310.
16. I. Seghedi, A. Szakacs, M. Kovacs, R. Rosu, Z. Pecskay, *Institute of Geology and Geophysics*, **1995**, *76, (7),* 49.
17. M. Radoane, N. Radoane, D. Dumitriu, C. Miclaus, *Carpathian Journal of Earth and Environmental Sciences*, **2006**, *1, (2),* 13.
18. J. Kimberley, K.T. Ramesh, O.S. Barnouin, *Journal of Geophysical Research*, **2010**, *115*, 1.
19. Y. Cudennec, A. Lecerf, *Solid State Sciences*, **2005**, *7 (5)*, 520.
20. R.V. Morris, H.V. Lauer, *Journal of Geophysics Research*, **1981**, *86, (B11),* 10893.